

1-1-1988

Thermodynamics of supercritical gas-polymer mixtures/

Eric J. Beckman

University of Massachusetts Amherst

Follow this and additional works at: https://scholarworks.umass.edu/dissertations_1

Recommended Citation

Beckman, Eric J., "Thermodynamics of supercritical gas-polymer mixtures/" (1988). *Doctoral Dissertations 1896 - February 2014*. 740.
https://scholarworks.umass.edu/dissertations_1/740

This Open Access Dissertation is brought to you for free and open access by ScholarWorks@UMass Amherst. It has been accepted for inclusion in Doctoral Dissertations 1896 - February 2014 by an authorized administrator of ScholarWorks@UMass Amherst. For more information, please contact scholarworks@library.umass.edu.

UMASS/AMHERST



312066007694783

THERMODYNAMICS OF SUPERCRITICAL GAS-POLYMER
MIXTURES

A Dissertation Presented

by

Eric J. Beckman

Submitted to the Graduate School of the
University of Massachusetts in partial fulfillment
of the requirements for the degree of

DOCTOR OF PHILOSOPHY

February, 1988

Polymer Science and Engineering

© Copyright by Eric John Beckman 1988

All Rights Reserved

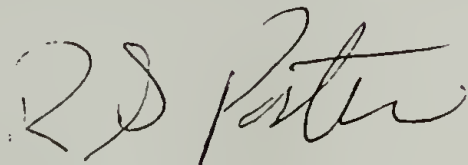
THERMODYNAMICS OF SUPERCRITICAL GAS-POLYMER
MIXTURES

A Dissertation Presented

by

Eric J. Beckman

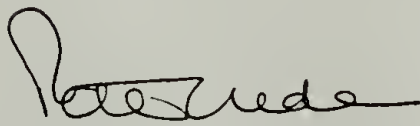
Approved as to style and content by:



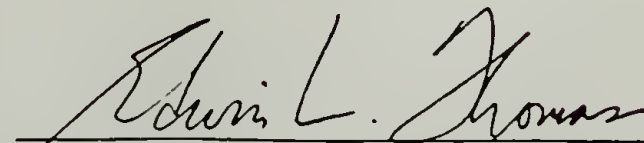
R.S. Porter, Chairman of Committee



F.E. Karasz, Member



P.C. Uden, Member



E.L. Thomas, Department Head
Polymer Science and Engineering Department

ACKNOWLEDGEMENTS

I would like to thank my research advisor, Dr. Roger S. Porter, for his support, good humor, and patience in allowing me to explore uncharted waters. I would also like to thank my committee members, Drs. F.E. Karasz and P.C. Uden, for their suggestions and comments. Special thanks goes to Drs. R. Koningsveld, L.A. Kleintjens, and W.J. MacKnight for quelling a lot of the anxiety and fear which seems to naturally accompany the word "thermodynamics".

I owe a great deal to Dr. Tom Hillegers at DSM, the man behind the development of the PEP computer program. In addition, the Thermodynamics Group at DSM Research in Geleen, Netherlands, particularly the always-suspicious Belgians, provided some excellent criticism and numerous timely coffee breaks.

I was fortunate in being part of a diverse and stimulating research group. There are too many names to mention, yet particular thanks goes to the "Class of 1982"; Jerry Parmer, Matt Muir, Youngchul Lee, and Kevin Schell for their never-ending harassment, inspired frisbee play, and bad jokes. In addition, Eleanor Thorpe should be commended on her ability to fight UMass red tape and interpret bizarre expense reports.

My family has always been there when I needed them and I am extremely grateful. Finally, thanks to Joanne for putting up with an absent-minded scientist and making the whole thing worthwhile.

ABSTRACT

THERMODYNAMICS OF SUPERCRITICAL GAS-POLYMER MIXTURES

February, 1988

Eric J. Beckman, B.S., Massachusetts Institute of Technology

Ph.D., University of Massachusetts

Directed by: Professor R.S. Porter

Supercritical fluids (SCF's) are commonly applied as extractants by the food and pharmaceutical industries due to their unique combination of properties. Whereas a large body of information concerning small molecule/SCF mixtures is available in the literature, studies of either the solubility of polymers in SCF's or models with which to predict the phase behavior of such systems, are few. In this work, predictions of the phase behavior of the poly(methyl methacrylate)-CO₂ and polystyrene-CO₂ systems are made using a generalized mean field lattice gas (MFLG) model and compared to experimental solubilities measured using a flow-through extraction unit. Because the necessary binary parameters are found via fitting of the model to published sorption data, calculations of dilute solution behavior are purely predictive. These predictions display the proper dependence of solubility on pressure and temperature, but underestimate the solubility, probably due to lack of segment density fluctuation terms in the MFLG model. Not surprisingly, CO₂ is a better solvent for PMMA than for PS.

Attempts to dissolve Bisphenol A polycarbonate in supercritical CO₂ were thwarted by the rapid solvent-induced crystallization (SINC) of the polymer. The extent and rate of crystallization are comparable to those observed in the SINC of polycarbonate by acetone. The behavior of the melting temperature implies that the T_g of the mixture passes through a minimum versus pressure, consistent with trends in other gas-polymer mixtures.

In addition, the MFLG model, in conjunction with postulated vitrification criteria, is used to predict the pressure-dependence of the T_g of a polymer-gas mixture. Three thermodynamic criteria are evaluated; iso-free volume, iso-entropy, and iso-viscosity, the latter represented by the quantity TS , as per the Adam-Gibbs derivation. Because the necessary model parameters were determined via fitting to phase behavior data, the subsequent T_g calculations involve no adjustable parameters. The constant- TS condition consistently produces the best prediction of the pressure and composition dependencies of the T_g . Predictions of the T_g of the PS-CO₂ and PMMA-CO₂ systems versus pressure are in excellent agreement with published results.

TABLE OF CONTENTS

	<u>page</u>
ACKNOWLEDGEMENTS	iv
ABSTRACT	v
LIST OF TABLES	xi
LIST OF FIGURES	xiii
 Chapter	
1 Introduction	1
1.1 Supercritical Gases: Novel Process Fluids for Polymers	1
1.2 Thermodynamic Modelling of Supercritical Gas-Polymer Systems	2
1.3 Scope of this Work	4
2 Modelling Pure Component Data I: A Comparison of Equations of State	7
2.1 Mean Field Lattice Models Which Include the Effect of Segmental Surface Areas	8
2.2 Comparison of MFLG and Rigid Lattice Models	14
2.3 Modelling Results for Pure Components	20
2.3.1 The Parameter Estimation Program (PEP)	20
2.3.2 Fitting Results for CO ₂ , SO ₂ , CF ₃ H, and PS	22
2.3.2.1 CO ₂	22
2.3.2.2 SO ₂ and CF ₃ H	31
2.3.2.3 Polystyrene (PS)	44
2.4 Comparison of the MFLG and Other Classes of Equation of State	55
2.5 Summary of Chapter 2	56

3	Modifying the Entropy of Mixing Expression of the MFLG Model: The First Order MFLG Model	58
3.1	Derivation of the First Order MFLG Model	58
3.2	Results for CO ₂ , SO ₂ , CF ₃ H, and Polystyrene	61
3.3	Summary of Chapter 3	72
4	Phase Separation Behavior of Binary Mixtures	73
4.1	Free Energy and Related Thermodynamic Quantities for the Zero and First Order MFLG Models	74
4.2	Phase Behavior of Polymer-Liquid Mixtures	80
4.2.1	Polystyrene-Cyclohexane	80
4.2.2	Polystyrene-SO ₂	88
4.2.3	Summary of Section 4.2	95
4.3	Phase Behavior of Polymer-Gas Mixtures	96
4.3.1	Experimental	96
4.3.2	Poly(Methyl Methacrylate)-CO ₂	98
4.3.3	Polystyrene-CO ₂	113
4.3.4	Summary of Section 4.3	118
5	Predicting the Pressure Dependence of the Glass Transition of Amorphous Polymers	120
5.1	Thermodynamic Criteria for the Glass Transition	121
5.1.1	Entropy: Comparison of MFLG and Gibbs-DiMarzio Model	123
5.1.2	Free Volume: Comparison of the Kanig and MFLG Models	124
5.1.3	Modifying the Temperature Dependence of the MFLG Free Energy Expression	127
5.2	Comparison of the Predictions of $\partial T_g/\partial p$ Produced by the Three Criteria: Results for Amorphous Polymers	129
5.3	Summary of Chapter 5	147

6 Predicting the Composition Dependence of the Glass Transition of Mixtures	148
6.1 Comparison with Other Models	149
6.2 Predicting the Glass Transition of Mixtures Using Thermodynamic Criteria	150
6.2.1 Effect of the Molecular Weight on the Glass Transition: Chain Ends as Diluent	152
6.2.2 Polymer-Liquid Mixtures: Polystyrene-Toluene and Polystyrene-Cyclohexane	153
6.3 Effect of Gas Pressure on the Glass Transition of Polymer	164
6.3.1 Examples from the Literature	165
6.3.2 Polycarbonate-Carbon Dioxide	166
6.3.2.1 Experimental	167
6.3.2.2 Results and Discussion	167
6.4 Predicting the T_g of Polymer-Gas Mixtures as a Function of Ambient Temperature and Pressure	175
6.4.1 Poly(Methyl Methacrylate)-CO ₂	175
6.4.2 Polystyrene-CO ₂	183
6.5 Summary of Chapter 6	188
7 Conclusions and Proposals for Future Work	190
7.1 Conclusions	190
7.2 Proposals for Future Work	195
7.2.1 Modelling	195
7.2.2 Applications	196

APPENDICES	198
A. Thermodynamic Relations for Pure Components Derived from the First Order MFLG Free Energy Expression	198
B. Equations Derived from the First Order MFLG Model Free Energy Expression and Defining Relations from Table 4.1	200
C. Derivation of the Volume Change on Mixing from the Degree of Swelling	208
BIBLIOGRAPHY	210

LIST OF TABLES

Table 1.1 Critical Constants of Some Common Gases	6
Table 2.1 Comparison of MFLG and other Lattice Equations of State	19
Table 2.2 Average Errors in Fitting Lattice Equations of State to pVT Data on CO ₂	25
Table 2.3 Lattice Model Parameters for CO ₂ Determined by Parameter Estimation Program (PEP)	26
Table 2.4 Average Errors in Fitting Lattice Equations of State to pVT Data on SO ₂	32
Table 2.5 Lattice Model Parameters for SO ₂ Determined by Parameter Estimation Program (PEP)	33
Table 2.6 Average Errors in Fitting Lattice Equations of State to pVT Data on CF ₃ H	38
Table 2.7 Lattice Model Parameters for CF ₃ H Determined by Parameter Estimation Program (PEP)	39
Table 2.8 Average Error in Fitting Lattice Equations of State to Polystyrene pVT Data	47
Table 2.9 Lattice Model Parameters for Polystyrene Determined by Parameter Estimation Program (PEP)	48
Table 2.10 Comparison of Molecular Surface Area Ratios Derived from MFLG Fitted Parameters and Using Bondi's Group Contribution Method	54
Table 3.1a Average Errors in Fitting Lattice Equations of State to pVT Data on CO ₂ , SO ₂ , CF ₃ H, and Polystyrene	64
Table 3.1b Average Errors in Fitting Lattice Equations of State to pVT Data on CO ₂ , SO ₂ , CF ₃ H, and Polystyrene	65

Table 3.2 Average Error in Fitting Lattice Equations of State to Polystyrene pVT Data	66
Table 3.3 First Order MFLG Model Parameters for CO ₂ , SO ₂ , CF ₃ H, and Polystyrene Determined by Parameter Estimation Program (PEP)	66
Table 3.4 Comparison of Molecular Surface Area Ratios Derived from First Order MFLG Fitted Parameters and Using Bondi's Group Contribution Method	71
Table 4.1 Thermodynamic Relationships for Mixtures for the Mean Field Lattice Gas (MFLG) Models	79
Table 4.2 Average Errors in Fitting MFLG Models to pVT Data on Cyclohexane	82
Table 4.3 Zero and First Order MFLG Parameters for Cyclohexane as Determined by the PEP	82
Table 4.4 MFLG Material Parameters for Poly(methyl methacrylate) and Carbon Dioxide and for the PMMA-CO ₂ Mixture	102
Table 4.5 Material Parameters for Polystyrene and PS-CO ₂ Mixture using MFLG Model	115
Table 5.1 Average Errors in Fitting MFLG Models to pVT Data on Cyclohexane, Toluene, and Benzene	133
Table 5.2 MFLG and Modified MFLG Parameters for Cyclohexane, Toluene, and Benzene as Determined by the PEP	134
Table 5.3 Fitting Results for Polystyrene, Poly(methyl methacrylate), Poly(vinyl acetate), and Bisphenol A Poly(carbonate) using MFLG Equation of State	135
Table 5.4 Values of FV, S, and T _g S for Polystyrene, Poly(methyl methacrylate), Poly(vinyl acetate), and Bisphenol A Polycarbonate using Modified MFLG Model	146
Table B.1 Terms for Equation B-1	207

LIST OF FIGURES

Figure 2.1 VLE data for CO ₂ and lattice model calculations	27
Figure 2.2 CO ₂ vapor pressure as a function of temperature and lattice model calculations	28
Figure 2.3 CO ₂ compressibility ($Z = PV/RT$) versus pressure at $T = 323K$ and lattice model calculations	29
Figure 2.4 CO ₂ compressibility ($Z = PV/RT$) versus pressure at $T = 372K$ and lattice model calculations	30
Figure 2.5 SO ₂ VLE data and lattice model calculations	34
Figure 2.6 SO ₂ vapor pressure as a function of temperature and lattice model calculations	35
Figure 2.7 SO ₂ compressibility ($Z = PV/RT$) versus temperature at $P = 101.3$ bar and lattice model calculations	36
Figure 2.8 SO ₂ compressibility ($Z = PV/RT$) versus temperature at $P = 304.0$ bar and lattice model calculations	37
Figure 2.9 CF ₃ H VLE data and lattice model calculations	40
Figure 2.10 CF ₃ H vapor pressure as a function of temperature and lattice model calculations	41
Figure 2.11 CF ₃ H compressibility ($Z = PV/RT$) versus pressure at $\rho = .5597$ g/cc and lattice model calculations	42
Figure 2.12 CF ₃ H compressibility ($Z = PV/RT$) versus pressure at $\rho = .7892$ g/cc and lattice model calculations	43
Figure 2.13 Polystyrene ($M_n = 2300$) density versus temperature at $P = 1$ bar and lattice model calculations	49
Figure 2.14 Polystyrene ($M_n = 20400$) density versus temperature at $P = 100$ bar and lattice model calculations	50
Figure 2.15 Polystyrene ($M_n = 20400$) density versus temperature at $P = 1500$ bar and lattice model calculations	51

Figure 2.16 Polystyrene ($M_n = 90700$) density versus temperature at $P = 800$ bar and lattice model calculations	52
Figure 2.17 Polystyrene ($M_n = 90700$) density versus temperature at $P = 1600$ bar and lattice model calculations	53
Figure 3.1 VLE data for CO_2 and lattice model calculations	67
Figure 3.2 CO_2 vapor pressure as a function of temperature and lattice model calculations	68
Figure 3.3 CO_2 compressibility ($Z = PV/RT$) versus pressure at $T = 323\text{K}$ and lattice model calculations	69
Figure 3.4 CO_2 compressibility ($Z = PV/RT$) versus pressure at $T = 372\text{K}$ and lattice model calculations	70
Figure 4.1 Cyclohexane pVT data versus MFLG models' descriptions	83
Figure 4.2 Polystyrene-Cyclohexane spinodal data (points) compared to Zero Order MFLG model description (curves) at three molecular weights (M_w 's)	84
Figure 4.3 Predictions of the spinodal curve of a 97,200 MW polystyrene in cyclohexane using the Zero Order model, parameter set 1 (see text); and parameter set 2; compared to cloud point data	85
Figure 4.4 Fit of the First Order MFLG model (curves) to spinodal data (points) for polystyrene-cyclohexane system	86
Figure 4.5 Prediction of the volume change on mixing of the polystyrene-cyclohexane system versus concentration by the Zero Order and First Order MFLG models compared to data derived from density measurements by Scholte [1970]	87
Figure 4.6 Vapor pressure suppression of a solution of 2330 MW polystyrene in liquid SO_2 (as compared to pure solvent) versus temperature	91

Figure 4.7 Predicted spinodals and binodals by Zero Order MFLG model and phase separation results by Albihn and Kubat [1981]	92
Figure 4.8 Predicted spinodals and binodals by Zero Order MFLG model and phase separation results by Albihn and Kubat [1981]	93
Figure 4.9 Predicted spinodals for Zero and First Order models and phase separation results by Albihn and Kubat [1981]	94
Figure 4.10 Fluitron Supercritical Extraction Unit	103
Figure 4.11 Fit of the Zero Order MFLG model "swelling binodal" equations to PMMA-CO ₂ sorption data at 315K by Liao and McHugh [1985]	104
Figure 4.12 Fit of the Zero Order MFLG model "swelling binodal" equations to PMMA-CO ₂ sorption data at 331.3K by Liao and McHugh [1985]	105
Figure 4.13 Fit of the Zero Order MFLG model "swelling binodal" equations to PMMA-CO ₂ sorption data at 341.2K by Liao and McHugh [1985]	106
Figure 4.14 Prediction of the volume change on mixing of the PMMA-CO ₂ mixture versus pressure by the Zero Order MFLG model compared to values calculated from swelling data by Liao and McHugh [1985] at three temperatures	107
Figure 4.15 Prediction (curves) of the density of CO ₂ versus literature data [Reynolds, 1979] (points) at two temperatures	108
Figure 4.16 Solubility measurements of 7000 MW PMMA in CO ₂ versus pressure at 313K compared to binodal and spinodal predictions by the Zero Order MFLG model	109
Figure 4.17 Solubility measurements of 7000 MW PMMA in CO ₂ at 333K compared to Zero Order MFLG model predictions	110

Figure 4.18 Solubility measurements of 24,300 MW PMMA in CO ₂ versus pressure at 313K compared to binodal and spinodal predictions by Zero Order MFLG model	111
Figure 4.19 Solubility measurements of 24,300 MW PMMA in CO ₂ versus pressure at 333K compared to Zero Order MFLG model predictions	112
Figure 4.20 Solubility of 2000 MW polystyrene in CO ₂ at 313K versus pressure (●) (and smoothed data by Bowman [1976] (■)) compared to spinodal predictions (—) by Zero Order MFLG model	116
Figure 4.21 Solubility measurements of 2000 MW polystyrene in CO ₂ at 353K versus pressure compared to Zero Order MFLG model spinodal prediction	117
Figure 5.1 Predictions of T _g versus pressure by MFLG model using constant FV, S, and TS criteria against literature data for PS by Gee [1966], Oels [1977], Zoller, <i>et al.</i> [1976] Quach and Simha [1971], Ichihara, <i>et al.</i> [1971] and Stevens, <i>et al.</i> [1986]	136
Figure 5.2 Predictions of T _g versus pressure by modified MFLG model using thermodynamic criteria	137
Figure 5.3 Predictions of density at T _g versus pressure using constant FV, S, and TS criteria and MFLG model against literature data for PS by Oels [1977]	138
Figure 5.4 Predictions of density at T _g versus pressure using modified MFLG model and thermodynamic criteria	139
Figure 5.5 Predictions of T _g versus pressure by MFLG model using constant FV, S, and TS criteria against literature data of PMMA by Olabisi and Simha [1975]	140
Figure 5.6 Predictions of T _g versus pressure by modified MFLG model using thermodynamic criteria	141

Figure 5.7 Predictions of T_g versus pressure by MFLG model using constant FV, S, and TS criteria against literature data for PVAc by McKinney and Goldstein [1974]	142
Figure 5.8 Predictions of T_g versus pressure by modified MFLG model using thermodynamic criteria	143
Figure 5.9 Predictions of T_g versus pressure by MFLG model using constant FV, S, and TS criteria against literature data for PC by Zoller [1982]	144
Figure 5.10 Predictions of T_g versus pressure by modified MFLG model using thermodynamic criteria	145
Figure 6.1 Predictions of T_g versus molecular weight using MFLG model and constant FV, constant S, and constant TS criteria compared with data by Ueberreiter and Kanig [1952], Cowie [1975], and Claudy, <i>et al.</i> [1983]	157
Figure 6.2 Calculated spinodals for polystyrene- toluene using Zero Order MFLG model and cloud points by Saeki, <i>et al.</i> [1973] at three molecular weights . . .	158
Figure 6.3 Predicted T_g of polystyrene-toluene mixture versus weight fraction polymer using MFLG model with constant FV, constant S, and constant TS criteria and data by Masa, <i>et al.</i> [1973], and Adachi, <i>et al.</i> [1975]	159
Figure 6.4 Predicted T_g of polystyrene-cyclohexane mixture versus weight fraction polymer using MFLG model with parameter set 1 and constant FV, constant S, and constant TS criteria and data by Masa, <i>et al.</i> [1973]	160
Figure 6.5 Predicted T_g of polystyrene-cyclohexane mixture versus weight fraction polymer using MFLG model with parameter set 2 and constant FV, constant S, and constant TS criteria	161

Figure 6.6 Predictions of ΔV_m of polystyrene-cyclohexane mixtures at $T=298K$ by MFLG model with parameter set 1 and parameter set 2 compared to data derived from solution density measurements of Scholte [1970]	162
Figure 6.7 Predictions of ΔV_m of polystyrene-toluene mixtures at $T=303K$ by MFLG model and data derived from solution density measurements of Scholte [1970]	163
Figure 6.8 DSC results of bisphenol A polycarbonate exposed to CO_2 for 4 hours at $75C$ at pressures from 100 to 500 atm.	171
Figure 6.9 DSC results of bisphenol A polycarbonate exposed to CO_2 for 4 hours at 300 atm. at temperatures of 50, 62.5, 75.0, and $87.5C$	172
Figure 6.10 Percent crystallinity of bisphenol A polycarbonate exposed to supercritical CO_2 for 4 hours versus exposure pressure at temperatures of 75.0 and $87.5C$	173
Figure 6.11 Percent crystallinity of bisphenol A polycarbonate exposed to supercritical CO_2 at 300 atm. at temperatures of 75.0 and $87.5C$ versus exposure time	174
Figure 6.12 Predictions of T_g versus pressure at $T_a= 308K$ for the CO_2 -PMMA mixture using the MFLG model with the constant FV, S, and TS conditions and data by Chiou, <i>et al.</i> [1985b]	177
Figure 6.13 Fit of the MFLG model swelling binodal equations to sorption data by Liao and McHugh [1985] at $315K$ (top graph) and $341.2K$ (bottom graph) using parameter set 1 and parameter set 2	178
Figure 6.14 Predictions of volume change on mixing for PMMA- CO_2 mixture at $315K$ (top graph) and $341.2K$ (bottom graph) using Zero Order model and parameter set 1 and parameter set 2 and data derived from swelling measurements of Liao and McHugh [1985]	179

Figure 6.15 Predictions of T_g versus pressure at $T_a=308K$ for the PMMA- CO_2 mixture using the Zero Order model and the three criteria	180
Figure 6.16 Predictions of T_g versus pressure for the CO_2 -PMMA mixture using the MFLG model and constant TS criterion at $T_a= 308K$, $T_a= 315K$, $T_a= 331.3K$, and $T_a= 341.2K$	181
Figure 6.17 Predictions of $(T_a - T_g)$ versus pressure for the CO_2 -PMMA mixture using MFLG model and constant TS criterion at $T_a= 308K$, $T_a= 315K$, $T_a= 331.3K$, and $T_a= 341.2K$	182
Figure 6.18 Prediction of T_g versus pressure of CO_2 -PS system using MFLG model and constant FV, S, and TS criteria and data by Wang [1981]	185
Figure 6.19 Prediction of T_g versus pressure for CO_2 -PS mixture using MFLG model and constant TS condition at $T_a= 318K$ and $T_a= 307K$ and data by Wang [1981] at 318K and 307K	186
Figure 6.20 Prediction of $(T_a - T_g)$ for CO_2 -PS at $T_a= 318K$ and CO_2 -PMMA at $T_a= 315K$ using MFLG model and constant TS condition	187

CHAPTER 1

Introduction

1.1 Supercritical Gases: Novel Process Fluids for Polymers

Supercritical gases have been used extensively by the food and pharmaceutical industries [Paulaitis, *et al.*, 1983; Randall, 1982] in extractions of high boiling or temperature sensitive compounds due to the interesting properties which gases display above the critical point, such as:

1. Supercritical fluids have liquid-like densities which can be adjusted over a significant range by changing the pressure. Thus the solvent power of a particular fluid can be varied without changing the composition of the fluid. Varying the solvent power of the gas will vary its selectivity towards a particular solute; consequently supercritical gases have been used to efficiently separate constituents of interest from mixtures, such as in the case of coffee decaffeination [Jasovsky and Gottesman, 1981].
2. Supercritical fluids have gas-like diffusivities and therefore contribute to high mass transfer rates [Schneider, 1983; King, *et al.*, 1983].
3. The critical temperatures and pressures of many of the gases commonly used in supercritical processes are low, less than 100°C and 100 atm. (see table 1.1).

The use of supercritical fluids in polymer processing has been "rediscovered" in the past five years. Since the 1940's, the high pressure polyethylene process has been operated at temperatures and pressures far above the critical point of ethylene. Not surprisingly, a great deal of phase behavior data has been gathered on this system [Ehrlich, 1965; Swelheim, *et al.*, 1965; de Loos, *et al.* 1983, 1984; Kleintjens, 1979; Luft and Lindner, 1976; Raetzsch, *et al.*, 1980; Spahl and Luft, 1981]. By contrast, many foamed polymer processes are conducted at pressures and temperatures above the critical point of the foaming gas, yet little or no information exists as to the phase behavior of such systems or the effect which the gas has on the glass transition of the polymer [Griskey, 1976; Bonner, 1977].

Phase behavior data on systems other than those involving polyethylene are few, yet interest in such systems has grown significantly over the past five years. Recent applications include fractionation [Krukonis, *et al.*, 1987], combined polymerization and fractionation [Kumar, *et al.*, 1986], and the use of supercritical gases to transport temperature sensitive additives into a polymer [Sand, 1986]. To support such advances, there is a continuing need for phase behavior data, which at present is scarce, on supercritical gas-polymer systems.

1.2 Thermodynamic Modelling of Supercritical Gas-Polymer Systems

Just as there is a lack of phase separation behavior data for polymer-supercritical gas systems, so too the number of thermodynamic models which have been shown to be suitable for describing such systems are also few [McHugh and Krukonis, 1986]. Modelling strategies commonly used for describing the solubility of low molecular weight solids in supercritical gases are inappropriate for use with polymers for several reasons:

1. In describing the solubility of non-polymeric solids in supercritical gases, it is usually assumed that the amount of gas sorbed by the solid is negligible, thus the chemical potential of the "solid" phase is calculated using the saturated vapor pressure and the Poynting correction [Paulaitis, *et al.*, 1983, McHugh and Krukonis, 1986]. This approximation is very poor for gas-polymer systems [Lundberg, *et al.*, 1969; Liao and McHugh, 1986]; in fact, often the reverse, that little or no polymer dissolves in the gas, is a more accurate assumption [Bowman, 1976].
2. The chemical potential of the gas is usually calculated via one of the cubic equations of state, such as Peng-Robinson, commonly used by chemical engineers [Kurnik, *et al.*, 1981]. Due to a lack of higher order reciprocal volume terms, such equations are inappropriate for use with high density liquids such as polymers. Thus, even without the restriction in item 1 above, there are still problems with using the low molecular weight solid modelling strategy.

Unfortunately, many of the thermodynamic models which have been successfully applied to polymer solutions, such as that by Flory and Huggins, will not accurately describe the behavior of supercritical systems due to lack of an explicit volume dependence of the free energy. As has been observed by Walsh and Dee [1987], and others, it is the volume, or equation of state, dependence that plays the major role in determining the phase diagram of polymer-gas mixtures at high pressure. Newer models, such as Flory's equation of state, while including a "free volume" dependence, are cell models, and as such, will not accurately describe the high compressibility of gases in the supercritical state [Liu and Prausnitz, 1980]. There is therefore a need to develop a model which will properly describe the thermodynamic behavior of both gases and polymers and mixtures thereof.

The glass transition of polymer-gas systems has received even less attention than has the phase behavior. One reason for this is that it is extremely difficult to measure the T_g of a gas-polymer mixture under pressure. Thus, use of models which require one or more adjustable parameters (and thus fitting to significant amounts of data) to calculate the T_g of a mixture would therefore be less than adequate for such systems. Likewise, because the T_g of such mixtures is affected by both gas concentration and pressure, a suitable model must also contain the proper pressure dependence. Knowledge of the course of the T_g -P curve of a polymer-gas mixture is important because the mass transfer rate of dilute systems and the potential processibility of concentrated mixtures are both related to the state of the polymer, glassy or rubbery, at the process temperature and pressure.

1.3 Scope of this Work

The goals of this research are the following:

1. Add to the fundamental data base of polymer solubility in supercritical gases.
2. Demonstrate the ability to reliably *predict* the phase behavior of supercritical gas-polymer mixtures.
3. For the first time, *predict* the glass transition temperature of a gas-polymer mixture at high pressure.

Three polymer-gas systems have been examined; polystyrene-CO₂, poly(methyl methacrylate)-CO₂, and polycarbonate-CO₂. Polystyrene was chosen because some solubility data is available in the literature to use as a guide. Poly(methyl methacrylate) and polycarbonate were chosen to attempt to take advantage

of chemical similarities between CO₂ and solute to maximize solubility. Initial results on the polycarbonate-CO₂ system showed that the gas had induced crystallization in the polymer rather than dissolve it. Further investigation on this system was therefore directed towards this crystallization process. Carbon dioxide was chosen as the solvent because it is non-toxic, non-flammable, and has a readily accessible critical region.

Literally hundreds of thermodynamic models are described in the literature of the past 15 years alone. Because of their past successes in the modelling of polymer solution data, the emphasis here has been directed towards lattice models. The effect of changes in volume on the phase diagram is represented by changes in the number of vacancies, or holes, which, along with the molecules, are postulated to occupy the lattice sites. After an extensive computer modelling comparison, the Mean Field Lattice Gas model of Kleintjens and Koningsveld [Kleintjens, 1979] was chosen to model the systems of interest. Modelling was directed towards the PS-CO₂ and the PMMA-CO₂ mixtures, as well as the PS-SO₂ system, for which some literature data exists.

In Chapter 2 the performance of various lattice models is compared using the description of the pVT behavior of the constituents of interest, *i.e.*, supercritical gases and polymers, as a benchmark. In Chapter 3 an attempt is made to redefine two of the heretofore empirical parameters in the MFLG model in terms of fundamental constants. Chapter 4 contains the modelling of the sorption of supercritical CO₂ by PMMA and PS and subsequent predictions of the solubility of these polymers in the gas versus data. Chapters 5 and 6 contain the procedure developed for predicting the T_g of polymer-supercritical gas mixtures.

Table 1.1

Critical Constants of Some Common Gases
 [Randall, 1982; Smith and Van Ness, 1975]

Gas	Critical Temperature (C)	Critical Pressure (atm.)	Critical Volume (cc/mole)
Carbon Dioxide	31.1	72.8	94.0
Ammonia	132.5	111.3	72.5
Methane	-82.6	45.4	99.0
Ethane	32.3	48.2	148.0
Propane	96.7	41.9	203.0
Butane	152.1	37.5	255.0
Ethylene	9.3	49.7	129.0
Nitrogen	-147.0	33.5	89.5
Nitrous Oxide	36.5	71.5	97.4
Sulfur Dioxide	157.7	77.8	122.0
Sulfur Hexafluoride	45.5	37.1	—
Trifluoromethane	25.6	47.7	—
1,1 Difluoroethane	113.5	46.9	—
Argon	-122.4	48.1	74.9
Xenon	16.6	57.6	118.0

CHAPTER 2

Modelling Pure Component Data I: A Comparison of Lattice Equations of State

Literally hundreds of equations of state have been developed over the past 15 years [Reid, 1983]. Whereas many of these equations have been shown to effectively describe low molecular weight liquid-liquid and liquid-gas phase separation behavior, a large portion of these models fail when a polymer is one of the constituents of the mixture due to lack of an explicit molecular weight dependence and increasing error as density increases. By contrast, lattice models, many of which were designed for the description of polymer solution behavior, can be successfully extended for use with gases and low molecular weight liquids. Thus this work concentrates on the evaluation of lattice models for the description of polymer and gas pVT behavior and the phase separation of mixtures thereof.

In Sections 2.1 and 2.2, a number of commonly used lattice equations of state are compared. In Section 2.3 the performance of five of these models is evaluated via fitting to pVT data of CO₂, SO₂, CF₃H, and polystyrene (PS). Section 2.4 contains a discussion of comparisons of the MFLG model with equations of state commonly used by chemical engineers. Section 2.5 concludes with a summary of the results presented in Chapter 2.

2.1 Mean Field Lattice Models Which Include the Effect of Segmental Surface Areas

The Flory-Huggins expression is, without a doubt, the most commonly used model for the description of the phase separation behavior of polymer solutions. Such a model cannot, however, be applied to polymer-gas mixtures without significant modification [Liau and McHugh, 1985; Maloney and Prausnitz, 1976]. The Flory-Huggins model contains no means by which to account for the effect of changes in volume (and consequently changes in pressure) on the free energy. The volume change on mixing, ΔV_m is assumed to be zero in the Flory-Huggins model which results in the situation that the Gibbs and Helmholtz free energies are equivalent. This approximation is adequate for the description of UCST-type phase separation behavior at low pressures, but, because LCST-type phase separation is a strong function of ΔV_m [Patterson, 1968], the Flory-Huggins model will not predict an LCST without empirical modification of the interaction parameter. In addition, contrary to experiment [Zeman, *et al.*, 1972; Zeman and Patterson, 1972], pressure plays no role in the determination of the phase diagram in the Flory-Huggins model. Finally, the Flory-Huggins interaction parameter is almost always found to vary with concentration, further limiting the predictive power of the model.

The effect of changes in volume and, consequently, pressure on the free energy can be modelled using one of two general strategies; that of the cell approach [Prigogine, 1957; Flory, *et al.*, 1964], and that of the lattice gas formulation. Whereas both methods have been shown to produce good descriptions of the effect of pressure on the phase diagrams of polymer mixtures the lattice gas method has been shown to provide a better representation of both pure component pVT data [McMaster, 1973; Nies, *et al.*, 1983], and the sorption of gases by

polymers [Liu and Prausnitz, 1980], in the vicinity of the solvent critical point. As will be seen in Chapter 4, accurate descriptions of gas sorption by polymers in this regime will be required to insure good predictions of polymer solubility in supercritical gases at high pressures. Therefore, this work will concentrate on the use of a lattice gas model to predict the phase behavior of polymer-gas mixtures.

The lattice gas approach, which has been in use since the 1920's [Schottky, 1929], is one in which vacant sites, or holes, are introduced into the lattice. Thus a pure component is assumed to be a pseudo-binary mixture, and changes in volume with pressure or temperature are modelled by changes in the concentration of the holes in the system. In the first approximation, the distribution of holes on the lattice is assumed to be random.

The other major drawback to the Flory-Huggins model mentioned above, that of the apparent concentration dependence of the interaction parameter, can be at least partially explained via the introduction of the concept of segmental contact surface areas during the formulation of the internal energy of mixing of holes and segments [Staverman, 1937]. Segments and holes are permitted distinct coordination numbers, z_{ii} , which are assumed to be proportional to their respective surface areas. Therefore, the total number of nearest neighbor contacts of a segment or hole, $2P_{ii} + P_{ij}$, is proportional to the contact surface area, σ_i :

$$2P_{11} + P_{10} = n_1 m_1 z_{11} = n_1 m_1 k \sigma_1 \quad (2-1)$$

$$2P_{00} + P_{01} = n_0 z_{00} = n_0 k \sigma_0 \quad (2-2)$$

where the n_i and m_i are the number of moles and number of lattice sites per molecule, respectively, of the segments and holes (holes are assumed to occupy

1 site each). The proportionality constant, k , is set to one in the first approximation and thus the ratio of the coordination numbers equals the surface area ratio. This approach is similar in concept to that used to construct decorated lattice models [Mermin, 1971; Fisher, 1968]. The lattice here has become an abstraction rather than a rigid construction with a mean coordination number, \bar{z} , which varies with hole concentration:

$$\bar{z} = \frac{\sum P_{ij}}{\sum n_i m_i} = z_{00}(1 - \gamma_1 \phi_1) = \sigma_0(1 - \gamma_1 \phi_1) \quad (2-3)$$

where $\gamma_1 = 1 - z_{11}/z_{00} = 1 - \sigma_1/\sigma_0$ and ϕ_1 is the volume fraction of the segments. The change in the internal energy upon mixing holes and segments, ΔU , is assumed to be equal to the change in the number of the various contact pairs on mixing, multiplied by their respective interaction energies:

$$\Delta U = \Delta P_{11}w_{11} + \Delta P_{10}w_{10} + \Delta P_{01}w_{01} + \Delta P_{00}w_{00} \quad (2-4)$$

which reduces to:

$$\Delta U = \Delta P_{11}w_{11} \quad (2-5)$$

if it is assumed that contact with a hole involves zero interaction energy. The number of the (1-1) contacts is calculated using Regular Solution Theory (*i.e.*, a mean field approach) and surface fractions, Φ_i , instead of volume fractions, or:

$$\begin{aligned} \Delta P_{11} &= \frac{n_1 m_1 \sigma_1}{2} (\Delta \Phi_1) = \frac{n_1 m_1 \sigma_1}{2} (\Phi_1 - 1) = \frac{-n_1 m_1 \sigma_1}{2} \Phi_0 \\ &= -\frac{n_1 m_1 \sigma_1}{2} \left(\frac{n_0 \sigma_0}{n_0 \sigma_0 + n_1 m_1 \sigma_1} \right) = -\frac{N_\phi \sigma_0}{2} \left(\frac{\phi_0 \phi_1 (1 - \gamma_1)}{1 - \gamma_1 \phi_1} \right) \end{aligned} \quad (2-6)$$

where N_ϕ is the total number of lattice sites. Combining equations (2-5) and (2-6):

$$\frac{\Delta U}{N_\phi RT} = \phi_0 \phi_1 \left(\frac{(1 - \gamma_1)}{1 - \gamma_1 \phi_1} \right) \left(\frac{g_{11}}{T} \right) \quad (2 - 7)$$

where:

$$g_{11} = - \left(\frac{w_{11} \sigma_0}{2R} \right)$$

Note that the effective interaction parameter, $(\Delta U / \phi_0 \phi_1 N_\phi RT)$, is dependent upon concentration without the use of purely empirical parameters (Note: in the original derivation of the Mean Field Lattice Gas model by Kleintjens [1979], the interaction parameter g_{11} is defined as $(-w_{11} \sigma_1 / 2R)$. This combines the factor $(1 - \gamma)$ from equation (2-7) with g_{11} yet does not affect the essential structure of the model.). If the change in the entropy on mixing holes and segments is assumed to follow the simple Flory-Huggins-Staverman expression, the Helmholtz free energy of mixing, ΔA , becomes:

$$\frac{\Delta A}{N_\phi RT} = \phi_0 \ln \phi_0 + \frac{\phi_1}{m_1} \ln \phi_1 + \frac{\phi_0 \phi_1 (1 - \gamma_1)}{1 - \gamma_1 \phi_1} \left(\frac{g_{11}}{T} \right) \quad (2 - 8)$$

Equation (2-8) is essentially the free energy expression derived by Kanig [1963] and will henceforth be referred to as the Kanig model.

During modelling of various gas-gas, gas-liquid, and polymer-liquid systems, Kleintjens and Koningsveld [Kleintjens, 1979; Kleintjens and Koningsveld, 1980; 1982] found that addition of two empirical parameters, α_1 and g_{10} , to equation (2-8) greatly improved the model description of the pVT behavior of gases and low molecular weight liquids. The free energy expression of this Mean Field Lattice Gas (MFLG) model is as follows:

$$\begin{aligned} \frac{\Delta A}{N_{\phi}RT} = & \phi_0 \ln \phi_0 + \frac{\phi_1}{m_1} \ln \phi_1 \\ & + \phi_0 \phi_1 \left(\alpha_1 + \left(\frac{(1 - \gamma_1)(g_{10} + g_{11}/T)}{(1 - \gamma_1 \phi_1)} \right) \right) \end{aligned} \quad (2-9)$$

The need for these empirical parameters was initially assumed to be due to deviations from the simple entropy of mixing expression used in the construction of the model. Possible molecular significance of α_1 and g_{10} will be discussed in later sections. Clearly, the Kanig model is a specific case ($\alpha_1, g_{10} = 0$) of the MFLG model.

The equation of state (EoS) is derived from the free energy (equation (2-9)) in the usual way, as shown below.

$$-p = \left(\frac{\partial A}{\partial V} \right)_T = \frac{1}{v_0} \left(\frac{\partial \Delta A}{\partial n_0} \right)_T \quad (2-10)$$

therefore:

$$\begin{aligned} \frac{-pv_0}{RT} = & \ln \phi_0 + \phi_1 \left(1 - \frac{1}{m_1} \right) \\ & + \phi_1^2 \left(\alpha_1 + \frac{(g_{10} + g_{11}/T)(1 - \gamma_1)^2}{Q} \right) \end{aligned} \quad (2-11)$$

where $Q = 1 - \gamma_1 \phi_1$. As mentioned above, the Kanig EoS is derived from equation (2-11) by setting g_{10} and α_1 to zero. In addition, the EoS of Panayioutou and Vera [1982b] is also a specific case of equation (2-11), that where α_1 alone vanishes. Whereas in the MFLG model γ_1 is considered to be an adjustable parameter, Panayioutou calculated γ_1 using Bondi's [1968] group contribution values.

Although the equation of state is sufficient to define the pVT behavior of high polymers, additional constraints, such as equations defining vapor-liquid equilibrium (VLE) and the gas-liquid critical point, are required to completely describe the behavior of gases and low molecular weight liquids. Vapor-liquid equilibrium is defined by equating the chemical potential of the segments and the holes (the latter is the same as equating the pressure) in the saturated liquid and vapor phases:

$$\mu_i^V = \mu_i^L; \quad \mu_i = \left(\frac{\partial \Delta A}{\partial n_i} \right)_{T, n_j}; \quad i = 0, 1 \quad (2-12)$$

Following the analysis of Kleintjens [1979], the critical condition for the MFLG model is expressed via equations (2-13) and (2-14):

$$\left(\frac{\partial^2 \Delta A}{\partial \phi_1^2} \right)_{T, V} = 0 \quad (2-13)$$

$$\left(\frac{\partial^3 \Delta A}{\partial \phi_1^3} \right)_{T, V} = 0 \quad (2-14)$$

The complete set of equations resulting from combinations of equations (2-9) and (2-12) – (2-14) can be found in [Kleintjens, 1979].

In both the MFLG and the Panayioutou-Vera models the volume per lattice site, v_0 , is fixed for all substances. Frenkel [1946] has asserted that v_0 for lattice models should approximate the size of small atoms and, as such, lie between 10 and 25 cc/mole. Panayioutou and Vera [1982b] used a value of 9.75, found by optimizing the fit of the equation of state to polystyrene pVT data; for the MFLG v_0 is presumed to be a scaling parameter and is initially set to 25 cc/mole for all substances. The effect of the value of v_0 on the quality of the model description will be examined in Section 2.3. Unlike the MFLG and

Panayioutou-Vera models, Kanig assumed that the volume per lattice site of the holes is fixed whereas that of the segments is temperature dependent, due to vibrations and rotations of the segments. This approach is similar to the cell-hole models of Arai and Saito [1972] and Simha and coworkers [Simha and Somcynsky, 1969; Nanda, *et al.*, 1966]. Despite the postulation of a cell-hole model, Kanig does not specify what the temperature dependence of the segment volume should be and therefore v_0 was held constant for the Kanig model during subsequent computer modelling. The effect of a temperature dependent m_1 (and consequently γ_1) on the performance of the lattice gas model will be examined in Chapter 5.

2.2 Comparison of MFLG and Rigid Lattice Models

As shown in Section 2.1, both the Kanig and Panayioutou-Vera equations of state are specific cases of the MFLG EoS. In this section, structural comparisons will be made between *rigid* lattice models and the MFLG. The term "rigid lattice" refers to those models which do not include the effect of segmental surface areas on the free energy and as such are constructed using a lattice with universal coordination number z . The internal energy of the system is assumed to be proportional to the number of non-bonded contacts per chain molecule, qz , and the "contact fraction", θ_1 , of segment-segment contacts:

$$U = \frac{n_1(qz)}{2} \theta_1 \epsilon_{11} = \frac{n_1(qz)}{2} \left(\frac{n_1(qz)}{z(n_0 + qn_1)} \right) \epsilon_{11} \quad (2-15)$$

where:

$$qz = (z - 2)m_1 + 2$$

and ϵ_{11} is the segment-segment interaction parameter. Note the similarity between equations (2-15) and (2-5)-(2-6). A partition function is constructed using

the energetic term from equation (2-15) and either the Guggenheim-Huggins-Miller [Guggenheim, 1952] or the Staverman [1950] approximation for the combinatorial term (use of either combinatorial expression leads to the same result in the equation of state [Sayegh and Vera, 1980]). Using the standard procedure, the sum over all states is approximated by the maximum term of the series, which is found by differentiation with respect to the number of holes. The resulting free energy expression can be shown to resemble that of the MFLG model with the quantity $\frac{z}{2}Q^* \ln Q^*$ in the place of $\phi_0\phi_1\alpha_1$, where:

$$Q^* = 1 - \left(\frac{2}{z} \left(1 - \frac{1}{m_1} \right) \phi_1 \right) \quad (2-16)$$

The equation of state is derived in the usual way:

$$-p = \left(\frac{\partial \ln \tilde{Z}}{\partial V} \right)_{T, n_1} \quad (2-17)$$

where \tilde{Z} is the maximum term of the partition function. The resulting equation of state for the rigid lattice model is therefore:

$$\frac{\tilde{P}}{\tilde{T}} = \ln \left(\frac{\tilde{V}}{\tilde{V} - 1} \right) + \frac{z}{2} \ln \left(\frac{\tilde{V} + q/m_1 - 1}{\tilde{V}} \right) - \frac{\Theta^2}{\tilde{T}} \quad (2-18)$$

where:

$$\tilde{P} = \frac{p}{P^*} = \frac{2v_0 p}{z\epsilon_{11}}$$

$$\tilde{T} = \frac{T}{T^*} = \frac{2RT}{z\epsilon_{11}}$$

The reduced volume is defined such that it equals the reciprocal of the segment fraction, $1/\phi_1$. The first term on the right-hand-side of equation (2-18) therefore equals $-\ln \phi_0$. Algebraic rearrangement of the second term, followed by expansion of the logarithm as a series, leads to:

$$\begin{aligned} \frac{z}{2} \ln \left(\frac{\tilde{V} + q/m_1 - 1}{\tilde{V}} \right) &= \phi_1 \left(\frac{1}{m_1} - 1 \right) - \frac{\phi_1^2}{z} \left(\frac{1}{m_1} - 1 \right)^2 \\ &+ \frac{4\phi_1^3}{3z^2} \left(\frac{1}{m_1} - 1 \right)^3 + \dots \end{aligned} \quad (2-19)$$

The term Θ^2 , which is defined as:

$$\Theta^2 = \left(\frac{qn_1}{qn_1 + n_0} \right)^2 \quad (2-20)$$

can easily be transformed to:

$$\left(\frac{qn_1}{qn_1 + n_0} \right)^2 = \frac{\phi_1^2 (q/m_1)^2}{(1 - \phi_1(1 - q/m_1))^2} \quad (2-21)$$

Thus the rigid lattice equation of state has the same general form as that for the MFLG model, yet displays two significant differences. The quantities which mirror the effect of the MFLG adjustable parameters γ_1 and α_1 are functions of z and m_1 in the rigid lattice formulation:

$$\gamma_{rigid} = \frac{2}{z} \left(1 - \frac{1}{m_1} \right) \quad (2-22)$$

$$\begin{aligned} -\alpha_{rigid} &= \frac{1}{z} \left(1 - \frac{1}{m_1} \right)^2 - \frac{4\phi_1}{3z^2} \left(1 - \frac{1}{m_1} \right)^3 \\ &+ \frac{2\phi_1^2}{z^3} \left(1 - \frac{1}{m_1} \right)^4 + \dots \end{aligned} \quad (2-23)$$

Given a lattice coordination number of approximately 10, the values of α_{rigid} and γ_{rigid} for polymers in the rigid lattice will tend universally towards .1 and

.2, respectively, and both parameters will approach zero for small molecules. As will be shown in a later section, the rigid lattice description as represented by equations (2-22) and (2-23) is too restrictive to allow for a good fit to both polymer and gaseous pVT data. This conclusion is also supported by the results of Costas, *et al.*, [1981], who did not introduce the concept of surfaces, but found it necessary to treat the quantity $\frac{2}{z}(1 - \frac{1}{m_1})$ as a material parameter to obtain a good description of pVT data. The rigid lattice model has been applied with $g_{10} = 0$, as by Gibbs and DiMarzio [1958], and Okada and Nose [1981], or with g_{10} non-zero, as by Panayioutou and Vera [1982], Kumar, *et al.*, [1987], or Kilian [1974]. The origin of equation (2-23) lends support to the hypothesis that the MFLG parameter α_1 arises due to deviations from the Flory-Huggins entropy of mixing expression.

Interestingly, if in the case of the MFLG ($\alpha_1 \rightarrow 0$, $\gamma_1 \rightarrow 0$, $g_{10} \rightarrow 0$), or in the case of the rigid model ($z \rightarrow \infty$), the equation of state is transformed to the lattice gas EoS by Trappeniers and coworkers [Trappeniers, *et al.*, 1970; Schouten, *et al.*, 1974]. Furthermore, if the volume per lattice site, v_0 , is designated a material parameter rather than a universal constant, the Trappeniers EoS is then transformed to the Sanchez-Lacombe equation of state [Sanchez and Lacombe, 1976; 1977]. While the transformation requirement $z = \infty$ seems to make little intuitive sense, in the case of the MFLG the constraint ($\alpha \rightarrow 0$, $g_{10} \rightarrow 0$, $\gamma_1 \rightarrow 0$) simply means that the surface areas of the holes and segments are equal, and as such cancel in expressions for the entropy or internal energy of mixing.

Table 2.1 summarizes the relationship of the various models mentioned in Sections 2.1 and 2.2 to the MFLG equation of state. In the next sections, the performance of several of these models will be compared to that of the MFLG in the description of the pVT behavior of polystyrene and of three gases which

will later be considered as supercritical solvents; carbon dioxide (CO_2), sulfur dioxide (SO_2), and fluoroform (CF_3H).

Table 2.1
Comparison of MFLG and other
Lattice Equations of State

Models	<u>Rigid</u> Lattice Models			
	v_0	γ_1	α_1	g_{10}
Panayioutou & Vera (1982a) [†]	Fixed	Non-zero	Non-zero	Non-zero
Gibbs & DiMarzio [†]	Fixed	Non-zero	Non-zero	0
Okada & Nose [†]	Fixed	Non-zero	Non-zero	0
Kilian	Fixed	0	0	Non-zero
Sanchez	Floating	0	0	0
Trappeniers	Fixed	0	0	0
	<u>Non-Rigid</u> Lattice Models			
MFLG	Fixed	Non-zero	Non-zero	Non-zero
Panayioutou & Vera (1982b) [*]	Fixed	Non-zero	0	Non-zero
Kanig	Fixed	Non-zero	0	0

[†] γ_1 and α_1 are tied to the number of segments per molecule and the lattice coordination number by equations (1-21) and (1-22).

^{*} γ_1 is derived from Bondi's group contribution values.

2.3 Modelling Results for Pure Components

In this section computer modelling is used to evaluate several of the models listed in Table 2.1. Throughout this section the term *MFLG* model will refer to the case where α_1 , g_{10} , and γ_1 are non-zero adjustable parameters; *Vera* model assumes $\alpha_1 = 0$, with g_{10} and γ_1 non-zero material constants; and the *Kanig* model uses a non-zero γ_1 and assumes $\alpha_1 = 0$ and $g_{10} = 0$. In each of these models, v_0 is set to 25 cc/mole and fixed. As can be seen, each of these three models is of the *non-rigid* variety. The rigid models are to be represented by the *Kilian* ($\alpha_1 = 0$ and $\gamma_1 = 0$) and the *Sanchez* equations ($\gamma_1 = 0$, $g_{10} = 0$, $\alpha_1 = 0$, and v_0 is an adjustable parameter). Because the three gases are small molecules, presumably with 1 segment per molecule, the rigid values for γ_1 and α_1 as represented by equations (2-22) and (2-23) should approach zero for these substances. Therefore the Kilian model is representative of the general class of rigid lattice models for the three gases. The Sanchez model is included to examine the effect of a floating v_0 on the quality of the model description of pVT behavior.

2.3.1 The Parameter Estimation Program (PEP)

Determination of the adjustable parameters for the various lattice models, as well as solution of the coupled equations needed to calculate VLE or critical behavior was carried out using the Parameter Estimation Program (PEP), developed at Dutch State Mines (DSM) Research (Geleen, Netherlands), and the University of Massachusetts Engineering Computer Center's DEC VAX cluster. The PEP finds the values of the parameters, λ_k , which are solutions to the minimization problem [Hillegers, 1986]:

Minimize:

$$\sum_{i=1}^n (x_i - x_i^{\circ})^T \Omega^{-1} (x_i - x_i^{\circ}) \quad (2-24)$$

subject to the constraints:

$$f_j(x_i, \lambda_k) = 0 \quad (2-25)$$

where the x_i are the calculated data points, the x_i° are the true values, and Ω is the error variance matrix. The constraints, f_j , are the appropriate equations (equation of state, VLE, critical point expressions) in the implicit form, as shown in equation (2-25). All variables are therefore assumed to have been measured with some error. The errors, or tolerances, which comprise Ω , are assumed to be random in nature and are set using suggested values from the literature. The errors can be assigned either absolute or relative (%) values. The best values for the parameters, therefore, are those which fit the surface represented by the constraints (equation 2-25) to the data x_i° such that the sum of the squares of the distance between x_i° 's and their projections onto the surface is minimal. The distances, $x_i - x_i^{\circ}$, are weighted by the corresponding tolerances. The problem is solved iteratively for the λ_k using a Gauss-Newton type of algorithm.

During the fitting of the models to the pVT data on the three gases, the tolerances were assigned the following values: temperatures, .25K absolute; densities and pressures, .5% relative. An exception is the critical point, where the temperature tolerance is lowered to .1K. In the fitting of the models to the polystyrene data, the temperature tolerances remain as above, the pressures were fixed, and the density tolerance lowered to .1% .

Because the PEP treats both parameters and data in fundamentally the same way (parameters are simply data with infinite tolerance), the PEP can be used to solve simultaneous equations (ie systems of n equations with n unknowns) quite easily. In this case the parameters and the independent variable are fixed. The tolerances for the dependent variable (or variables) are then set to infinity and the system iterated until all equations are solved (*i.e.* convergence). In this way the solution to a system of equations can be solved quickly for a list of the independent variable.

2.3.2 Fitting Results for CO₂, SO₂, CF₃H, and PS

2.3.2.1 CO₂

The models were fit to VLE [Perry and Chilton, 1973] and supercritical pVT data [Michels and Michels, 1936; Michels, *et al.*, 1936]. Average errors for the five models are shown in Table 2.2 and the quality of the various model descriptions is displayed graphically in Figures 2.1 – 2.4. The parameter values for the models are provided in Table 2.3.

The usefulness of the segmental surface area concept is made readily apparent by comparing the results for the Vera model with those for the Kilian model. A non-zero γ_1 provides a significantly better “concentration” (here this translates to density dependence of pressure) dependence of the effective interaction parameter, as evidenced by the superiority of the Vera model description of the supercritical isotherms (Figures 2.3 and 2.4). Interestingly, the floating v_0 employed by the Sanchez model partially compensates for the lack of a surface dependence in the free energy (compare Sanchez to Kanig to Vera models). However, the optimum value of v_0 for the Sanchez model is unrealistically small

(smaller than a hydrogen atom) which leads to the odd conclusion that CO_2 , in the context of the Sanchez model, comprises nearly 8 segments (Table 2.3).

The mean field concept, which is the basis for the construction of the lattice models under consideration, is, of course, only an approximation. Non-mean field behavior, which is certainly present to some degree in all substances, can take three forms. One is the presence of specific interactions, such as hydrogen bonding, which can probably be discounted in the case of the three gases under study here. Second, segment density fluctuations due to the connectivity of the segments in chain molecules will affect the shape of the VLE curve. Since this non-mean field contribution vanishes when the number of segments drops to unity, this effect can also be discounted in discussions of the behavior of the three gases. Finally, there are those segment density fluctuations which occur near the critical point. These, of course, cannot be ignored in discussions of the quality of the description of a lattice model since the critical point determines two of the five constraining equations for the system. From the results for CO_2 , it appears that the g_{10} parameter, and to a lesser degree α_1 , compensate for the lack of an explicit dependence of the critical conditions on segment density fluctuations in the lattice model (compare the critical point error of MFLG to Vera to Kanig model in Table 2.2).

In addition to a role in the compensation for the fluctuations near the critical point, the α_1 parameter also appears to play a role in fine tuning the ϕ_0 dependence of the model at high densities (compare critical and saturated liquid densities of Vera and MFLG models). This is consistent with the hypothesis that α_1 arises due to deviations from the Flory-Huggins entropy of mixing expression, and as such contains a ϕ_0 dependence as shown by equation (2-23). This hypothesis will be explored in greater detail in Chapter 3.

With the exception of the Sanchez model, the value of v_0 was fixed at 25 cc/mole during the fitting of the lattice equations of state. In order to evaluate the importance of the value of v_0 to the quality of the models' descriptions v_0 was varied between 10 and 30 (the prescribed limits by Frenkel) and the total error (χ^2) noted. The value of v_0 displayed a minimal effect on the accuracy of the MFLG model with an increasing dependence as the number of parameters was lowered from five (MFLG) to three (Kanig, Kilian).

In terms of overall accuracy, the MFLG and Vera models are clearly superior in their descriptions of the pVT data of CO₂. The inclusion of a non-zero α_1 parameter by the MFLG model, though displaying little effect on the supercritical pVT data, provides some improvement over the Vera model in the description of the VLE and critical point data.

Table 2.2

Average Errors in Fitting Lattice Equations of State
to pVT Data on CO₂

Model	Number of of Points	Temp. (K)	<u>VLE Data</u>		
			Vapor Pressure-%	Vapor Density-%	Liquid Density-%
MFLG	15	.6	1.2	.5	2.3
Vera	15	.9	1.5	1.7	3.6
Kanig	15	12.5	8.2	14.2	17.9
Kilian	15	2.5	7.0	4.6	9.5
Sanchez	15	1.2	5.4	4.5	2.7

Model	<u>Critical Point</u>			Number of Points	<u>Equation of State</u>		
	Temp. (K)	Press. %	Dens. %		Press. %	Temp. (K)	Dens. %
MFLG	1.7	.1	7.7	66	1.0	-	4.9
Vera	2.4	.6	13.6	66	.9	-	4.2
Kanig	12.3	1.3	23.7	66	3.4	-	10.7
Kilian	11.1	27.1	3.1	66	4.0	-	13.6
Sanchez	6.7	15.3	12.1	66	2.6	-	9.2

Table 2.3

Lattice Model Parameters for CO₂ Determined by
Parameter Estimation Program (PEP)

Model	v_0	m_1	α_1	g_{10}	g_{11}	γ_1
MFLG	25.0	1.31	.91499	-1.1446	519.82	-1.2010
Vera	25.0	1.28	0	-1.1160	725.30	-.67302
Kanig	25.0	1.48	0	0	393.35	-.49967
Kilian	25.0	1.70	0	-1.3241	909.97	0
Sanchez	3.7081	7.62	0	0	288.4	0

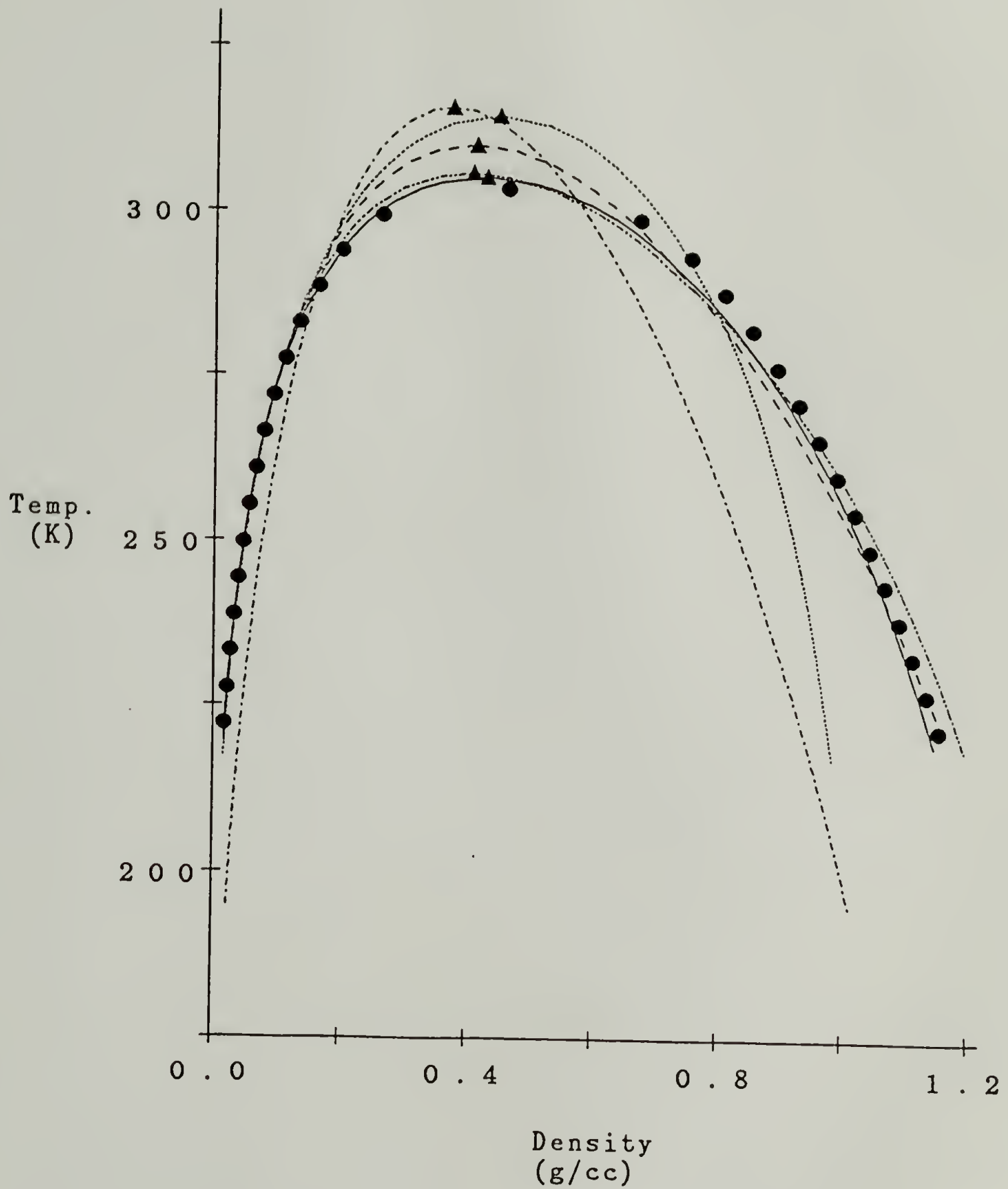


Figure 2.1

VLE data for CO_2 (\bullet) and lattice model calculations; MFLG ($—$), Vera ($\cdots\cdots$), Kanig ($-\cdots-$), Kilian ($\cdot\cdots\cdot$), and Sanchez ($- - -$). \blacktriangle 's are calculated critical points.

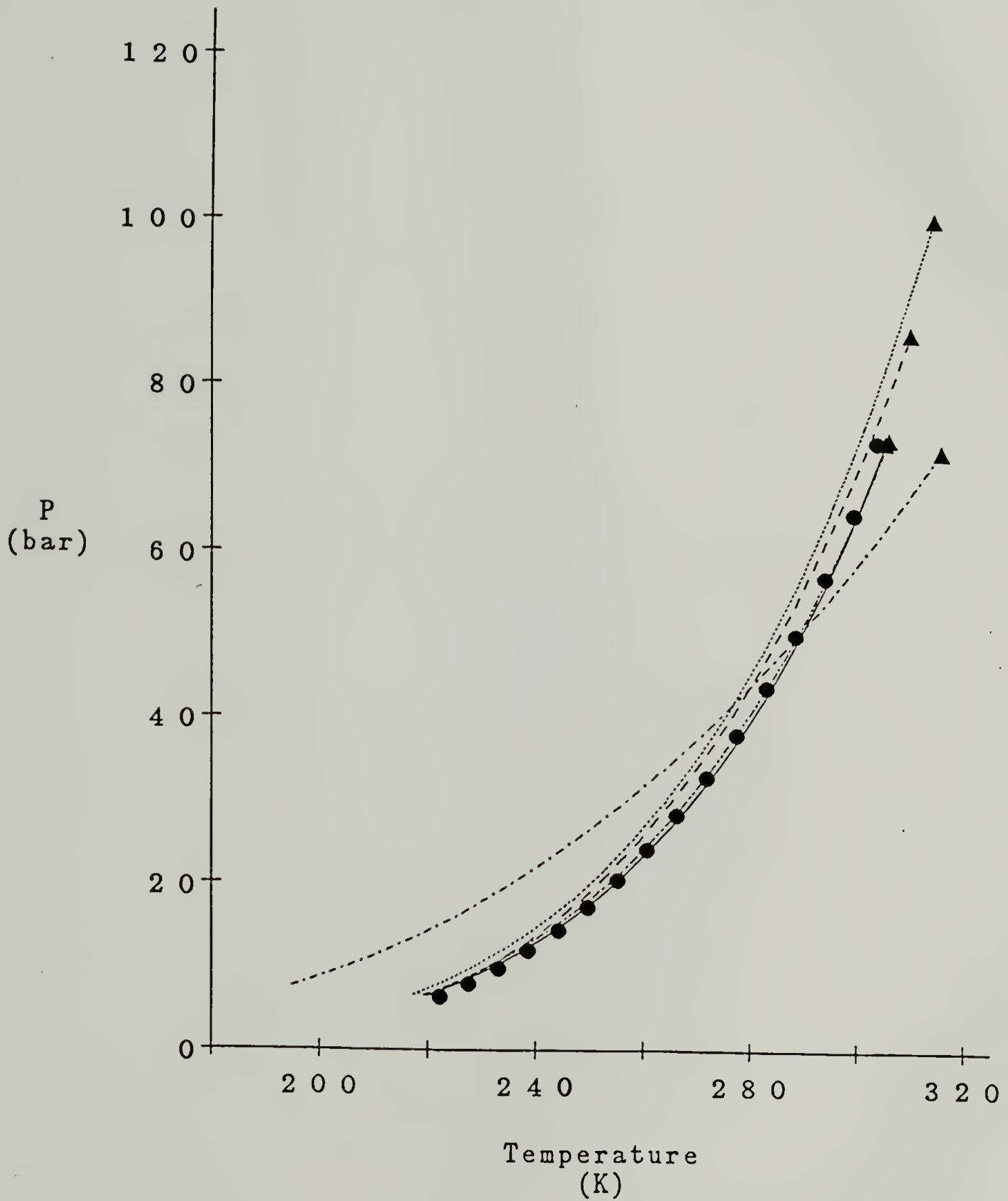


Figure 2.2

CO₂ vapor pressure as a function of temperature and lattice model calculations; symbols same as in Figure 2.1.

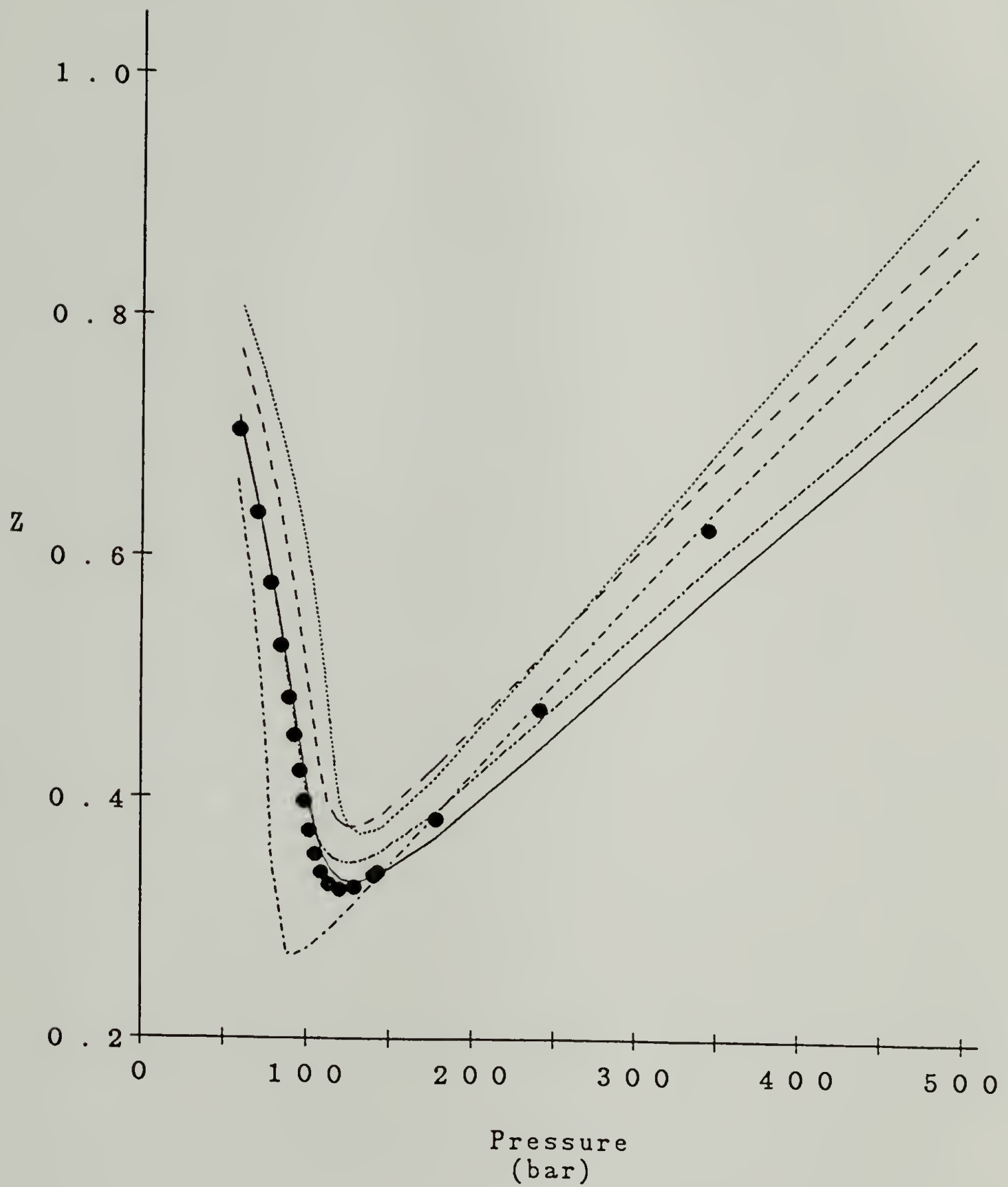


Figure 2.3

CO₂ compressibility ($Z = PV/RT$) versus pressure at $T = 323K$ and lattice model calculations; symbols same as in Figure 2.1.

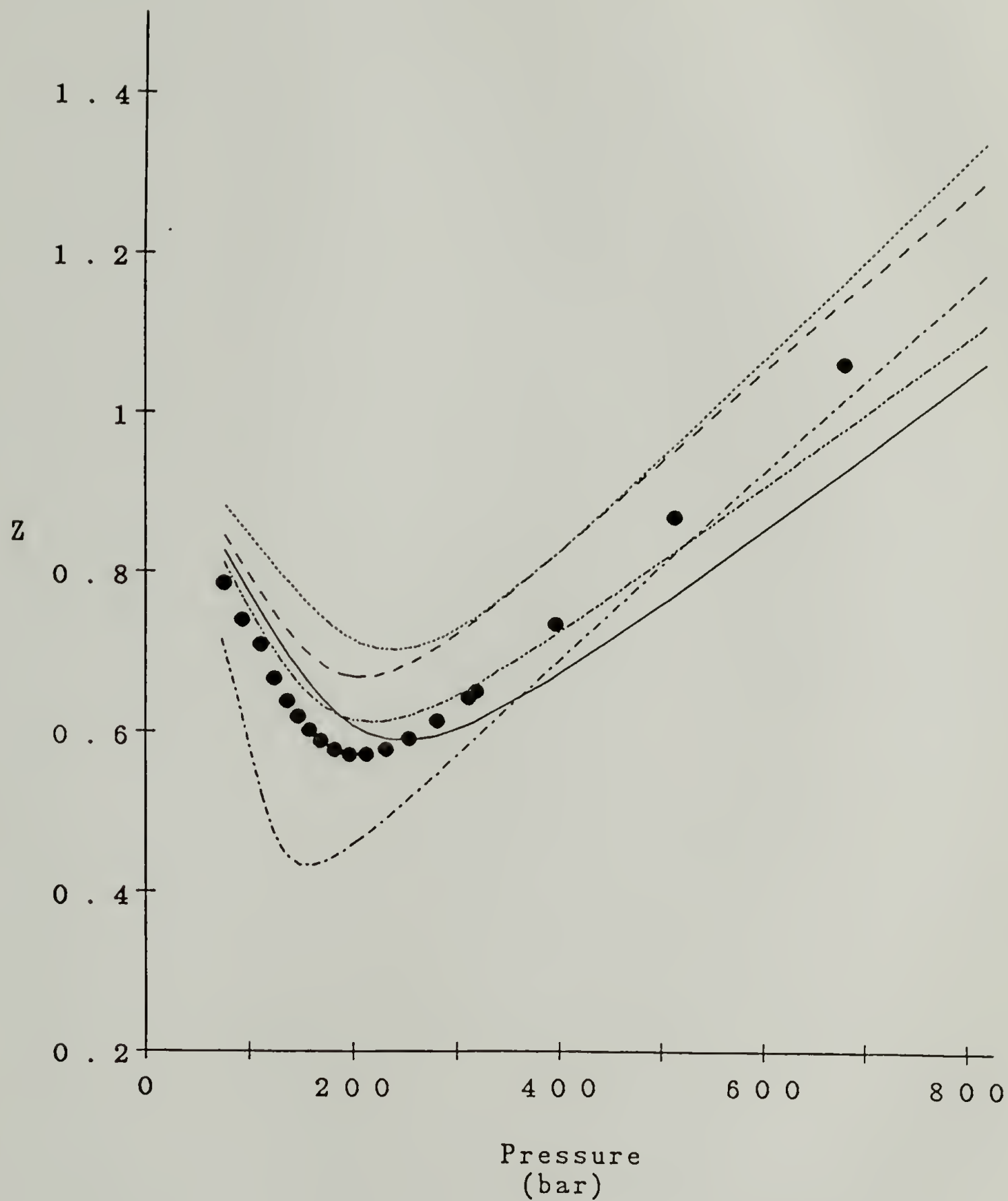


Figure 2.4

CO₂ compressibility ($Z = PV/RT$) versus pressure at $T = 372K$ and lattice model calculations; symbols same as in Figure 2.1.

2.3.2.2 SO₂ and CF₃H

The models were fit to literature VLE and pVT data for SO₂ [Perry and Chilton, 1973; Kang, *et al.*, 1961] and CF₃H [Perry and Chilton, 1973; Hou and Martin, 1959]. Results are shown in Tables 2.4 and 2.5 and Figures 2.5 – 2.8 for SO₂, and Tables 2.6 – 2.7 and Figures 2.9 – 2.12 for CF₃H. The trends for these two gases are essentially the same as reported for CO₂. They can be summarized as follows:

1. The surface contribution (non-zero γ_1) is needed to obtain the proper dependence of pressure on density (compare Kilian and Vera model results).
2. The non-zero g_{10} helps to compensate for the lack of an explicit reference to density fluctuations near the critical point (compare Kanig and Vera critical point results).
3. The non-zero α_1 parameter also contributes to increased accuracy near the critical point and also helps to fine tune the dependence of the equation of state on ϕ_0 at high densities.

The MFLG, Vera, and Kanig equations of state are examples of non-rigid lattice models whereas the Kilian and Sanchez are of the rigid variety, albeit with effectively infinite values of the lattice coordination number. However, because the compounds here are gases which comprise approximately 1 segment each on the lattice, the rigid values of γ_1 and α_1 , as represented by equations (2-23) and (2-24), approach zero even for rigid lattice models with less-than-infinite coordination numbers. Thus the behavior of the entire class of rigid lattice models can be represented by the performance of the Kilian model for the three gases under consideration. As can be seen by the modelling results, the rigid lattice models produce an inferior description of the pVT behavior of low molecular weight gases.

Table 2.4

Average Errors in Fitting Lattice Equations of State
to pVT Data on SO₂

VLE Data

Model	Number of of Points	Temp. (K)	Vapor Pressure-%	Vapor Density-%	Liquid Density-%
MFLG	19	2.4	1.7	2.1	2.4
Vera	19	1.9	.7	2.6	4.9
Kanig	19	21.7	12.4	22.1	46.8
Kilian	19	1.5	4.6	3.7	10.7
Sanchez	19	1.0	3.6	2.6	3.2

Critical PointEquation of State

Model	Temp. (K)	Press. %	Dens. %	Number of Points	Press. %	Temp. (K)	Dens. %
MFLG	.9	.4	9.4	32	—	.7	3.4
Vera	2.2	1.8	14.8	32	—	.7	3.3
Kanig	28.5	7.8	35.1	32	—	1.4	10.8
Kilian	12.4	29.8	.3	32	—	2.8	13.2
Sanchez	7.9	16.2	12.9	32	—	1.7	8.9

Table 2.5

Lattice Model Parameters for SO₂ Determined by
Parameter Estimation Program (PEP)

Model	v_0	m_1	α_1	g_{10}	g_{11}	γ_1
MFLG	25.0	1.57	.80814	-1.1162	695.77	-1.2619
Vera	25.0	1.55	0	-1.1480	968.10	-.71102
Kanig	25.0	2.54	0	0	604.83	-.006158
Kilian	25.0	2.03	0	-1.4446	1281.5	0
Sanchez	4.0538	8.66	0	0	393.56	0

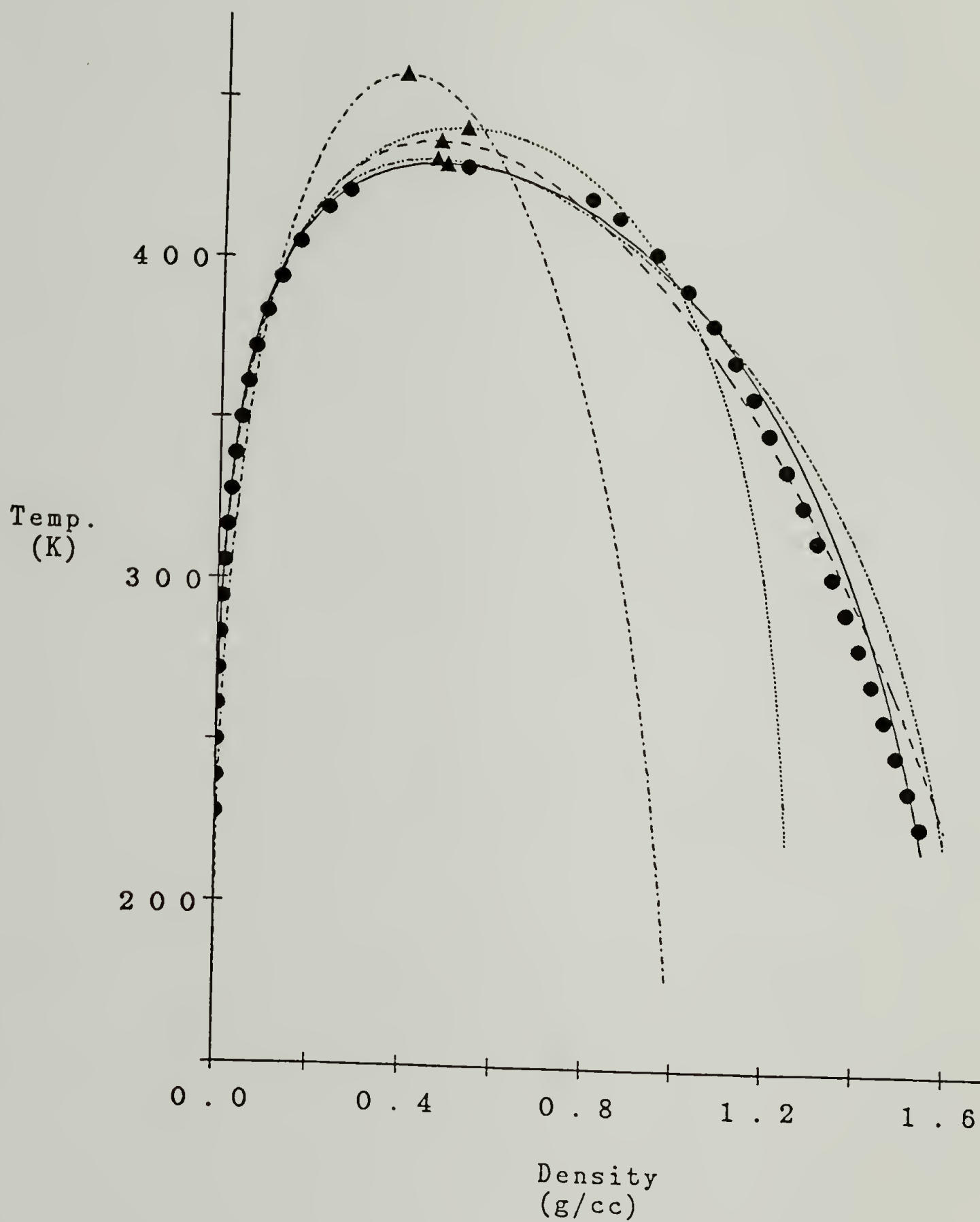


Figure 2.5

SO₂ VLE data (●) and lattice model calculations; MFLG (—), Vera (·-·-·-), Kanig (-·-·-), Kilian (·-·-·), and Sanchez (- - -). ▲'s are calculated critical points.

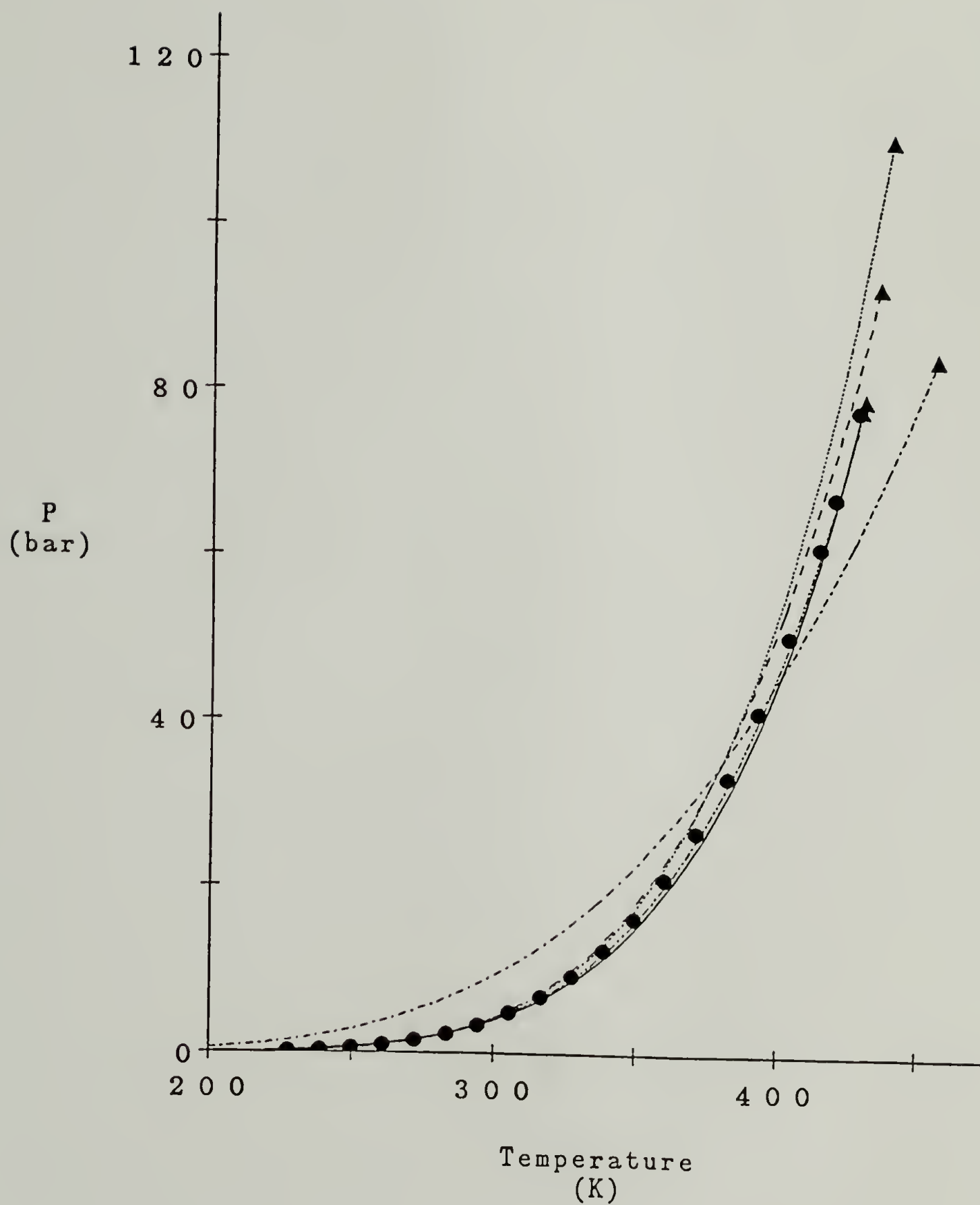


Figure 2.6

SO₂ vapor pressure as a function of temperature and lattice model calculations; symbols same as in Figure 2.5.

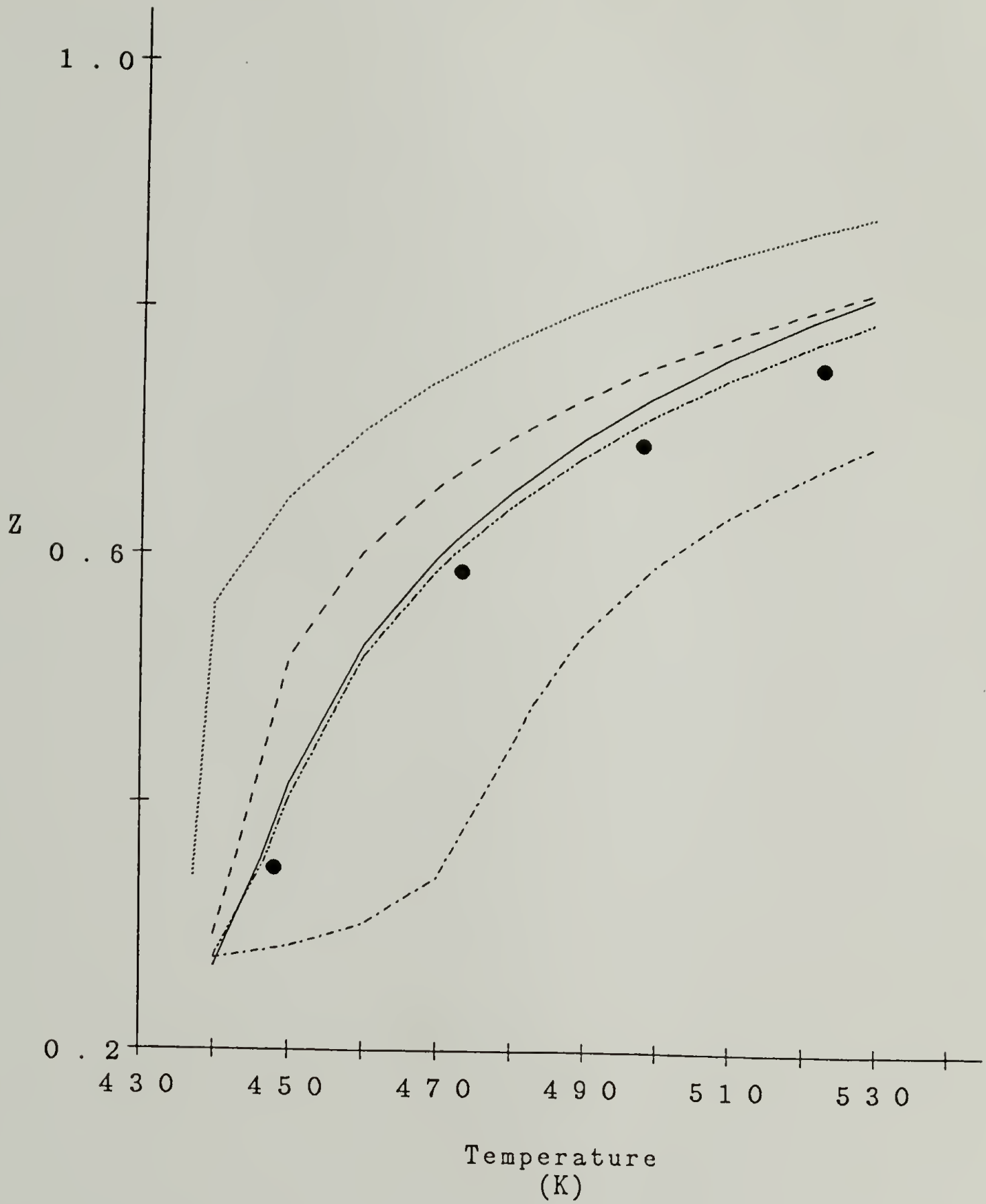


Figure 2.7

SO_2 compressibility ($Z = PV/RT$) versus temperature at $P = 101.3$ bar and lattice model calculations; symbols same as in Figure 2.5.

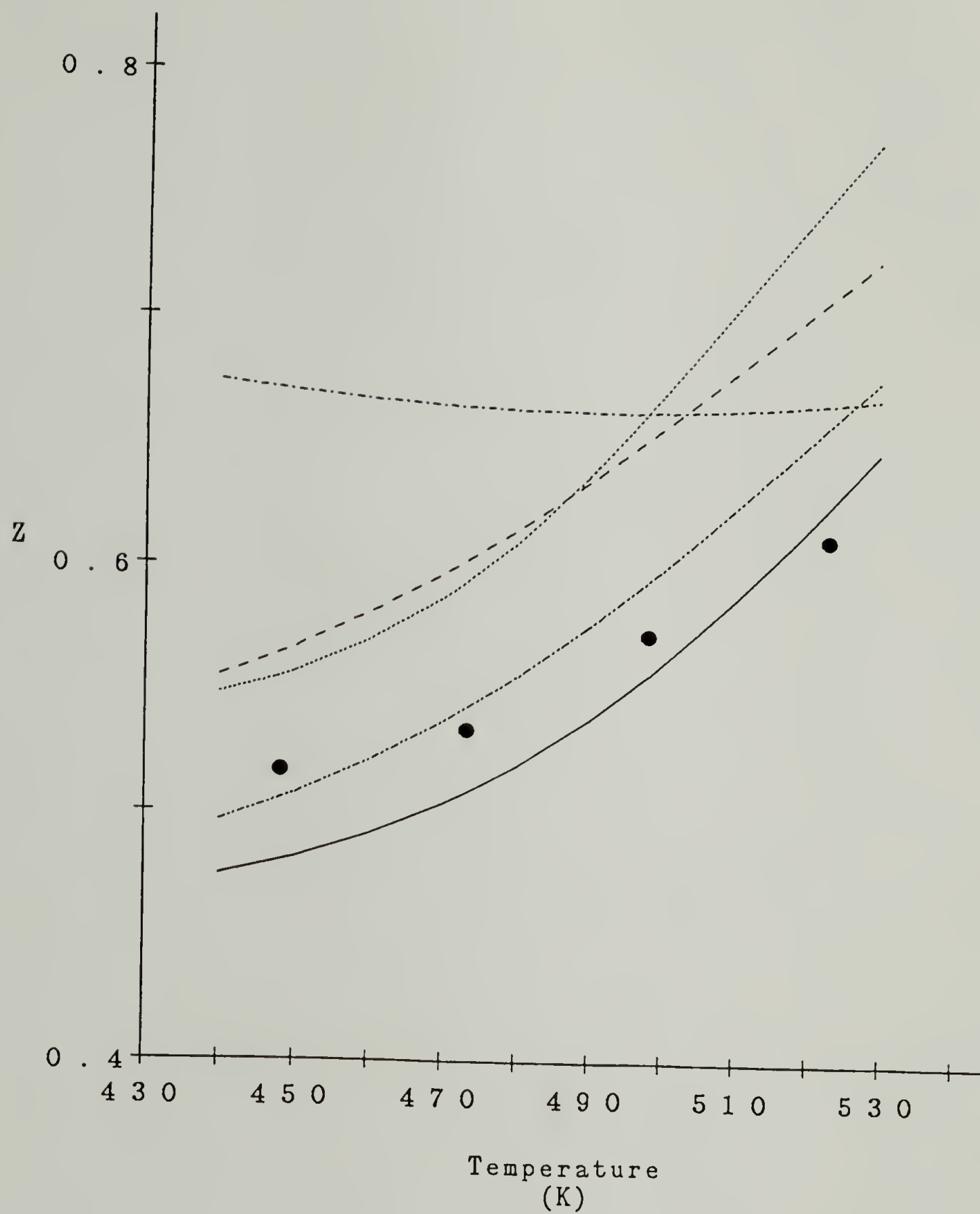


Figure 2.8

SO₂ compressibility ($Z = PV/RT$) versus temperature at $P = 304.0$ bar and lattice model calculations; symbols same as in Figure 2.6.

Table 2.6
Average Errors in Fitting Lattice Equations of State
to pVT Data on CF₃H

<u>VLE Data</u>							
Model	Number of of Points	Temp. (K)	Vapor Pressure-%	Vapor Density-%	Liquid Density-%		
MFLG	15	2.7	1.8	3.1	2.9		
Vera	15	2.5	1.4	3.8	5.1		
Kanig	15	24.7	9.6	19.6	13.5		
Kilian	15	2.4	5.2	5.4	11.4		
Sanchez	15	1.3	4.5	4.3	2.7		

<u>Critical Point</u>				<u>Equation of State</u>			
Model	Temp. (K)	Press. %	Dens. %	Number of Points	Press. %	Temp. (K)	Dens. %
MFLG	2.3	.7	13.9	78	2.8	.9	—
Vera	4.3	3.5	18.0	78	2.5	1.0	—
Kanig	20.9	22.8	12.2	78	6.9	2.8	—
Kilian	13.3	32.6	1.6	78	6.5	2.1	—
Sanchez	10.8	22.4	11.0	78	4.6	1.5	—

Table 2.7

Lattice Model Parameters for CF_3H Determined by
Parameter Estimation Program (PEP)

Model	v_0	m_1	α_1	g_{10}	g_{11}	γ_1
MFLG	25.0	1.69	.76250	-.98262	438.71	-1.2983
Vera	25.0	1.65	0	-.98651	609.01	-.75940
Kanig	25.0	2.12	0	0	401.99	-.16847
Kilian	25.0	2.19	0	-1.1825	808.36	0
Sanchez	4.8114	8.02	0	0	283.68	0

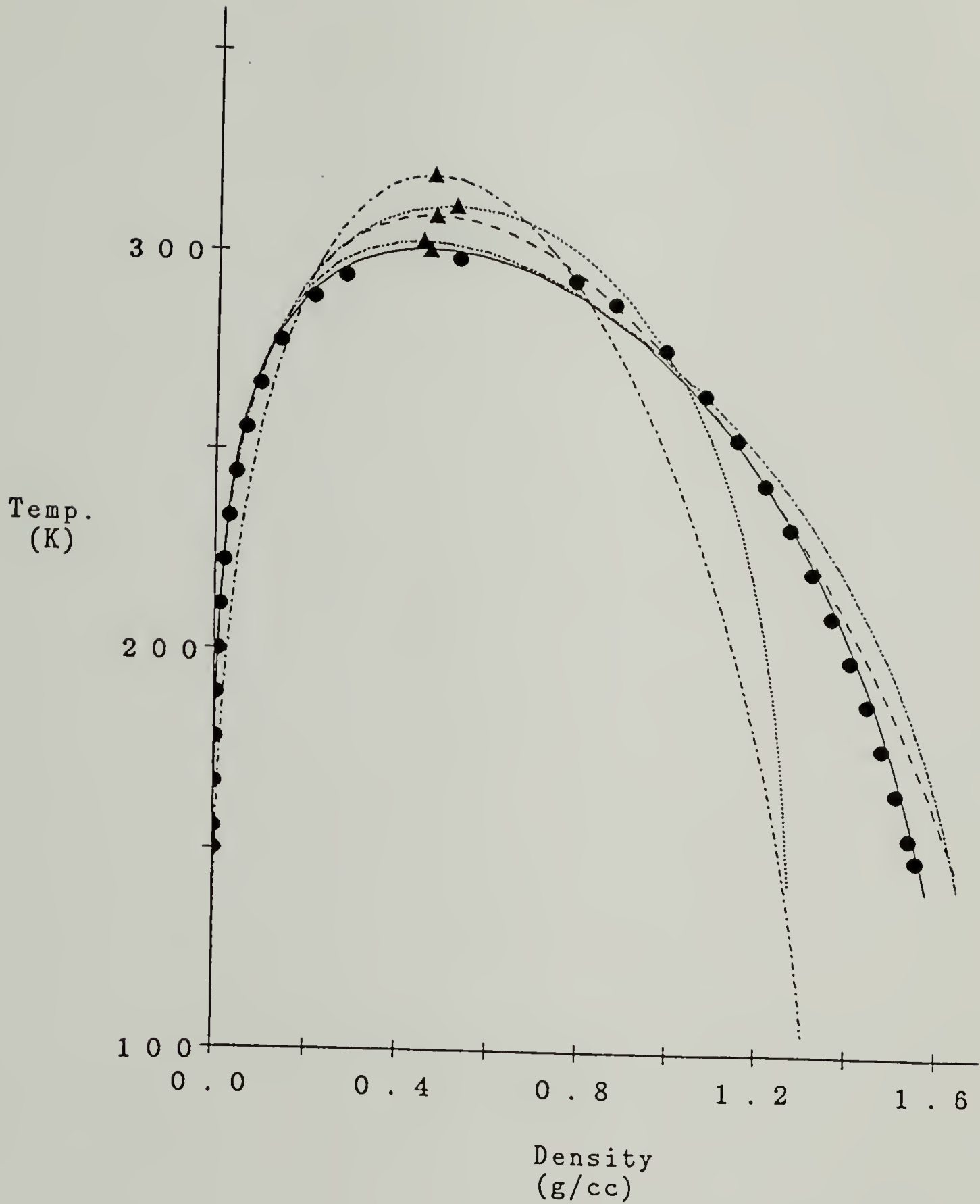


Figure 2.9

CF_3H VLE data (\bullet) and lattice model calculations; MFLG (—), Vera ($\cdots\cdots$), Kanig ($\cdots\cdots$), Kilian (\cdots), and Sanchez (---). \blacktriangle 's are calculated critical points.

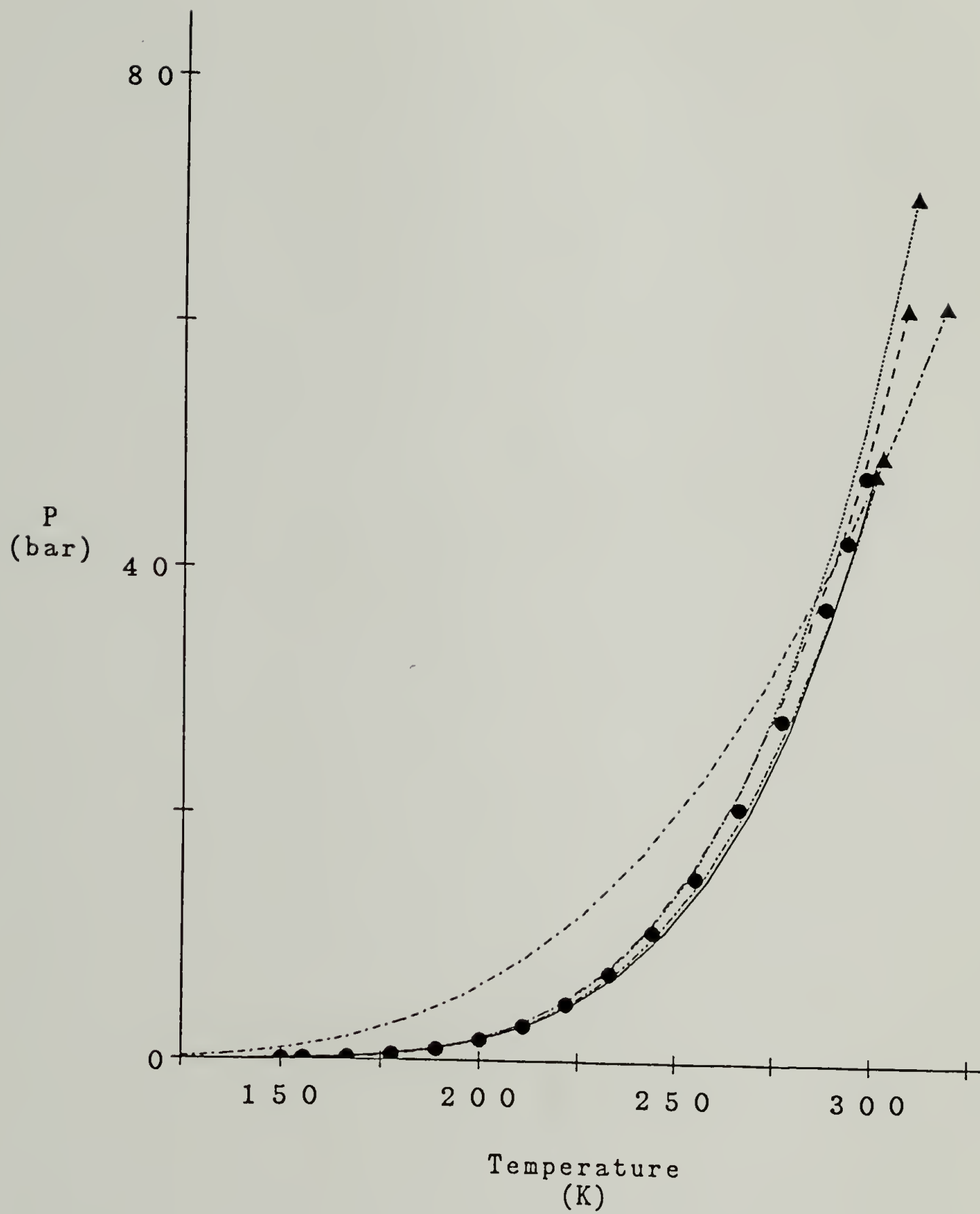


Figure 2.10

CF_3H vapor pressure as a function of temperature and lattice model calculations; symbols same as in Figure 2.9.

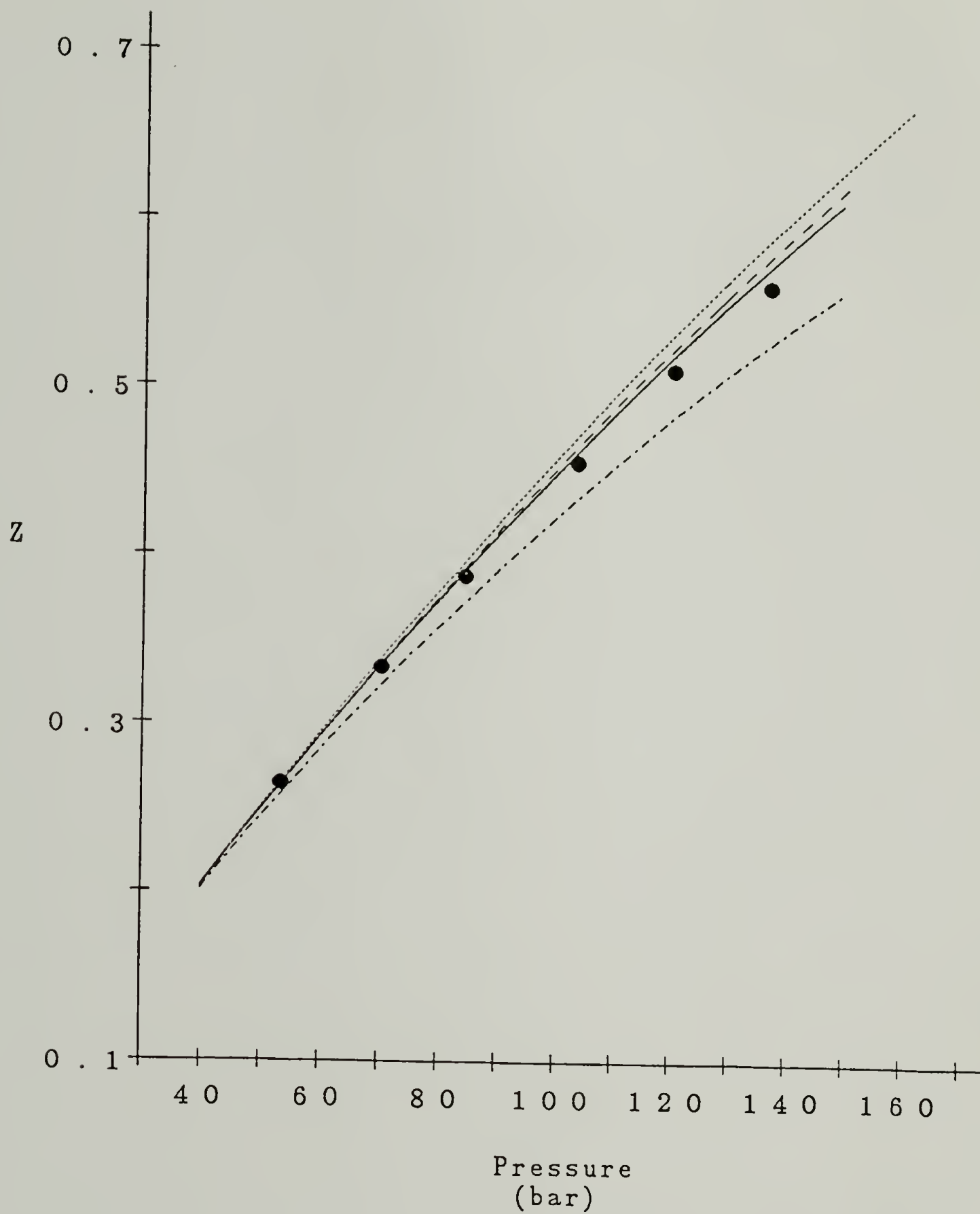


Figure 2.11

CF_3H compressibility ($Z = PV/RT$) versus pressure at $\rho = .5597 \text{ g/cc}$ and lattice model calculations; symbols same as in Figure 2.9.

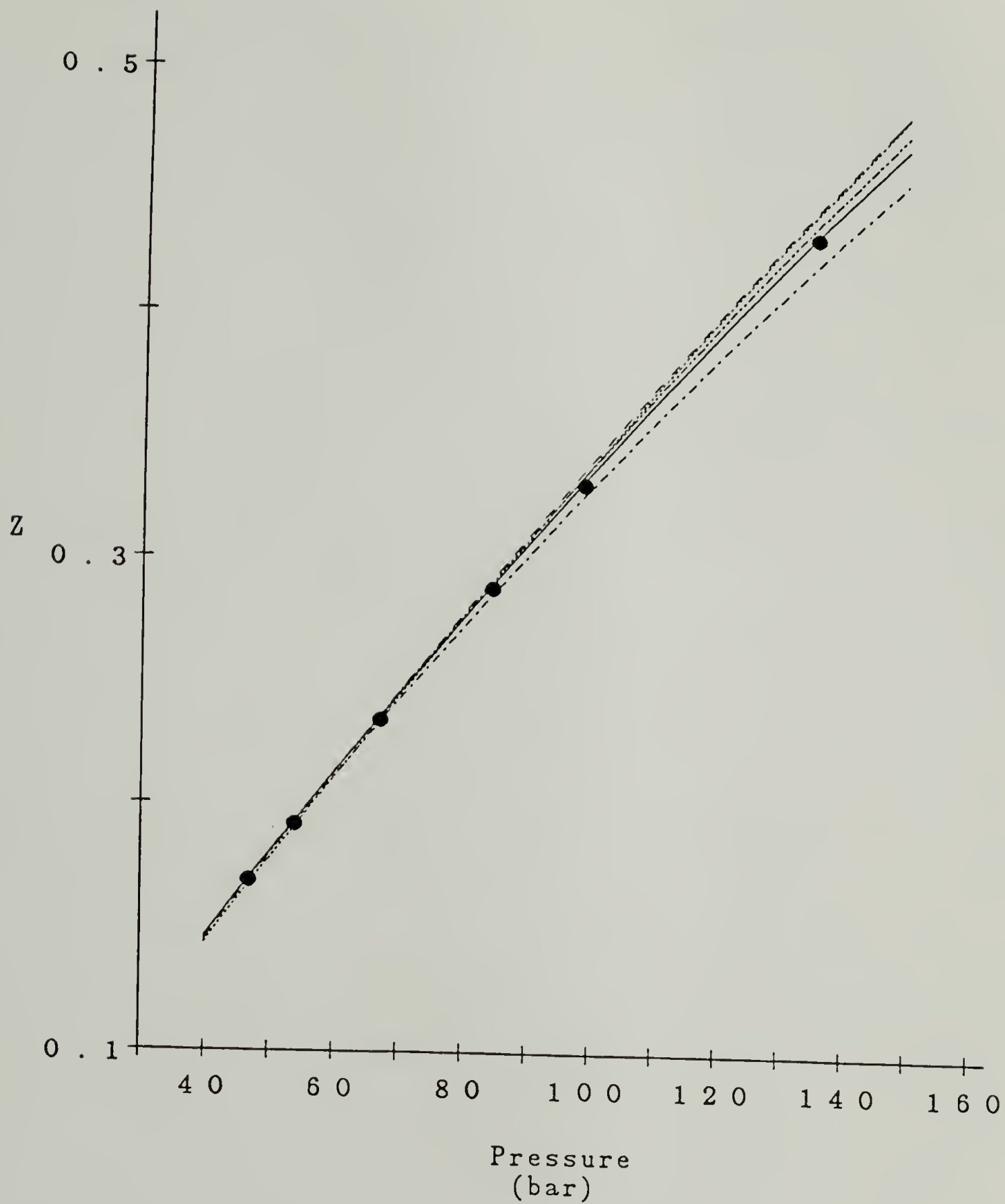


Figure 2.12

CF_3H compressibility ($Z = PV/RT$) versus pressure at $\rho = .7892$ g/cc and lattice model calculations; symbols same as in Figure 2.9.

2.3.2.3 Polystyrene (PS)

Unlike the three gases, polystyrene pVT behavior is governed by only one constraining equation, the equation of state. Thus there are five adjustable parameters (in the case of the MFLG model) yet only one equation for use in the fitting. In an attempt to avoid correlation between the parameters, pVT data for polystyrene at five molecular weights; 2300, 3650, 20400, 90700, and 125000, were evaluated [Ueberreiter and Laupenmuhlen, 1953; Oels, 1977; Quach and Simha, 1971; Zoller, *et al.*, 1976]. The use of five constraining equations allowed the fitting of the MFLG to the PS data without restrictions being placed on any of the parameters. Although there was a high degree of correlation between g_{10} and α_1 , the system converged without the necessity of fixing one of these two parameters.

Results for the PS fitting are shown in Tables 2.8 – 2.9 and in Figures 2.13 – 2.17.

In the previous two sections, the hypothesis was advanced that the g_{10} parameter partially accounts for the density fluctuations near the critical point. If this is its sole function, then g_{10} should have little effect on the quality of the description of the polystyrene pVT data. As can be seen by comparing the Vera and Kanig results, this is not entirely true. Whereas the effect of a non-zero g_{10} is less significant than that of a non-zero α_1 (compare Vera and MFLG results), it is not negligible. Thus the need for the g_{10} parameter arises both due to non-mean field corrections and to other effects. A clue as to the nature of these “other effects” can be found by examining the heat capacity, ΔC_v , which is derived from the second temperature derivative of the free energy. For the MFLG model, ΔC_v is identically zero, clearly an unsatisfactory result. If, instead of deriving ΔC_v from the free energy, ΔC_v is assumed to vary with

temperature linearly, the free energy should therefore vary with temperature as in equation (2-26):

$$\frac{\Delta A}{N_{\phi}RT} \sim C_1 + \frac{C_2}{T} + C_3T + C_4 \ln T \quad (2 - 26)$$

Thus if the interaction energy is assumed to be an interaction free energy, then g_{10} , as well as other parameters, are natural consequences [Koningsveld, 1968; Smirnova and Victorov, 1987; Kehiaian, *et al.*, 1981]. Because the heat capacity results from the vibrations and rotations of the segments, it is also possible that one of the cell-hole models, which model the effect of segmental vibrations via a cell which changes size with temperature, could accurately model the temperature dependence of the free energy without expanding the interaction function as in equation (2-26). The addition of a "cell" contribution to the MFLG model will be investigated in Chapter 5.

As in the cases of the three gases, a non-zero α_1 helps to fine tune the density-pressure relationship at high densities. Again, the floating v_0 in the Sanchez model accurately mimics the effect of a non-zero γ_1 , yet for polystyrene also produces a reasonable optimized value for v_0 . However, if it became necessary to model a mixture of polystyrene and, eg., one of the gases from the previous two sections, a mixing rule for the quite disparate pure component v_0 's would have to be devised.

As mentioned in Section 2.2, Panayioutou used Bondi's group contribution increments to calculate the value of γ_1 during modelling of the pVT behavior of high MW polystyrene [Panayioutou and Vera, 1982b]. Table 2.10 shows a comparison of surface area ratios calculated using MFLG-fitted values of γ_1 and m_1 against those found using Bondi's [1968] values. Ratios are presented because the surfaces are themselves used by the model as ratios and because use

of ratios precludes the need to determine a value for σ_0 (which, like v_0 , should be a simple scaling parameter). As can be seen, MFLG-calculated ratios involving PS, CO₂, and SO₂ are within 10% of the Bondi ratios. The disagreement in the CF₃H -based ratios may be due to the chemically asymmetric nature of this molecule. It may be necessary to introduce the concept of group contributions and specific interactions [Smirnova and Victorov, 1987; Kehiaian, *et al.*, 1978] to produce a γ_1 for CF₃H which better agrees with Bondi's estimate. In general, it appears that ratios of Bondi's values, used in conjunction with a previously calculated γ_1 , such as that for CO₂, will produce a good first approximation for the γ_1 of a system where only a limited amount of data are available.

Table 2.8

Average Error in Fitting Lattice Equations of State
to Polystyrene pVT Data

Model	Number of Points	Press. (%)	Temp. (K)	Dens. (%)
MFLG	117	-	.1	.12
Vera	117	-	.1	.20
Kanig	117	-	.15	.32
Kilian	117	-	.15	.34
Sanchez	117	-	.12	.26

Table 2.9

Lattice Model Parameters for Polystyrene Determined
by Parameter Estimation Program (PEP)

Model	v_0	m_1^*	α_1	g_{10}	g_{11}	γ_1
MFLG	25.0	3.70	-6.8354	4.8622	1110.0	-1.0889
Vera	25.0	3.79	0	-.60738	876.09	-433.32
Kanig	25.0	3.81	0	0	707.91	-.85766
Kilian	25.0	3.83	0	-.16630	857.09	0
Sanchez	16.798	5.60	0	0	734.44	0

* segments per monomer unit

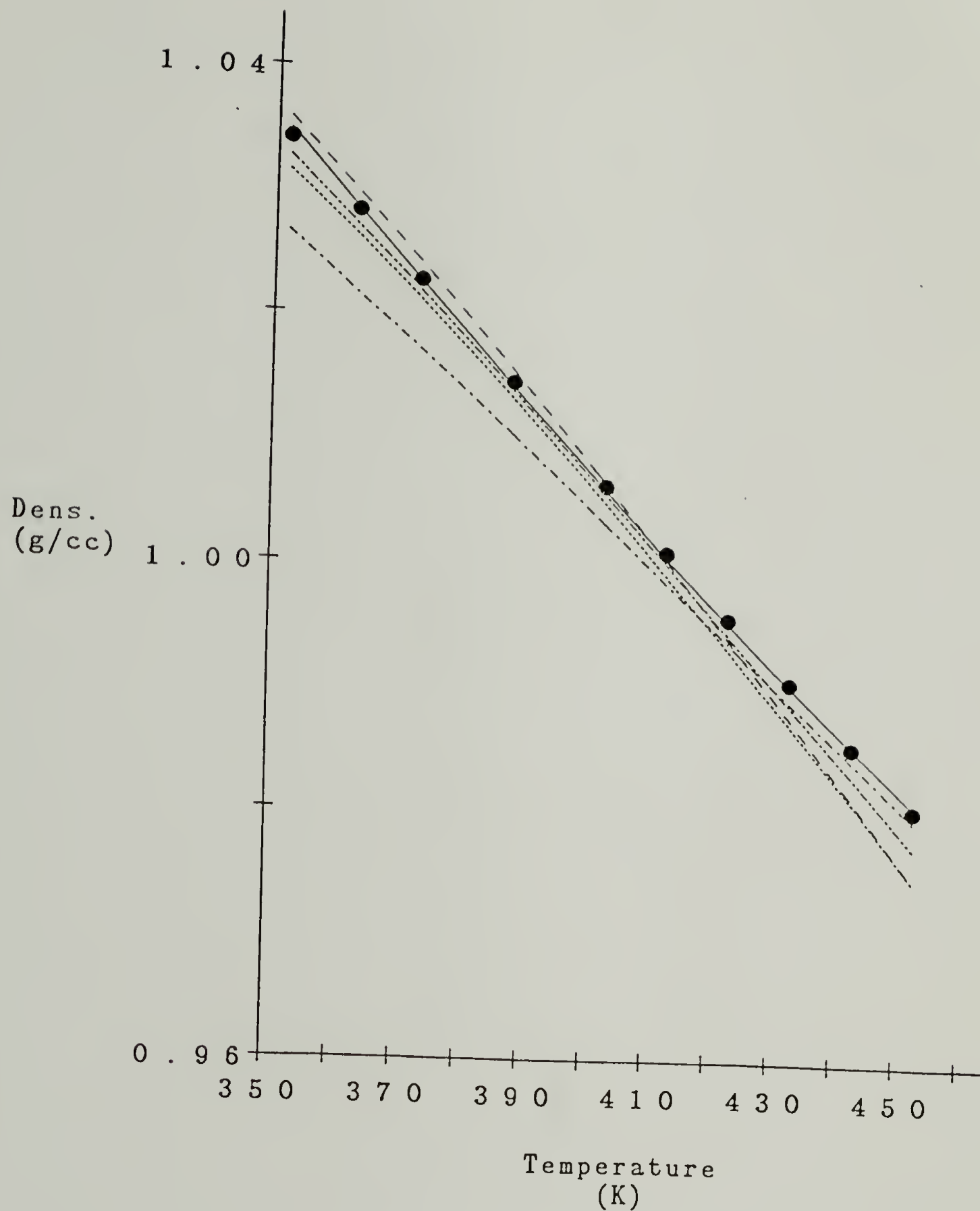


Figure 2.13

Polystyrene ($M_n = 2300$) density versus temperature at $P = 1$ bar and lattice model calculations; MFLG (—), Vera (.....), Kanig (---), Kilian (···) and Sanchez (- - -).

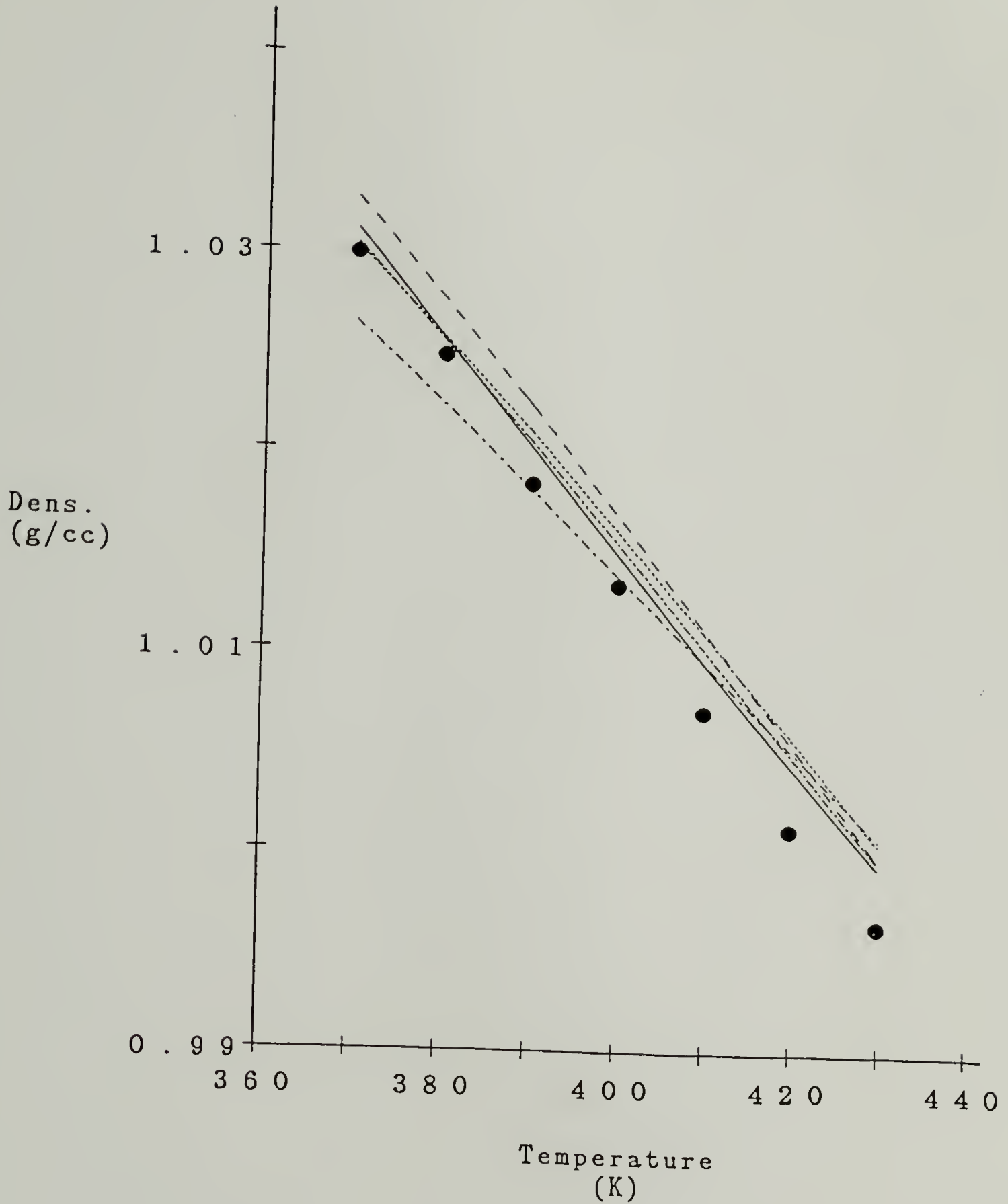


Figure 2.14

Polystyrene ($M_n = 20400$) density versus temperature at $P = 100$ bar and lattice model calculations; symbols same as in Figure 2.13.

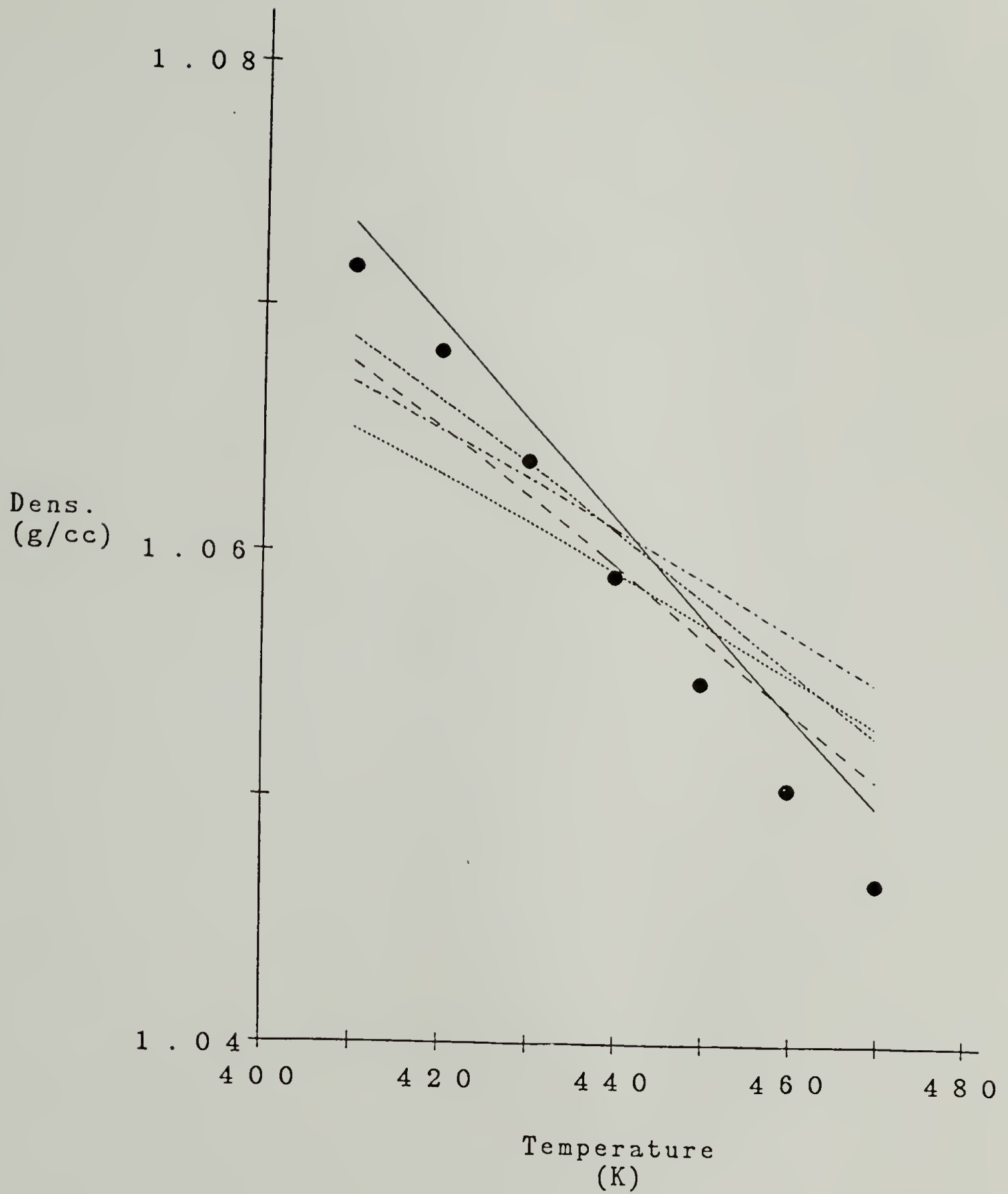


Figure 2.15

Polystyrene ($M_n = 20400$) density versus temperature at $P = 1500$ bar and lattice model calculations; symbols same as in Figure 2.13.

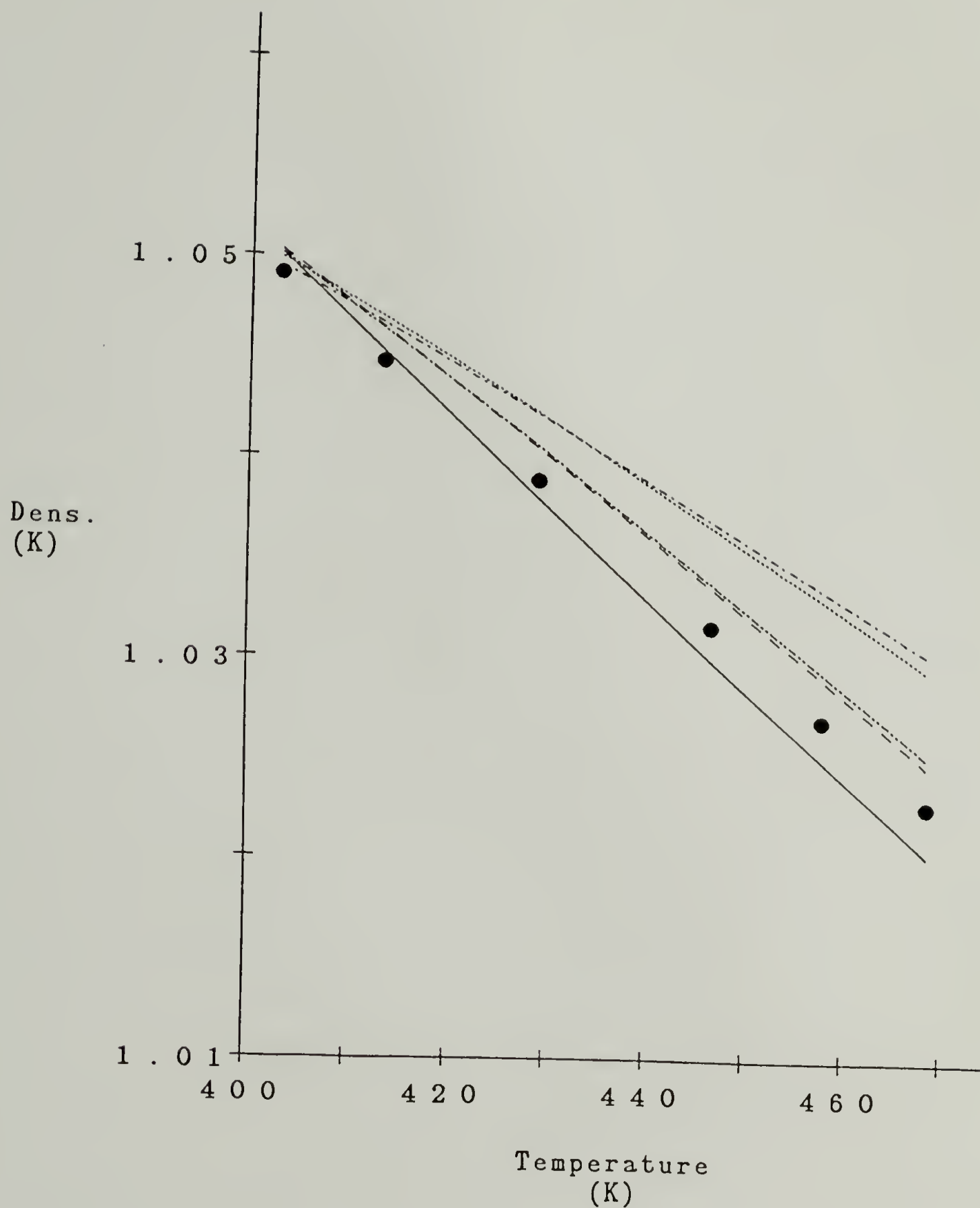


Figure 2.16

Polystyrene ($M_n = 90700$) density versus temperature at $P = 800$ bar and lattice model calculations; symbols same as in Figure 2.13.

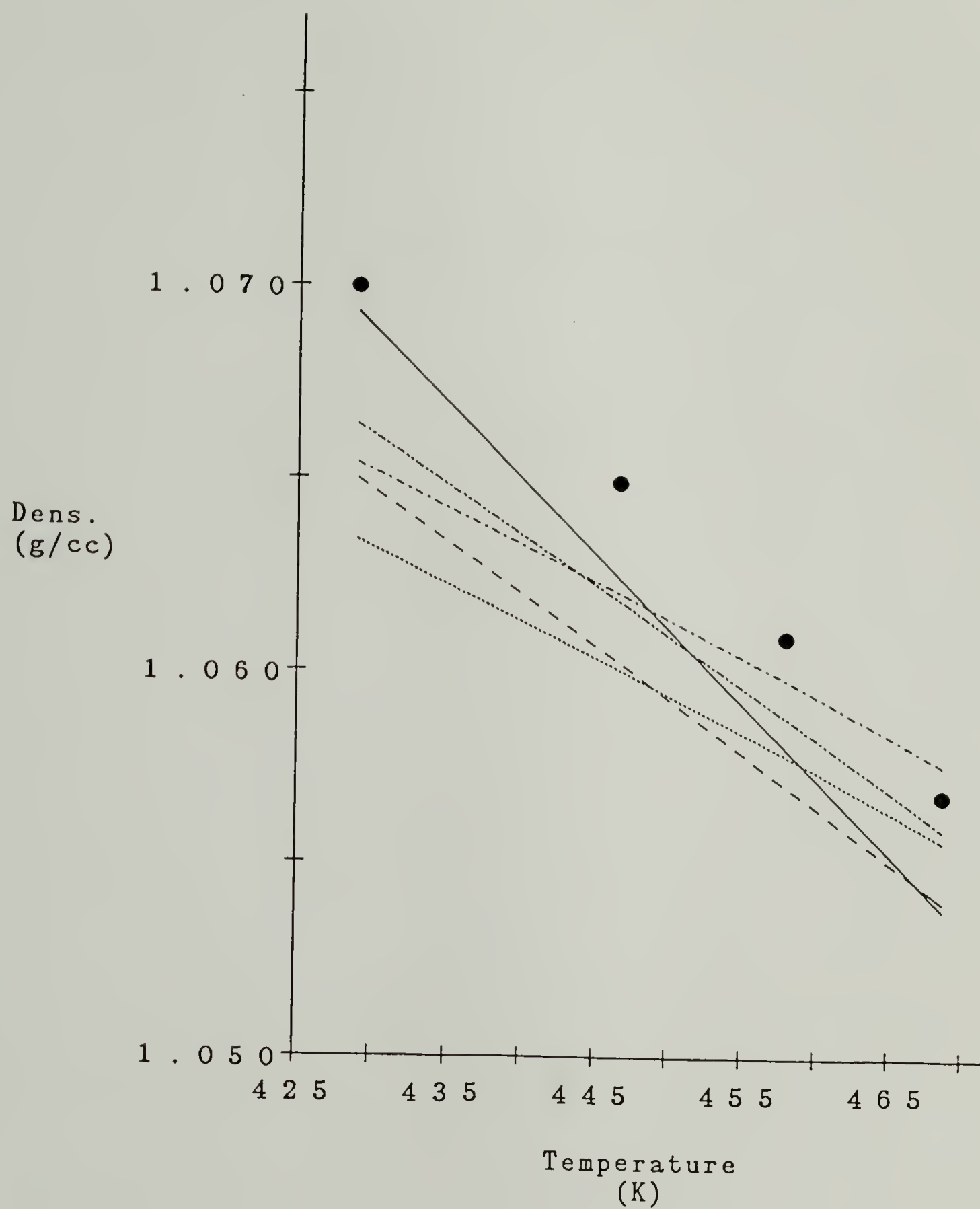


Figure 2.17

Polystyrene ($M_n = 90700$) density versus temperature at $P = 1600$ bar and lattice model calculations; symbols same as in Figure 2.13.

Table 2.10

Comparison of Molecular Surface Area Ratios Derived
from MFLG Fitted Parameters and Using Bondi's
Group Contribution Method

	CO ₂	SO ₂	CF ₃ H	PS
CO ₂	—	.81/.84	.74/.64	.37/.36
SO ₂	1.23/1.19	—	.91/.77	.46/.43
CF ₃ H	1.35/1.56	1.09/1.31	—	.50/.56
PS	2.68/2.81	2.17/2.35	1.99/1.80	—

Note: Entries in Table 2.10 are derived by dividing the molecular surface area of the row component by that in the column. Values are presented in the format (MFLG value/Bondi value) for comparison. MFLG values are calculated via the relation $((1 - \gamma_1)m_1 / (1 - \gamma_2)m_2)$. The Bondi values are calculated using the group contribution increments from reference [Bondi, 1968]; CO₂ - 2.58, SO₂ - 3.08, CF₃H - 4.02, and PS - 7.25.

2.4 Comparison of the MFLG and other Classes of Equation of State

In this section the MFLG equation of state will be compared to several non-lattice models. Nies and coworkers [1983], compared the performance of the MFLG model to that of the Simha-Somcycnsky (SS) cell-hole construction. Whereas a structural comparison of the two equations of state (such as that in Section 2.2) reveals few similarities, a comparison of the quality of the description of the pVT data of ethylene showed similar overall accuracy for the two models. The SS model produced a more accurate fit of the saturated liquid densities yet the MFLG model provided a better accounting of the data in the near-critical regime.

A general comparison of the MFLG EoS and those equations of state commonly encountered in chemical engineering practice can be made via a simple transformation of the MFLG EoS. If the term $\ln \phi_0$ from equation (2-11) is expanded as a series, followed by the substitution $\phi_1 = m_1 v_0 / V$, the MFLG EoS becomes:

$$p = \frac{RT}{V} + \frac{K_1(T)}{V^2 - 2K_2V + K_2^2} + \frac{K_3}{V^2} + \frac{K_4}{V^3} + \frac{K_5}{V^4} + \dots \quad (2-27)$$

where:

$$K_1 = Rm_1^2 v_0 (1 - \gamma_1)^2 (g_{10}T + g_{11})$$

$$K_2 = \gamma_1 m_1 v_0$$

$$K_3 = m_1^2 v_0 \left(\frac{1}{2} - \alpha_1 \right)$$

$$K_4 = \frac{RT}{3} (m_1 v_0)^3$$

$$K_5 = \frac{RT}{4} (m_1 v_0)^4$$

demonstrating that the MFLG EoS can be represented as a modified virial equation. Comparison with the Peng-Robinson (PR) [Peng and Robinson, 1976] or Soave [Soave, 1972] modifications of the Redlich-Kwong equation of state reveal some interesting similarities yet significant differences:

Peng-Robinson:

$$p = \frac{RT}{V - b} - \frac{a(T)}{V^2 + 2bV - b^2} \quad (2 - 28)$$

Soave:

$$p = \frac{RT}{V - b} - \frac{a(T)}{V^2 + bV} \quad (2 - 29)$$

Because neither the PR or Soave equations include terms higher in order than $1/V^2$, it would be expected that the MFLG model would describe the high density liquid region (and therefore polymer behavior) better than these two equations. Nitsche, *et al.*, [1983; 1984] and Kilpatrick [1986] found this to be the case in a comparison of the performance of the MFLG model and the PR equation in the description of the VLE data of water, CO₂, ammonia, and methanol. As $V \rightarrow \infty$ all three equations reduce to the ideal gas relation.

2.5 Summary of Chapter 2

In this Chapter, it has been shown that many lattice models fall into one of two broad categories, depending on whether or not the effect of segmental contact surface areas has been included. Further, it has been shown that those which do not employ the contact surface concept, the rigid lattice models, are specific cases of those which do, the non-rigid models. In computer modelling

studies of the pVT behavior of CO₂, SO₂, CF₃H, and polystyrene, the non-rigid form of the lattice model has been demonstrated to be superior, based on the quality of the description.

In the case of the non-rigid class of lattice models, it has been shown that several equations of state are specific cases of the Mean Field Lattice Gas model of Kleintjens and Koningsveld. Setting the parameter α_1 to zero yields the equation of state by Panayioutou and Vera; this requirement plus the constraint that g_{10} vanishes leads to Kanig's model. Retaining both parameters produces a superior description of the phase behavior of both the gases and polystyrene. It appears that the g_{10} parameter partially accounts for the lack of model terms which describe non-mean field density fluctuations near the critical point (in the case of the gases), and possibly makes up for neglect of a cell-like vibrational contribution to the EoS (for polystyrene). The α_1 parameter helps to fine-tune the dependence of the EoS on ϕ_0 at high densities, and as such, is possibly required due to deviations from the simple Flory-Huggins entropy of mixing expression used to construct the MFLG model.

CHAPTER 3

Modifying the Entropy of Mixing Expression of the MFLG Model: The First Order MFLG Model

Comparison of the performance of the various lattice models in Chapter 2 showed that the empirical α_1 parameter helps improve the ϕ_0 dependence of the equation of state at high densities. Inspection of the derivation of the generalized rigid lattice model revealed that a non-zero α_1 may originate in deviations from the Flory-Huggins entropy of mixing expression due to the introduction of a molecular surface dependence to the free energy. Indeed, the MFLG free energy expression (equation 2-9) is inconsistent because it combines entropy of mixing terms based on identical coordination numbers (and therefore surface areas) with a relation for the internal energy of mixing (equation 2-7) arising from a contact-statistical treatment. In this Chapter, the question of whether it is this inconsistency that prompts the need for empirical corrections such as α_1 . As in Chapter 2, computer modelling of the pVT behavior of CO₂, SO₂, CF₃H, and polystyrene will be used to evaluate the performance of the new derivation.

The derivation of the modified MFLG model is presented in Section 3.1. Computer modelling results are given in Section 3.2 and Section 3.3 concludes with a summary of this Chapter.

3.1 Derivation of the First Order MFLG Model

It is assumed that because the segments and holes are permitted distinct contact surface areas, the Flory-Huggins expression for calculating the number of ways of arranging the molecules and holes on the lattice, Ω_0 , must be adjusted

to account for the number of unlike contact pairs, P_{ij} , as calculated using contact statistics as in Section 2.1 [Staverman, 1937]. The Flory-Huggins derivation of Ω_0 is of the general form [Flory, 1953]:

$$\Omega_0 = \left(\frac{(n_0 + n_1)!}{n_0!n_1!} \right) \left(\frac{V^*}{V} \right)^{n_1(m_1-1)} \quad (3-1)$$

where V^* is a parametric volume which compensates for limitations in segment placement on the lattice after the first segment has been affixed. It is assumed that this parameter is independent of concentration and as such vanishes during the calculation of the entropy of mixing from equation (3-1).

The composition-dependent correction to equation (3-1) is assumed to take the form (z_{ij}/\bar{z}) , where z_{ij} is the number of unlike contacts per segment and \bar{z} is the average coordination number of the system at a given concentration as defined by equation (2-2). The number of arrangements of molecules and holes on the lattice, Ω_1 , is therefore:

$$\Omega_1 = \Omega_0 \left(\frac{z_{01}}{\bar{z}} \right)^{P_{01}} \left(\frac{z_{10}}{\bar{z}} \right)^{P_{10}} = \Omega_0 \left(\frac{z_{01}z_{10}}{\bar{z}^2} \right)^{P_{10}} \quad (3-2)$$

where the number of unlike contact pairs, P_{10} , is calculated as per equation (2-6). As before, the ratio of the surface areas is assumed to be equal to the ratio of the like-pair coordination numbers (z_{11}/z_{00}). The entropy of mixing, derived from equation (3-2) in the usual way ($S = -R \ln \Omega_1$), when added to the internal energy of mixing expression derived for the MFLG model (equation (2-7)), results in the following free energy equation:

$$\begin{aligned} \frac{\Delta A}{N_\phi RT} = & \phi_0 \ln \phi_0 + \frac{\phi_1}{m_1} \ln \phi_1 + \frac{\phi_0 \phi_1 (1 - \gamma_1)}{Q} (2z_{00} \ln Q) \\ & + \frac{\phi_0 \phi_1 (1 - \gamma_1)}{Q} \left(-z_{00} \ln z + \frac{g_{11}}{T} \right) \end{aligned} \quad (3-3)$$

where:

$$Q = 1 - \gamma_1 \phi_1 = 1 - \left(1 - \frac{z_{11}}{z_{00}}\right) \phi_1$$

$$z = \left(\frac{z_{10} z_{01}}{z_{00}^2}\right)$$

A comparison of equation (3-3) with (2-9) shows that not only α_1 , but also g_{10} have been redefined in this First Order MFLG model:

$$\alpha_1 = \frac{2z_{00}(1 - \gamma_1) \ln Q}{Q} \quad (3-4)$$

$$g_{10} = -z_{00} \ln z \quad (3-5)$$

The equation of state, critical point, and VLE equations for the First Order MFLG model are provided in Appendix A.

Comparison of the free energy expressions of the First Order MFLG and the rigid lattice model (see Chapter 2) shows that while both contain a contribution to the entropy of mixing (given below as α) due to the number of contacts per segment, both the form and limiting values of α differ substantially:

Rigid Model:

$$\alpha \sim Q^* \ln Q^*; \text{ where } Q^* = 1 - \left(\frac{2}{z} \left(1 - \frac{1}{m_1}\right)\right) \phi_1 \quad (3-6)$$

$$\alpha \rightarrow 0 \text{ as } m_1 \rightarrow 1$$

First Order MFLG:

$$\alpha \sim \frac{\ln Q}{Q}; \text{ where } Q = 1 - \gamma_1 \phi_1 \quad (3-7)$$

$$\alpha \rightarrow 0 \text{ as } \sigma_1 \rightarrow \sigma_0 \text{ } (\gamma_1 \rightarrow 0)$$

Thus the excess entropy contribution due to contact statistics to the First Order MFLG model is non-vanishing even for small molecules, a significant difference from the rigid lattice models.

In the next section, the PEP is used to evaluate the performance of the First Order MFLG model via modelling of the pVT behavior of CO₂, SO₂, CF₃H, and polystyrene, as in Chapter 2. The First Order MFLG description is compared to that of the Zero Order MFLG, as well as that of the Kanig and Kilian. The Kanig model is included in the comparison because it contains no α_1 or g_{10} contribution and thus serves as a type of “control”. As was shown in Chapter 2, in the case of the gases, the Kilian model is representative of the general class of rigid lattice models. Comparing the Kilian and First Order descriptions will therefore present a means by which to compare the “rigid” and non-rigid derivations of α_1 .

3.2 Results for CO₂, SO₂, CF₃H, and Polystyrene

Average errors between calculated and actual pVT data for all four compounds under consideration are shown in Tables 3.1a, 3.1b, and 3.2. Parameter values are provided in Table 3.3. In addition, a graphical comparison of the First and Zero Order Models is given for the CO₂ description in Figures 3.1 – 3.4. The data used in the modelling are the same as was used in Chapter 2.

The quantity z_{00} , the hole like-pair coordination number, should be a simple scaling quantity like the lattice site volume v_0 . To test this assumption, the value of z_{00} was varied between the natural limits 6 and 12 and the total error (χ^2) for the CO₂ system compared. As suspected, the value of z_{00} has little effect

on the overall accuracy of the description, within the prescribed limits, and was therefore set to 10.0.

As can be seen by the results in Tables 3.1 – 3.2, the derivation of α_1 and g_{10} in the First Order model is clearly superior to the case where both parameters are zero (Kanig) and to the rigid model description of their contribution (Kilian). However, the First Order model cannot, except in a few instances, equal the description of the Zero Order model. The performance of the First Order model is particularly poor near the critical point (see also Figures 3.1 and 3.2). Apparently the First Order model derivation of α_1 and g_{10} does not compensate for the fluctuations near T_c as well as the two-empirical-parameter approach of the Zero Order model. This conclusion is supported by the results for polystyrene; in a situation where the critical point is absent, the First Order model produces a description of pVT behavior equal to that of the Zero Order MFLG and while using one fewer adjustable parameter.

In addition to a reasonable description of pVT behavior, the First Order model results in values of the surface area ratio which are in surprisingly good agreement with Bondi's values (see Table 3.4). The exceptions are those entries which involve SO_2 ; if the model-calculated value of the molecular surface area was approximately 15% lower these values too would agree with Bondi's ratios.

Following testing of the First Order MFLG model, an attempt was made to further modify the free energy expression to correct another possible inconsistency. Heretofore the like-pair coordination numbers, z_{ii} , have been assumed to be constants, proportional to the surface areas. However, it is clear that these coordination numbers should vary with concentration in a real random packing of segments. Therefore these coordination were assumed to vary linearly with volume fraction (such that at the limits $\phi_1 = 0, 1$ the description is

exact) and the resulting model evaluated [Beckman, *et al.*, 1987]. The description of this Second Order model proved to be much poorer than that of the First Order model and therefore this approach was abandoned. It appears that further improvements should concentrate on the concentration and temperature dependence of the segment density fluctuations near the critical point since the greatest error in the First Order model is in the critical region.

Table 3.1a

Average Errors in Fitting Lattice Equations of State
to pVT Data on CO₂, SO₂, CF₃H, and Polystyrene

Model	Number of of Points	Temp. (K)	<u>VLE Data</u>		
			Vapor Pressure-%	Vapor Density-%	Liquid Density-%
CO ₂ - Zero	15	.6	1.2	.5	2.3
- First	15	1.0	4.3	3.5	7.4
- Kanig	15	12.5	8.2	14.2	17.9
- Kilian	15	2.5	7.0	4.6	9.5
SO ₂ - Zero	19	2.4	1.7	2.1	2.4
- First	19	.8	2.9	2.4	4.5
- Kanig	19	21.7	12.4	22.1	46.8
- Kilian	19	1.5	4.6	3.7	10.7
CF ₃ H - Zero	15	2.7	1.8	3.1	2.9
- First	15	1.0	3.6	3.6	6.2
- Kanig	15	24.7	9.6	19.6	13.5
- Kilian	15	2.4	5.2	5.4	11.4

Table 3.1b

Average Errors in Fitting Lattice Equations of State to
pVT Data on CO₂, SO₂, CF₃H, and Polystyrene

Model	<u>Critical Point</u>			Number of Points	<u>Equation of State</u>		
	Temp. (K)	Press. %	Dens. %		Press. %	Temp. (K)	Dens. %
CO ₂ - Zero	1.7	.1	7.7	66	1.0	—	4.9
- First	4.0	5.0	19.3	66	1.1	—	2.8
- Kanig	12.3	1.3	23.7	66	3.4	—	10.7
- Kilian	11.1	27.1	3.1	66	4.0	—	13.6
SO ₂ - Zero	.9	.4	9.4	32	—	.7	3.4
- First	2.9	8.8	17.1	32	—	.5	4.3
- Kanig	28.5	7.8	35.1	32	—	1.4	10.8
- Kilian	12.4	29.8	.3	32	—	2.8	13.2
CF ₃ H - Zero	2.3	.7	13.9	78	2.8	.9	—
- First	2.6	11.1	18.3	78	3.3	.5	—
- Kanig	20.9	22.8	12.2	78	6.9	2.8	—
- Kilian	13.3	32.6	1.6	78	6.5	2.1	—

Table 3.2

Average Error in Fitting Lattice Equations of State
to Polystyrene pVT Data

Model	Number of Points	Press. (%)	Temp. (K)	Dens. (%)
Zero	117	-	.1	.12
First	117	-	.1	.12
Kanig	117	-	.15	.32
Kilian	117	-	.15	.34

Table 3.3

First Order MFLG Model Parameters for CO₂, SO₂, CF₃H,
and Polystyrene Determined by Parameter Estimation Program (PEP)

Model	m_1	z_1	g_{11}	γ_1
CO ₂	1.20	1.4813	1830.6	.1031
SO ₂	1.65	1.2860	1824.5	.051184
CHF ₃	1.715	1.2236	1223.6	.04328
PS	3.67	.7974	1297.1	.21954

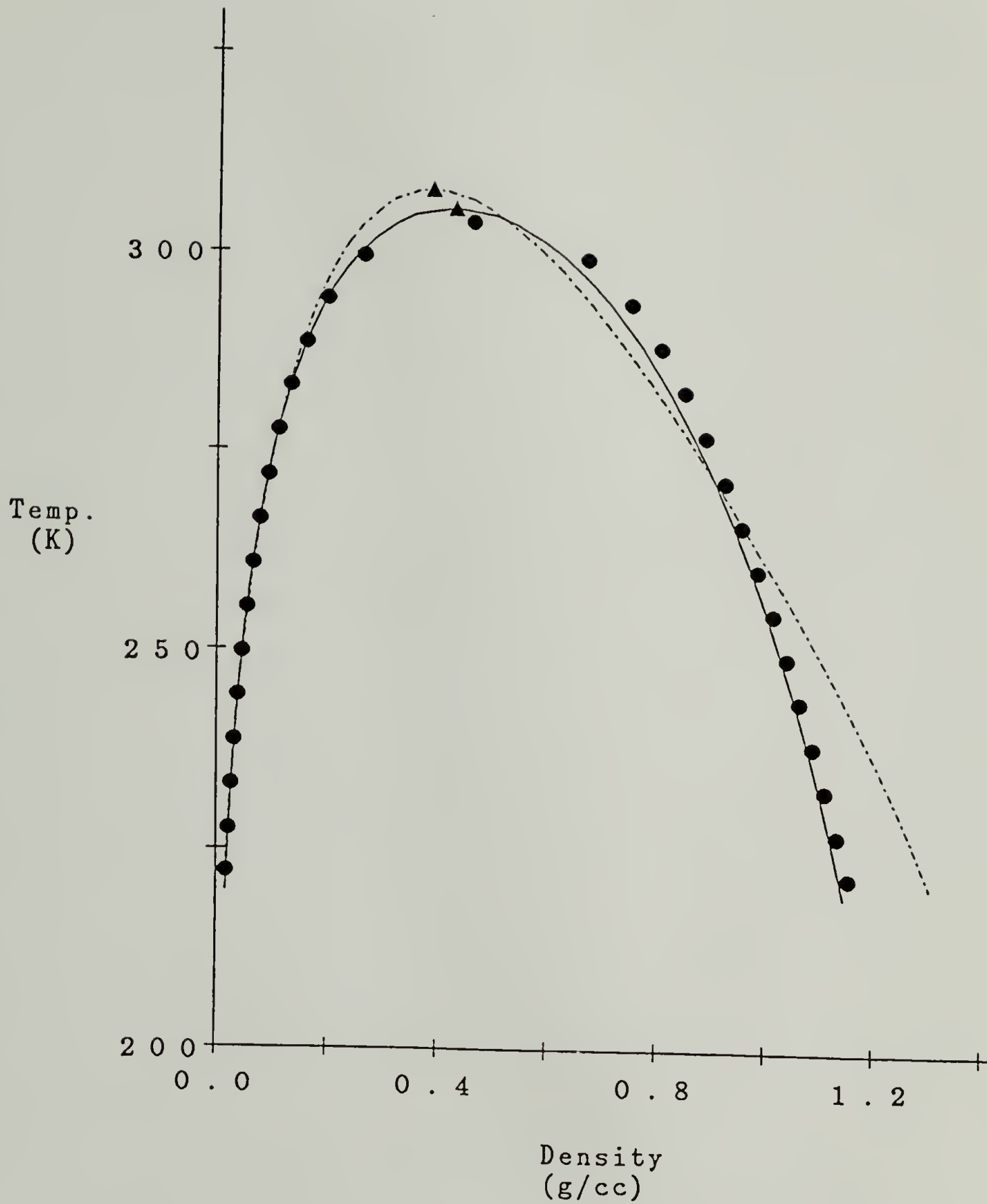


Figure 3.1

VLE data for CO_2 (\bullet) and lattice model calculations; Zero Order MFLG ($-$), First Order MFLG (\cdots). \blacktriangle 's are calculated critical points.

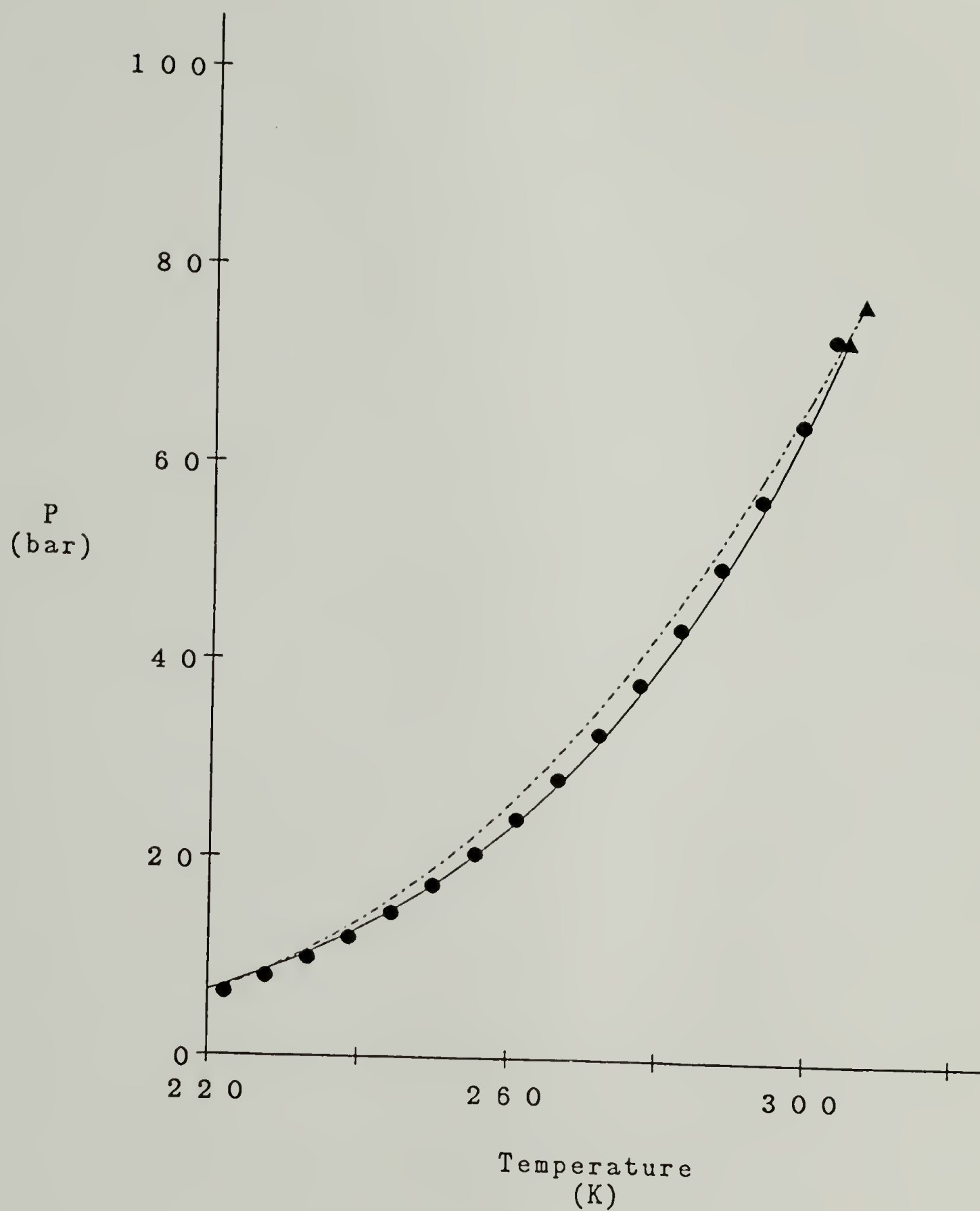


Figure 3.2

CO₂ vapor pressure as a function of temperature and lattice model calculations; symbols same as in Figure 3.1.

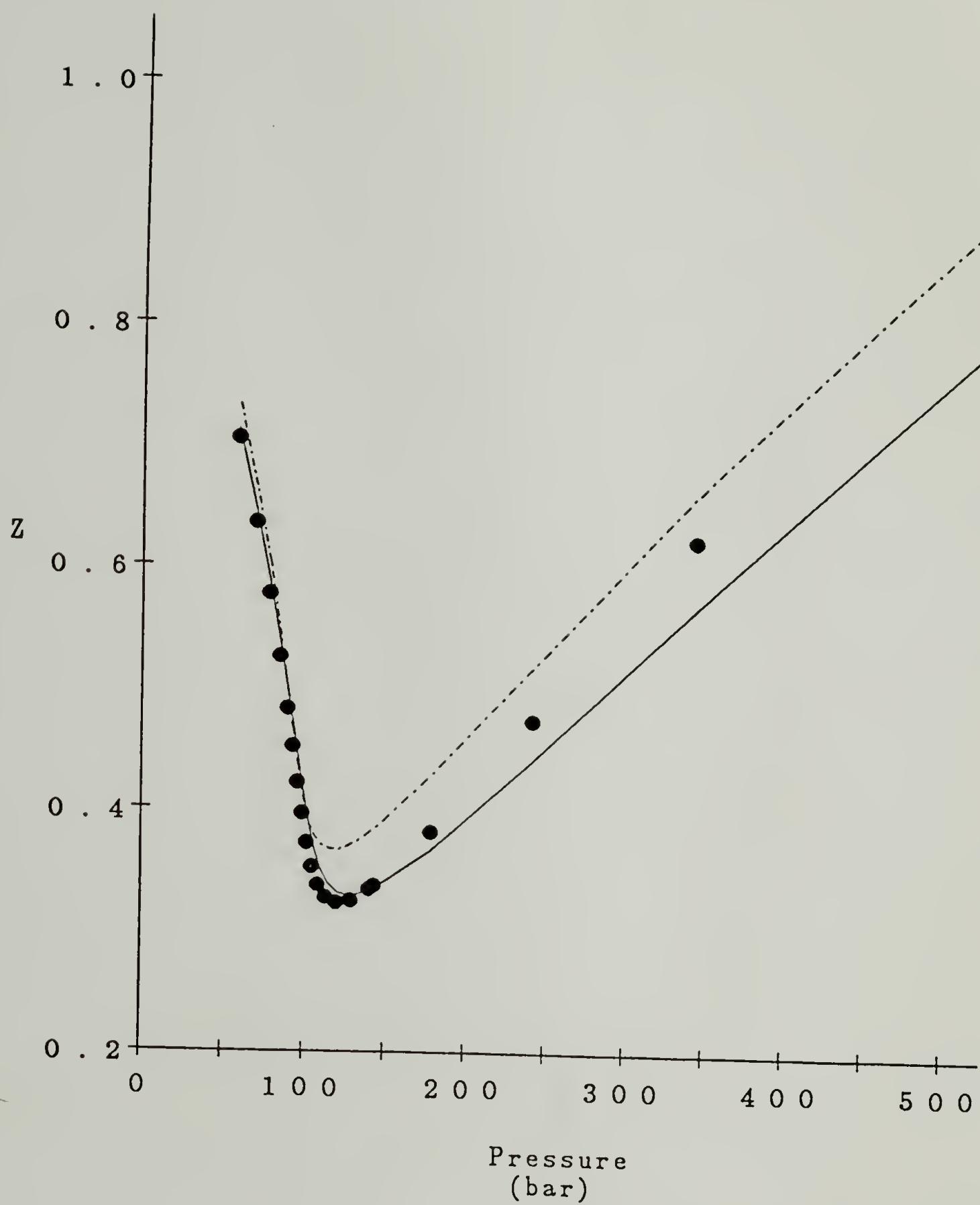


Figure 3.3

CO₂ compressibility ($Z = PV/RT$) versus pressure at $T = 323K$ and lattice model calculations; symbols same as in Figure 3.1.

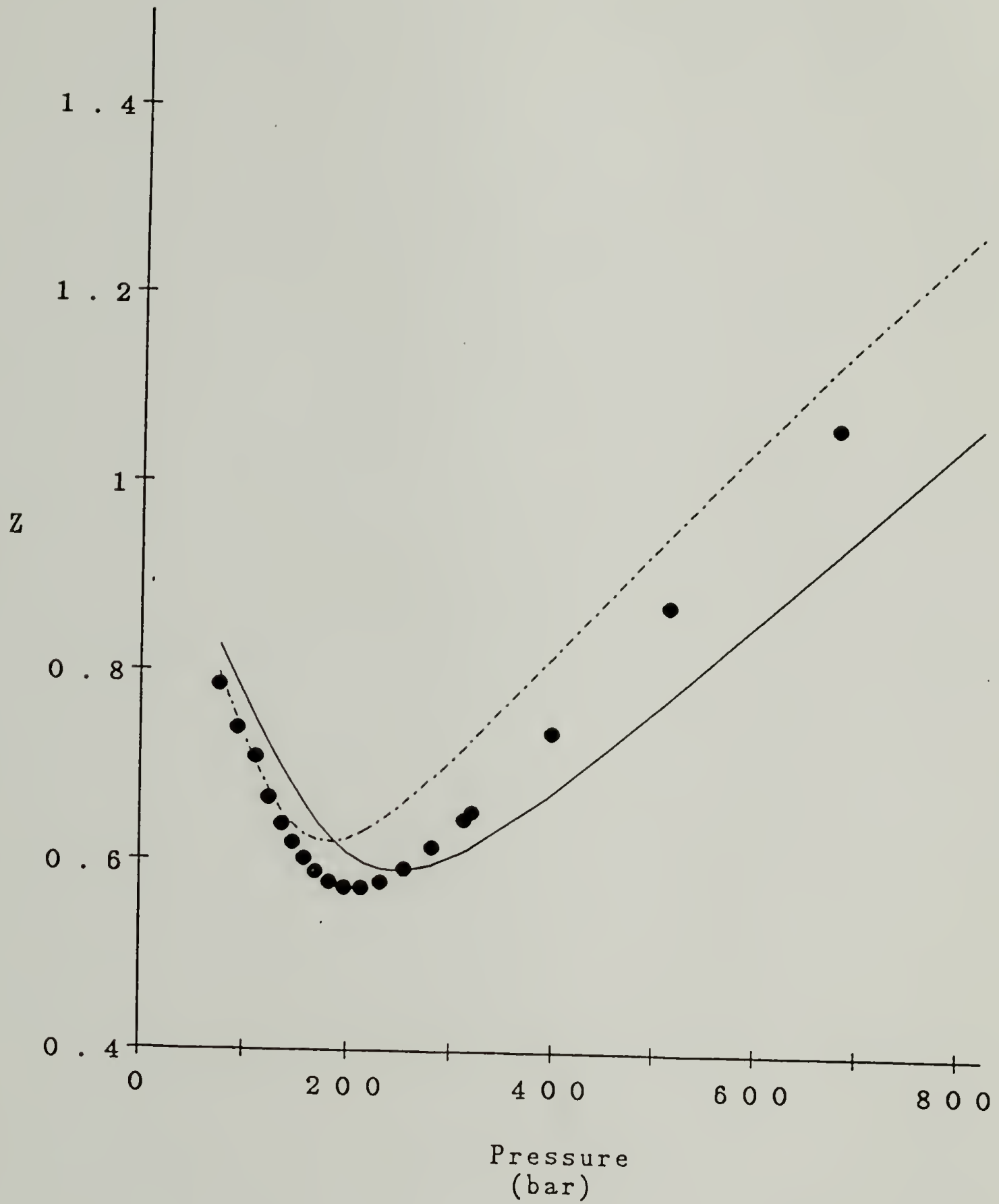


Figure 3.4

CO₂ compressibility ($Z = PV/RT$) versus pressure at $T = 372K$ and lattice model calculations; symbols same as in Figure 3.1.

Table 3.4

Comparison of Molecular Surface Area Ratios Derived from First Order MFLG Fitted Parameters and Using Bondi's Group Contribution Method

	CO ₂	SO ₂	CF ₃ H	PS
CO ₂	—	.69/.84	.66/.64	.38/.36
SO ₂	1.45/1.19	—	.95/.77	.55/.43
CF ₃ H	1.52/1.56	1.05/1.31	—	.57/.56
PS	2.66/2.81	1.83/2.35	1.75/1.80	—

Note: Entries in Table 3.4 are derived by dividing the molecular surface area of the row component by that in the column. Values are presented in the format (First Order MFLG value/Bondi value) for comparison. First Order MFLG values are calculated via the relation $((1 - \gamma_1)m_1 / (1 - \gamma_2)m_2)$. The Bondi values [Bondi, 1968] are calculated using group contribution increments and are; CO₂ - 2.58, SO₂ - 3.08, CF₃H - 4.02, and PS - 7.25.

3.3 Summary of Chapter 3

In this Chapter, the fundamental nature of the heretofore MFLG empirical parameters α_1 and g_{10} was investigated via modifications to the MFLG entropy of mixing expression and subsequent computer modelling. The Flory-Huggins entropy of mixing relation was modified to attempt to account for the dependence of the total number of configurations on the distinct surface areas of the segments and holes. The resulting free energy expression, designated the First Order model, provided apparently molecular definitions for both α_1 and g_{10} and required one fewer adjustable parameter than the Zero Order model. Computer modelling of the pVT behavior of CO_2 , SO_2 , CF_3H , and polystyrene showed that whereas the First Order model produces a significantly better description than the case where $(\alpha_1, g_{10}=0)$ or that of the general rigid lattice model, it falls short of equalling the performance of the parent model. Lacking the empirical g_{10} parameter to compensate for the segment density fluctuations in the region near T_c , the First Order model displays large errors in this regime. Consequently, in situations where critical conditions are not relevant, such as modelling of the pVT behavior of polystyrene, the First Order model performs as well as the Zero Order MFLG, despite one fewer adjustable constant.

In the next Chapter, the performance of the Zero and First Order models will be compared in the modelling of the phase separation behavior of polymer-liquid and polymer-gas mixtures.

CHAPTER 4

Phase Separation Behavior of Binary Mixtures

The results in this section are divided into two areas; those from modelling of polymer-liquid mixtures and those from polymer-gas mixtures.

In Section 4.2.1, modelling results on the systems PS-cyclohexane and PS-SO₂ are presented. The purpose for this work is twofold; both to compare the performance of the Zero Order and First Order MFLG models in describing phase behavior and to evaluate two types of modelling strategies. The first strategy involves finding the values of the necessary binary parameters via fitting of the appropriate model equations against dilute solution data (PS-cyclohexane) while the second uses mixture data on concentrated solutions (PS-SO₂). The choice of strategy is important because the mean field approximation breaks down in the case of very dilute polymer solutions, due to the large fluctuations in segment density owing to the isolated nature of individual polymer coils. Thus it would be expected that binary interaction parameters found via fitting against concentrated solution data would be more useful in subsequent model predictions than those determined using dilute solution results.

In Section 4.2.2, binary parameters found by fitting the appropriate model equations against sorption data (polymer weight fractions of .75 and above) from the systems PS-CO₂ and poly(methyl methacrylate)-CO₂ are used to predict the solubility of the two polymers in supercritical CO₂ versus pressure. These predictions are then compared to data measured using a flow-through supercritical extraction unit.

4.1 Free Energy and Related Thermodynamic Quantities for the Zero and First Order MFLG Models

Just as the MFLG represents a pure substance as a quasi-binary (holes and segments), a mixture of two constituents is modelled as a quasi-ternary. The internal energy is derived using the same general procedure as outlined in Section 2.1, *i.e.*, the number of (1-1), (2-2), and (1-2) contacts are calculated using surface fractions and Regular Solution Theory. The free energy expression for binary mixtures for the Zero Order MFLG model is therefore:

$$\begin{aligned}
 \frac{\Delta A}{N_{\phi}RT} = & \phi_0 \ln \phi_0 + \frac{\phi_1}{m_1} \ln \phi_1 + \frac{\phi_2}{m_2} \ln \phi_2 \\
 & + \phi_0 \phi_1 \left(\alpha_1 + \frac{\beta_1(1 - \gamma_1)}{(1 - \gamma_1 \phi_1 - \gamma_2 \phi_2)} \right) - O(\phi_1) \\
 & + \phi_0 \phi_2 \left(\alpha_2 + \frac{\beta_2(1 - \gamma_2)}{(1 - \gamma_1 \phi_1 - \gamma_2 \phi_2)} \right) - O(\phi_2) \\
 & + \phi_1 \phi_2 \left(\alpha_m + \frac{\beta_m(1 - \gamma_1)(1 - \gamma_2)}{(1 - \gamma_1 \phi_1 - \gamma_2 \phi_2)} \right)
 \end{aligned} \tag{4-1}$$

where:

$$\gamma_i = 1 - \sigma_i / \sigma_0$$

$$\beta_i = g_{i0} + g_{i1} / T$$

and where the other symbols have been defined previously. The two terms $O(\phi_i)$ are required because ΔA refers to the difference in free energy between a mixture of type 1 segments, type 2 segments, and holes, and the initial states type 1 segments plus holes and type 2 segments plus holes. However, since these terms vanish during the derivations of the binary equation of state, binodal, spinodal, and critical point, they need not be discussed further.

The entropy of mixing correction, which is the basis for the First Order MFLG model, is derived in a fashion analogous to that of the pure component case. The total number of arrangements of segments and holes on the lattice, Ω_1 , is assumed to be:

$$\Omega_1 = \Omega_0 \prod_{i=0}^2 \prod_{\substack{j=0 \\ j \neq i}}^2 \left(\frac{z_{ij}}{\bar{z}} \right)^{P_{ij}} \quad (4-2)$$

where:

$$\Omega_0 = \left(\frac{(n_0 + n_1 + n_2)!}{n_0!n_1!n_2!} \right) \prod_{i=1}^2 \left(\frac{V_i^*}{V} \right)^{n_i(m_i-1)}$$

As before, \bar{z} is the average coordination number of the system at a given concentration:

$$\bar{z} = \left(\sum_0^2 2P_{ii} + \sum_{\substack{0 \\ j \neq i}}^2 P_{ij} \right) / N_\phi \quad (4-3)$$

The number of like and unlike-contact pairs, P_{ii} and P_{ij} , are calculated as for the Zero Order MFLG model:

$$P_{ij} = n_i m_i z_{ii} \frac{n_j m_j z_{jj}}{\sum_0^2 n_i m_i z_{ii}} \quad i \neq j \quad (4-4)$$

$$P_{ii} = \frac{1}{2} \frac{(n_i m_i z_{ii})^2}{\sum_0^2 n_i m_i z_{ii}} \quad (4-5)$$

The entropy of mixing calculated from equation (4-2) is added to the Zero Order internal energy of mixing, yielding the First Order MFLG binary free energy expression:

$$\begin{aligned}
\frac{\Delta A}{N_\phi RT} = & \phi_0 \ln \phi_0 + \frac{\phi_1}{m_1} \ln \phi_1 + \frac{\phi_2}{m_2} \ln \phi_2 \\
& + \frac{\phi_0 \phi_1 (1 - \gamma_1)}{Q} (2z_{00} \ln Q - z_{00} \ln z_1 + \beta_1) - O(\phi_1) \\
& + \frac{\phi_0 \phi_2 (1 - \gamma_2)}{Q} (2z_{00} \ln Q - z_{00} \ln z_2 + \beta_2) - O(\phi_2) \\
& + \frac{\phi_1 \phi_2 (1 - \gamma_1)(1 - \gamma_2)}{Q} (2z_{00} \ln Q - z_{00} \ln z_m + \beta_m)
\end{aligned} \tag{4-6}$$

where:

$$\beta_i = g_{i1}/T \quad i = 1, 2, m$$

$$Q = 1 - \gamma_1 \phi_1 - \gamma_2 \phi_2$$

$$\gamma_i = 1 - z_{ii}/z_{00} \quad i = 1, 2$$

$$z_i = z_{0i} z_{i0} / z_{00}^2 \quad i = 1, 2$$

$$z_m = z_{12} z_{21} / z_{00}^2$$

The binary equation of state, binodal, spinodal, and critical conditions are derived from the free energy expressions (equations (4-1) and (4-6)) in the usual way [Gibbs, 1874; Modell and Reid, 1974], as shown in Table 4.1. The complete set of equations for the Zero Order MFLG model, as defined by the relations in Table 4.1, are provided in reference [Kleintjens, 1979]. The corresponding equations for the First Order model are shown in Appendix B. The volume fractions (ϕ_i 's) can be related to quantities commonly measured during analysis of phase separation behavior, such as weight fraction (w_i) and solution density (ρ_{sol}), by equations (4-7)-(4-9):

$$\phi_1 = \frac{(1 - \phi_0)c_1 w_1}{c_1 w_1 + c_2 w_2} \tag{4-7}$$

$$\phi_2 = \frac{(1 - \phi_0)c_2w_2}{c_1w_1 + c_2w_2} \quad (4-8)$$

$$\rho_{sol} = \left(\frac{\phi_1}{c_1} + \frac{\phi_2}{c_2} \right) \frac{1}{v_0} \quad (4-9)$$

where the $c_i = m_i/M_i$.

Not all multi-phase situations can be described by the equations in Table 4.1. The determination of the binary parameters for the SO₂-polystyrene system (see Section 4.2), for example, was accomplished by fitting the model to vapor pressure suppression measurements of a constant composition solution (versus the pure solvent) at six temperatures. The appropriate model equations for this example are those which govern the "swelling binodal", or:

$$\mu_o^\circ = \mu_0^{sol} \quad (4-10)$$

$$\mu_1^\circ = \mu_1^{sol} \quad (4-11)$$

where the μ_i° and μ_i^{sol} are the chemical potentials of the holes and solvent segments in the pure gas and solution states, respectively. Equations (4-10) and (4-11), in conjunction with the binary EoS, are used to model not only the SO₂-PS system, but also the sorption of CO₂ by poly(methyl methacrylate) [PMMA] and polystyrene at high pressures (see Section 4.3). In the latter two cases, it is assumed that the dilute phase is essentially pure solvent (CO₂), thus permitting use of equations (4-10) and (4-11). The MFLG equations governing such "swelling binodal" situations, as defined by equations (4-10) and (4-11), are:

$$\begin{aligned}
\ln \frac{\phi'_0}{\phi_0} = & \Delta \left\{ \phi_1(1 - 1/m_1) + \phi_1^2 \alpha_1 + (\phi_1/Q^2) \beta_1(1 - \gamma_1)^2 \right\} \\
& + \phi_2(1 - 1/m_2) + \phi_2(\phi_1 + \phi_2) \alpha_2 \\
& + \phi_1 \phi_2 \left(\alpha_1 + \frac{\beta_1(1 - \gamma_1)(1 - \gamma_2)}{Q^2} \right) \\
& + \frac{\phi_2 \beta_2(1 - \gamma_2)(Q - \phi_0)}{Q^2} \\
& - \phi_1 \phi_2 \left(\alpha_m + \frac{\beta_m(1 - \gamma_1)(1 - \gamma_2)}{Q^2} \right)
\end{aligned} \tag{4-12}$$

and:

$$\begin{aligned}
\frac{1}{m_1} \ln \frac{\phi'_1}{\phi_1} = & \Delta \left\{ \phi_0(1/m_1 - 1) + \phi_0^2 \alpha_1 + (\phi_0/Q^2) \beta_1(1 - \gamma_1) \right\} \\
& + \phi_2(1/m_1 - 1/m_2) + \phi_2(\phi_0 + \phi_2) \alpha_m \\
& + \phi_0 \phi_2 \left(\alpha_1 + \frac{\beta_1(1 - \gamma_1)(1 - \gamma_2)}{Q^2} \right) \\
& + \frac{\phi_2 \beta_m(1 - \gamma_1)(1 - \gamma_2)(\phi_0 + \phi_2(1 - \gamma_2))}{Q^2}
\end{aligned} \tag{4-13}$$

where:

$$Q' = 1 - \gamma_1 \phi'_1$$

$$Q = 1 - \gamma_1 \phi_1 - \gamma_2 \phi_2$$

and $\Delta\{x\}$ refers to the difference in the value of x of the heavy and light phases, or $x - x'$. The corresponding equations for the First Order MFLG model are presented in Appendix B.

Table 4.1

Thermodynamic Relationships for Mixtures for the
Mean Field Lattice Gas (MFLG) Models

Binary Equation of State:

$$-p = \frac{1}{v_0} \left(\frac{\partial \Delta A}{\partial n_0} \right)_{T, n_1, n_2}$$

Binodal:

$$\mu_i = \mu'_i \quad i = 0, 1, 2$$

$$\mu_i = \left(\frac{\partial \Delta A}{\partial n_i} \right)_{T, n_j}$$

Spinodal:

$$J_{sp} = \begin{vmatrix} A_{11} & A_{12} \\ A_{21} & A_{22} \end{vmatrix} = A_{11}A_{22} - A_{12}A_{21} = 0$$

where:

$$A_{ij} = \frac{\partial^2 \Delta A}{\partial \phi_i \partial \phi_j}$$

Critical Condition:

$$\begin{pmatrix} \frac{\partial J_{sp}}{\partial \phi_1} & \frac{\partial J_{sp}}{\partial \phi_2} \\ A_{21} & A_{22} \end{pmatrix} = \begin{pmatrix} \frac{\partial J_{sp}}{\partial \phi_1} \end{pmatrix} A_{22} - \begin{pmatrix} \frac{\partial J_{sp}}{\partial \phi_2} \end{pmatrix} A_{21} = 0$$

4.2 Polymer-Liquid Mixtures

4.2.1 Polystyrene-Cyclohexane

Pure component parameters for cyclohexane were found by fitting the model unary equations to literature data [Kerns, *et al.*, 1974; Washburn, 1928; Young, 1910; Timmermans, 1965; Hales and Townsend, 1972]. The fitting results for the two models are shown in Figure 4.1 and in Tables 4.2 and 4.3. Binary parameters for the PS-cyclohexane system were found by fitting the Zero and First Order MFLG spinodal equations to data by Derham and coworkers [1974]. While solution densities are not reported by Derham, *et al.*, they can be calculated from the results of Scholte [1970], who made density measurements in the same temperature and concentration range as Derham's data. Some additional fitting was carried out using cloud point data by Saeki, *et al.* [1973].

The fit of the Zero Order MFLG model to the UCST-region data is very good, but deceiving (see Figure 4.2); subsequent prediction of the LCST-region spinodal for a 97200 MW polystyrene displays the proper shape but is located approximately 100K too low in temperature (see Figure 4.3). A second set of binary parameters was found using 10 cloud points (modelled as spinodal points) from both the UCST and LCST regimes. Whereas the predicted 97200 MW LCST-region spinodal is more accurate in temperature than the first attempt (Figure 4.3), the predicted shape of the curve is much poorer.

These results demonstrate the problems which are encountered when fitting mean field models to dilute polymer solution data. Such data reflect the contributions of segment-density fluctuations due both to the presence of a critical

point and to the isolated nature of polymer coils in dilute solution. Although the MFLG model does not contain an explicit dependence of the free energy on these segment density fluctuations, the results in Figure 4.2 show that the binary parameters g_{m0} and α_m can adequately compensate for this deficiency over small ranges in temperature. This compensation, however, comes at the expense of a reduced useful temperature range of the model, as seen in Figure 4.3. Non-mean field corrections to the MFLG model could come in the form of an expanded temperature dependence of the interaction parameter [Nies, *et al.*, 1985], a function which bridges the dilute and concentrated contact statistics [Koningsveld, *et al.*, 1974; Irvine and Gordon, 1980], or a contribution to the free energy which directly addresses the effect of the fluctuations [Edwards, 1966; Muthukumar, 1986].

The First Order model, which uses two binary parameters (z_m, g_{m1}) to three for the Zero Order MFLG (α_m, g_{m0}, g_{m1}), produces a poor description of the UCST-region spinodal data (see Figure 4.4). The two-parameter description apparently cannot effectively compensate for the lack of non-mean field contributions to the free energy in the dilute regime. Despite the less accurate predicted temperature dependence of the First Order model as compared to the Zero Order MFLG, it might be expected that the ϕ_0 dependence of the First Order model would be better than that of the parent model. Thus predictions of ΔV_m , the volume change on mixing, defined as:

$$\Delta V_m = V - x_1 V_1 - x_2 V_2 \quad (4 - 14)$$

were compared. Results (Figure 4.5) show that whereas the First Order model predicts the correct sign (negative), the dependence on weight fraction is grossly overestimated.

Table 4.2
Average Errors in Fitting MFLG Models to pVT Data
on Cyclohexane

Model	<u>VLE Data</u>				
	Number of of Points	Temp. (K)	Vapor Pressure-%	Vapor Density-%	Liquid Density-%
MFLG - Zero	19	1.2	1.0	1.2	2.5
- First	19	1.2	3.1	1.8	4.1

Model	<u>Critical Point</u>			<u>Equation of State</u>			
	Temp. (K)	Press. %	Dens. %	Number of Points	Press. %	Temp. (K)	Dens. %
MFLG - Zero	.9	8.2	5.6	56	.3	-	.3
- First	1.8	10.5	15.6	56	1.4	-	1.1

Table 4.3
Zero and First Order MFLG Parameters for Cyclohexane
as Determined by the PEP

Model	m_1	α_1	z_1	g_{10}	g_{11}	γ_1
MFLG - Zero	3.56	.91134	-	-.53522	369.02	-1.4931
- First	4.03	-	1.0645	-	967.5	.010157

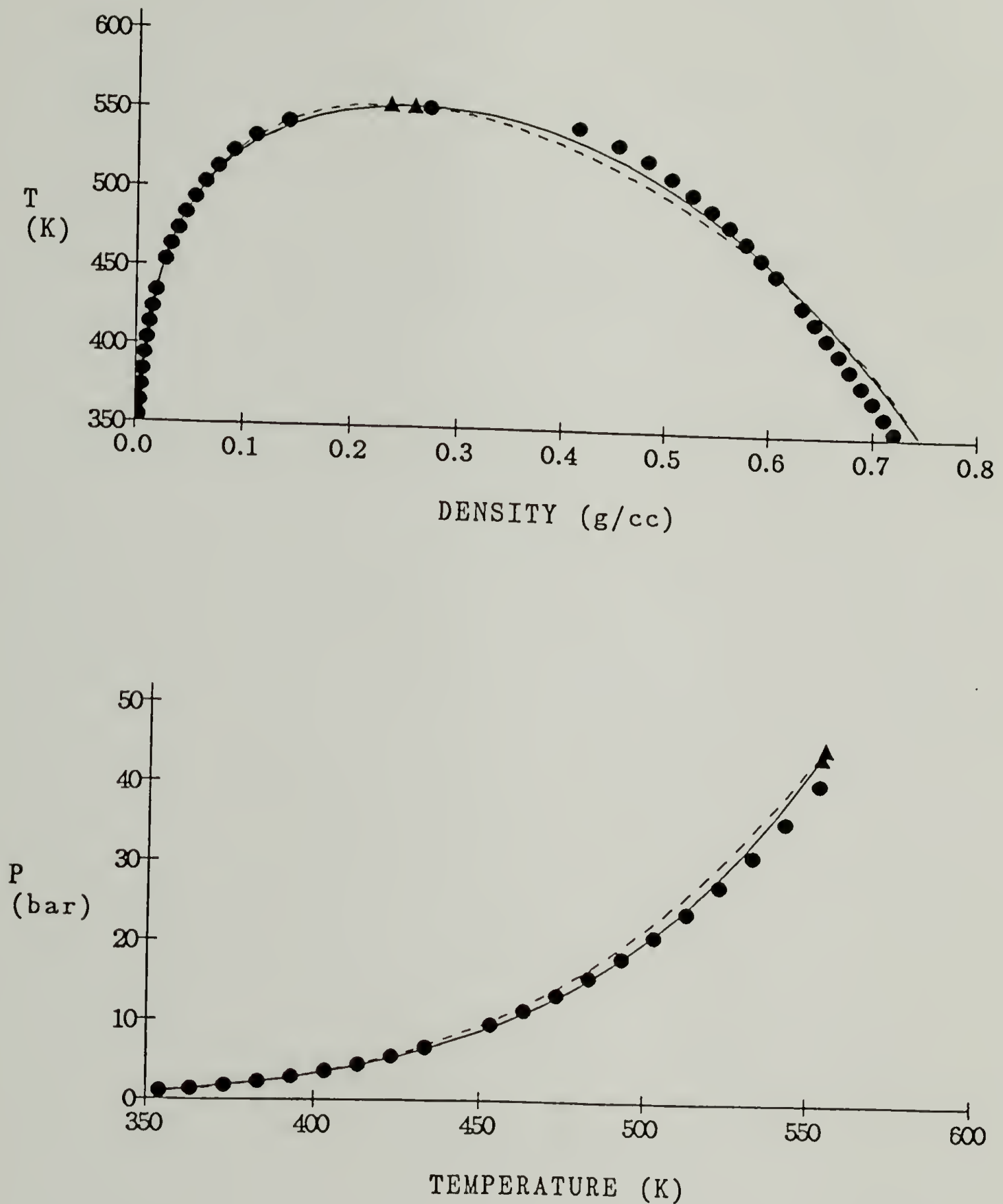


Figure 4.1

Cyclohexane pVT data (●) versus MFLG models' descriptions. (top graph) VLE data and description by Zero Order MFLG (—) and First Order MFLG (- - -) models. ▲'s are calculated critical points. (bottom graph) Vapor pressure versus temperature data and models' descriptions; symbols same as in top graph.

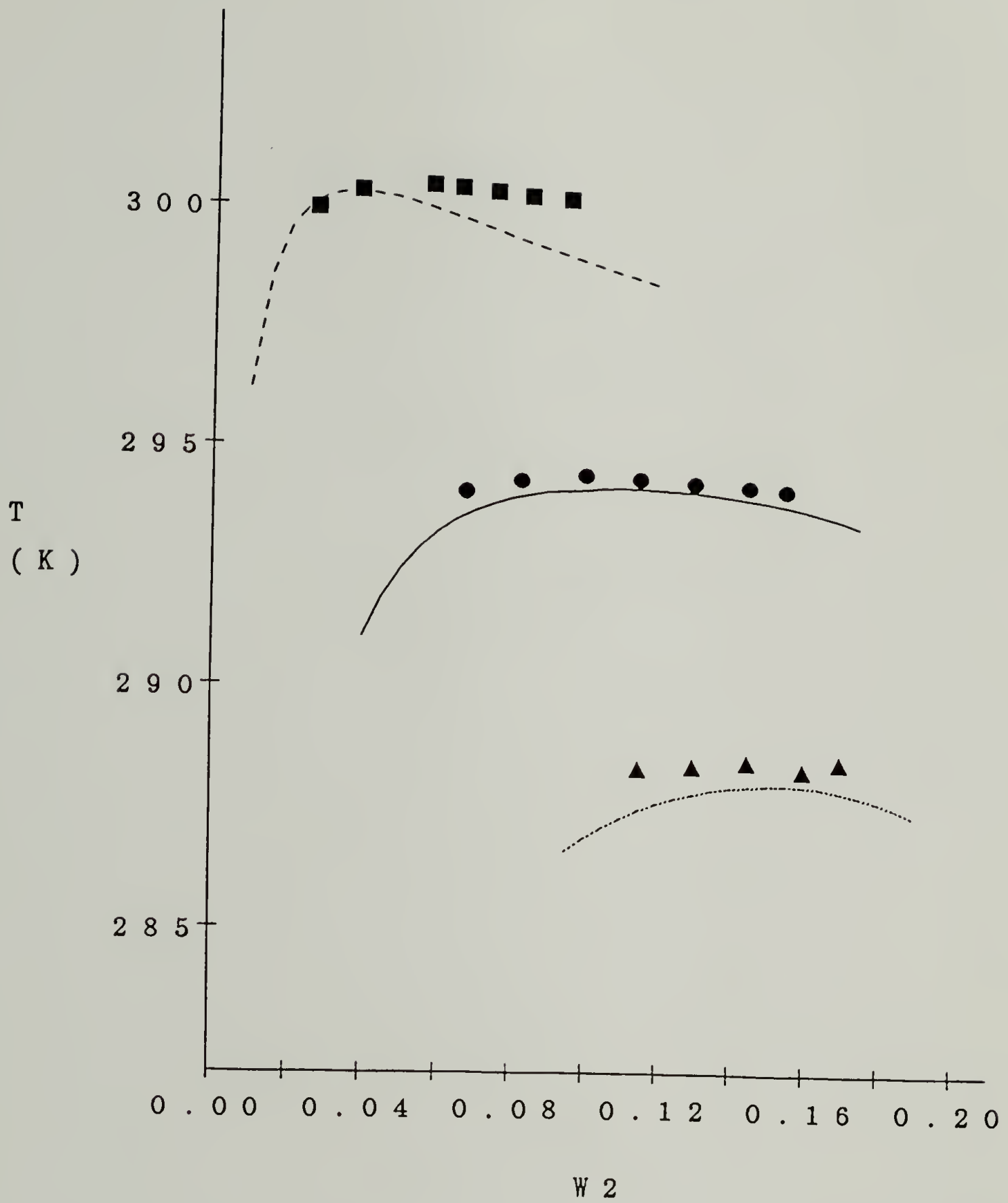


Figure 4.2

Polystyrene-Cyclohexane spinodal data (points) compared to Zero Order MFLG model description (curves) at three molecular weights (M_w 's): 527,000 (- - -), (\blacksquare); 111,000 (—), (\bullet); (51,000) (\cdots), (\blacktriangle).

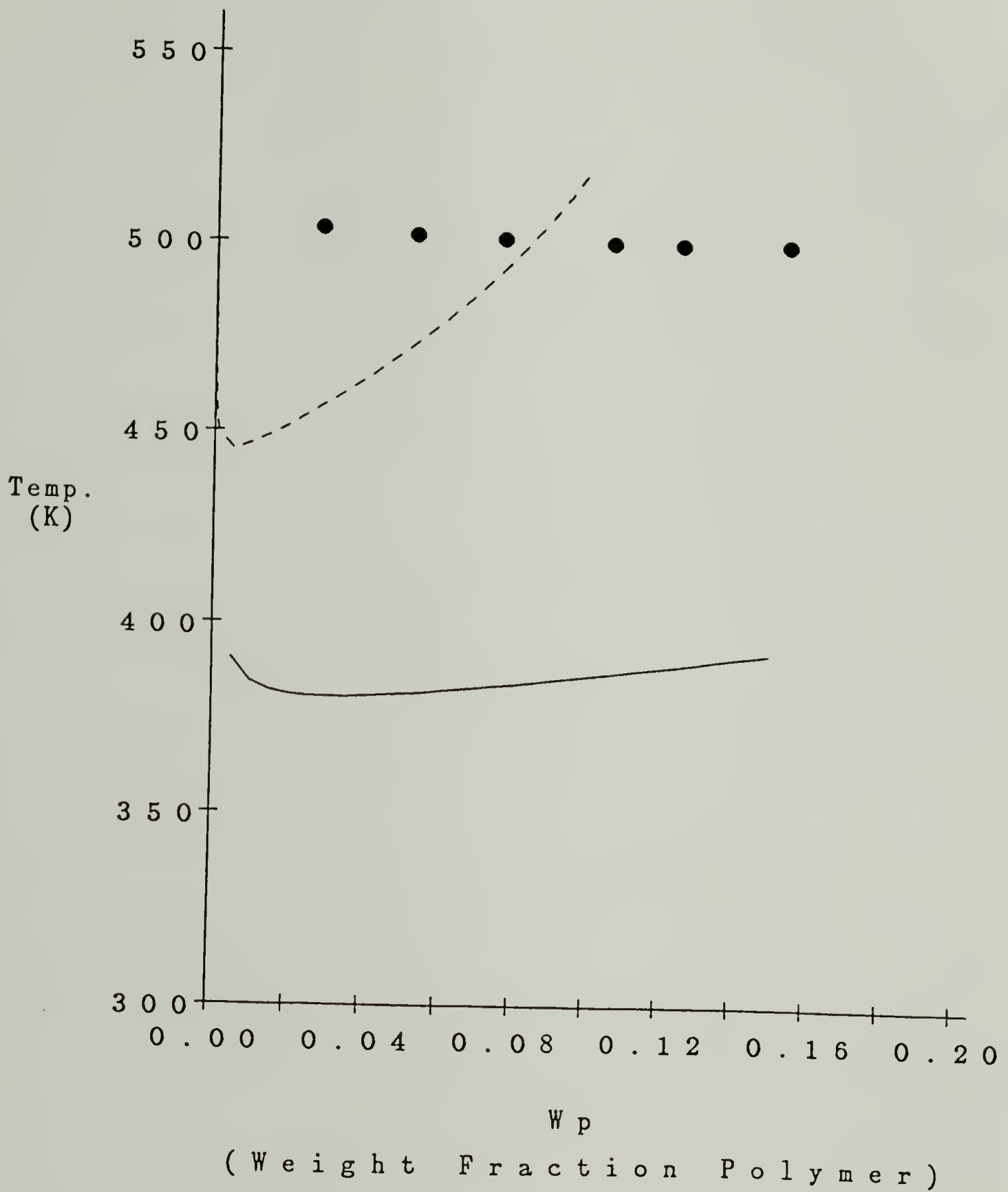


Figure 4.3

Predictions of the spinodal curve of a 97,200 MW polystyrene in cyclohexane using the Zero Order model, parameter set 1 (see text) [—]; and parameter set 2 [···]; compared to cloud point data (•).

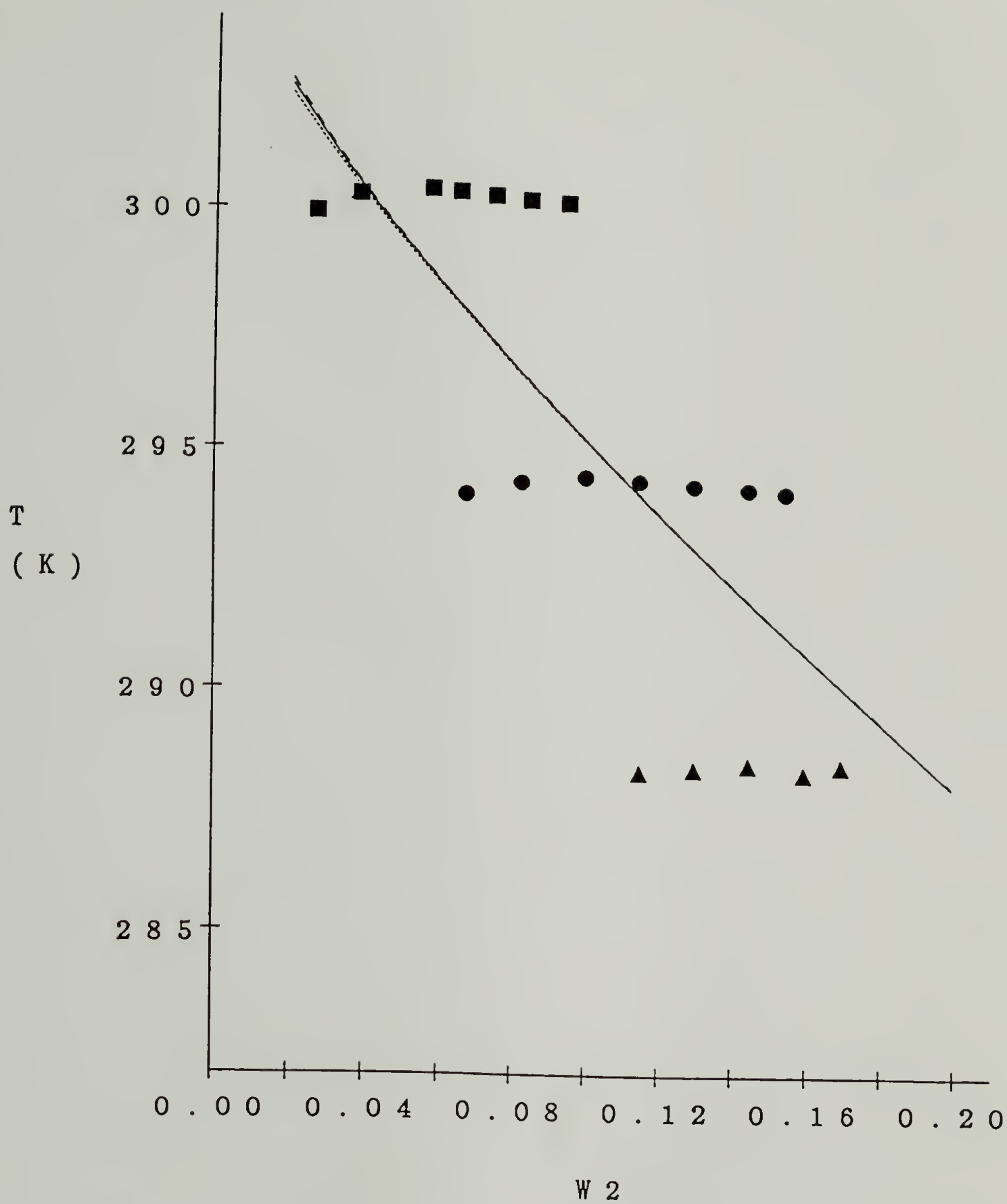


Figure 4.4

Fit of the First Order MFLG model (curves) to spinodal data (points) for polystyrene-cyclohexane system; symbols same as for Figure 4.2.

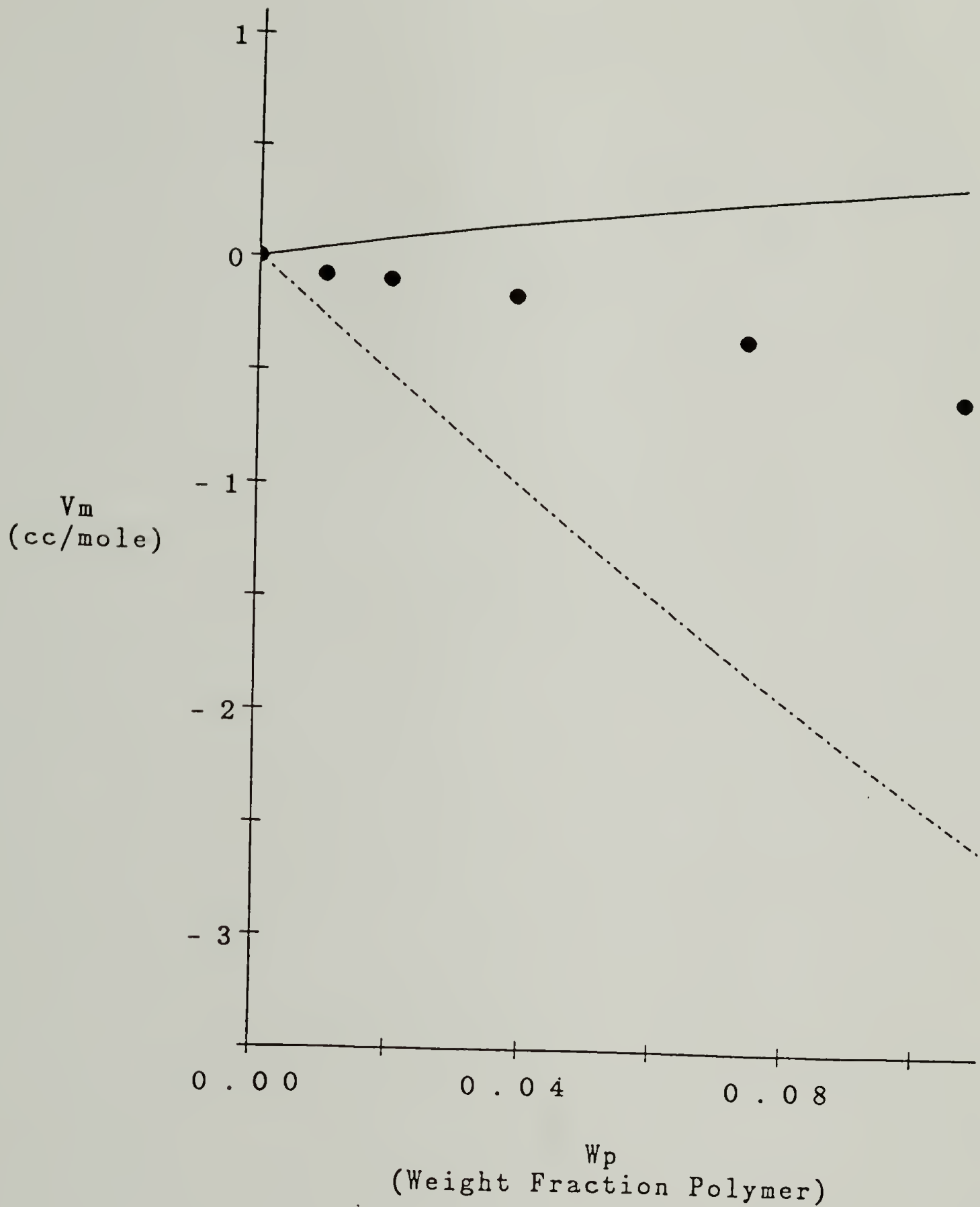


Figure 4.5

Prediction of the volume change on mixing of the polystyrene-cyclohexane system versus concentration by the Zero Order (—) and First Order (- - -) MFLG models compared to data derived from density measurements by Scholte [1970] (•).

4.2.2 Polystyrene-SO₂

Pure component parameters used for SO₂ and PS were those determined in Section 2.2. Binary parameters were determined by fitting the "swelling binodal" equations for the two models (see Section 4.1) to the vapor pressure suppression results of Albihn and coworkers [1979; 1981]. Albihn measured the difference in vapor pressure between a 64.8% solution of 2330 MW polystyrene and pure SO₂ at six temperatures between 240-300K. The fitting results are excellent for both models (Figure 4.6).

Albihn also measured the phase behavior of three higher molecular weight polystyrenes in SO₂ at 293K. These experiments consisted of immersion of an amount of polystyrene in SO₂ (1:5 by weight), prolonged shaking, and analysis of the composition of the two phases. Using the binary parameters found above, binodals and spinodals for the three cases were calculated. The binodal calculations assume the equilibrium of an essentially pure vapor phase with two liquid phases. Thus the situation can be described by the following equations:

$$\mu_0^V = \mu_0^{L_1} = \mu_0^{L_2} \quad (2 \text{ independent equations})$$

$$\mu_1^V = \mu_1^{L_1} = \mu_1^{L_2} \quad (2 \text{ independent equations})$$

$$\mu_2^{L_1} = \mu_2^{L_2} \quad (4 - 15)$$

$$-\frac{pv_0}{RT} = \mu_0^V$$

Therefore, given the temperature, there are six independent equations for the six unknowns: density of each phase (3), weight fraction polymer in each liquid phase (2), and the equilibrium pressure (1). The spinodal is represented by the appropriate equation from Table 4.1 and an equilibrium between holes and solvent segments in the vapor and metastable liquid phases.

Because Albihn used polystyrenes with broad molecular weight distributions, not surprisingly, phase separation in SO_2 segregated the polystyrene by molecular weight between the two phases. However, because initial molecular weight distribution curves were not available, the multi-component approach [Koningsveld and Staverman, 1967; Solc, 1970] to modelling phase separation behavior could not be used. Therefore the initial molecular weight averages were used to calculate the phase boundaries for the concentrated side of the diagram whereas the dilute solution molecular weight averages, as measured by Albihn, were used to predict the dilute phase boundaries. Results are shown in Figures 4.7 and 4.8.

The agreement between experiment and prediction is quite good, especially considering how few data were used in the fitting of the binary parameters. That the absolute value of the predicted spinodal composition at 293K is more accurate for the concentrated side of the diagram is not surprising; the dilute solution effect mentioned in Section 4.2.1 for the polystyrene-cyclohexane system holds true here as well. This effect can also be seen by examining the effective molecular weight cutoff (the point at which the polymer concentration drops below .0001%) in the dilute phase. The model predicts a cutoff at approximately 12,000 whereas the data show a cutoff nearer 50,000. However, because the model was fitted to concentrated regime data, where the mean field approximation is expected to be valid, the predicted temperature dependence of the phase diagram is better than that for polystyrene-cyclohexane. This accuracy is confirmed by Albihn, who noted that the two phases do not merge as the temperature is raised to the critical point and beyond. In addition, the predicted phase diagrams also confirm the observation that the composition of the dilute phase above the critical temperature drops below .1% even for oligomeric polystyrene (see Figure 4.8). Interestingly, the Flory-Huggins model, as applied

by Albihn to the vapor pressure suppression data, would predict an ovate-shaped phase diagram, contrary to the experimental observations.

Again, the First Order model produces a much poorer prediction of the phase behavior than the Zero Order MFLG (see Figure 4.9). The temperature dependence of the spinodals is opposite to that of both the Zero Order model and experimental observations.

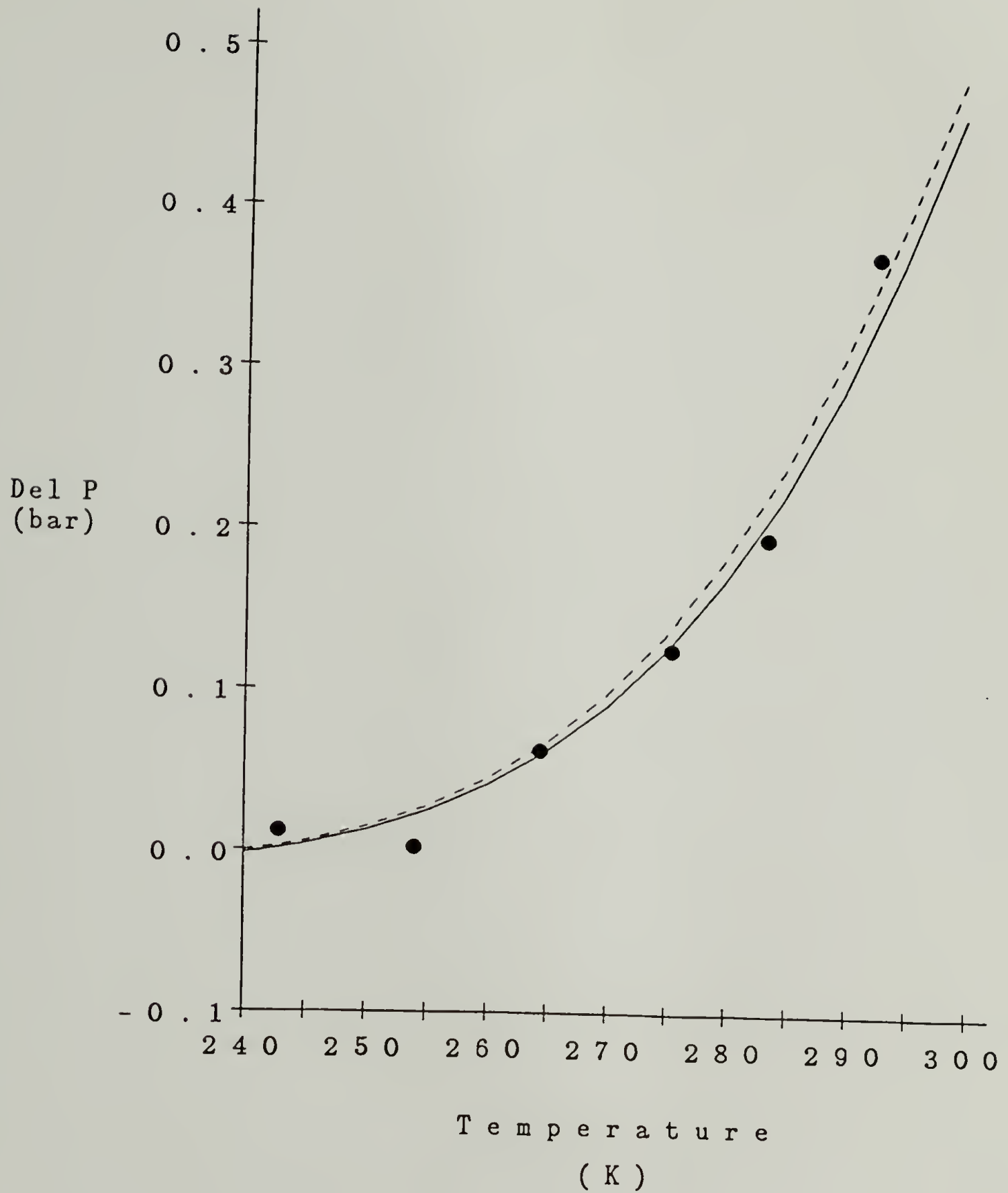


Figure 4.6

Vapor pressure suppression of a solution of 2330 MW polystyrene in liquid SO_2 (as compared to pure solvent) versus temperature. The fit of the Zero (—) and First Order (- - -) MFLG models is compared to data (•). [Albihn and Kubat, 1981]

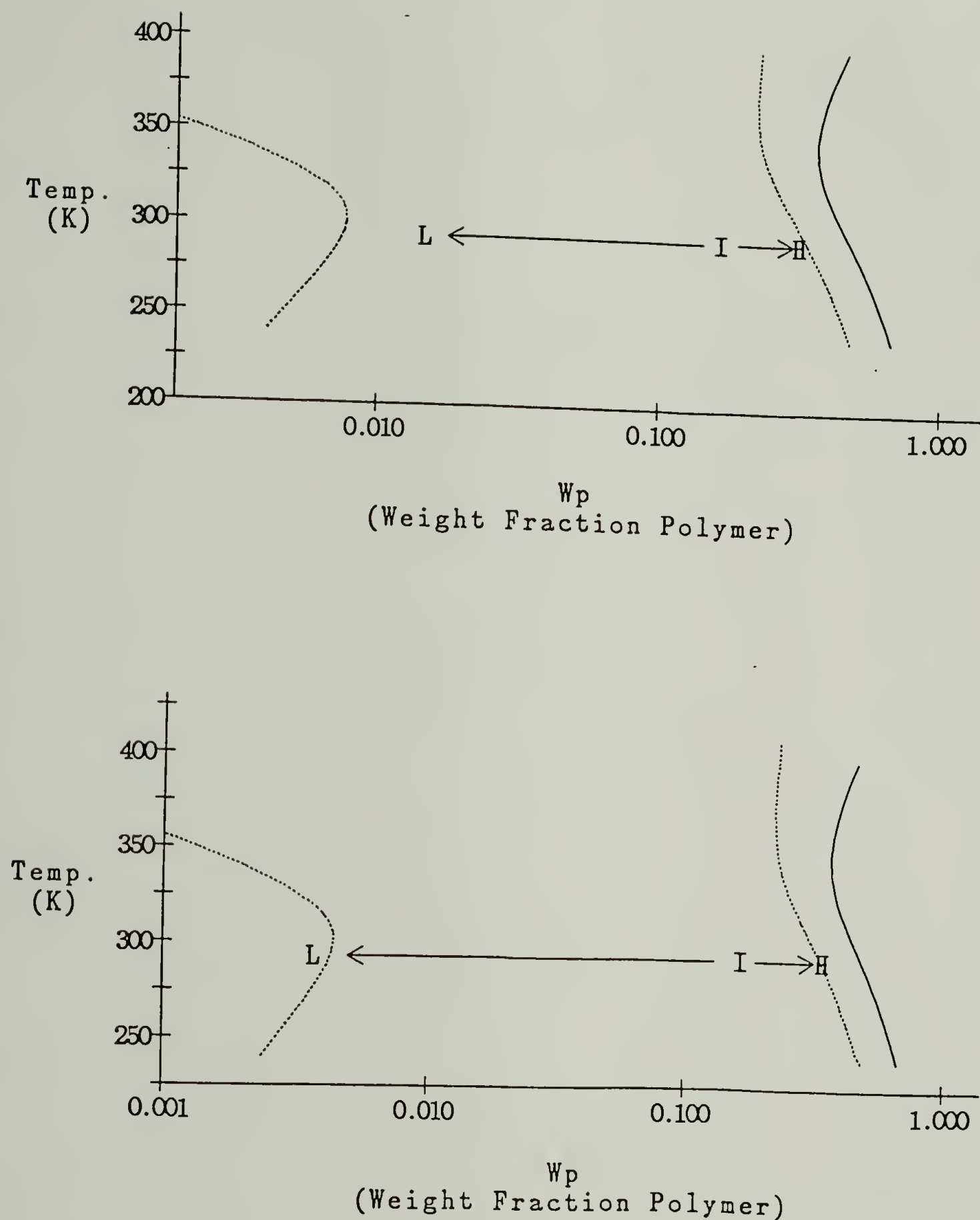


Figure 4.7

Predicted spinodals (\cdots) and binodals ($—$) by Zero Order MFLG model and phase separation results by Albihn and Kubat [1981]; initial concentration [I]; light [L] and heavy [H] phase concentrations after equilibration at 293.2K. Top graph; $M_n = 15,600$, $M_w = 35,400$. Bottom graph; $M_n = 66,700$, $M_w = 196,500$.

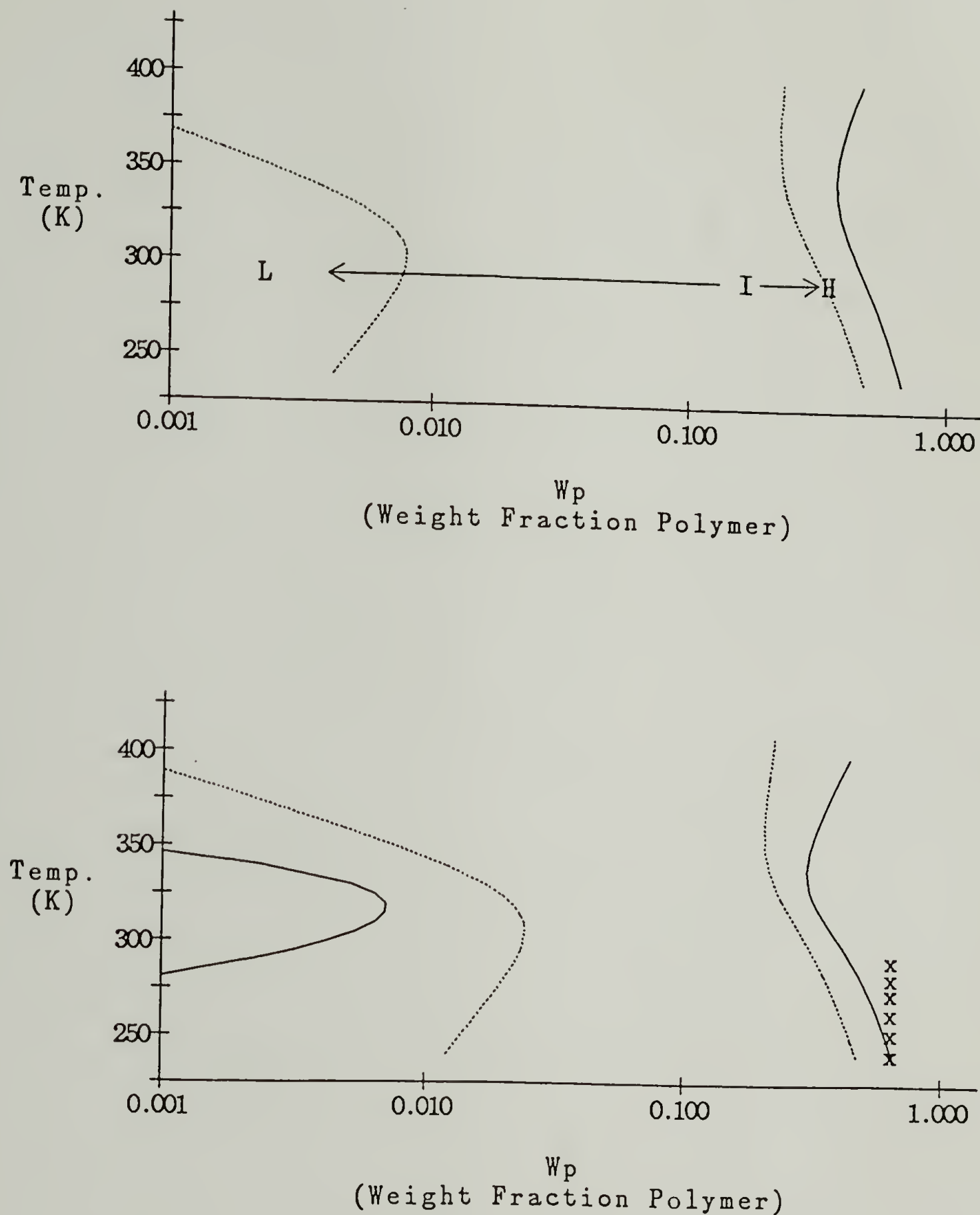


Figure 4.8

Predicted spinodals (\cdots) and binodals ($—$) by Zero Order MFLG model and phase separation results by Albihn and Kubat [1981]; symbols same as in Figure 4.7. Top graph; $M_n = 136,000$, $M_w = 402,000$. Bottom graph; $M_n = 2330$, $M_w = 3650$ (projected phase diagram of material used during fitting, x 's are temperature-composition locations of points used).

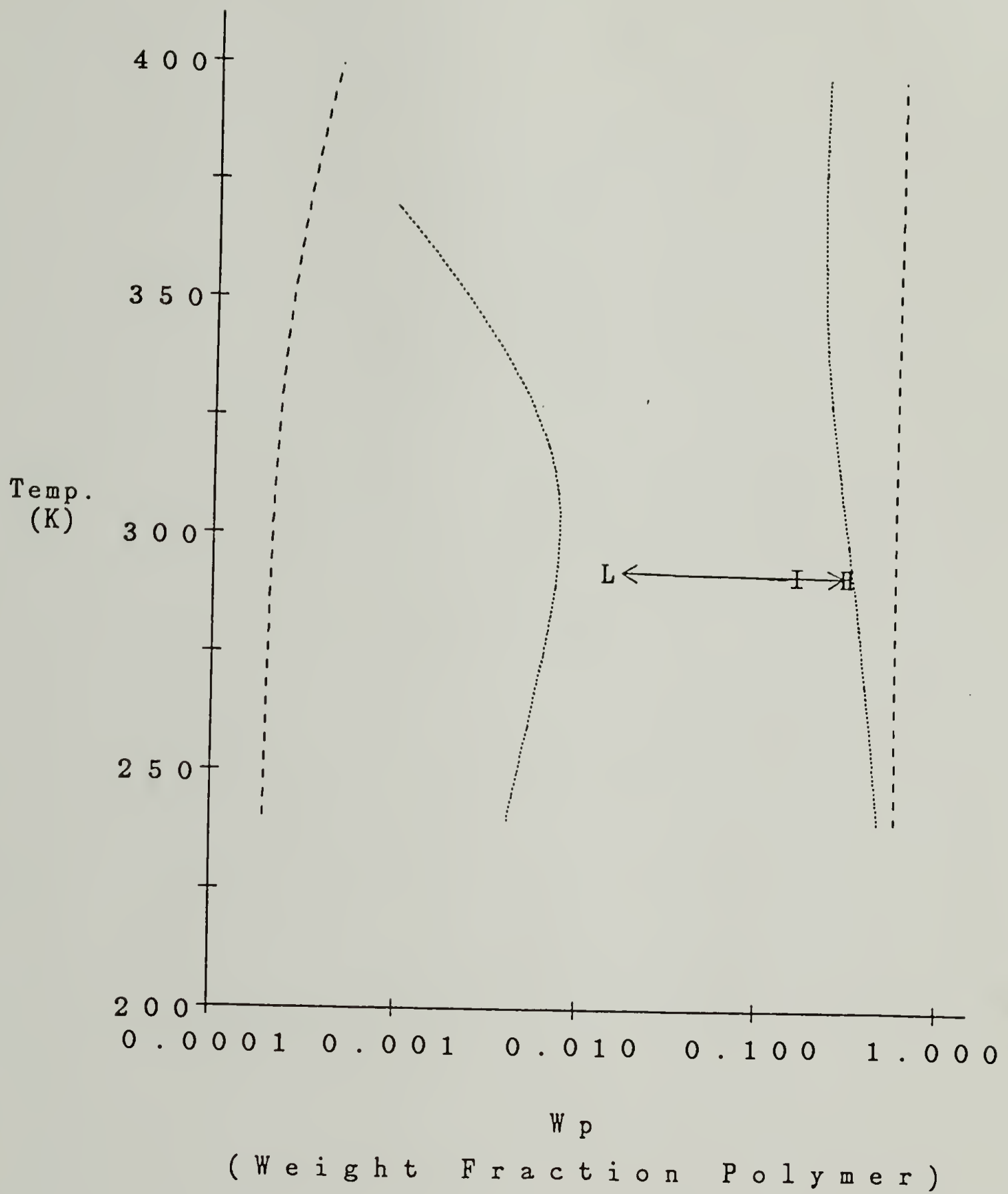


Figure 4.9

Predicted spinodals for Zero (\cdots) and First Order ($- - -$) MFLG models and phase separation results by Albihn and Kubat [1981]; symbols same as in Figure 4.7. Molecular weights are same as for top panel of Figure 4.7.

4.2.3 Summary of Section 4.2

The breakdown of the mean field approximation in the very dilute region causes significant problems if binary parameters for the MFLG models are found via use of data from this region. The use of the three binary parameters in the Zero Order model partially compensates for the dilute solution problem over small temperature ranges, but phase behavior predictions at temperatures outside the fitting range cannot be made with confidence. The MFLG models perform much better using parameters found with concentrated solution data. While subsequent predictions of dilute phase behavior will still generally underestimate the equilibrium concentration (by overestimating the number of polymer-solvent contacts), the predicted temperature dependence and shape of the phase diagrams will be more accurate.

The prediction of phase separation behavior by the Zero Order MFLG is significantly more accurate than that of the First Order model. The two-binary-parameter description of the First Order model does not produce the proper temperature dependence of the phase diagrams, although the volume change on mixing prediction is somewhat improved. Apparently, though the First Order model properly describes the ϕ_0 dependence of the empirical parameters α_1 and g_{10} , more work needs to be done on the temperature dependence of these parameters. Therefore, the prediction of the phase behavior of polymer-gas mixtures will be handled using the Zero Order model alone.

4.3 Phase Behavior of Polymer-Gas Mixtures

4.3.1 Experimental

Solubility of PMMA and PS in supercritical CO₂ was measured using a Fluitron Supercritical Extraction Unit (Fluitron, Inc., Ivyland, PA), a flow diagram of which is shown in Figure 4.10. Approximately 2-3 grams of polymer is suspended in the flow-through column in a porous, cellulose Soxhlet extraction thimble. Gas is charged to the column to the required pressure after which the system is allowed to equilibrate for approximately three hours. During this time the pressure and temperature can be maintained to within ± 50 psi and $\pm .5$ K, respectively. The extraction unit is rated for use at pressures up to 30,000 psi and temperatures to 150C. Following equilibration, the compressor is reactivated followed by the opening of the heated metering valve. The higher the run pressure, the higher the metering valve must be heated to insure freedom from Joule-Thompson icing and therefore a smooth and steady gas flow to the collection vessel. As the gas expands through the metering valve, the polymer drops out of solution and is recovered in the collection vessel, which contains an organic solvent which is known to readily dissolve the polymer under study (Toluene was used in both cases). Use of the organic solvent facilitates removal of the solute from the collection vessel. A run is continued until approximately the equivalent of approximately 300 cc (3 times the column volume) has been extracted. The metering valve is then closed and the column maintained at the run pressure while the toluene solution is removed from the collection vessel. Following this transfer, the toluene is removed by evaporation and vacuum treatment and the amount of solute is measured gravimetrically. Blank runs involving only the toluene were made in order that impurities in the solvent

not be mistaken for dissolved polymer. The volume of the gas expended during the run is recorded by the totalizer, and is converted to a weight basis using the literature value for the density (The totalizer has been calibrated against the flow meter and flow sensor such that 1 count equals 50cc of CO₂ at room temperature and pressure). Two runs are made consecutively and the solubility is taken to be the total amount of solute extracted over the 2 runs divided by the total amount of gas expended during those runs.

Narrow molecular weight polystyrene and poly(methyl methacrylate) standards were obtained from Pressure Chemical Co., Pittsburgh PA. Nominal molecular weights are 2000 for the polystyrene ($M_w/M_n \leq 1.06$) and 7000 and 24300 for the PMMA's ($M_w/M_n = 1.15, 1.10$, respectively). Linde Bone Dry CO₂, obtained from Merriam-Graves Corp., West Springfield, MA, and Fisher Scientific Spectro-Grade Toluene (T-330), were used as received. Although the polymers used have narrow molecular weight distributions, extracted polymer was continually re-combined with material left in the column after a pair of runs to avoid molecular weight stripping and consequently biased results.

Errors in the solubility come mainly from two sources, both random in nature. Errors in weighing will be approximately $\pm 4\%$. Temperature fluctuations in the room will lead to errors in the density assumed for CO₂ in the collection vessel. These errors will also be approximately 4% or less. Thus the solubility measurements should be assumed to be $\pm 8 - 9\%$. Indeed, measurements of the solubility of the 2000 MW PS in CO₂ at 40C are 5-10% lower than the measurements of Bowman [1976].

4.3.2 Poly(Methyl Methacrylate)-CO₂

Pure component MFLG parameters for CO₂ were determined in Section 2.3. Pure component parameters for poly(methyl methacrylate) [PMMA] were determined by fitting the MFLG equation of state to pVT data by Olabisi and Simha [1975]. Because data on only one molecular weight species is available in the literature, only one constraining equation (see Section 2.3.1) could be used to fix the parameters, resulting in a high degree of correlation between the α_1 , g_{10} , and γ_1 parameters. Consequently the value of γ_1 for PMMA was linked to the number of segments per monomer, m , and the corresponding polystyrene values via the following:

$$\frac{(1 - \gamma_{PMMA})m_{PMMA}}{(1 - \gamma_{PS})m_{PS}} = \text{Bondi monomer surface ratio} \quad (4 - 16)$$

The values of the parameters for PMMA are shown in Table 4.3. Average error in calculated density for the 40 data points is .03%.

The sorption behavior of CO₂ by atactic PMMA has been reported by Liau and McHugh [1985]. Liau measured the volume change of the polymer upon swelling by the gas, as well as the equilibrium weight fraction CO₂ absorbed, at three temperatures over an extensive range in pressure. The volume change on mixing can be calculated from the combination of the swelling and sorption results using:

$$\Delta V_m = \frac{\left(\frac{S}{\rho_p} - \left(\frac{1-w_p}{w_p} \right) \frac{1}{\rho_{CO_2}} \right)}{\frac{1}{M_p} + \left(\frac{1-w_p}{w_p} \right) \frac{1}{M_{CO_2}}} \quad (4 - 17)$$

where S is the fractional increase in volume upon swelling, the ρ_i and M_i are the densities and molecular weights of the gas and polymer, and w_p is the weight fraction polymer. The derivation of equation (4-17) is shown in Appendix C.

The sorption data were fitted to the "swelling binodal" equations (equations (4-12) and (4-13)) to determine the binary parameters, which are shown in Table (4-3). The literature and calculated isotherms are compared in Figures 4.11 – 4.13. Significantly, the model correctly predicts that the isotherms will intersect, a phenomenon observed in many gas-polymer mixtures [Lundberg, *et al.*, 1969; Maloney and Prausnitz, 1976]. The average error in the predicted weight fraction over all three isotherms is 1.6%.

The ΔV_m 's derived from Liao's measurements using equation (4-17) and those predicted by the MFLG model are compared in Figure 4.14. Although the form of the model description is correct, the absolute values of the predicted ΔV_m 's are too low, particularly at higher pressures. This is a result of both an overestimation of the pure CO₂ density Figure 4.15 and an overestimation of the change in volume change upon swelling of the PMMA.

To test the useful temperature range of the model, predictions of sorption of CO₂ by PMMA using the binary parameters found above were made at $T = 461.53K$ and $T = 298.2K$ and compared to measurements by Durrill and Griskey [1966], and Berens [1987].

The experimental data at 461.53K are in the form of a Henry's Law constant, which is the slope of the sorption-pressure curve at low pressures, and is given in units of ($cc(STP)/g PMMA$). Therefore, to compare the model prediction with the experimental result, equations (4-12) and (4-13) and the model parameters from Table 4.2 were used to calculate sorption versus pressure (up

to 20 bar) at $T = 461.53K$. The results were converted to a $cc(STP)$ versus $g PMMA$ basis and then linearized using a standard regression procedure to find the slope. The calculated result, .326, is greater than the experimental value of .260, but the agreement is reasonable considering the high temperature at which the prediction was made.

Berens measured the sorption by PMMA of liquid CO_2 at its vapor pressure at $298K$. Prediction of sorption under these conditions requires the solution of equations for three phase equilibrium (liquid-liquid-vapor), or:

$$\mu_0^V = \mu_0^L = \mu_0^P \quad (2 \text{ independent equations}) \quad (4 - 18)$$

$$\mu_1^V = \mu_1^L = \mu_1^P \quad (2 \text{ independent equations}) \quad (4 - 19)$$

$$\frac{-pv_0}{RT} = \frac{\mu_0^V}{RT} \quad (4 - 20)$$

where the μ_i^j are the chemical potentials of the holes and CO_2 segments in the vapor, liquid, and swollen polymer phases. Thus there are five independent equations for the five unknowns; pressure, CO_2 liquid and vapor densities, weight fraction CO_2 absorbed by the polymer, and the density of the swollen polymer phase. The calculated result, $25.6 (g CO_2/g PMMA)$, is within experimental error of the measured value, $27.0 \pm 2.0 (g CO_2/g PMMA)$.

The binodal and spinodal equations, in conjunction with the equation of state, were used to predict the phase behavior of dilute solutions of PMMA in CO_2 , given the binary parameters found above. Results are shown in Figures 4.16 - 4.19 (The binodal at $M = 24,300$, $T = 313.2K$ is predicted to lie at concentrations less than $1.E-08$ and therefore does not appear in the figures). Because the binodal is often associated with the cloud point curve, and because the spinodal is a meta-stable condition, it is expected that the solubility would fall between the two yet generally follow the course of the binodal. Assuming this, though the dependence of the solubility on pressure, temperature

and molecular weight are all described correctly, the model underpredicts the solubility in each case.

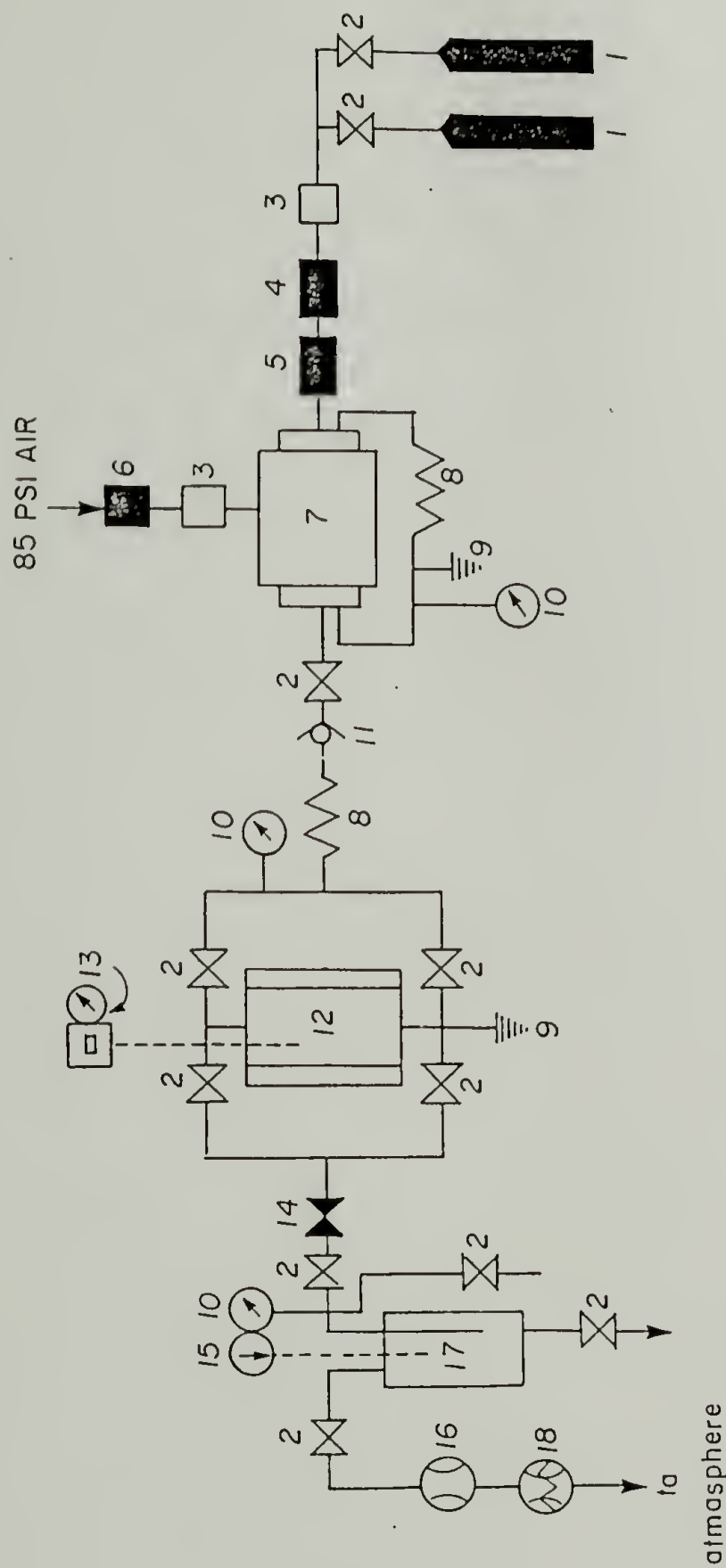
The underprediction of the binodals is due to several factors. First, in the determination of the adjustable parameters using Liao's sorption data, it was assumed that the light phase during equilibrium swelling of the 33,200 MW PMMA was essentially pure CO_2 . Based on the experimental solubility results using the 24,300 MW PMMA, this may not be so. Second, as mentioned previously, mean field models do not account for the large fluctuations in monomer segment density in dilute polymer solutions (due to the isolated nature of the individual polymer coils) and consequently do not usually predict dilute polymer solution data accurately. Finally, that the binodal curve is too "sharp" at high pressure is partially due to errors in the prediction of the volume of mixing at higher pressure.

Table 4.4

MFLG Material Parameters for Poly(methyl methacrylate) and Carbon Dioxide and for the PMMA-CO₂ Mixture

Parameter	CO ₂	Zero Order Model	
		PMMA	PMMA-CO ₂
m	1.31	3.13*	—
α	.91498	-9.0493	—
g_{10}	-1.1445	6.1068	—
g_{11}	519.82	1361.0	—
γ	-1.2010	-1.286	—
α_m	—	—	4.2339
g_{m0}	—	—	-1.7716
g_{m1}	—	—	87.572

* segments per monomer unit



- | | | | | | |
|---|----------------------------|----|---------------------------------------|----|------------------------|
| 1 | Gas cylinders | 7 | Compressor | 13 | Temperature controller |
| 2 | Manual valves | 8 | Heat exchanger | 14 | Metering valves |
| 3 | Regulator | 9 | Rupture disc | 15 | Temperature readout |
| 4 | Filter, molecular sieve | 10 | Pressure gauge | 16 | Flow meter |
| 5 | Filter, activated charcoal | 11 | Check valve | 17 | Separation valve |
| 6 | Filter, mesh | 12 | Extraction column with heating jacket | 18 | Flow totalizer |

Figure 4.10

Fluitron Supercritical Extraction Unit

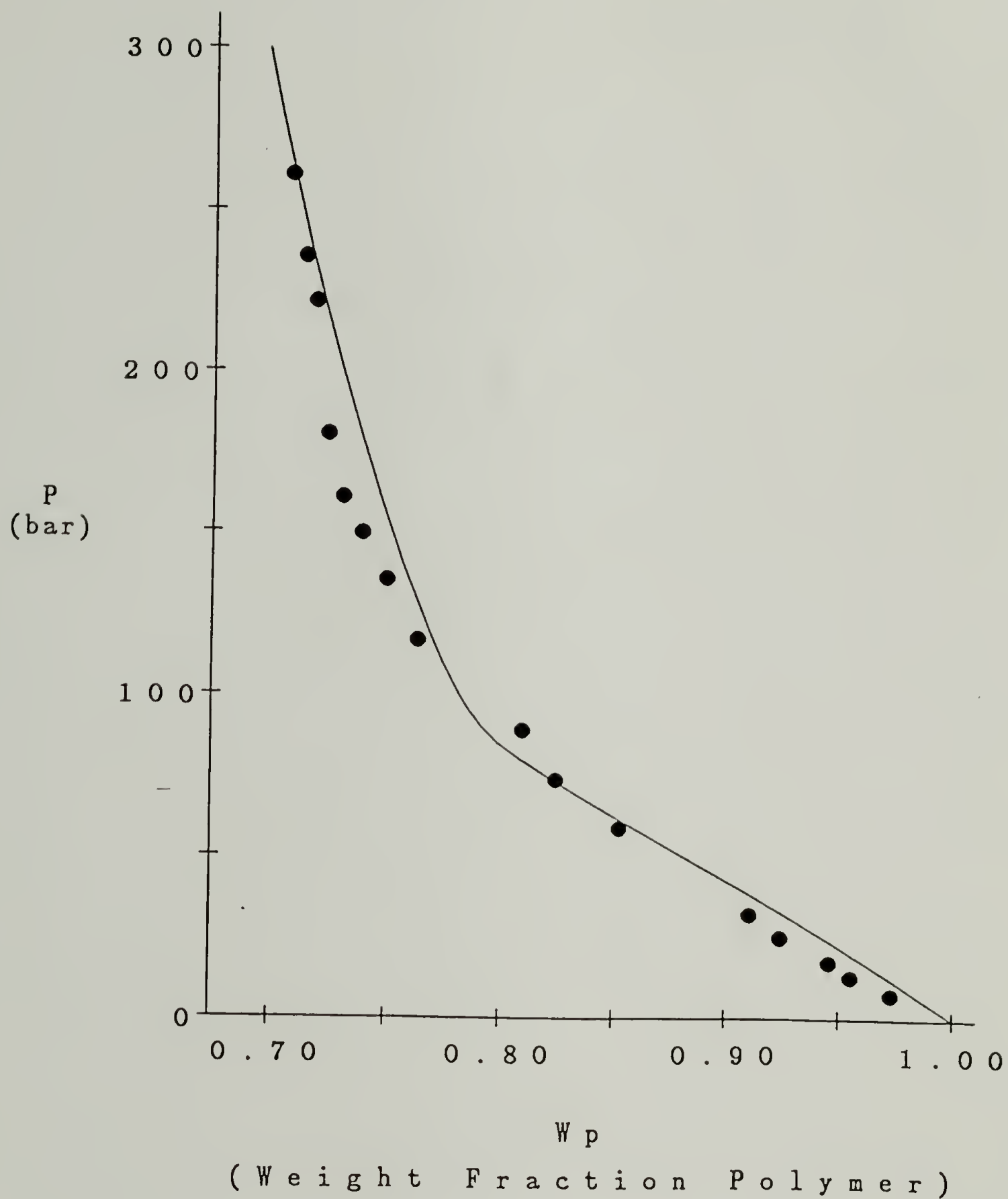


Figure 4.11

Fit of the Zero Order MFLG model "swelling binodal" equations (—) to PMMA-CO₂ sorption data (•) at 315K by Liao and McHugh [1985].

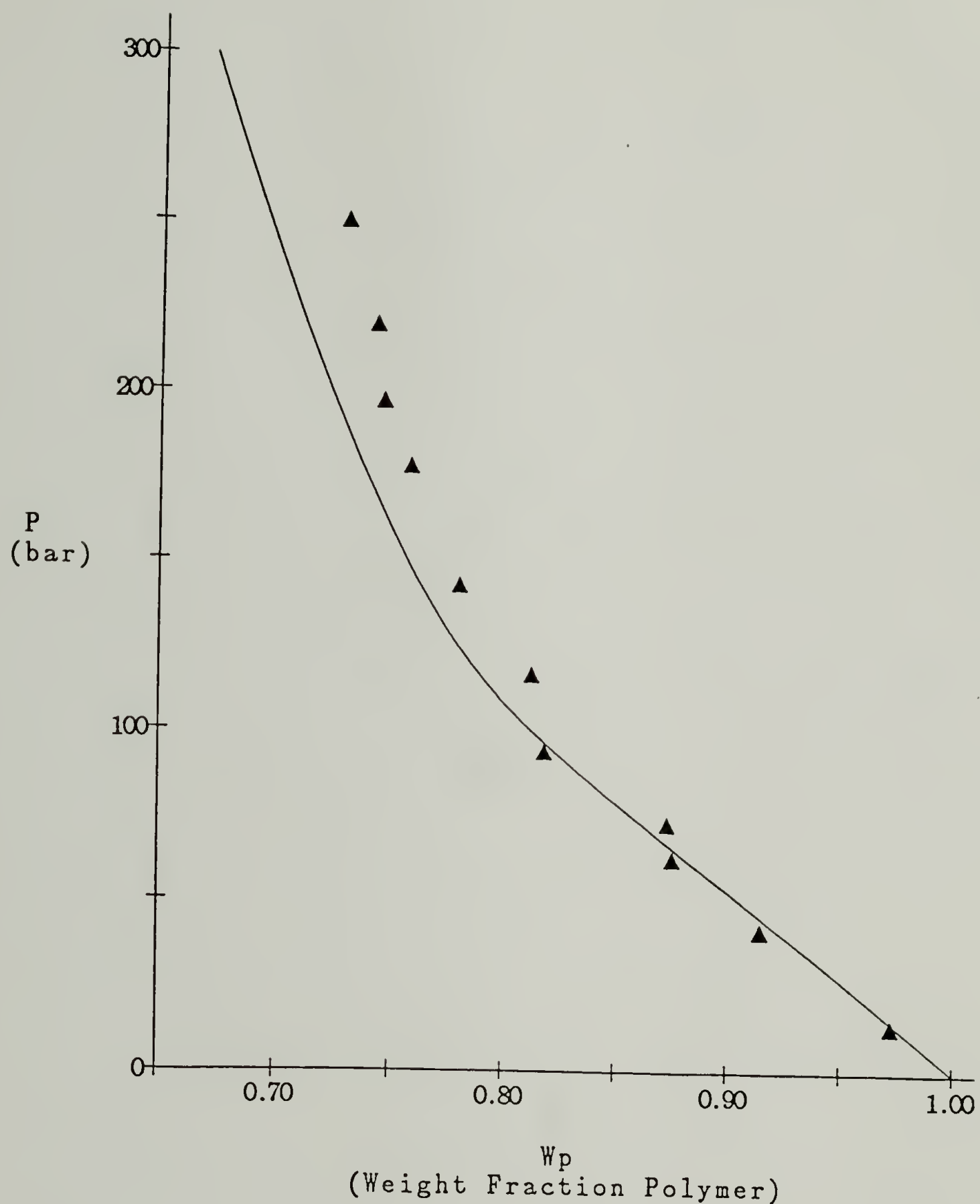


Figure 4.12

Fit of the Zero Order MFLG model "swelling binodal" equations to PMMA-CO₂ sorption data at 331.3K by Liau and McHugh [1985]; symbols same as in Figure 4.11.

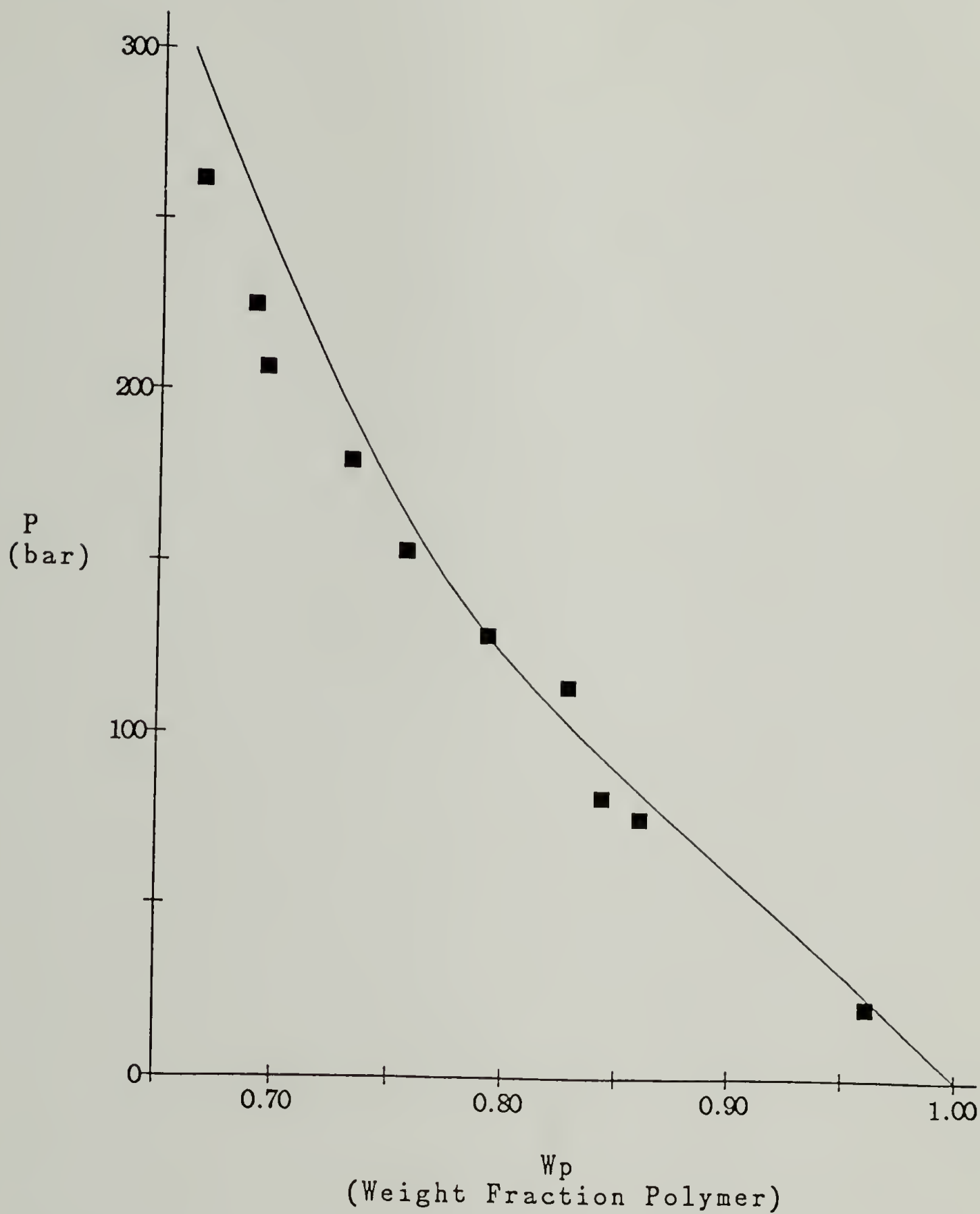


Figure 4.13

Fit of the Zero Order MFLG model "swelling binodal" equations to PMMA-CO₂ sorption data at 341.2K by Liao and McHugh [1985]; symbols same as in Figure 4.11.

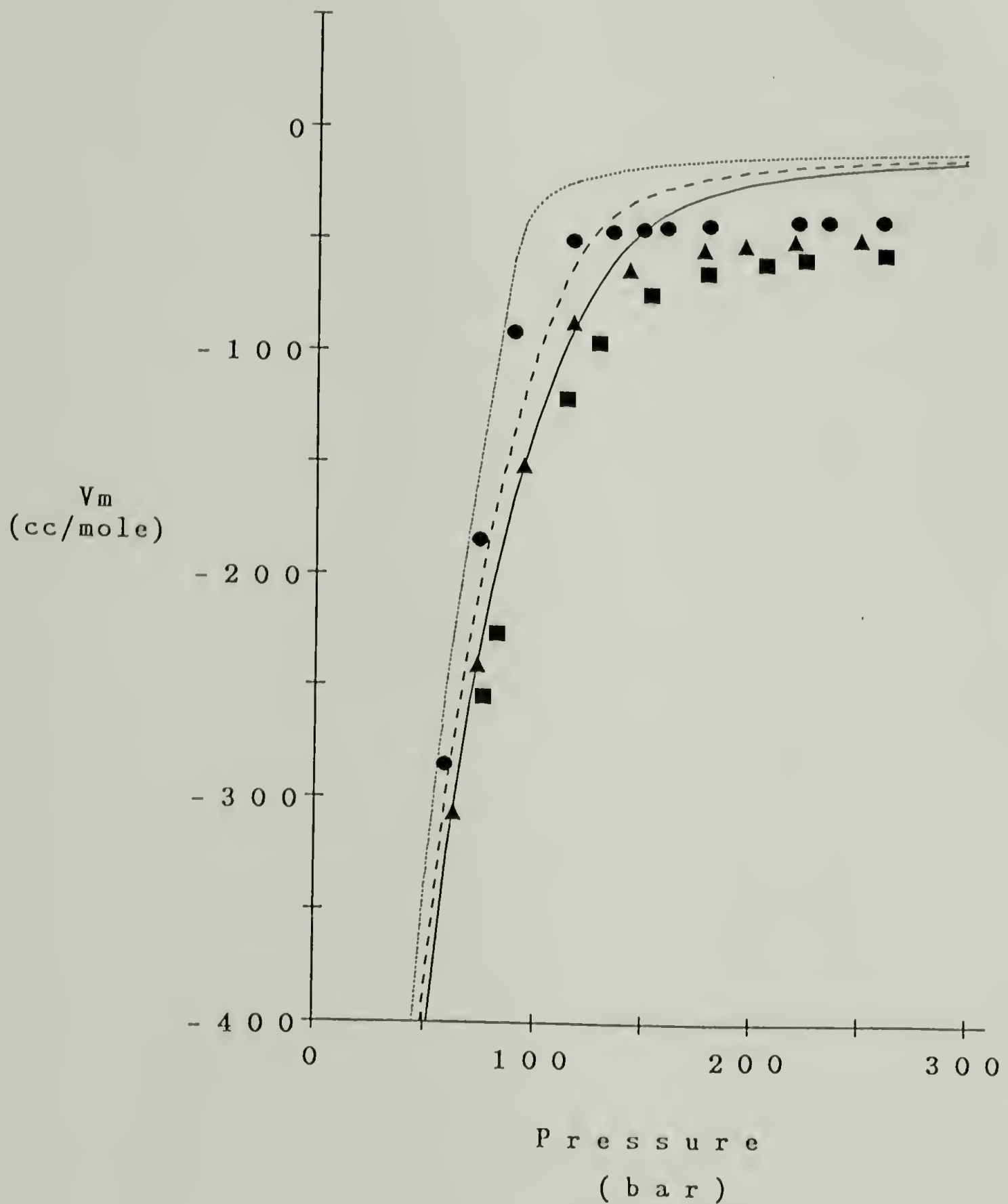


Figure 4.14

Prediction of the volume change on mixing of the PMMA-CO₂ mixture versus pressure by the Zero Order MFLG model (curves) compared to values calculated from swelling data (points) by Liau and McHugh [1985] at three temperatures: $T = 315K$, (—), (•); $T = 331.3K$, (- - -), (▲); $T = 341.2$, (···), (■).

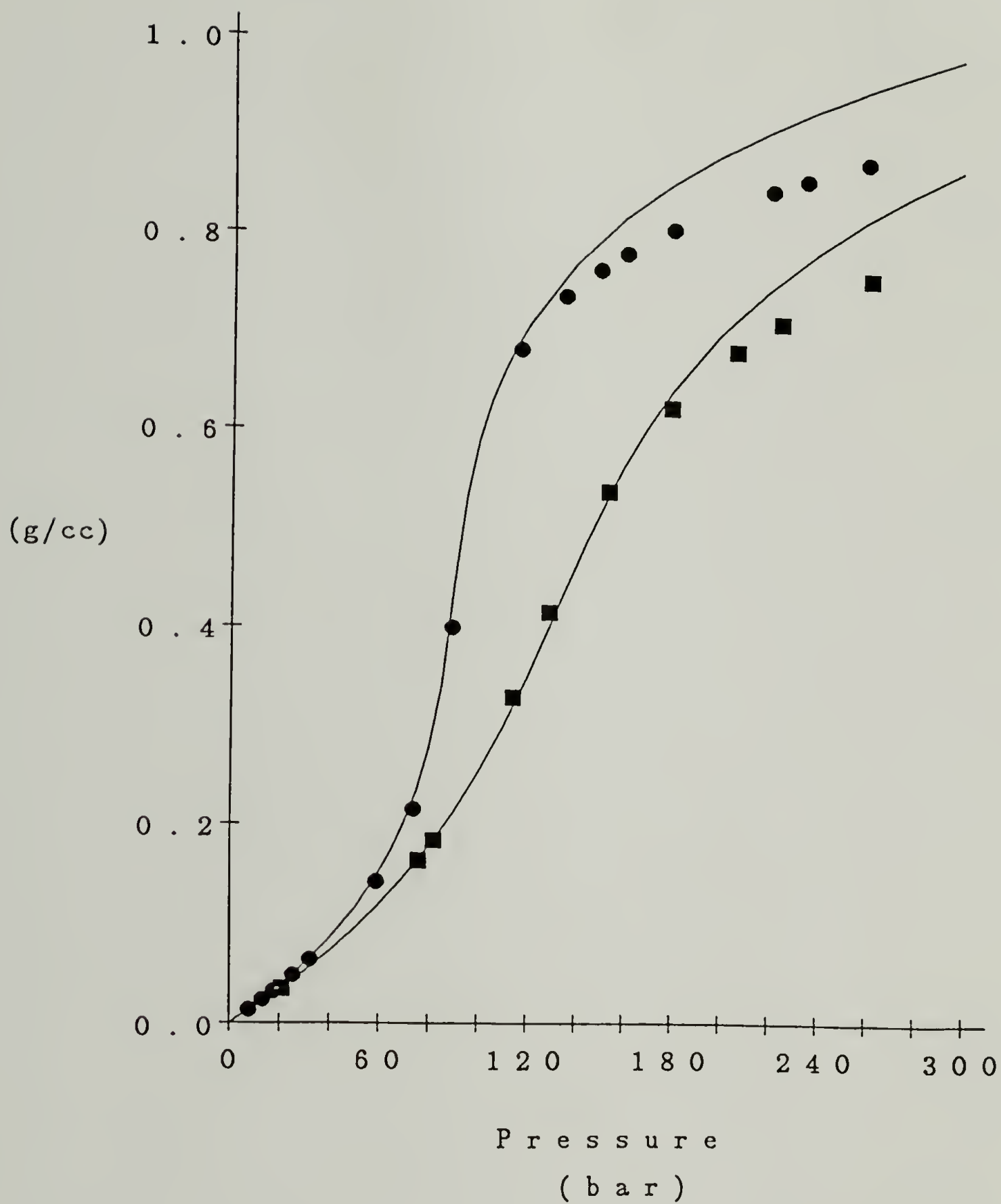


Figure 4.15

Prediction (curves) of the density of CO₂ versus literature data [Reynolds, 1979] (points) at two temperatures: $T = 315K$; (\bullet), (—); $T = 341.2K$; (\blacksquare) (- - -).

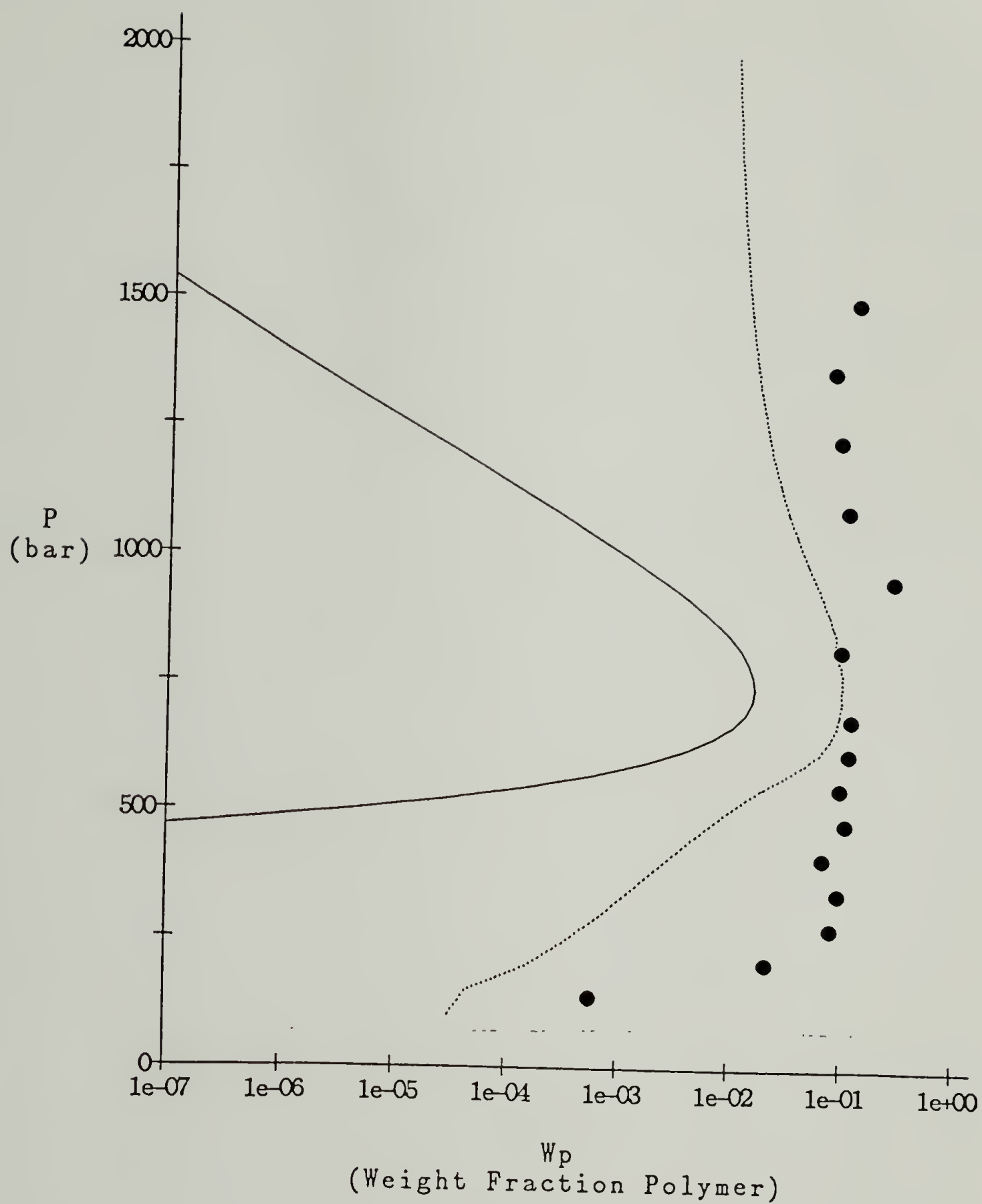


Figure 4.16

Solubility measurements of 7000 MW PMMA in CO_2 versus pressure at 313K (•) compared to binodal (—) and spinodal (- - -) predictions by the Zero Order MFLG model.

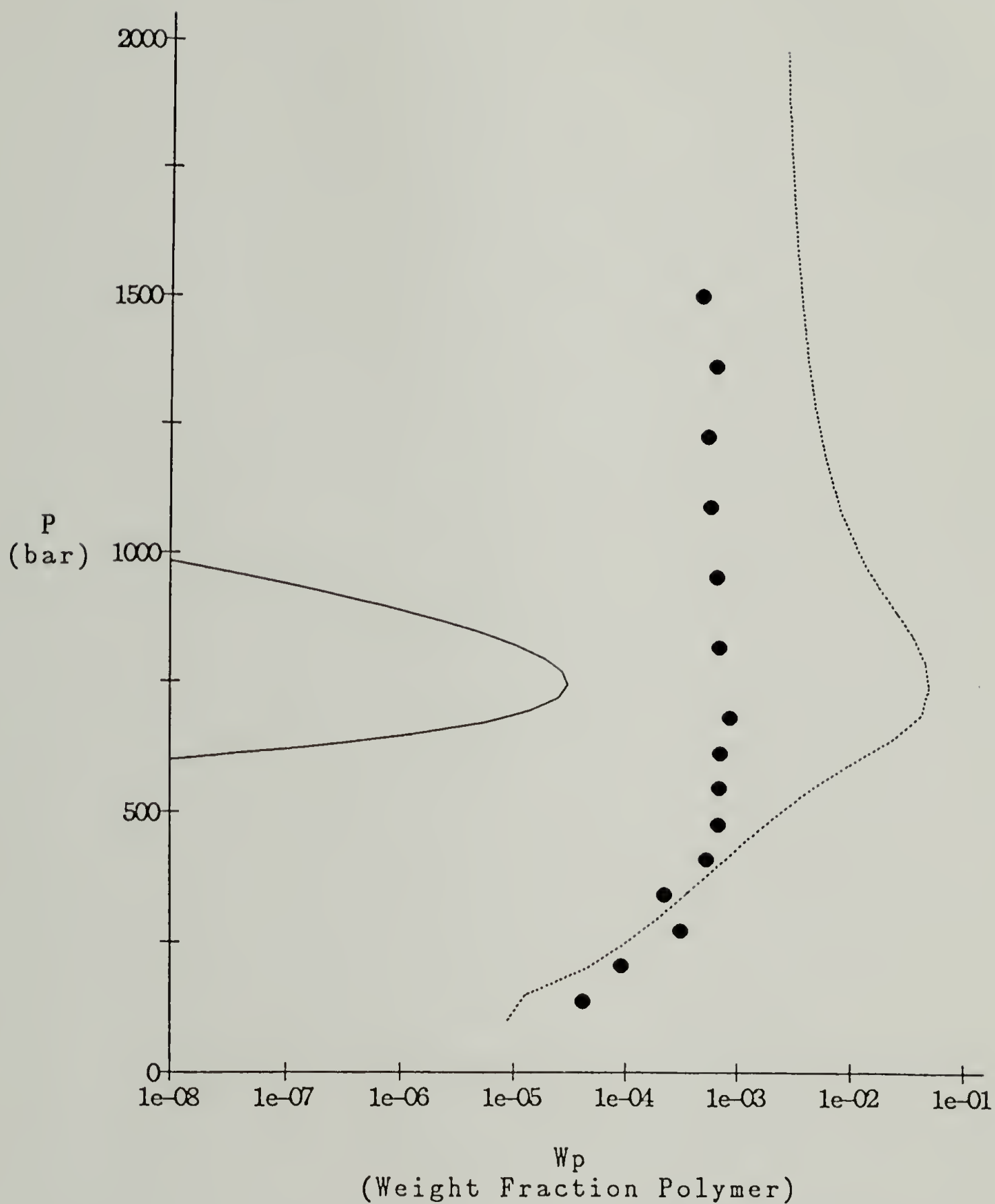


Figure 4.17

Solubility measurements of 7000 MW PMMA in CO_2 at 333K compared to Zero Order MFLG model predictions; symbols same as in Figure 4.16.

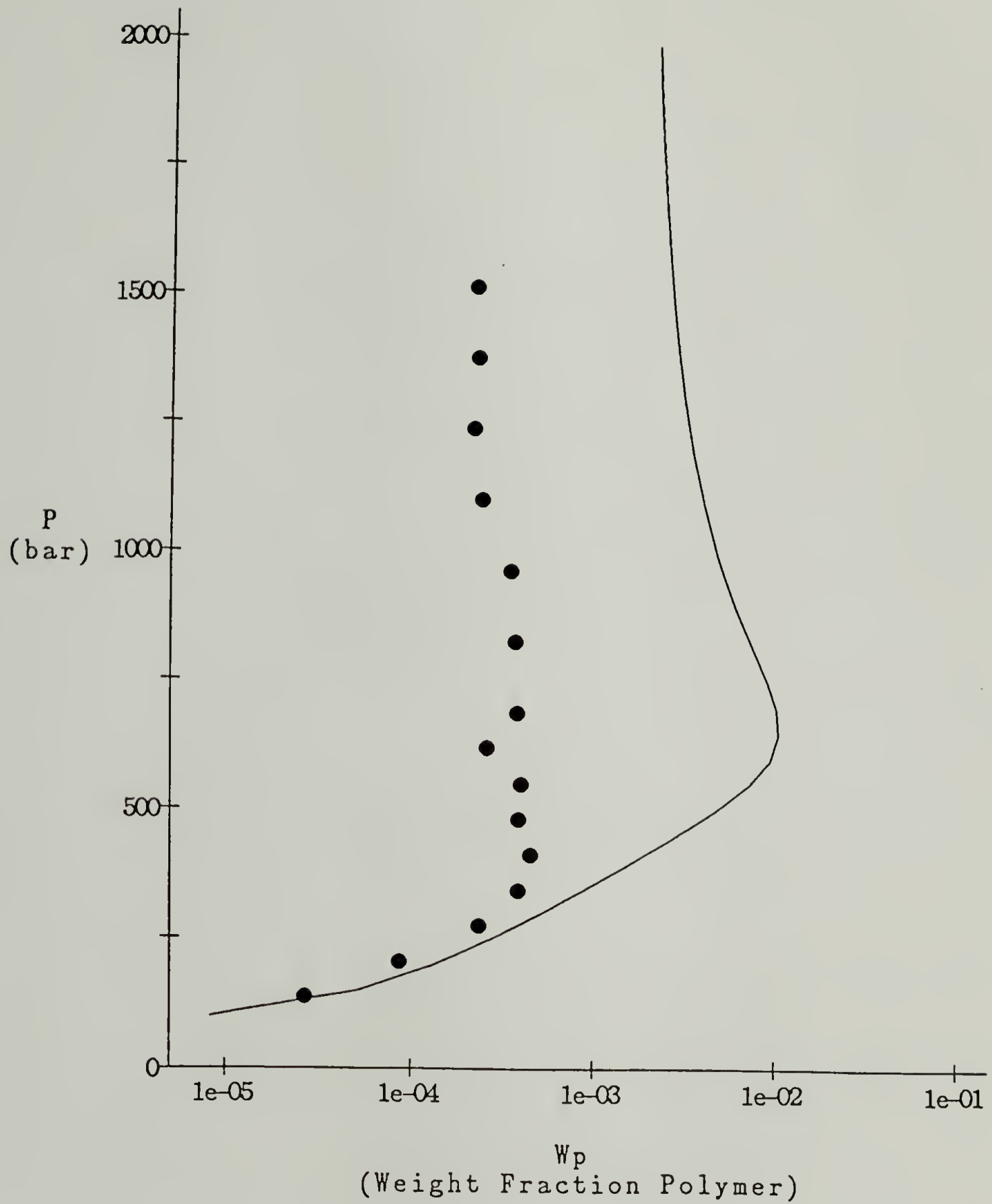


Figure 4.18

Solubility measurements of 24,300 MW PMMA in CO_2 versus pressure at 313K (•) compared to binodal (—) and spinodal (- - -) predictions by Zero Order MFLG model.

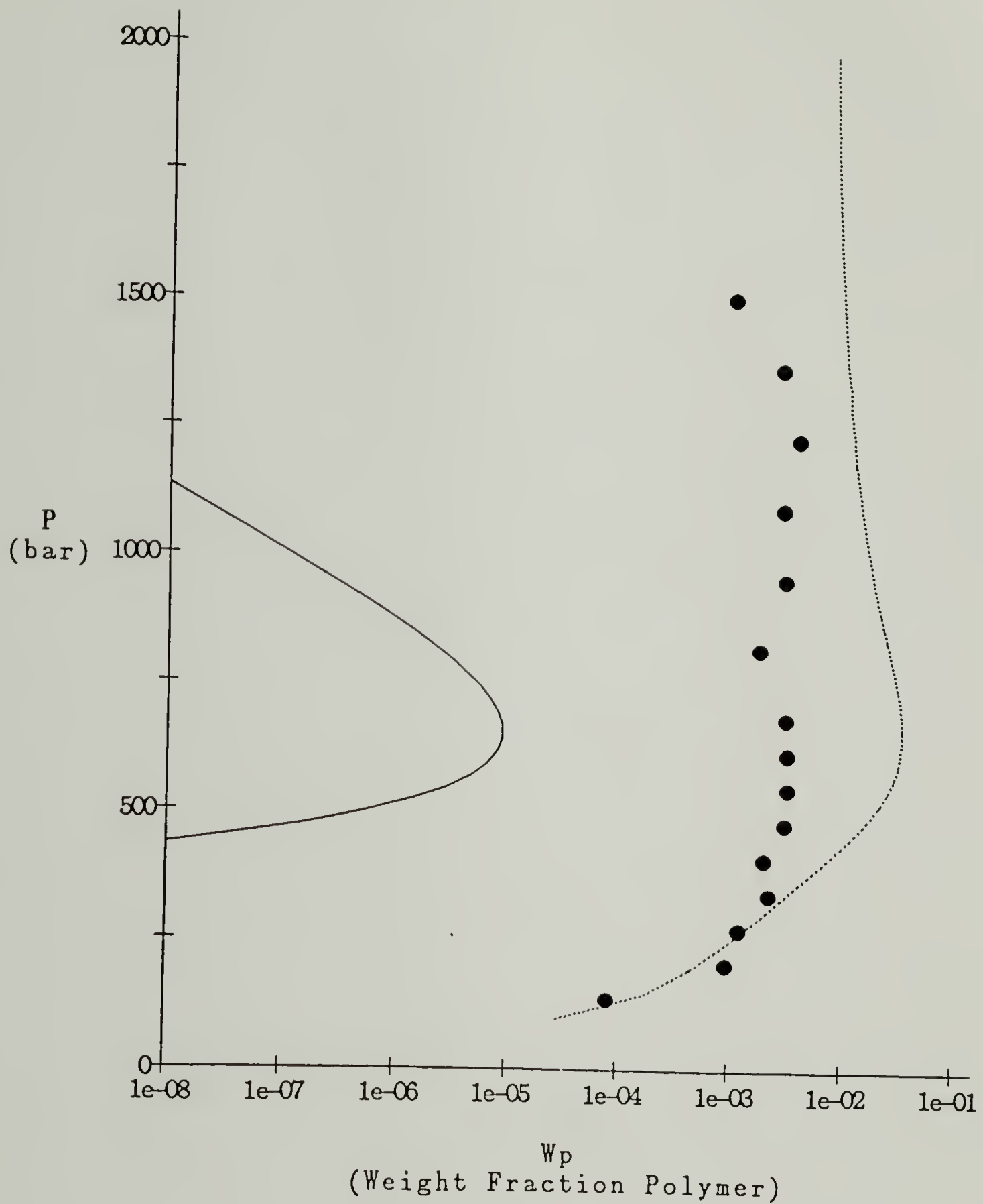


Figure 4.19

Solubility measurements of 24,300 MW PMMA in CO₂ versus pressure at 333K compared to Zero Order MFLG model predictions; symbols same as in Figure 4.18.

4.3.3 Polystyrene-CO₂

Pure component parameters for both constituents were determined in Section 2.3. Unfortunately, sorption data on the PS-CO₂ binary are relatively scarce. The binary parameters for the model were determined by fitting the sorption equations against Henry's Law region data at several temperatures [Durrill and Griskey, 1966; Morel and Paul, 1982]. Due to the lack of volume of mixing data (solution densities were set to the density of pure PS and assigned a tolerance of 10% during fitting), α_m could not be determined with any confidence and was consequently set to zero. All of the material parameters for PS and the PS-CO₂ binary are shown in Table 4.5. The error between calculated and actual Henry's Law constants is less than .1%.

The predicted sorption at $T = 298K$, 5.7 ($g\ CO_2/g\ PS$), is much lower than the measured value [Berens, 1987] of 13.5. The large error in this prediction, as compared to the corresponding calculation for PMMA-CO₂, is due to both the ambiguity in the binary parameters owing to the scarcity of sorption data and to the distinct possibility that polystyrene, under these conditions, (CO₂ vapor at 298.2K) is in the glassy state. Because the MFLG model is predicated on an *equilibrium* distribution of segments and holes, it is not rigorously applicable to non-equilibrium materials such as polymer glasses. Sorption of gases by glasses is better represented by a model of the dual-mode variety [Morel and Paul, 1982].

The predictions of the dilute solution behavior of PS-CO₂ are shown in Figures 4.20 and 4.21. The trends are similar to those found for PMMA-CO₂, although, not surprisingly, it appears that CO₂ is a much better solvent for PMMA than for PS. Unlike the PMMA-CO₂ system, the approximation made during the determination of the binary parameters, that high molecular weight

polymer does not dissolve in the gas over the pressure range of the sorption data, holds quite well for the PS-CO₂ binary [Bowman, 1976].

Table 4.5

Material Parameters for Polystyrene and PS-CO₂ Mixture
using MFLG Model

Parameter	Polystyrene	Polystyrene-CO ₂
m	3.7*	-
α	-6.8354	-
g_{10}	4.8622	-
g_{11}	1110.0	-
γ	-1.0889	-
α_m	-	0
g_{m0}	-	-.17450
g_{m1}	-	279.51

* segments per monomer unit

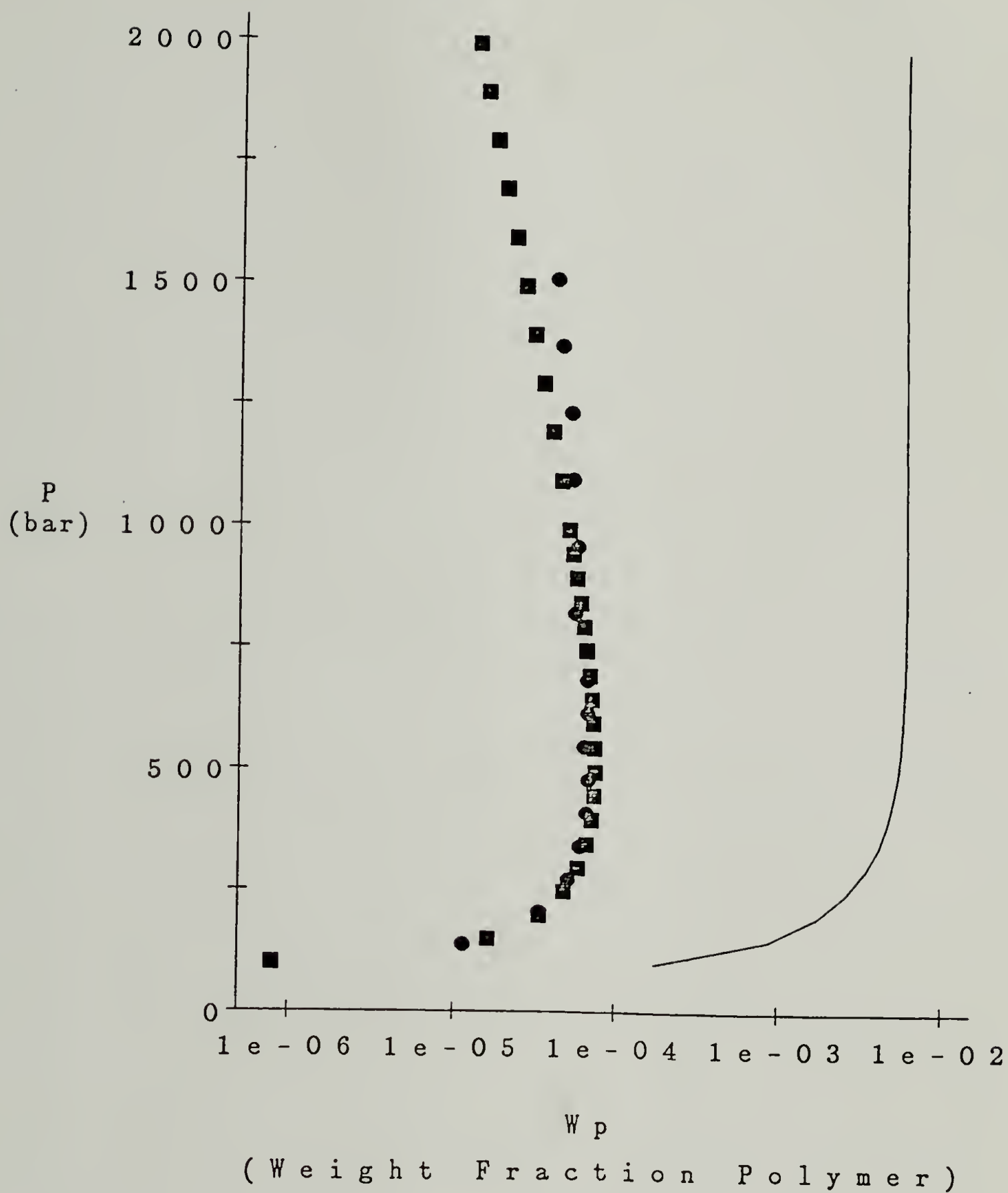


Figure 4.20

Solubility of 2000 MW polystyrene in CO_2 at 313K versus pressure (\bullet) (and smoothed data by Bowman [1976] (\blacksquare)), compared to spinodal predictions (—) by Zero Order MFLG model.

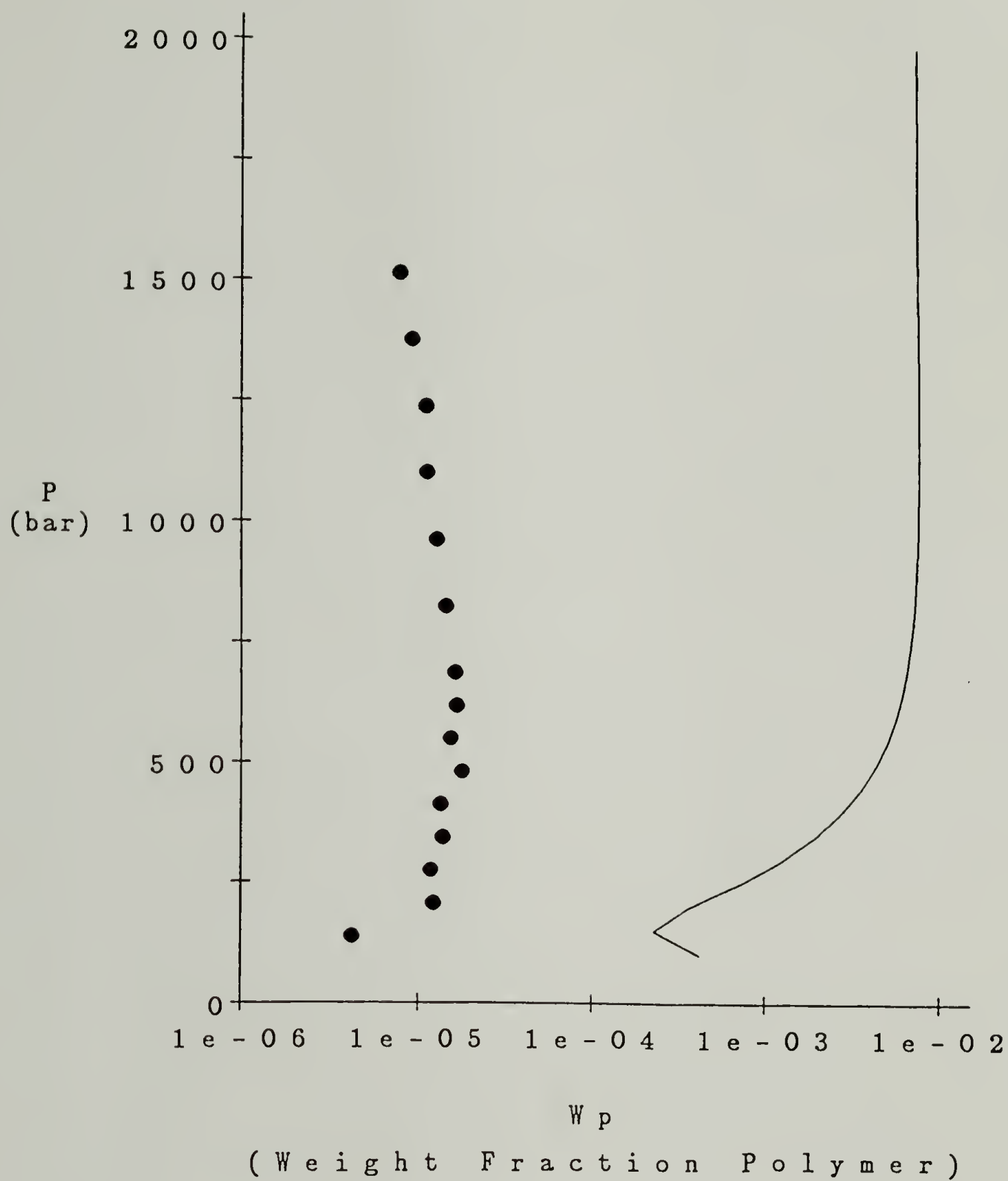


Figure 4.21

Solubility measurements of 2000 MW polystyrene in CO_2 at 353K versus pressure (\bullet) compared to Zero Order MFLG model spinodal prediction ($-$).

4.3.4 Summary of Section 4.3

The MFLG model produces an accurate description of the sorption of supercritical CO₂ by atactic PMMA in the concentration region where the mean field approximation is expected to be valid. Using the binary parameters found by fitting the appropriate model equations to the literature sorption data at temperatures between 315K and 341.2K, accurate predictions of sorption have been made at temperatures of 298.2K and 461.53K, thus demonstrating the large useful temperature range of the model. Predictions of the volume change on mixing, while displaying the proper trends versus temperature and pressure, show deviations from the data at high pressure.

In general, though correctly describing the effects of temperature, pressure, and molecular weight on dilute solution phase behavior, the model underpredicts the solubility of PMMA in CO₂. This is due both to the assumptions made during the determination of the binary parameters (that no 33,200 MW PMMA dissolves in CO₂ up to pressures of 300 bar) and to the breakdown of the mean field approximation in very dilute polymer solutions.

The predictions in the PS-CO₂ system were made using a minimal amount of data during the fitting procedure. Despite this, the model solubility predictions qualitatively describe the dilute solution behavior, but as in the PMMA-CO₂ binary, underpredict the solubility. Not surprisingly, CO₂ is a much better solvent for PMMA than for PS.

Clearly, dilute polymer solutions present a problem for the model in its present form. A number of authors have attempted to bridge the gap between dilute and concentrated polymer solution thermodynamics [Koningsveld, *et al.*,

1974; Irvine and Gordon, 1980; Edwards, 1966; Muthukumar, 1986; Sanchez and Lohse, 1981; des Cloizeaux, 1975]. Of these, the bridging theories of Koningsveld, *et al.*, and Irvine and Gordon, the cell model by Sanchez and Lohse, or the field theoretical approach of Muthukumar seem to be the most readily adaptable to a lattice model such as the MFLG since each of these builds from an existing mean field approach.

CHAPTER 5

Predicting the Pressure Dependence of the Glass Transition of Amorphous Polymers

As stated in Chapter 1, one of the goals of this research is to predict the T_g of a gas-polymer mixture as a function of gas pressure. This means that the model must be able to successfully predict:

1. The effect of hydrostatic pressure alone on the T_g of a pure polymer;
2. The effect of diluent concentration on the T_g of a mixture;
3. And the effect of pressure on the amount of gas a polymer will absorb.

In Chapter 4, it has been shown that the MFLG model will accurately predict the sorption of a high pressure gas by a polymer. In this chapter, the effect of hydrostatic pressure on the T_g of a pure polymer is examined.

The dependence of T_g on pressure is predicted by considering the glass transition as a state of constant Cr , where Cr is a criterion calculated from the thermodynamic properties of the material under study. Three criteria are evaluated; the iso-free volume (FV), iso-entropy (S), and iso-viscosity or iso-relaxation time. The latter is represented in the first approximation by the quantity TS , as originally derived by Adam and Gibbs [1965]. Because the model material constants are determined by fitting of the MFLG EoS to literature pVT data, the calculation of $\partial T_g/\partial p$ is a *prediction*, requiring no additional adjustable parameters. Predictions of $\partial T_g/\partial p$ for the amorphous polymers PS, PMMA, poly(vinyl acetate) [PVAC] and Bisphenol A polycarbonate (PC) are made using each of the criteria and compared with literature data.

As shown in Chapters 2 and 4, the Zero Order model has been shown to provide good descriptions of the volumetric properties of substances, yet it contains a fundamental flaw in that the change in heat capacity upon mixing holes and segments, ΔC_v is *identically zero*. Thus, the temperature dependence of the Zero Order model free energy expression will be modified. The adjustment is necessary at this point because the heat capacity is an entropy derivative and since the entropy plays a large role in the T_g predictions, it is obviously important to obtain as good a description of the entropy as possible. The modification will be made in the form of a "softening" of the segments, or a cell-hole type of model.

5.1 Thermodynamic Criteria for the Glass Transition

The glass transition can be thought of as a freezing- in process [Lipatov, 1978] where one or more configurational properties, which depend upon temperature and pressure in the melt, are constants for the glass. Oels and Rehage [1977] has shown that as a first approximation, the glass transition-pressure line for atactic polystyrene (and possibly other polymers) can be assumed to depend on only one order parameter. Proposals for the identity of this order parameter have centered on the free volume, entropy, and relaxation time.

Although free volume-based theories of the glass transition are the most numerous of the three types mentioned above, predictions of $\partial T_g / \partial p$ using free volume criteria are few. Sanditov and Bartenev [1975], using Eyring's hole model for fluids and a constant hole volume criterion, showed $\partial T_g / \partial p$ to be a material constant. While this is a reasonable first approximation, it is not reliable for most polymers. Kanig [1963], from V-T curves of both liquid and glassy polystyrene of various chain lengths, concluded that the ratio of the "vibration" free volume

(*i.e.*, that portion of the free volume which does not freeze in at T_g) to the total free volume is a material constant at T_g . While the use of Kanig's lattice equation of state to define the free volume ratio made it possible, in principle, to calculate $\partial T_g / \partial p$, only the effect of diluents was modeled.

The most widely used of the entropy models is the Gibbs-DiMarzio (GD) theory [Gibbs and DiMarzio, 1958; DiMarzio and Gibbs, 1958]. The Gibbs-DiMarzio theory assumes that T_g is a second order transition, which, under conditions of infinitely slow cooling, occurs when the configurational entropy drops to zero. While this theory can describe qualitatively the effects of pressure [DiMarzio, *et al.*, 1976] on the T_g , the calculated transition temperature, T_2 , is usually $\approx 20 - 50K$ below the actual T_g . Practically speaking, modelling the pressure dependence of T_g using the GD theory would be similar to a specific case of the freeze-in constant entropy condition, *i.e.*, $S = 0$. The GD model will be covered more thoroughly in a separate section to follow.

Although not strictly an entropy-based model, the theory of DiBenedetto [1987] also assumes the glass transition to be a second order transition. Employing the idea of corresponding states, the DiBenedetto model assumes all substances to have the same reduced glass transition temperature. Thus this model is similar to that used here with the constant reduced T_g acting as the vitrification criterion. However, because DiBenedetto avoids deriving the equation of state, the effect of pressure on the T_g cannot be calculated with this theory.

Turnbull [1969], Miller [1968; 1978a,b], and also McKinney and Goldstein [1974], have postulated that the glass transition is an iso-viscous, or iso-relaxation time state. Adam and Gibbs [1965] showed that as a first approximation,

the relaxation time is a function of the quantity TS , where S is the configurational entropy. (The configurational entropy is taken to mean the difference between the total entropy and the ideal crystalline entropy.) In an experimental study on poly(vinyl chloride), Naoki and Owada [1984] found that use of the constant TS condition was superior to both constant entropy alone and constant free volume in the description of $\partial T_g/\partial p$. Nose [1971], using a cell-hole model for polymer liquids and glasses, also found the iso- TS criterion to be superior to both the iso-entropy and iso-free volume models in describing $\partial T_g/\partial p$ for polystyrene, poly(vinyl acetate), poly(methyl methacrylate), and other polymers. Miller [1968], however, found the Adam-Gibbs criterion to provide an accurate description of the glass transition only if the conformational entropy is substituted for the configurational entropy. Despite this, the configurational entropy, as derived from the MFLG model, will be used to calculate the Adam-Gibbs criterion.

5.1.1 Entropy: Comparison of MFLG and Gibbs-DiMarzio Model

The Gibbs-DiMarzio (GD) model [Gibbs and DiMarzio, 1958; DiMarzio and Gibbs, 1958] employs the general rigid lattice formulation, as described in Chapter 2, with a zero g_{10} . Thus the GD equation of state is a specific case of the MFLG EoS, and as has been shown in Section 2.3, is significantly less accurate in its descriptions of the pVT behavior of both gases and polystyrene. However, the unique feature of the model derives from the assumption that segments can exist in a number of rotational states, each with its own particular energy. An isobaric-isothermal partition function is constructed in which the sum over states is replaced by a sum over the allowed values of both n_0 , the number of holes, and f_i , the fraction of molecules in rotational state i . Using the standard procedure, the sum is replaced by its maximum term which is obtained by

differentiation with respect to both n_0 and f_i . Equating the derivatives to zero yields the equilibrium values of n_0 (the equation of state) and f_i . As a further simplification, the rotational isomer approximation is invoked, thus reducing the number of allowable states to two. The fraction of segments in high energy wells is found to be:

$$f = \frac{(z - 2) \exp(-\Delta\epsilon/kT)}{1 + (z - 2) \exp(-\Delta\epsilon/kT)} \quad (5 - 1)$$

where $\Delta\epsilon$ is the energy difference between the two states. Because the terms in the GD free energy expression which are functions of $f(\Delta\epsilon, T)$ are linear in ϕ_1 , they vanish during the calculation of the chemical potential of either holes or segments. Thus, while the equations of state of the two models are somewhat similar, use of the multiple rotational state approximation by Gibbs-DiMarzio adds temperature-dependent terms to the entropy not found in the analogous expression for the MFLG. As in the case of the EoS, we can set the Gibbs-DiMarzio expression for the entropy in terms of MFLG symbols:

$$\begin{aligned} \frac{\Delta S}{N_\phi} = & -R \left\{ \phi_0 \ln \phi_0 + \frac{\phi_1}{m_1} \ln \phi_1 - \frac{\phi_1}{m_1} \ln \left(\frac{m_1 z(z-1)}{4} \right) - \frac{z}{2} Q \ln Q \right\} \\ & - \frac{\phi_1}{m_1} \left\{ f \ln f + (1-f) \ln(1-f) \right\} \end{aligned} \quad (5 - 2)$$

where Q is defined as in equation (3-6). For a polymer, assuming that $z \approx 10$, the first group of terms on the right-hand side of equation (5-2) will be negative while the f -dependent group will be positive. The entropy will therefore vanish at a temperature which depends on the values of z , $\Delta\epsilon$, r , and g_{11} . By contrast, the entropy expression for the MFLG model reads as follows:

$$\frac{\Delta S}{N_\phi} = -R \left(\phi_0 \ln \phi_0 + \frac{\phi_1}{m_1} \ln \phi_1 + \phi_0 \phi_1 \left\{ \alpha + \frac{g_{10}(1-\gamma)}{1-\gamma\phi_1} \right\} \right) \quad (5 - 3)$$

For the polymers studied so far [polystyrene, poly(methyl methacrylate, poly(vinyl acetate), and bisphenol A polycarbonate], the terms inside the curly braces in equation (5-3) are always negative. Therefore the configurational entropy, as defined by equation (5-3), will never be zero for these polymers, so long as there are holes present, even if the Gibbs-DiMarzio terms which include the effect of the two rotational states (*i.e.* the f -dependent terms) are added in.

While the Gibbs-DiMarzio zero entropy criterion cannot be used verbatim with the MFLG model, the f -dependent terms could be included in the MFLG entropy expression and the value of $\Delta\epsilon$ could be found by fitting against $\partial T_g/\partial p$ data. This would presume the entropy to be the dominant force in determining T_g , whereas one of the goals of this work is to try to objectively compare the three criteria. A different approach to modifying the MFLG entropy expression will therefore be used (see Section 5.1.3).

5.1.2 Free Volume: Comparison of the Kanig and MFLG Models

The approach of Kanig [1963] is, in many respects, the most closely related to that of this work. Kanig constructed a lattice model in which, like the MFLG, holes and segments are permitted different contact surface areas for the purposes of calculating the free energy (see Chapter 2). The Kanig EoS is consequently of the same form as that of the MFLG with the added constraints that $\alpha = 0$ and $g_{10} = 0$. The performance of the Kanig and MFLG equations of state has been compared in Section 2.3.

The major difference between Kanig's model and the MFLG is that Kanig assumed there to be two types of free volume, that due to holes and "vibration" volume, or that due to vibrations of the segments about their lattice locations.

Kanig did not attempt to define the "vibration" volume from fundamental principles, but rather related it to experimentally observable quantities by assuming that the holes completely freeze in at T_g . Kanig found, by observation of the volumetric behavior of polystyrenes of molecular weights ranging from 200 to 90,000, that the value of ϕ_h , the free volume fraction due to the holes (and consequently ϕ_v , the free volume fraction due to vibration volumes) at T_g is essentially constant. Taking the constant ϕ_h as the criterion for T_g , Kanig was able to derive the Gordon-Taylor [Gordon and Taylor, 1952] empirical equation for the T_g of a copolymer from his model, and to show good fits to polystyrene T_g versus diluent concentration data.

The Kanig criterion for T_g is approximately that of the constant FV used herein. The difference lies in Kanig's use of the "vibration" volumes, such that $(\partial\phi_0/\partial T)_V \neq 0$. In Section 5.1.3, the MFLG model will be modified in an attempt to describe the temperature dependence of these vibration volumes and thereby add a volume-dependent intramolecular contribution to the configurational entropy.

5.1.3 Modifying the Temperature Dependence of the MFLG Free Energy Expression

The MFLG can successfully model the pVT behavior (volume derivatives of the free energy) of liquids, gases, and polymers. However, quantities based on the higher order temperature derivatives of the free energy are not as well described by the model in its present form. For example, using equation (2-9) or (5-3) we find:

$$-\left(\frac{\partial \Delta S}{\partial T}\right)_{V,n_1} = \left(\frac{\partial^2 \Delta A}{\partial T^2}\right)_{V,n_1} = -\Delta C_V/T \equiv 0 \quad (5-4)$$

which is clearly unsatisfactory where real fluids are concerned. An attempt will therefore be made to improve the temperature dependence of the MFLG model. The modified model will be compared to the original formulation in the description of the pVT behavior of liquids as well as in the prediction of $\partial T_g/\partial p$ for the four polymers.

One solution to the problem with the MFLG temperature dependence, as shown by the unrealistic constraint to ΔC_v , is to "soften" the segments somewhat, by allowing the number of segments/molecule, and therefore the surface area per segment, to vary with temperature. This is analogous to the cell-hole approach to the lattice model which has been pursued in depth by Simha and coworkers [Simha and Somcynsky, 1968] and follows the suggestion of Kanig. As a first approximation we divide the monomer unit into a number of chemical groups, G, and allow the radius of each group to vary linearly with temperature due to anharmonic vibrations. Initially all groups in the monomer are considered equivalent. If r is the radius of a group:

$$r = A + BT$$

therefore:

$$m_1 = \frac{4\pi G}{3v_0}(A + BT)^3 \quad (5-5)$$

and:

$$\sigma_1/\sigma_0 = K \left(\frac{3v_0}{\sigma_0} \right) \left(\frac{1}{(A + BT)} \right) = 1.814K \left(\frac{1}{(A + BT)} \right) \quad (5-6)$$

where K is a constant which allows for segment surface/volume ratios other than that of spheres (the holes, however, are assumed to be spheres). Thermodynamic derivatives at constant temperature, such as the equation of state, are not affected by these changes, while the entropy of mixing of holes and segments becomes:

$$\begin{aligned} \frac{\Delta S}{N_\phi} = & -R \left(\phi_0 \ln \phi_0 + \frac{\phi_1}{m_1} \ln \phi_1 + \phi_0 \phi_1 \left(\alpha + \frac{g_{10}(1 - \gamma_1)}{1 - \gamma_1 \phi_1} \right) \right) \\ & - RT \phi_1' \left(\left(\frac{1}{m_1} - 1 \right) - \ln \phi_0 + (\phi_0 - \phi_1) \alpha \right) \\ & - RT \phi_1' \left(\frac{(\phi_0 - \phi_1 + \gamma_1 \phi_1^2)(1 - \gamma_1) \beta}{(1 - \gamma_1 \phi_1)^2} \right) \\ & + RT \gamma_1' \left(\frac{\phi_0^2 \phi_1 \beta}{(1 - \gamma_1 \phi_1)^2} \right) \end{aligned} \quad (5-7)$$

where:

$$\phi_1' = \left(\frac{\partial \phi_1}{\partial T} \right)_{V, n_1}$$

$$\gamma_1' = \left(\frac{\partial \gamma_1}{\partial T} \right)_{V, n_1}$$

The temperature dependence assumed for m_1 and γ_1 is overly simplistic in that the groups are allowed to change size independently, *i.e.*, the vibrations and rotations of one group do not affect its neighbors, and there is no upper bound to the size of a segment. Since all groups are assumed to be chemically equivalent, the values of A and B, found via fitting against pVT data, will represent smoothed net effects over the whole chain. Finally, no coupling is assumed between the number of holes and the temperature dependence of m_1 and γ . However, these changes to the model are meant only as a first approximation.

5.2 Comparison of the Predictions of $\partial T_g/\partial p$ Produced by the Three Criteria: Results for Amorphous Polymers

Because only the equation of state is available as a constraint for the fitting of thermodynamic models to pVT data on polymers, comparative testing of the Zero Order MFLG and modified MFLG model (Section 5.1.3) was performed on literature data for cyclohexane [Kerns, *et al.*, 1974; Washburn, 1928; Young, 1910; Timmermans, 1965], toluene [Washburn, 1928; Young, 1910; Timmermans, 1965; Hales and Townsend, 1972], and benzene [Kudchaker, *et al.*, 1968; Vargaftik, 1975; Gehrig and Lentz, 1977]. Results are shown in Tables 5.1 and 5.2. The modified model, as expected, improves the fit over that of the Zero Order MFLG to the saturated liquid densities. In other areas the average error of the modified model is equal or less than that of the parent.

Fitting of the Zero Order MFLG model to PS and PMMA data has been discussed previously (see Sections 2.3 and 4.3.2). Because literature pVT data is available for only one molecular weight species of PVAc [McKinney and Goldstein, 1974] and PC [Zoller, 1982], the γ_1 parameter was linked to the number of segments per monomer unit, the corresponding values for PS, and the Bondi

ratio as in Section 4.3.2. Determination of the parameters for the four polymers using the modified model was handled in the same way. All parameters were allowed to float during the fitting of the PS data whereas the K parameters of the other three polymers were set by the PS result and the Bondi ratios.

The results of the fitting for the four polymers are shown in Table 5.3. These results are for the MFLG; results for the modified model are not significantly different.

Once the parameters for the four polymers had been set using the pVT data, the course of the T_g versus pressure curve was calculated using each of the three criteria without further need of adjustable parameters. The procedure is as follows: the value of the criterion of interest per segment, free volume (FV), entropy (S), or TS, is calculated at T_g ($p = 0$) and then fixed. The pressure is then raised and the values of the glass transition and density at T_g are found via simultaneous solution of the EoS and the defining equation for the criterion in question. Entropy (and consequently TS) is defined by equation (5-3) for the MFLG and equation (5-6) for the modified version. Rather than simply using a constant ϕ_0 as the free volume constant, this criterion was defined in terms of the number of segment-hole contacts per segment, or:

$$FV = \frac{\sigma_0 \phi_0 (1 - \gamma)}{1 - \gamma \phi_1} \quad (5 - 7)$$

Although for the MFLG, where $\gamma \neq f(T)$, this is equivalent to treating ϕ_0 at T_g as a material constant (*i.e.*, the Miller [1968] criterion), the case of the modified model is more complex. Either case provides more flexibility than simply setting ϕ_0 at T_g to a universal value.

Figures 5.1 and 5.2 show the results of the T_g versus pressure predictions for the models for PS. In the case of the MFLG model (Figure 5.1), because both the entropy and free volume criteria depend implicitly on temperature via the temperature dependence of ϕ_0 in the EoS, these two give identical results. The TS criterion produces a more accurate prediction but one which remains linear with pressure whereas the data show substantial curvature at higher pressures. Using the modified version of the model (Figure 5.2), the TS criterion again gives the most accurate prediction and improves upon the performance of the MFLG model in both absolute error and in the predicted shape of the curve.

Figures 5.3 and 5.4 show the predicted density of PS at T_g versus pressure using each of the three criteria. As in Figures 5.1 and 5.2, the constant TS criterion produces the best prediction and the modified version of the model shows improvement over the prediction of the MFLG. The prediction of a constant density at T_g versus pressure made using the FV and S criteria and the MFLG model can again be traced to the explicit dependence of S and FV on ϕ_0 alone.

Results for PMMA and PVAc are shown in Figures 5.5 – 5.8. The trends are similar to those found for PS; namely that the constant TS prediction is the most accurate and that use of the modified version of the MFLG model brings improvement to the prediction.

Results for polycarbonate are given in Figures 5.9 and 5.10. Like the results for the other three polymers, the TS criterion provides the most accurate predictions; unlike the previous results, the modified version of the MFLG does not improve the prediction. This could be a result of the overly simplistic approximations which were made to derive the modified version of the model. In addition, because the MFLG model treats polymers as completely flexible, it may be necessary to add a flexibility dependence [Huggins, 1970; Lacombe and

Callahan, 1981] to the entropy of mixing of holes and segments to adequately model such polymers as polycarbonate.

Table 5.4 shows the calculated values of the three criteria for the four polymers. The purpose for presenting this data is to show that as far as the MFLG model is concerned, none of the criteria can be considered as universal values. Miller [1967; 1968], however, has postulated that the quantity $Z_g P^*$ should equal a universal constant (here Z_G is the number of segments in a cooperative unit at T_g and P^* is the criterion for the glass transition). Using values for Z_g calculated by Warfield and Hartmann [1982], there still appears to be no universal value of any of the three criteria at T_g .

Although the constant TS criterion provides good results, a model such as the MFLG naturally cannot fully describe the vitrification process. Use of the equilibrium MFLG model reveals nothing of the time dependence of the glass transition process, thus the predictions made here must be considered pseudo-equilibrium, or long time results. The equilibrium nature of the model also prevents analysis of the pVT behavior of the glass itself. Despite these problems, the one order parameter model using the MFLG theory and the constant TS criterion gives a good first approximation for the pressure dependence of T_g .

Table 5.1
Average Errors in Fitting MFLG Models to pVT Data
on Cyclohexane, Toluene, and Benzene

Model	<u>VLE Data</u>						
	Number of of Points	Temp. (K)	Vapor Pressure-%	Vapor Density-%	Liquid Density-%		
Toluene - MFLG	10	.8	2.5	3.7	4.3		
- Mod. MFLG	10	.5	3.0	3.7	.7		
Cyclohex. - MFLG	19	1.2	1.0	1.2	2.5		
- Mod. MFLG	19	.9	1.1	1.3	1.8		
Benzene - MFLG	25	.9	1.0	1.2	3.2		
- Mod. MFLG	25	.8	.9	1.2	2.7		

Model	<u>Critical Point</u>			<u>Equation of State</u>			
	Temp. (K)	Press. %	Dens. %	Number of Points	Press. %	Temp. (K)	Dens. %
Toluene - MFLG	.6	4.2	2.0	19	.2	-	3.0
- Mod. MFLG	.2	.8	.7	19	.1	-	3.0
Cyclohex. - MFLG	.9	8.2	5.6	56	.3	-	.3
- Mod. MFLG	.4	3.9	4.7	56	.4	-	.3
Benzene - MFLG	6.9	10.6	13.9	48	5.4	7.2	-
- Mod. MFLG	7.0	10.0	15.0	48	5.3	6.6	-

Table 5.2

MFLG and Modified MFLG Parameters for Cyclohexane, Toluene,
and Benzene as Determined by the PEP

Compound	m_1	α_1	<u>MFLG model</u>		
			g_{10}	g_{11}	γ_1
Cyclohexane	3.56	.91134	-.53522	369.02	-1.4931
Toluene	3.48	1.0020	-.31244	233.03	-2.7879
Benzene	3.36	.25694	-.68961	802.46	-.31630

Compound	A	B	<u>Modified MFLG</u>			
			α_1	g_{10}	g_{11}	γ_1
Cyclohexane	1.7823	-.70187e-03	.50246	-.25216	346.41	3.46
Toluene	1.5162	-.20832e-03	.96348	-.24820	214.47	5.24
Benzene	1.5039	-.25248e-04	-.39215	-.24922	892.26	1.80

Table 5.3

Fitting Results for Polystyrene, Poly(methyl methacrylate),
Poly(vinyl acetate), and Bisphenol A Poly(carbonate)
using MFLG Equation of State

Polymer	Number of Data Points	Average Error-%	Average Error- g/cc
PS	117 [†]	± .12	± .0012
PMMA	40	± .03	± .0004
PVAc	110	± .015	± .0002
PC	104	± .14	± .0016

[†] Data on PS with molecular weights (M_n) of 2300, 3650, 20000, 91000, and 125000.

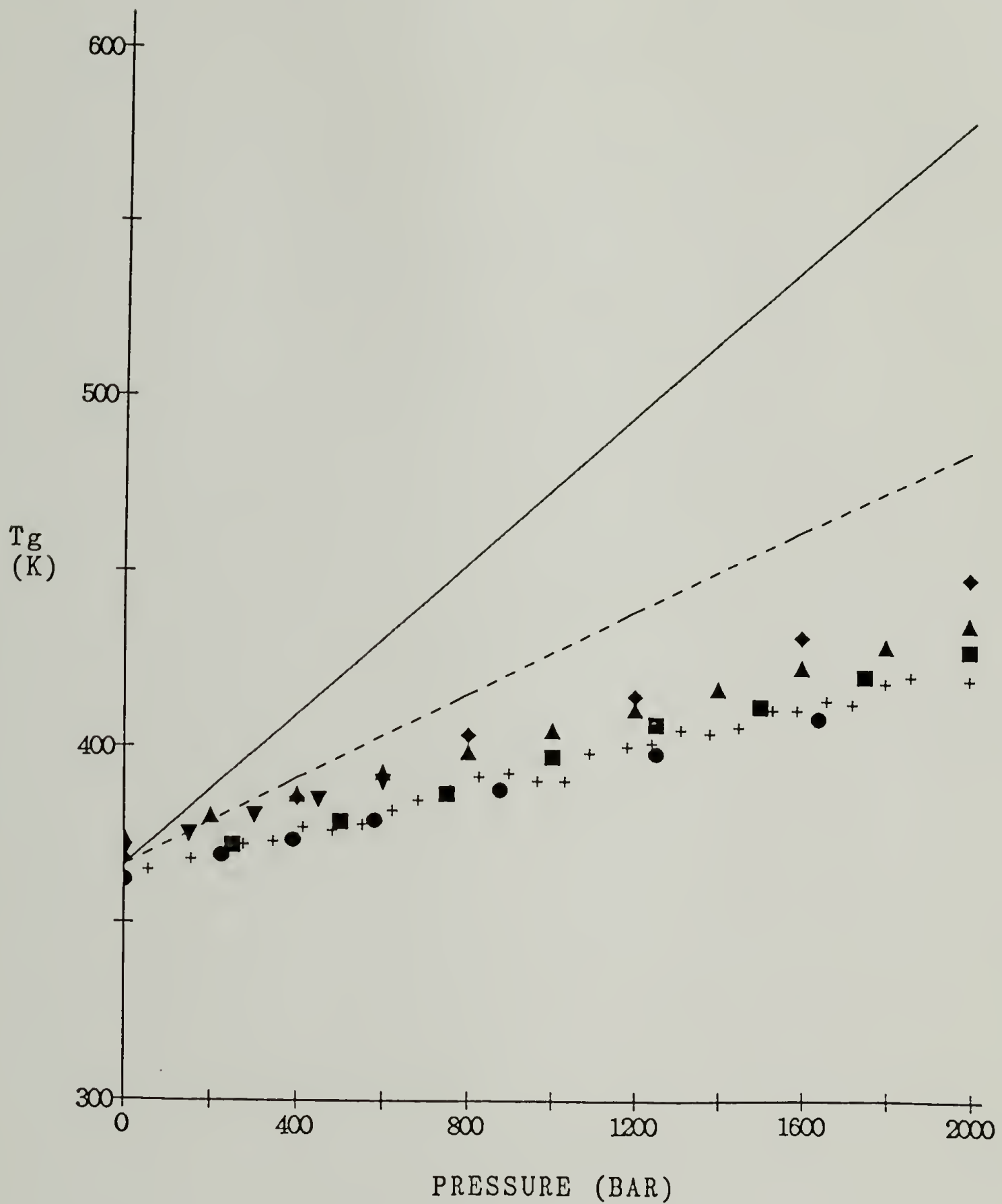


Figure 5.1

Predictions of T_g versus pressure by MFLG model using constant FV (—), S (···), and TS (- - -) criteria against literature data for PS by Gee [1966] (●), Oels [1977] (■), Zoller, *et al.* [1976] (◆), Quach and Simha [1971] (▲), Ichihara, *et al.* [1971] (▼), and Stevens, *et al.* [1986] (+).

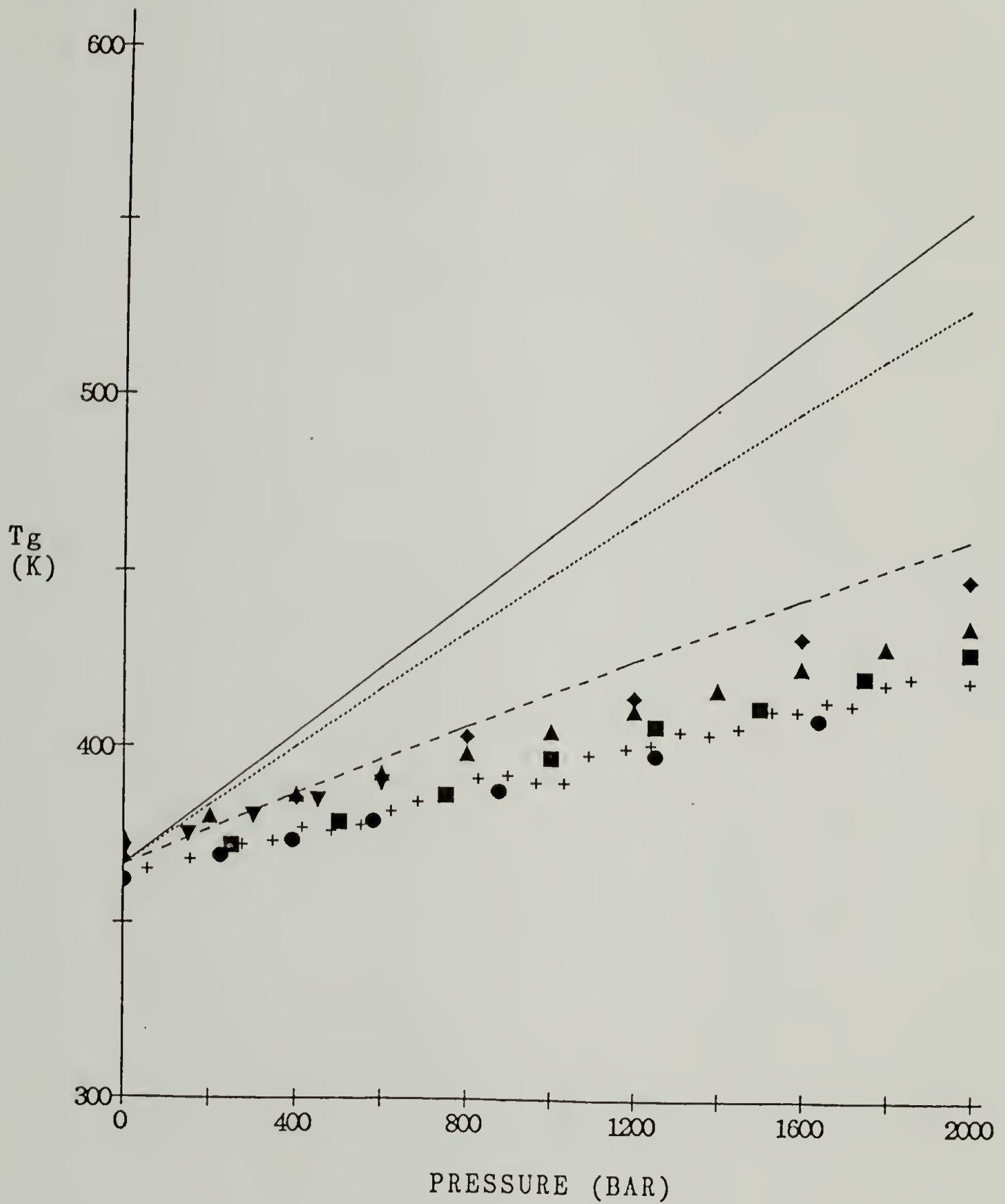


Figure 5.2

Predictions of T_g versus pressure by modified MFLG model using thermodynamic criteria; symbols same as in Figure 5.1.

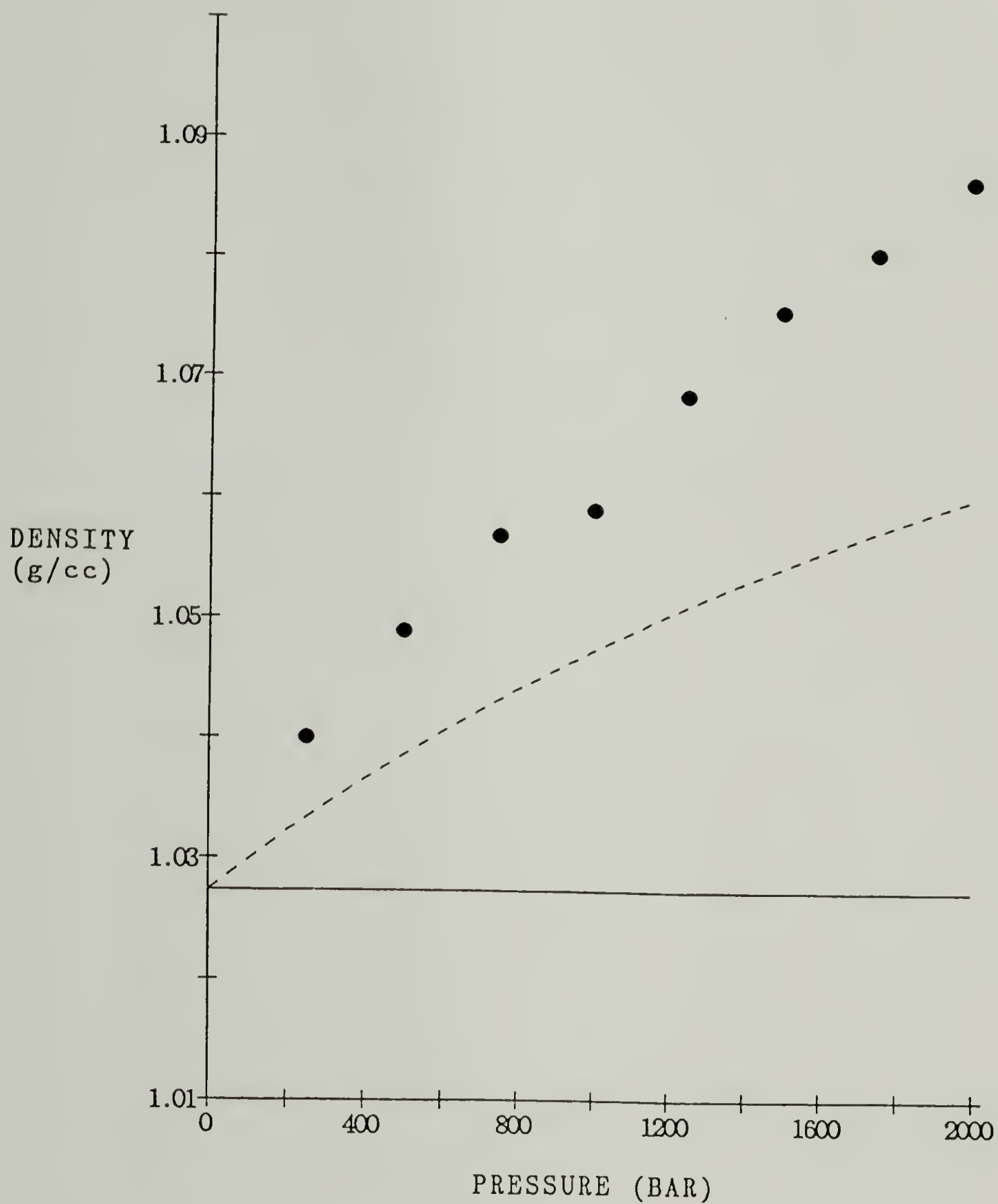


Figure 5.3

Predictions of density at T_g versus pressure using constant FV (—), S (···), and TS (- - -) criteria and MFLG model against literature data for PS by Oels [1977] (•).

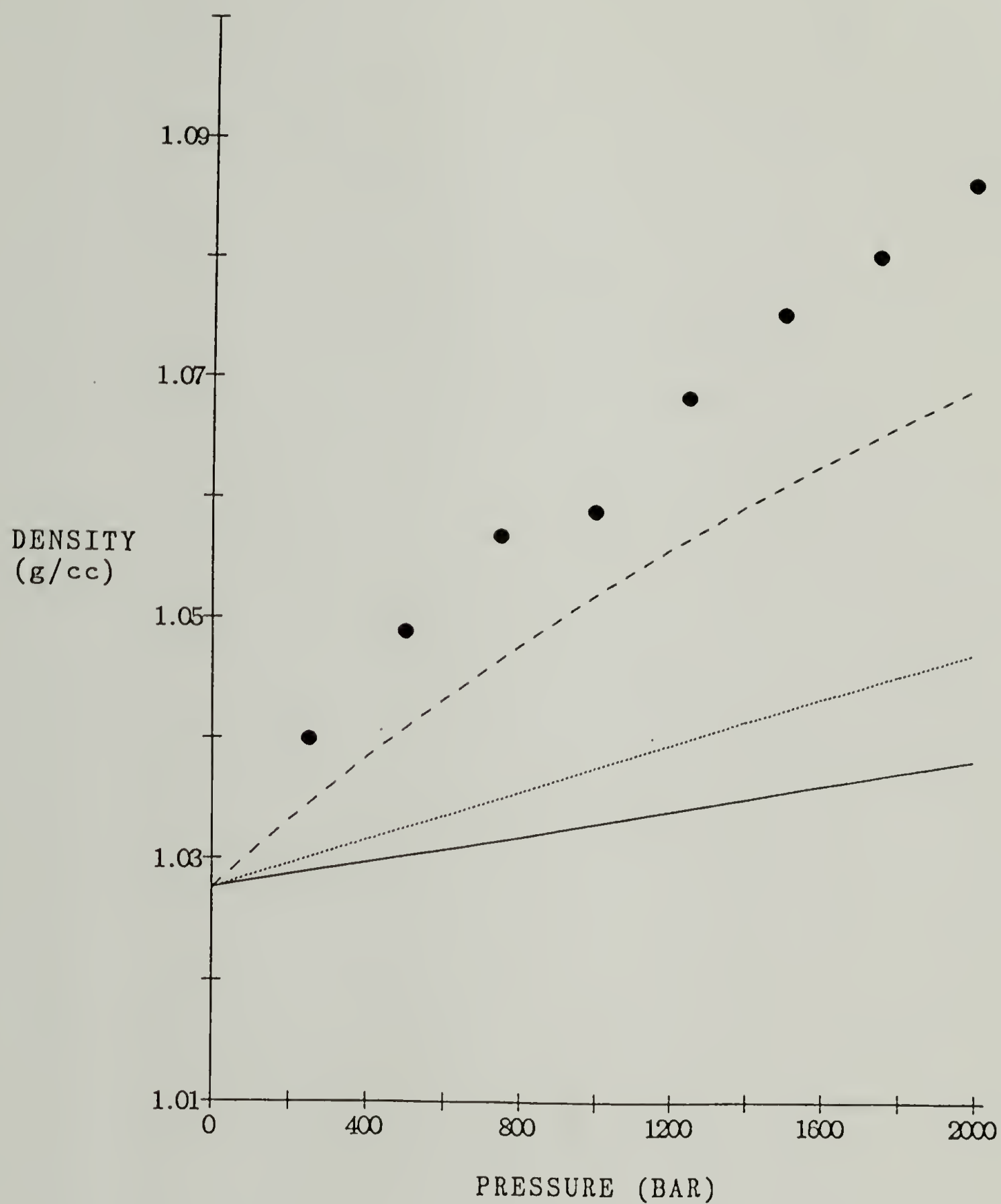


Figure 5.4

Predictions of density at T_g versus pressure using modified MFLG model and thermodynamic criteria; symbols same as in Figure 5.3.

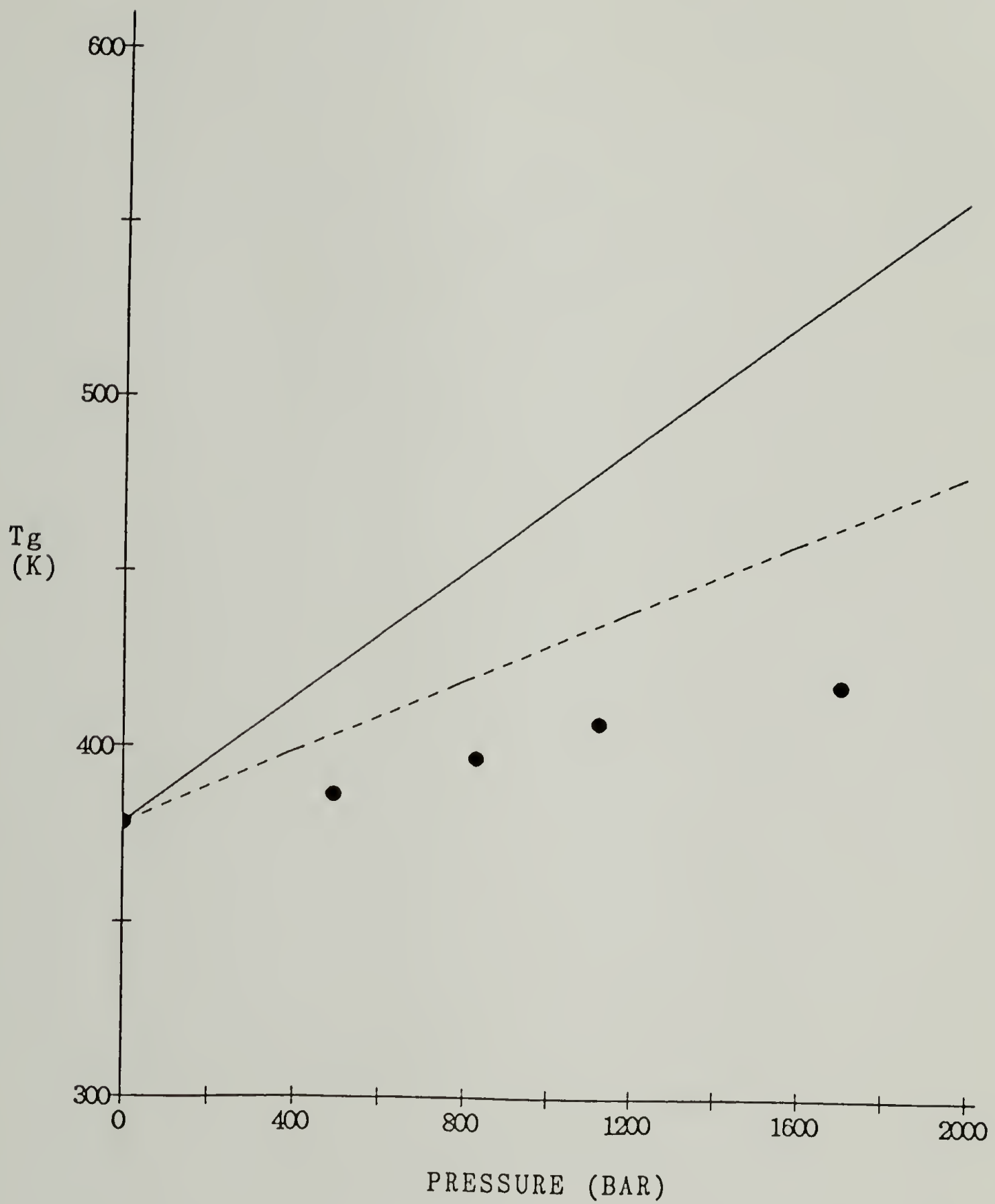


Figure 5.5

Predictions of T_g versus pressure by MFLG model using constant FV (—), S (···), and TS (- - -) criteria against literature data of PMMA by Olabisi and Simha [1975] (•).

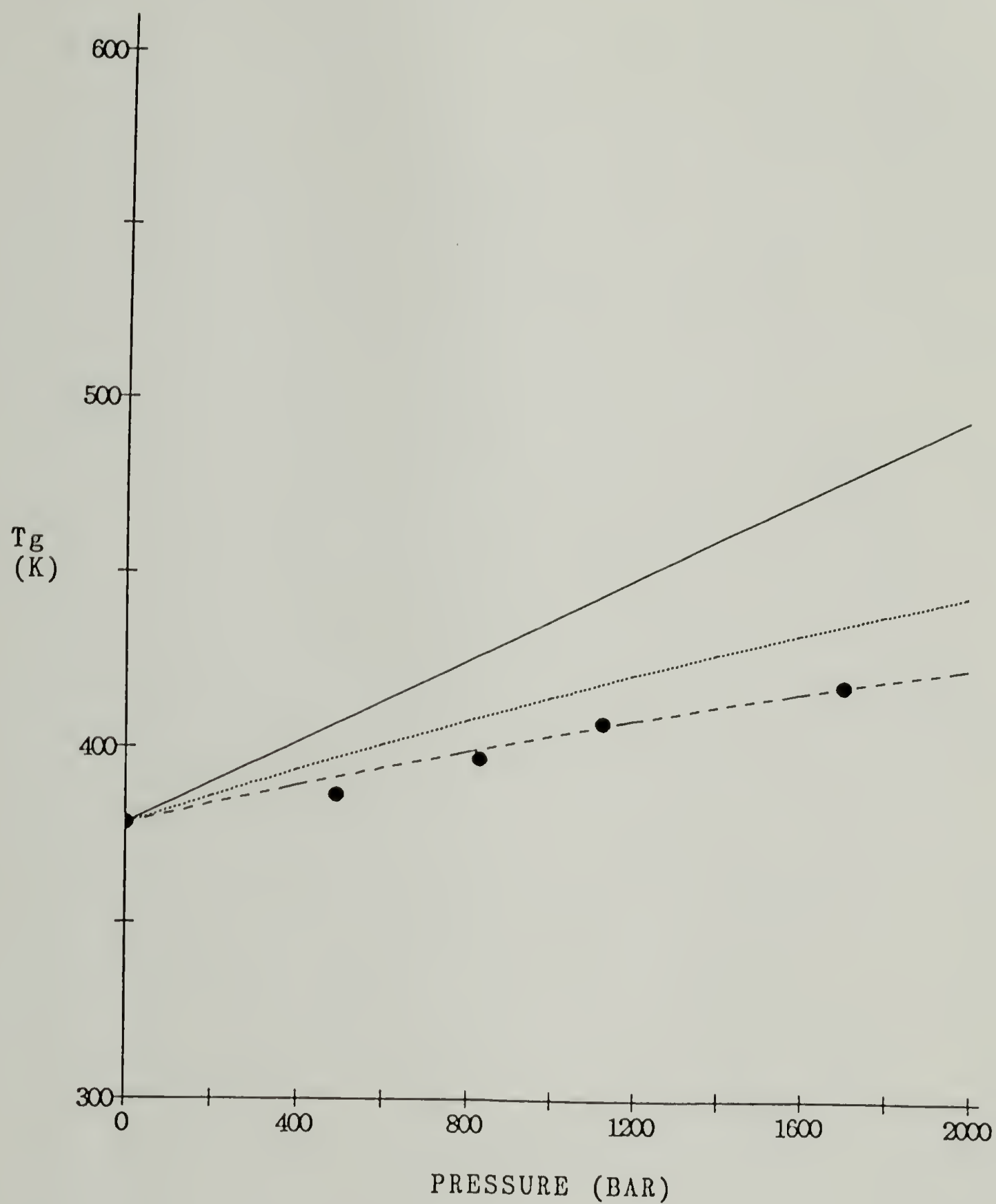


Figure 5.6

Predictions of T_g versus pressure by modified MFLG model using thermodynamic criteria; symbols same as in Figure 5.5.

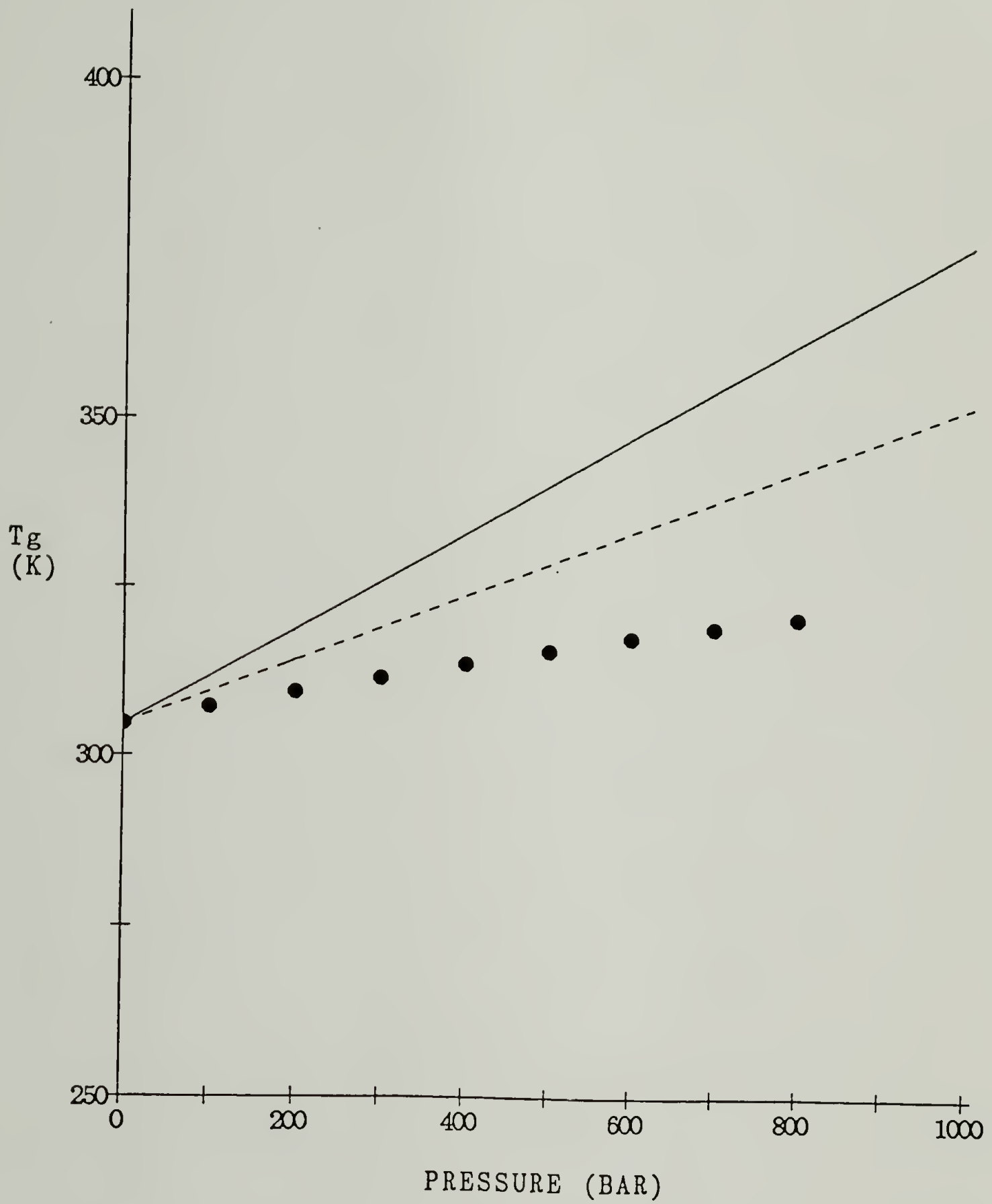


Figure 5.7

Predictions of T_g versus pressure by MFLG model using constant FV (—), S (···), and TS (- - -) criteria against literature data for PVAc by McKinney and Goldstein [1974] (•).

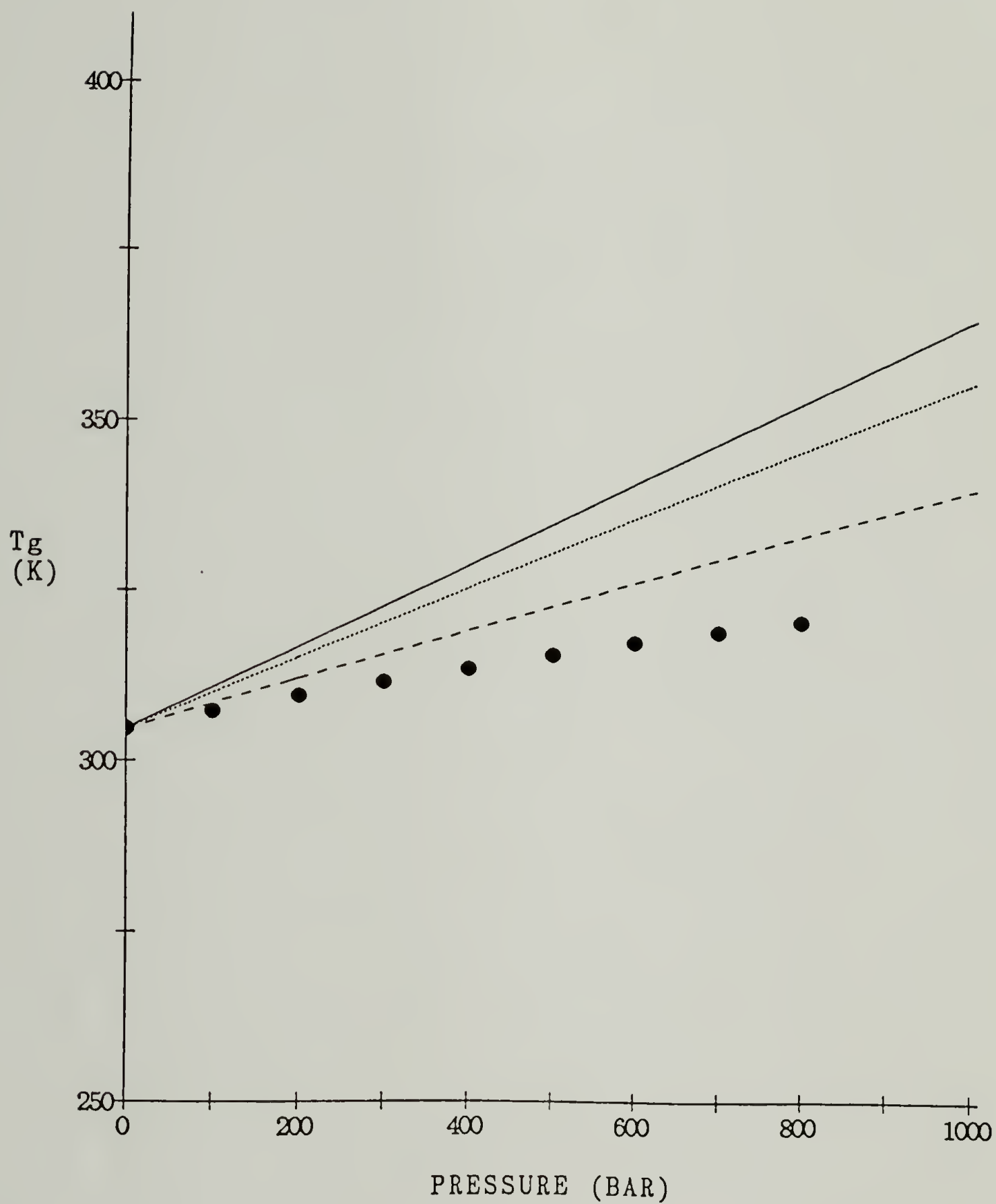


Figure 5.8

Predictions of T_g versus pressure by modified MFLG model using thermodynamic criteria; symbols same as in Figure 5.7.

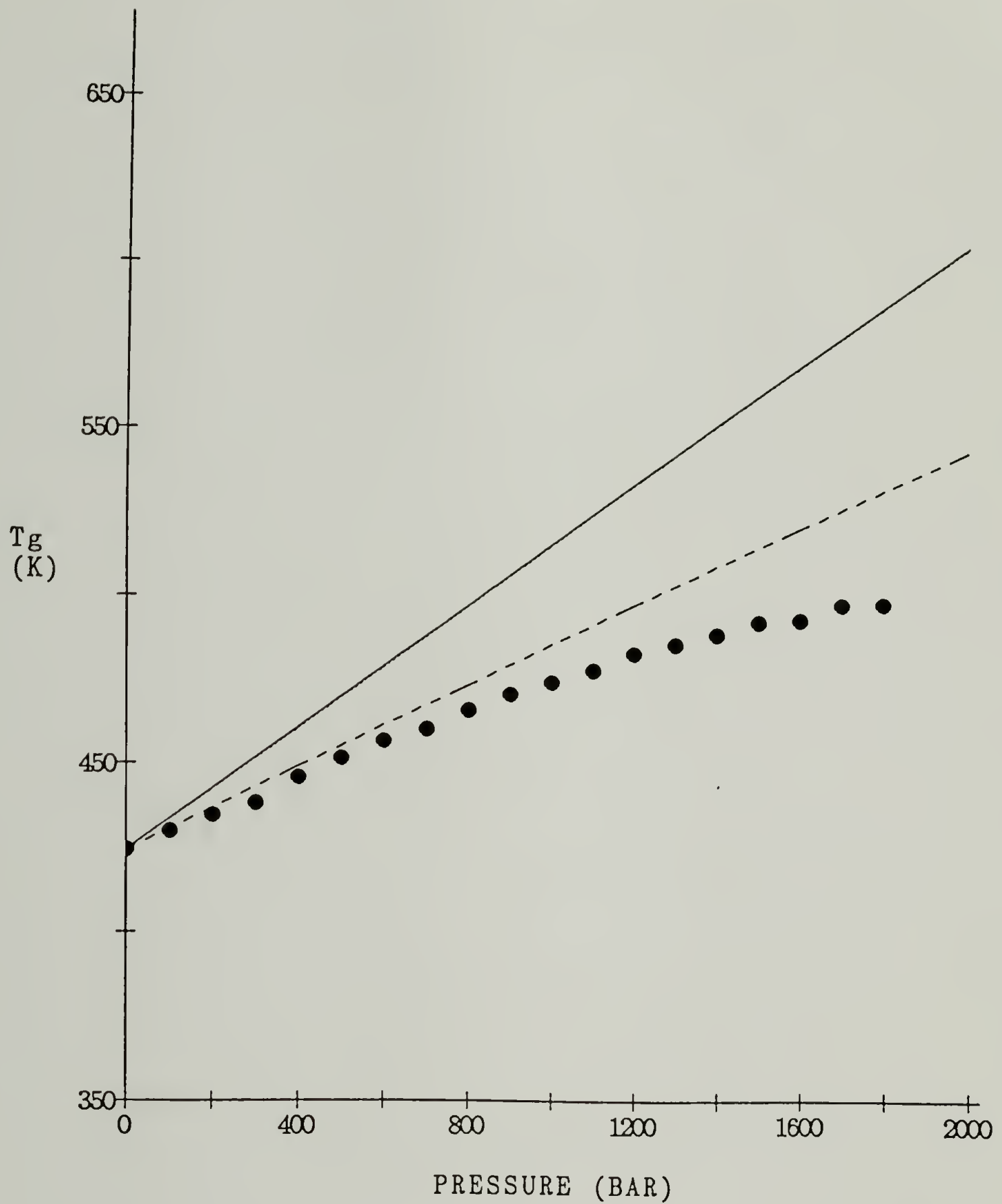


Figure 5.9

Predictions of T_g versus pressure by MFLG model using constant FV (—), S (\cdots), and TS (- - -) criteria against literature data for PC by Zoller [1982] (\bullet).

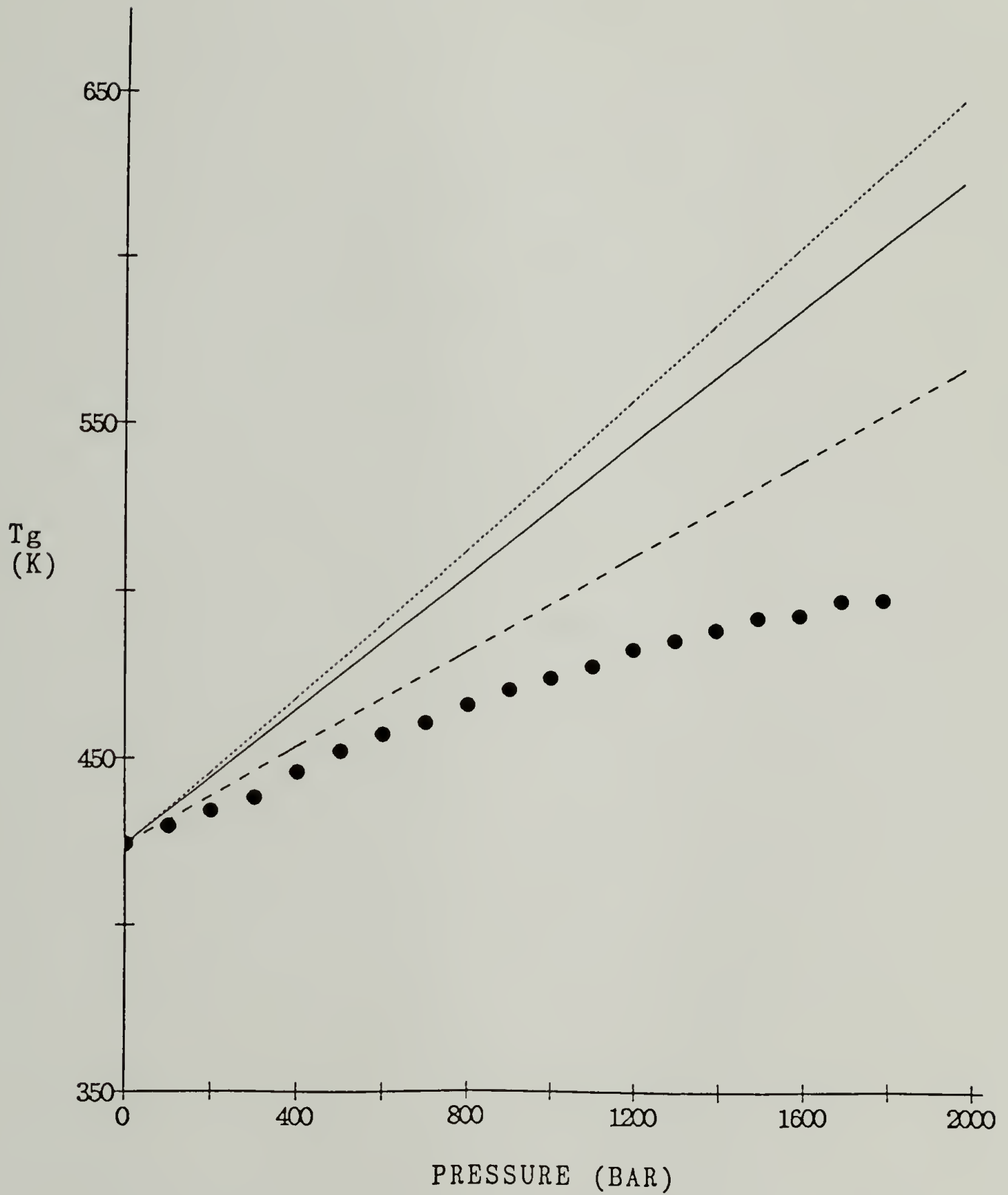


Figure 5.10

Predictions of T_g versus pressure by modified MFLG model using thermodynamic criteria; symbols same as in Figure 5.9.

Table 5.4

Values of FV, S, and T_gS for Polystyrene, Poly(methyl methacrylate), Poly(vinyl acetate), and Bisphenol A Polycarbonate using Modified MFLG Model

Polymer	FV	S	T_gS	$(Zg \times FV)$	$(Zg \times S)$	$(Zg \times T_gS)$
PS	.0874	3.23	1182	9.70	358	1.31×10^5
PMMA	.0831	4.34	1640	5.54	289	1.09×10^5
PVAc	.0726	3.69	1123	2.94	149	4.5×10^4
PC	.0738	2.52	1068	N.A.	N.A.	N.A.

Note: $Zg = N \times c_1 \times M_0$ where N is the number of monomer units involved in a cooperative unit at T_g [Warfield and Hartmann, 1982], M_0 is the molecular weight per monomer unit, and $c_1 = m_1/M$.

5.3 Summary of Chapter 5

The glass transition has been approximated as a freezing-in process involving one order parameter. Three separate parameters have been considered; free volume, entropy, and relaxation time, the latter represented by the quantity TS as derived by Adam and Gibbs [1965]. Using the MFLG model, the $\partial T_g/\partial p$ curve has been calculated for the four amorphous polymers polystyrene, poly(methyl methacrylate), poly(vinyl acetate), and polycarbonate using each of the criteria mentioned above. Because all of the necessary material constants are found via fitting of pVT data against the MFLG equation of state, no adjustable parameters are involved in the calculation of $\partial T_g/\partial p$.

Predictions of $\partial T_g/\partial p$ and $\partial \rho_g/\partial p$ employing the constant TS criterion are significantly more accurate than either the iso-entropy or iso-free volume situations for all four polymers. A modification to the MFLG model, which allows the number of segments per molecule, as well as the surface area per segment, to vary with temperature, further increases the accuracy of the predictions for three of the four polymers studied.

CHAPTER 6

Predicting the Composition Dependence of the Glass Transition of Mixtures

Chapter 6 is broken into two main sections. In the first, the three thermodynamic criteria used in Chapter 5 to predict the T_g of polymers versus pressure are evaluated in calculations of the T_g of polymer-solvent mixtures as a function of composition. The second section brings together the results from Chapters 4 and 5 and the first part of Chapter 6, *i.e.*,

1. Predictions of sorption of gases by polymers versus pressure.
2. Predictions of $\partial T_g / \partial p$ of pure polymers versus pressure.
3. Predictions of T_g of mixtures versus composition.

to predict the T_g of the PS-CO₂ and PMMA-CO₂ systems at pressures above the critical point of the gas.

Although the modified version of the MFLG model showed promise in calculations of the pressure effect on the T_g of amorphous polymers in Chapter 5, it is not clear how mixing will affect the temperature dependence of the segments. Therefore, the calculations of the effect of diluent concentration on the T_g of a polymer will be performed using only the Zero Order MFLG model.

6.1 Comparison with other Models

A number of expressions, both empirical and based on fundamental principles, have been proposed to describe the behavior of T_g versus diluent concentration. Application of many of these models to the prediction of the T_g of a gas-polymer mixture would be difficult, owing either to the necessity of determining one or more adjustable parameters [Fox, 1956; Wood, 1958; Gordon, *et al.*, 1977; Chow, 1980;], or to lack of an explicit pressure dependence of the T_g of the polymer itself [Kelley and Bueche, 1961; Couchman, 1979]. Two notable exceptions are the Gibbs-DiMarzio (GD) model [Gibbs and DiMarzio, 1958] and the lattice model of Kanig [1963]. An extensive comparison of the MFLG and GD models has been made in Chapter 5. To summarize:

1. The GD equation of state (EoS) is of the same general form as that of the MFLG, but since the GD model is based on use of a "rigid" lattice, both α and γ are tied to the lattice coordination number and to m (in addition, $g_{10} = 0$). This form of the EoS has been shown to be less accurate than the MFLG in describing both polymer and non-polymer pVT behavior. On the other hand, the GD entropy expression contains an added temperature dependence not found in the analogous MFLG expression, a result of the inclusion of the postulated effect of barriers to segmental rotation by Gibbs and DiMarzio.
2. Inclusion of the GD terms which account for the effect of barriers to rotation in the MFLG entropy expression, along with stipulation of zero entropy at T_g , is not a viable route to modelling T_g behavior in that, in many cases, due to the values of the adjustable parameters (found by fitting the MFLG EoS against pVT data, as before), the entropy can never be zero, so long as there are holes present, despite the added temperature dependent terms.

Use of the extra GD terms with merely a constant entropy, rather than a zero entropy, as the condition for T_g is possible, but still unsatisfactory as it would lead to additional adjustable parameters which could only be found via fitting against T_g versus pressure (or diluent concentration) data. It is desired at this time to avoid such a situation.

As shown in Chapter 5, the Kanig approach is closely related to that used herein, albeit with a less accurate model for describing pVT and phase separation data. The difference between Kanig's criterion and the constant FV condition used here lies in Kanig's use of the "vibration" volumes, such that $(\partial\phi_0/\partial T)_V \neq 0$. Using the constant vibration/hole volume ratio criterion, Kanig was able to show good fits to the polystyrene T_g versus diluent concentration data of Jenkel and Heusch [1953]. However, while Kanig fit his equation for the T_g to the data, the necessary binary interaction parameters of the MFLG model will be found via fitting against phase separation data, thus rendering the modelling of T_g versus diluent concentration a prediction rather than a fit.

6.2 Predicting the Glass Transition of Mixtures Using Thermodynamic Criteria

The thermodynamic criteria for T_g to be compared are those three examined in Chapter 5, the constant free volume (FV), constant entropy (S), and the constant relaxation time, represented by a constant TS, as derived by Adam and Gibbs [1965]. The entropy of a mixture is defined in the usual way:

$$S = -\left(\frac{\partial\Delta A}{\partial T}\right)_{V, n_i} = -\left(\frac{\partial\Delta A}{\partial T}\right)_{n_0, n_1, n_2} \quad (6-1)$$

Therefore, substituting the MFLG model expression for the free energy (equation 4-9) into equation (6-1):

$$\begin{aligned} \frac{S}{N_\phi} = & -R \left(\phi_0 \ln \phi_0 + \frac{\phi_1}{m_1} \ln \phi_1 + \frac{\phi_2}{m_2} \ln \phi_2 \right) \\ & - R \left(\phi_0 \phi_1 \left(\frac{\alpha_1 + g_{10}(1 - \gamma_1)}{Q} \right) + \phi_0 \phi_2 \left(\alpha_2 + \frac{g_{20}(1 - \gamma_2)}{Q} \right) \right) \quad (6-2) \\ & - R \left(+\phi_1 \phi_2 \left(\alpha_m + \frac{g_{m0}(1 - \gamma_1)(1 - \gamma_2)}{Q} \right) \right) \end{aligned}$$

Equation (6-2) defines the constant S and constant TS criteria for the model. The constant free volume criterion is defined as the number of hole-segment contacts rather than simply by the hole fraction. For the binary case the FV is therefore:

$$\frac{FV}{N_\phi} = \frac{\sigma_0 \phi_0 (\phi_1(1 - \gamma_1) + \phi_2(1 - \gamma_2))}{1 - \gamma_1 \phi_1 - \gamma_2 \phi_2} \quad (6-3)$$

Following the determination of all of the necessary material parameters, both pure component and binary (see Chapters 2 and 4), the segmental values for each of the three T_g criteria (FV, S, TS) for each component were calculated using T_g 's from the literature and the defining equations for the criteria of pure components (see Chapter 5). The T_g versus weight fraction diluent is then calculated via the simultaneous solution of the binary EoS and:

$$\frac{Cr_{sol}}{N_\phi} = \phi_1 Cr_1^0 + \phi_2 Cr_2^0 \quad (6-4)$$

where the Cr_i^0 are the segmental values of the criterion of interest for the pure components and Cr_{sol} is the analogous value for the binary mixture as defined by equations (6-2) and (6-3). In the case where the diluent is a gas, and the

desired result is a prediction of T_g versus pressure, the swelling equations, (4-12) and (4-13), are used to calculate the ϕ_i 's versus temperature and pressure followed by the procedure outlined above.

6.2.1 Effect of the Molecular Weight on the Glass Transition: Chain Ends as Diluent

The observed decrease of T_g as the molecular weight of a polymer decreases has, in the past, been attributed to the plasticizing effect of the chain ends. Assuming that the chain ends of a polymer act as a diluent, the influence of molecular weight on the T_g can be modelled using the simplest form of binary mixture:

1. All binary parameters (α_m, g_{m0}, g_{m1}) are set to zero.
2. Pure component parameters are identical for diluent and polymer.
3. Diluent concentration, w_1 , is $2/DP$, where DP is the degree of polymerization.

Modelling of T_g versus molecular weight as outlined above was tested against literature data for polystyrene [Ueberreiter and Kanig, 1952; Cowie, 1975; Claudy, *et al.* 1983]. Results are shown in Figure (6.1). While the constant TS condition produces the most accurate predictions, it should be noted that the mixture of chain ends and "middles" is assumed to be ideal such that the volume change on mixing and heat of mixing are assumed to be zero. The effect of these excess functions on calculations of T_g as a function of diluent concentration will be discussed in the next section.

6.2.2 Polymer-Liquid Mixtures: Polystyrene-Toluene and Polystyrene-Cyclohexane

Pure component parameters for toluene and for cyclohexane were found by fitting the applicable unary MFLG expressions against literature data in Chapters 4 and 5. Ideally, as demonstrated in Chapter 4, binary parameters for the MFLG model should be determined by fitting of the appropriate equations to concentrated solution data, because the mean field approximation is expected to be valid in this concentration regime. Unfortunately, only dilute solution phase data was available for the PS-cyclohexane and PS-toluene systems.

Binary parameters for the PS-cyclohexane system were determined by fitting the MFLG spinodal equation to data versus molecular weight measured by Derham, et al. [1974] in Section 4.2.1. In the case of the PS-toluene binary, the available data consist of cloud point curves (CPC's) of various molecular weight PS's in the vicinity of the critical point [Saeki, *et al.* 1973]. While the CPC is normally associated with the binodal, because the coexisting concentrations were not determined, the MFLG binodal equations could not be used to find the binary parameters. In addition, the critical points (LCST's) had not been measured but had been estimated from the minima of the CPC's by Saeki, *et al.*. The CPC's are very flat near the critical point which could bring large error to such an estimation. Therefore it was decided to find the binary parameters for the PS-toluene system by fitting the MFLG spinodal to the CPC data. Some results are shown in Figure 6.2.

The T_g of toluene was assumed to be 115K [16,17] and that of cyclohexane was estimated to be approximately 80K based on the T_g 's of various alkyl-cyclohexane compounds [Carpenter, *et al.* 1967; Angell, *et al.* 1978]. Using these values and the measured T_g of polystyrene, the three criteria were calculated

for each component. The T_g versus diluent concentration was then determined using the previously outlined procedure and equation (6-2) or (6-3) as required. Results are given in Figures 6.3 and 6.4.

From the results in Figures 6.3 and 6.4, it would appear that the FV condition produces the best prediction for the PS-cyclohexane binary whereas the TS criterion provides the most accurate results in the case of PS-toluene. However, because dilute solution data were used to fit the binary parameters, these results were examined more closely.

As shown in Chapter 4, the temperature dependence of the initial set of binary parameters for the PS-cyclohexane binary was poor. By fitting the model to dilute solution data, the values of the parameters compensated for the lack of a non-mean field dependence to the MFLG model at the expense of the useful temperature range of the model. Therefore, a second set of binary parameters was determined whose temperature dependence is better but which cannot describe the shape of the phase diagram as well as parameter set #1. Binary parameter set # 2 was also used to construct a T_g versus concentration diagram for the polystyrene-cyclohexane mixture (see Figure 6.5).

As can be seen, the FV-based prediction is not as severely influenced by the choice of parameter set as the curves based on either a constant S or TS. Intuitively, it would be expected that the prediction of T_g made using the FV criterion would be strongly influenced by ΔV_m , the volume change on mixing. Predictions of ΔV_m versus weight fraction using parameter sets 1 and 2 for the PS-cyclohexane system are compared to values calculated from Scholte's [1970] density measurements in Figure 6.6. The relative magnitude of the change in the position of the constant FV curve on switching from parameter set 1 to 2

appears to be related to the magnitude of the change in the calculated ΔV_m on changing parameter sets.

As can be seen in Figure 6.6, the predicted sign of ΔV_m is wrong, yet the prediction of the T_g using the FV criterion is still the most accurate. To investigate this observation, a third set of binary parameters was found in which the fitting was heavily biased towards a very accurate prediction of ΔV_m . This was accomplished by assigning a tolerance to the solution densities an order of magnitude lower than that for either the temperatures or the weight fractions during the fitting. The resulting predictions of ΔV_m were naturally correct in both sign and magnitude yet this third parameter set did not significantly change the predicted T_g curve from that calculated using parameter set 1. It would appear that only the magnitude of ΔV_m is important in the FV-based prediction of T_g .

Toluene is a better solvent for polystyrene than is cyclohexane; consequently the PS-toluene binary exhibits only LCST type phase separation. Therefore the only available measure of the accuracy of the temperature dependence of the binary parameters is the fit to the cloud points in Figure 6.2. Thus it would appear that if the binary parameters show the proper temperature dependence, the TS criterion will produce an accurate prediction of the T_g .

Because solution densities were not available in the temperature range of the cloud points used in the fitting of the PS-toluene system, the densities had to be estimated. Naturally this brought large error to the prediction of the volume change on mixing Figure 6.7. The large error in ΔV_m translates to a large error in the FV-based prediction of the T_g .

It appears that if the temperature dependence of the binary parameters is accurate, then the constant TS condition will produce a good description of the behavior of the T_g of a polymer-diluent mixture. It also appears that if the volume change on mixing is close to zero, then the FV criterion will also produce an accurate prediction of the T_g . These conjectures will be explored further in the next section on gas-polymer mixtures. In these systems the binary parameters were found using concentrated solution data, thereby eliminating the ambiguity present in the fitting of the PS-cyclohexane and PS-toluene systems. In addition, the volume change on mixing for such systems is highly non-ideal, which will provide a good test for both the MFLG model and the FV criterion.

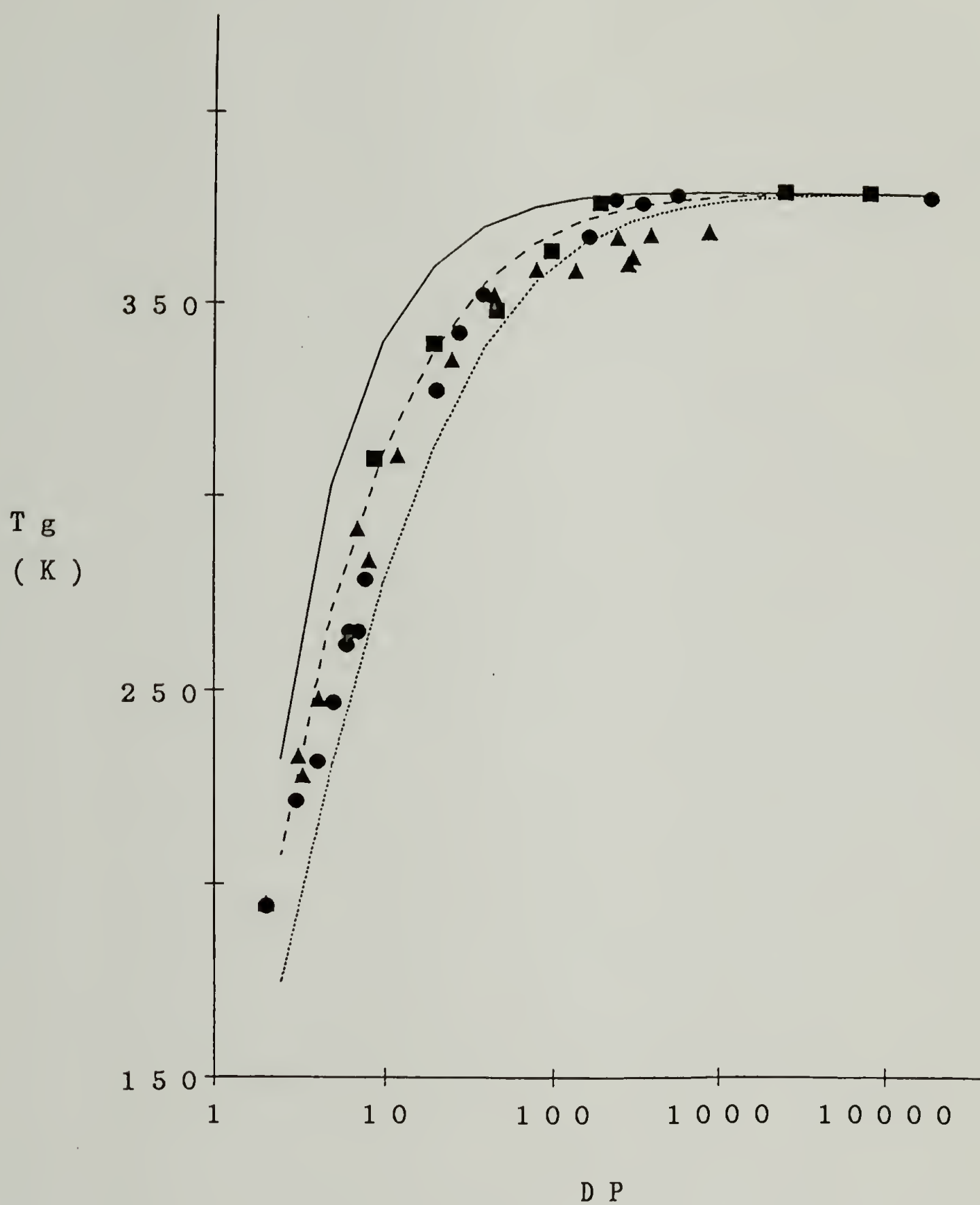


Figure 6.1

Predictions of T_g versus molecular weight using MFLG model and constant FV (—), constant S (···), and constant TS (- - -) criteria compared with data by Ueberreiter and Kanig [1952] (\blacktriangle), Cowie [1975] (\blacksquare), and Claudy, *et al.* [1983] (\bullet).

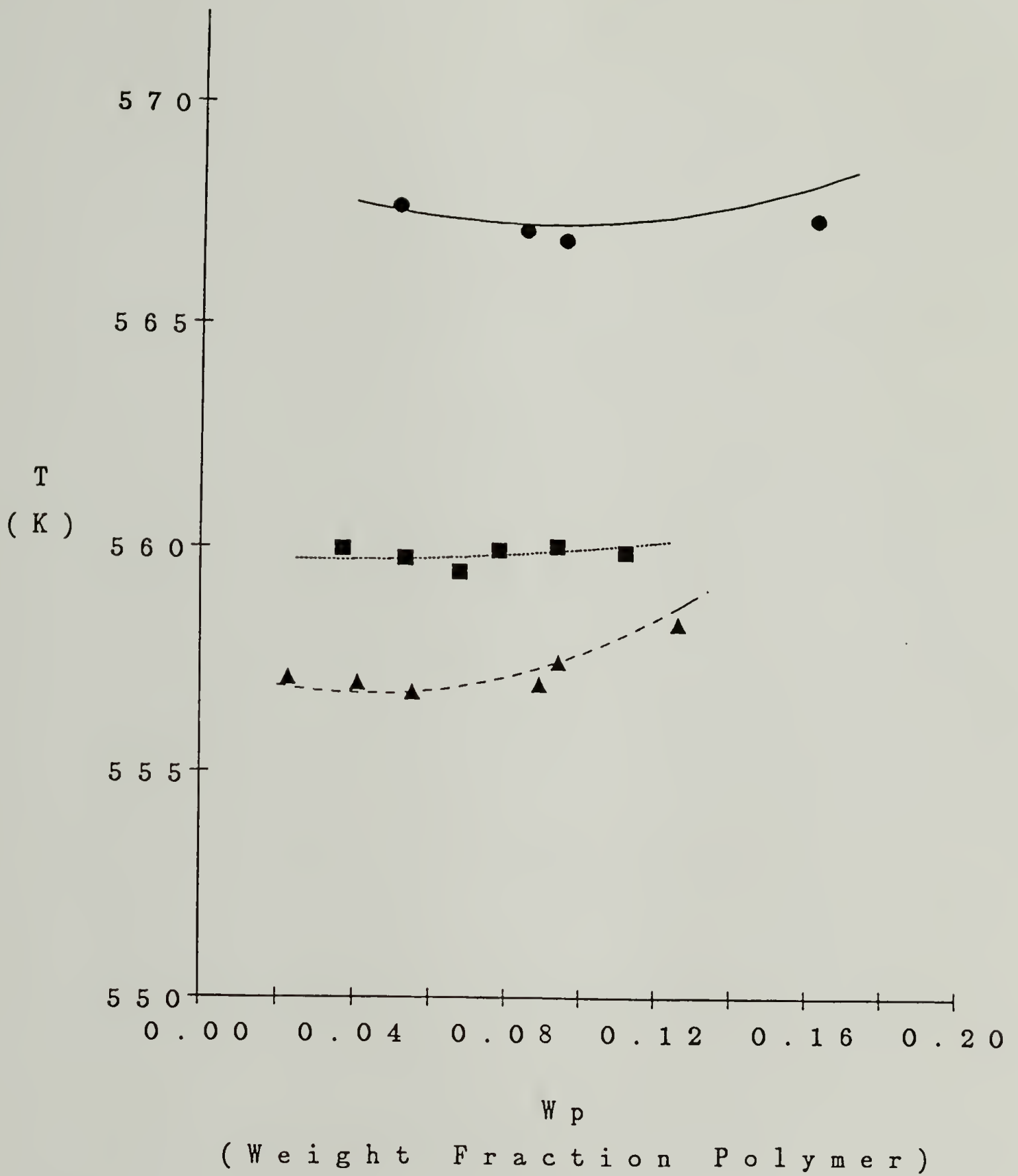


Figure 6.2

Calculated spinodals for polystyrene-toluene using Zero Order MFLG model and cloud points by Saeki, *et al.* [1973] at three molecular weights: (—),(•), $M_w=37,000$; (···),(■), $M_w=97,000$; (- - -),(▲), $M_w=200,000$.

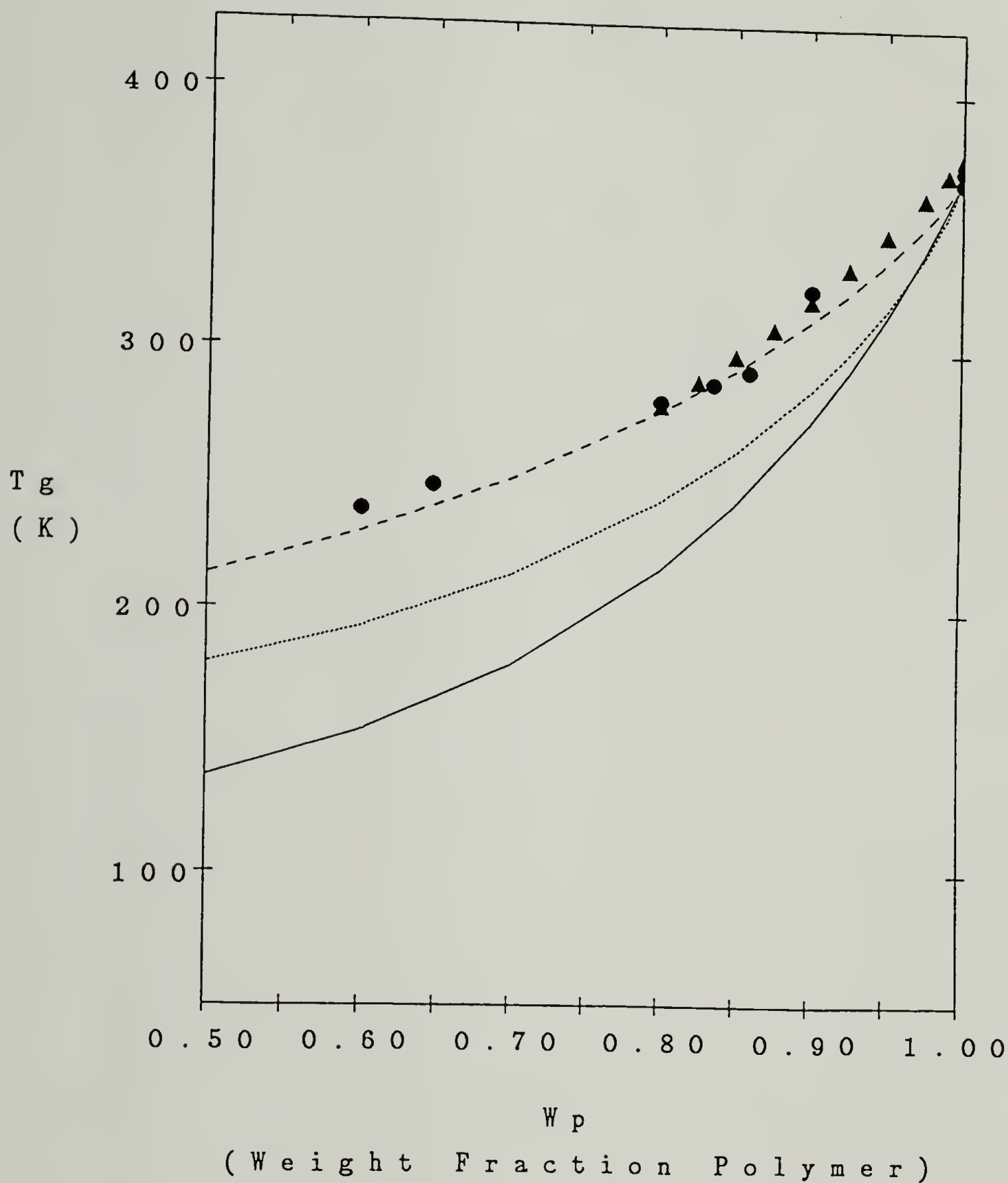


Figure 6.3

Predicted T_g of polystyrene-toluene mixture versus weight fraction polymer using MFLG model with constant FV (—), constant S (···), and constant TS (- - -) criteria and data by Masa, et al [1973] (▲), and Adachi, et al. [1975] (●).

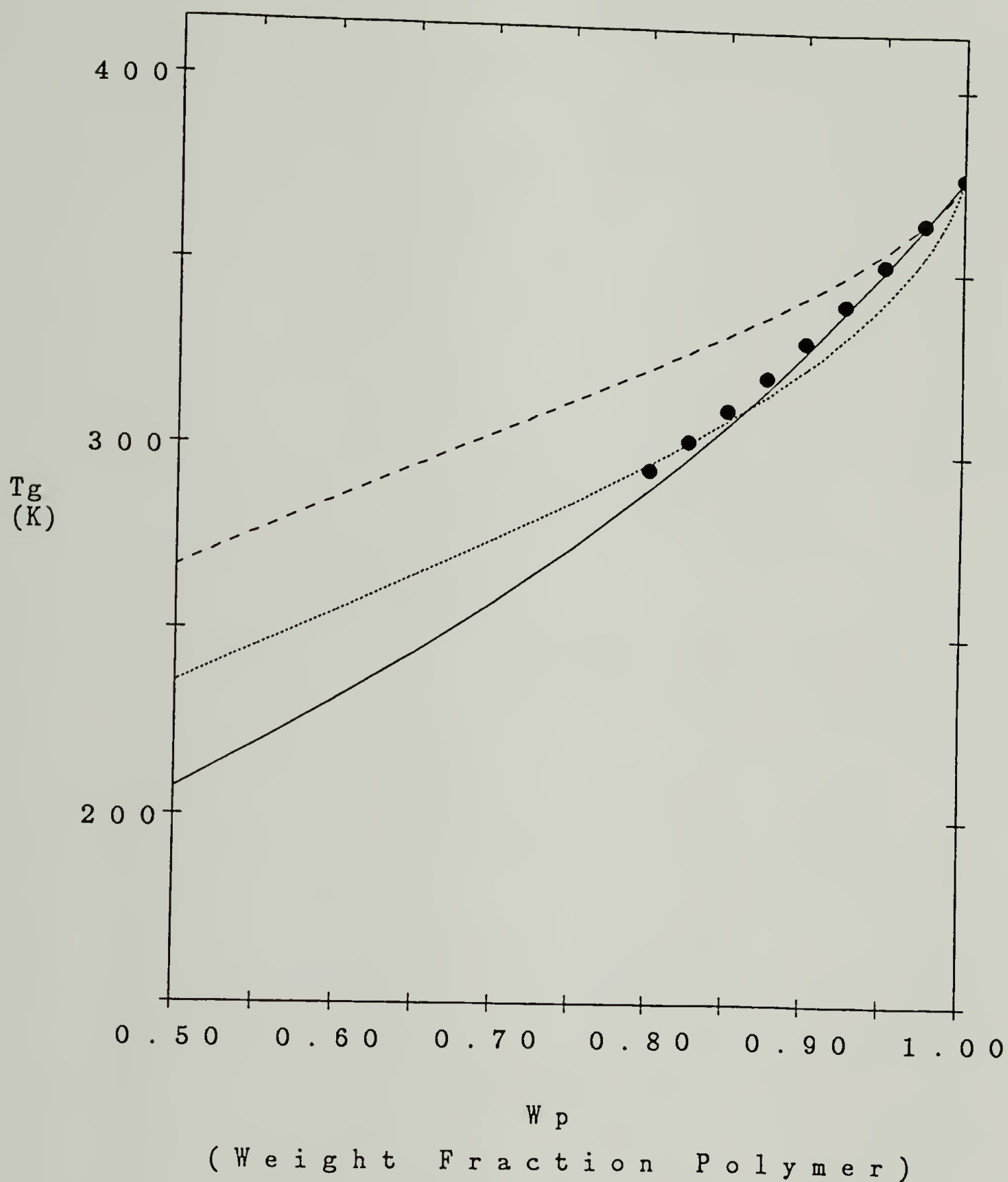


Figure 6.4

Predicted T_g of polystyrene-cyclohexane mixture versus weight fraction polymer using MFLG model with parameter set 1 and constant FV (—), constant S (···), and constant TS (- - -) criteria and data by Masa, *et al.* [1973] (●).

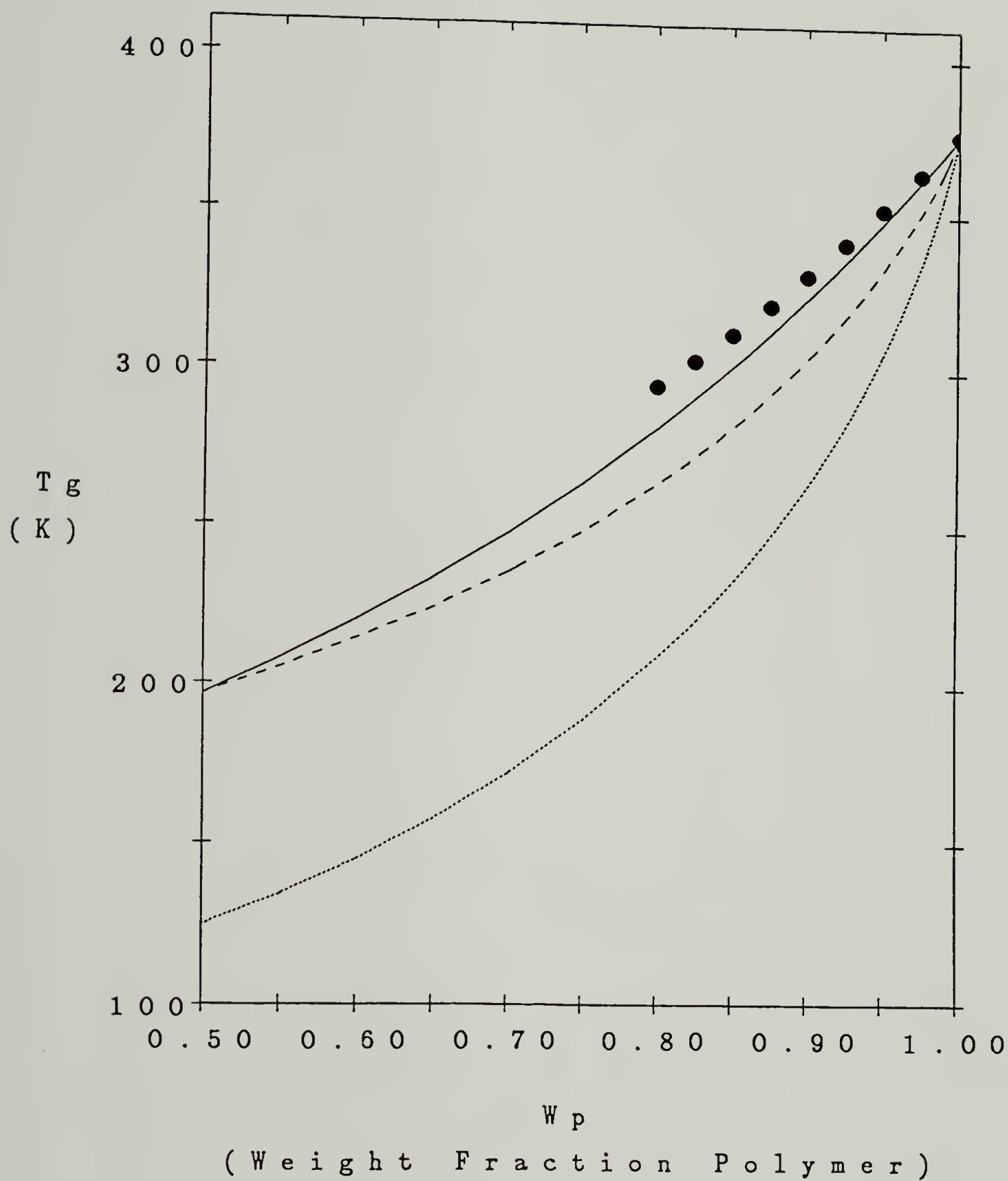


Figure 6.5

Predicted T_g of polystyrene-cyclohexane mixture versus weight fraction polymer using MFLG model with parameter set 2 and constant FV, constant S, and constant TS criteria; symbols same as for Figure 6.4.

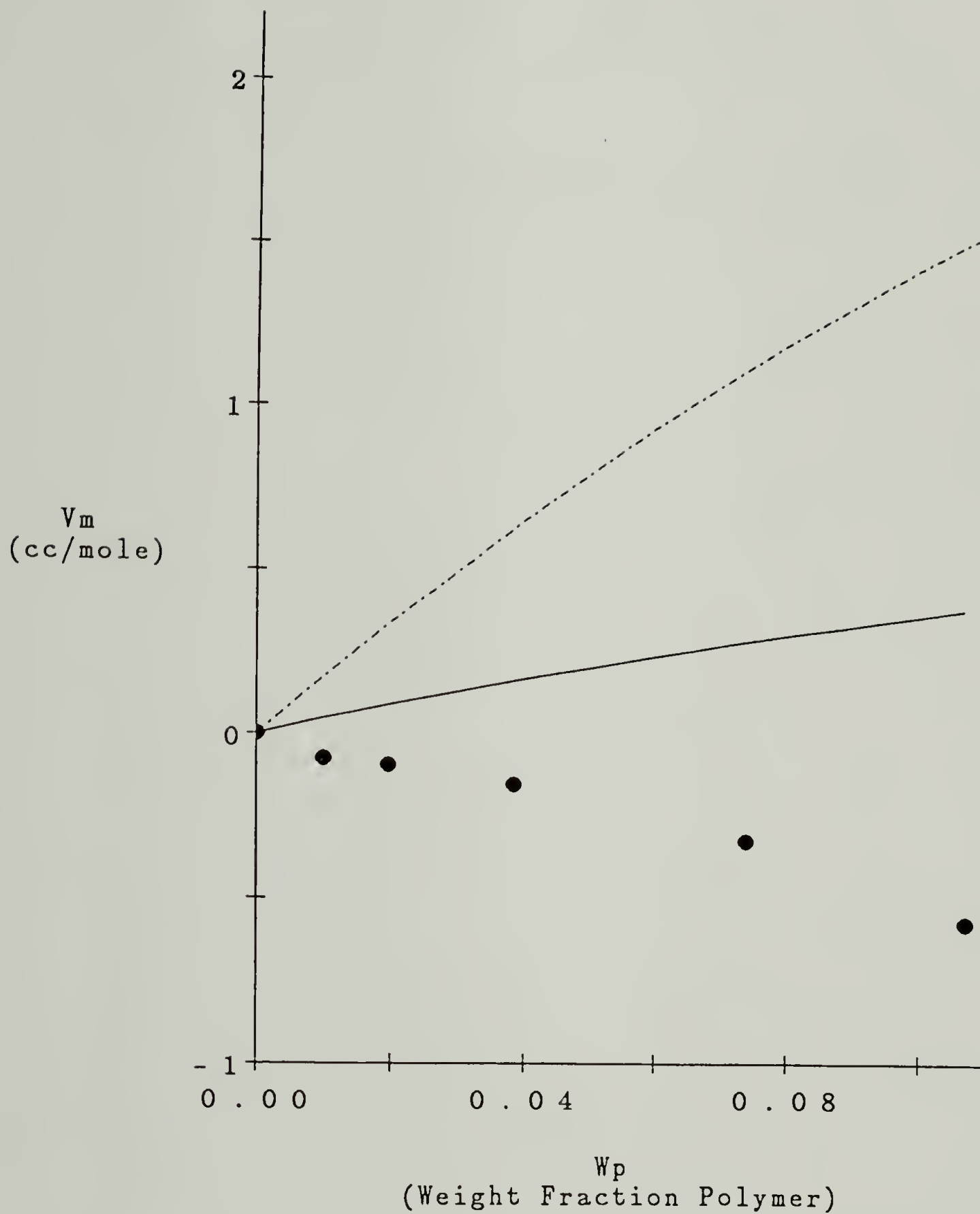


Figure 6.6

Predictions of ΔV_m of polystyrene-cyclohexane mixtures at $T=298K$ by MFLG model with parameter set 1 (—) and parameter set 2 (···) compared to data derived from solution density measurements of Scholte [1970] (●).

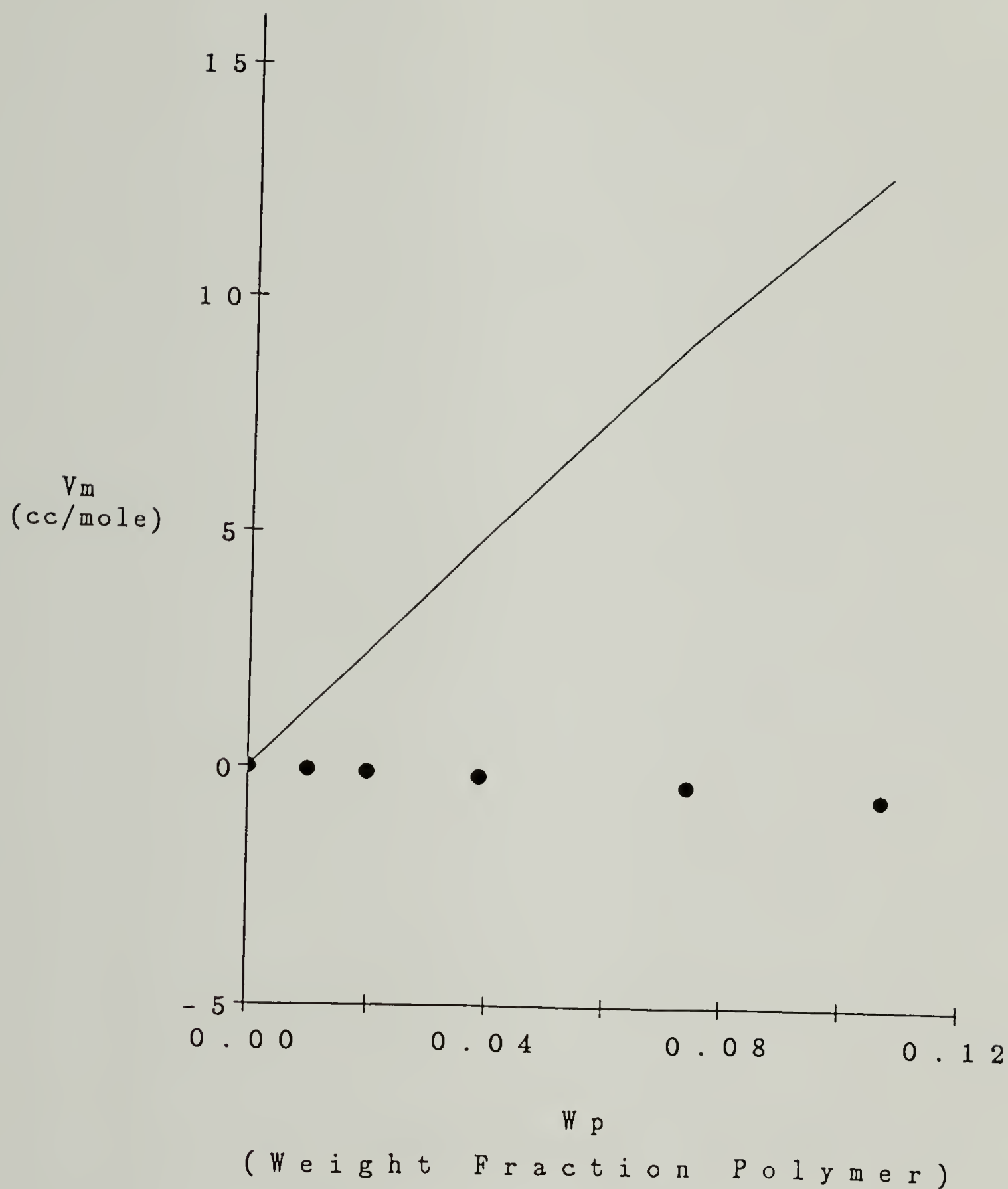


Figure 6.7

Predictions of ΔV_m of polystyrene-toluene mixtures at $T=303K$ by MFLG model (—) and data derived from solution density measurements of Scholte [1970] (●).

6.3 Effect of Gas Pressure on the Glass Transition of Polymer

Knowledge of the behavior of $\partial T_g/\partial p$ for a polymer in a high pressure gas environment is important in that the extent of sorption of gases by polymers [Morel and Paul, 1982; Sefcik, 1986], the solubility of polymers in supercritical fluids [Schroeder and Van Arndt, 1976], and the ability of polymers to undergo solvent-induced crystallization [Chiou, *et al.*, 1985a], all depend on the difference between the ambient temperature and T_g . However, it is difficult to measure the T_g of a polymer in a high pressure gas environment. A means by which to predict the T_g of a polymer-gas mixture versus gas pressure without the need for determining adjustable parameters would therefore be quite useful.

Gases, like low molecular weight liquids, readily plasticize amorphous polymers [Chiou, *et al.* 1985b]. Since the amount of gas absorbed by a polymer generally increases with increasing pressure, the magnitude of the T_g suppression will initially increase as gas pressure is raised. A point of diminishing returns will eventually be reached, however, as increasing hydrostatic pressure by itself raises T_g , acting against the plasticizing effect of the gas. The T_g of a polymer in such an environment will consequently pass through a minimum versus pressure [Wang, *et al.*, 1982]. The chemical potential of a gas, and consequently the amount absorbed by a particular polymer, is a function of both temperature and pressure. Since, as stated above, the T_g is a function of both pressure and diluent concentration, the position of the T_g minimum in a gas-polymer mixture is a function of both temperature and pressure.

6.3.1 Examples from the Literature

Because it is difficult to measure the glass transition of a polymer-gas mixture at high pressure, the available literature " T_g " results on such systems are usually indirect measurements. For example, in the study by Wang [1981] on the polystyrene- CO_2 system, the data were calculated using the WLF equation and shift factors found by superimposing creep curves of PS exposed to high pressure CO_2 . The data are therefore reasonable approximations. In a study by Schroeder and Van Arndt [1976] on the PVC- CO_2 mixture, it was observed that the slope of each of the isobaric solubility-temperature curves display a discontinuity. Extrapolation of these kinks back to zero pressure yields the T_g of the pure PVC; thus the T_g of the mixture was estimated to be the kink point. Both of these indirect observations indicate that the T_g of the polymer-gas mixtures develops a minimum at some point as pressure is increased.

In addition to these two studies, experimental results on the polycarbonate- CO_2 mixture also imply the existence of a T_g minimum. The original aim of this work was to attempt to measure the solubility of polycarbonate in supercritical CO_2 , since, by inspection, CO_2 should be a reasonably good solvent for this polymer. The first several runs in the supercritical extraction unit showed little or no solubility and either a significant embrittlement or a whitening of the extracted films, or both. Subsequent DSC and WAXS measurements showed the whitened material to be semi-crystalline whereas the films were initially completely amorphous. This solvent-induced process was investigated further.

6.3.2 Polycarbonate-Carbon Dioxide

Chiou and coworkers [Chiou, *et al.* 1985a,b] have shown that CO₂ will plasticize and thereby induce crystallization in poly(ethylene terephthalate) and in poly(vinylidene fluoride)/poly(methyl methacrylate) blends at temperatures below their respective T_g's. Carbon dioxide was also shown to plasticize bisphenol A polycarbonate, but apparently not to the extent required to cause crystallization. Chiou, *et al.*, conducted experiments only up to a pressure of 35 atm., yet the degree of plasticization might be expected to increase markedly above the critical point of CO₂ (304.2K and 73.8 bar), as is the case in the PMMA-CO₂ system. Theory also supports this hypothesis [Flory, 1970; Patterson, 1972] in that CO₂ density increases rapidly above the critical point, thus decreasing the free volume difference between the polymer and gas. The entropy of mixing therefore becomes more positive, increasing the size of the homogeneous region of the phase diagram.

As previously stated, in the course of experiments to determine the solubility of bisphenol A polycarbonate in supercritical CO₂, the gas was observed to induce significant crystallinity in the PC films. Because CO₂ is both the pressure-transmitting medium and a diluent whose properties vary significantly with temperature and pressure, these two variables combine to affect the crystallization rate, degree of crystallinity, and the melting temperature of the crystals so formed.

6.3.2.1 Experimental

Lexan 0.003 in. polycarbonate film from the General Electric Plastics Co., Pittsfield, MA, was used as received. Differential Scanning Calorimetry (DSC) showed the film to be amorphous with a T_g of $147C$.

Polycarbonate strips, 1 X 15 cm, were clamped at each end to a stainless steel frame. These sample assemblies were then inserted into the pressure cell of the Fluitron supercritical extraction unit, and the cell flushed with CO_2 . The temperature was raised from the ambient, after which the cell was rapidly pressurized using the two-stage diaphragm compressor. Samples were exposed to CO_2 for up to 12 hours. Following depressurization the samples were allowed to degas at room temperature for 2 hours prior to thermal analysis. Both the results of thermogravimetry, no weight loss below $300C$, and the position of the T_g 's of the treated films, $145 \pm 3C$, indicate that CO_2 was essentially absent from the polycarbonate samples after the degassing.

Melting endotherms and T_g 's were determined using a Perkin-Elmer DSC-4 with a TADS computer control and analysis system. Unless otherwise noted, the scanning rate was $10C/min.$. The percent crystallinity was calculated using a value of 26.2 cal/g for the heat of fusion of bisphenol A polycarbonate [Mercier and Legras, 1970].

6.3.2.2 Results and Discussion

Films of polycarbonate were exposed to CO_2 at pressures up to 600 atm. and temperatures of 50.0, 62.5, 75.0, 87.5, and $100C$. At 50.0 and at $62.5C$, the films remain transparent but become brittle after 4 hours of CO_2 exposure.

DSC thermograms reveal no signs of crystal growth, although some display an enthalpy relaxation at T_g , indicating annealing at sub- T_g conditions.

After CO_2 exposure at 75.0°C and 125 atm., the polycarbonate film whitens and deforms. Thermal analysis of the whitened samples shows two melting peaks (see figure 6.8). The higher melting peak (I) occurs between 210 and 230°C , whereas the lower (II) appears at 180 - 205°C . Peak II represents small crystallites formed due to the plasticizing effect of the CO_2 , whereas peak I is probably the result of simultaneous melting and recrystallization of portions of peak II during the DSC scan. This contention is supported by the results of a heating rate study. As the scan rate was increased from 2 to $80^\circ\text{C}/\text{min.}$, the proportion of the total melting endotherm associated with peak I drops from 100% to less than 5%. This type of double melting peak has been observed in the melting behavior of other thermoplastics as well [Sweet and Bell, 1972; Lemstra, *et al.* 1972; Todoki and Kawaguchi, 1977; Lee and Porter, 1987].

As the CO_2 pressure is increased, the volume fraction of CO_2 absorbed by the polycarbonate increases, lowering the T_g . As the T_g drops significantly below the ambient temperature, the chains become mobile and, prompted by the large undercooling, will crystallize. The low melting temperature of peak II (see Figures 6.8 and 6.9) indicates that the crystallites formed due to the CO_2 exposure are small, a result consistent with the high nucleation density found in solvent-induced crystallization of bisphenol A polycarbonate. Although raising the pressure increases chain mobility by increasing the CO_2 sorption thus lowering the T_g , a point of diminishing returns will eventually be reached, as mentioned in Section 6.3.1. While the slope of the sorption-pressure curve will begin to level out, the high pressure itself will work to raise T_g (by approximately $5^\circ\text{C}/100$ atm. [Zoller, 1982]). The net result is that the T_g may pass through a minimum as pressure is increased at constant ambient temperature. The

data in figure 6.10 show a rapid increase in crystallinity up to 350-400 atm., following the trend of the CO₂ density, but then flatten out, possibly due to a T_g minimum, whereas the CO₂ density continues to increase. The degree of crystallinity attainable in bisphenol A polycarbonate, 20-25%, is similar to that achieved when acetone or methylene chloride is used as the plasticizer [Mercier, *et al.* 1967; Kambour, *et al.* 1966].

As can be seen in Figure 6.8, the position of peak II initially moves upfield as pressure is increased but then reverses direction above 400 atm.. Crystallite size and perfection, and consequently melting temperature, are functions of the nucleation density, chain mobility during crystallization, and the degree of undercooling. Kambour *et al.* [1966], have suggested that chain mobility plays the dominant role in determining T_m in acetone-induced crystallization of polycarbonate. If the T_g of the polycarbonate-CO₂ mixture were to experience a minimum versus pressure, then chain mobility would observe a maximum, consistent with the behavior of peak II in Figure 6.8. In addition, this behavior occurs in spite of the effect of pressure alone on the size of the crystallites, which should raise the T_m .

Increasing the temperature at constant pressure will have two effects on the crystallization of polycarbonate. First, depending on whether the mixture exhibits upper critical or lower critical mixing behavior in that portion of the supercritical region under consideration, the solubility of the CO₂ in the polymer will either increase or decrease. Thus the T_g of the polycarbonate-CO₂ mixture could either increase or decrease owing to an increase in temperature. Second, a temperature increase will by itself promote chain mobility. The two effects could cancel or add together. A comparison of the DSC results for polycarbonate film exposed to CO₂ at 75 and 87.5°C shows that the percent crystallinity has increased, which implies additivity of the two effects and therefore UCST

behavior, or dominance of the effect of temperature over the effect of changes in diluent concentration.

Crystallization of bisphenol A polycarbonate induced by supercritical CO₂ proceeds at a rate similar to that of acetone- or methylene chloride-induced crystallization [Mercier, *et al.* 1967] (see Figure 6.11).

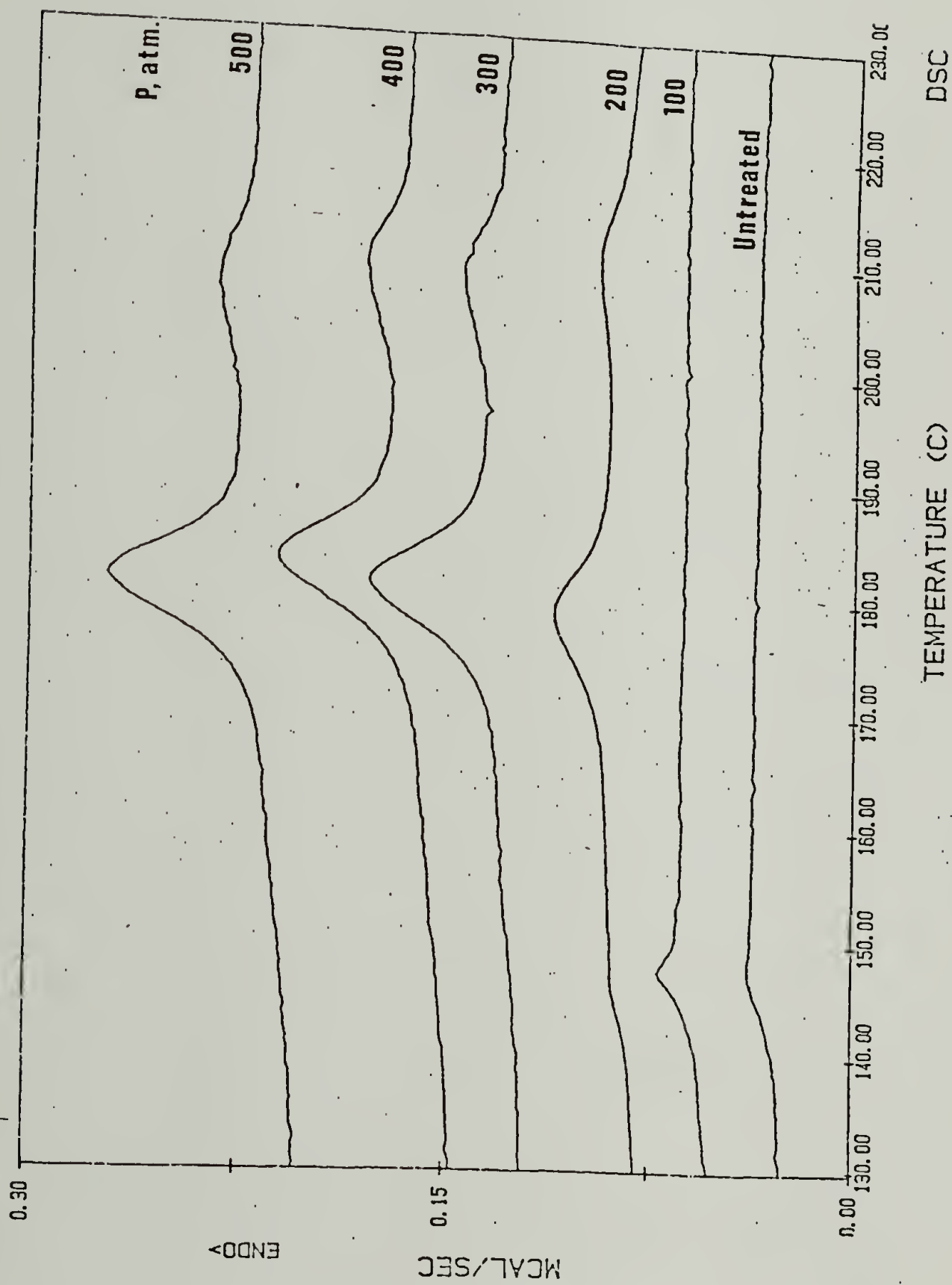


Figure 6.8

DSC results of bisphenol A polycarbonate exposed to CO₂ for 4 hours
at 75°C at pressures from 100 to 500 atm..

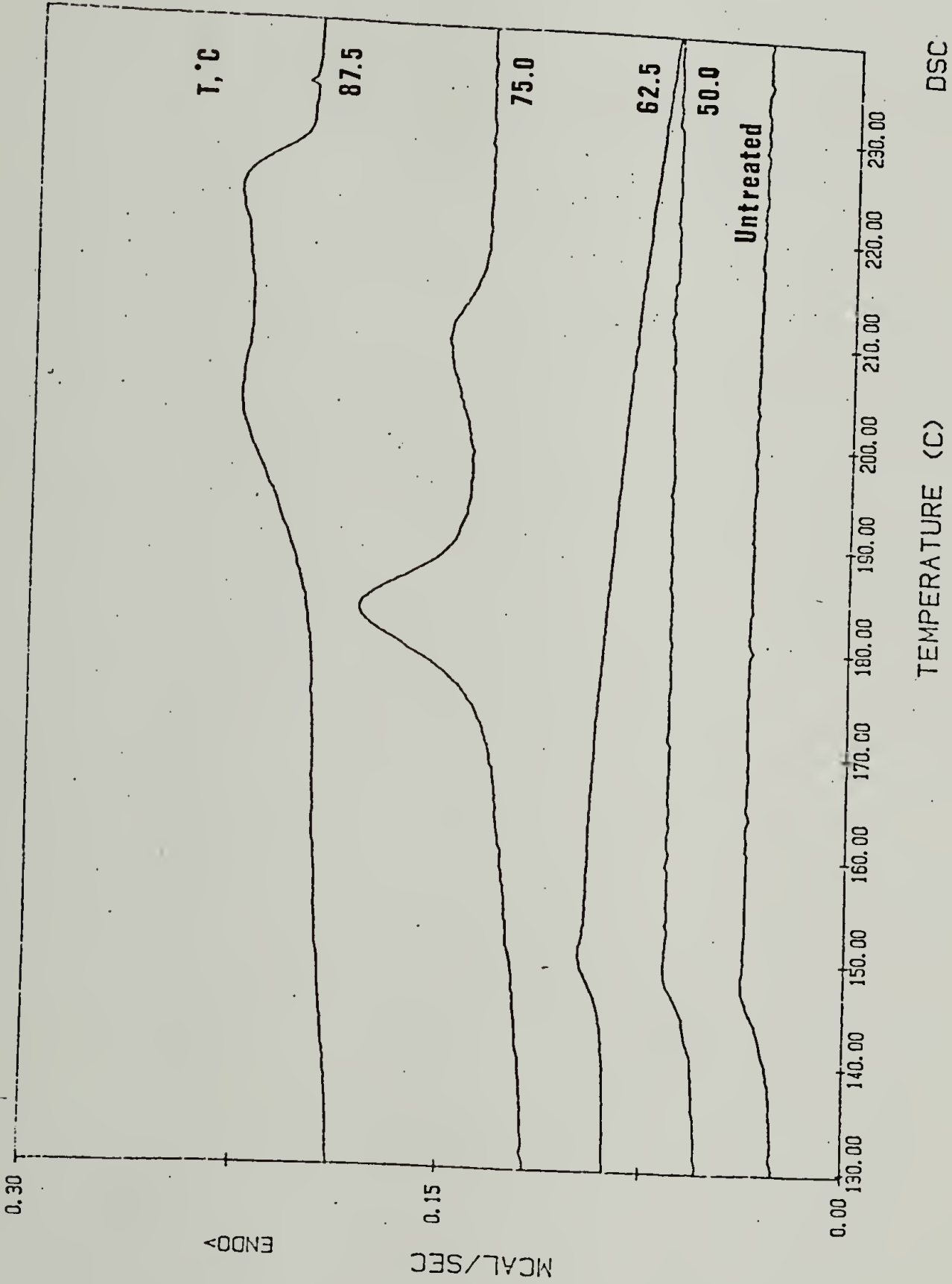


Figure 6.9

DSC results of bisphenol A polycarbonate exposed to CO₂ for 4 hours at 300 atm. at temperatures of 50, 62.5, 75.0, and 87.5C.

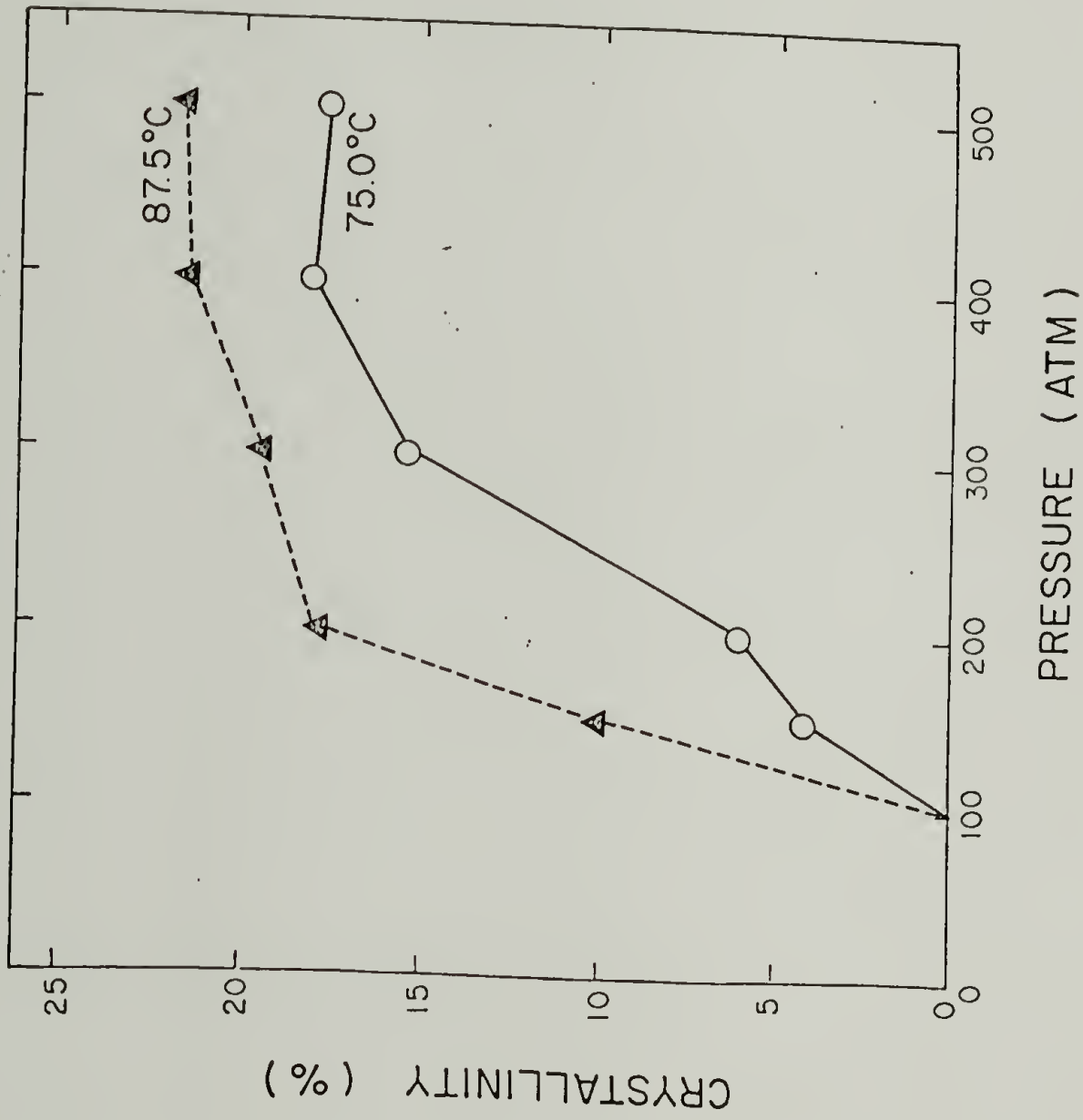


Figure 6.10

Percent crystallinity of bisphenol A polycarbonate exposed to supercritical CO₂ for 4 hours versus exposure pressure at temperatures of 75.0 and 87.5C.

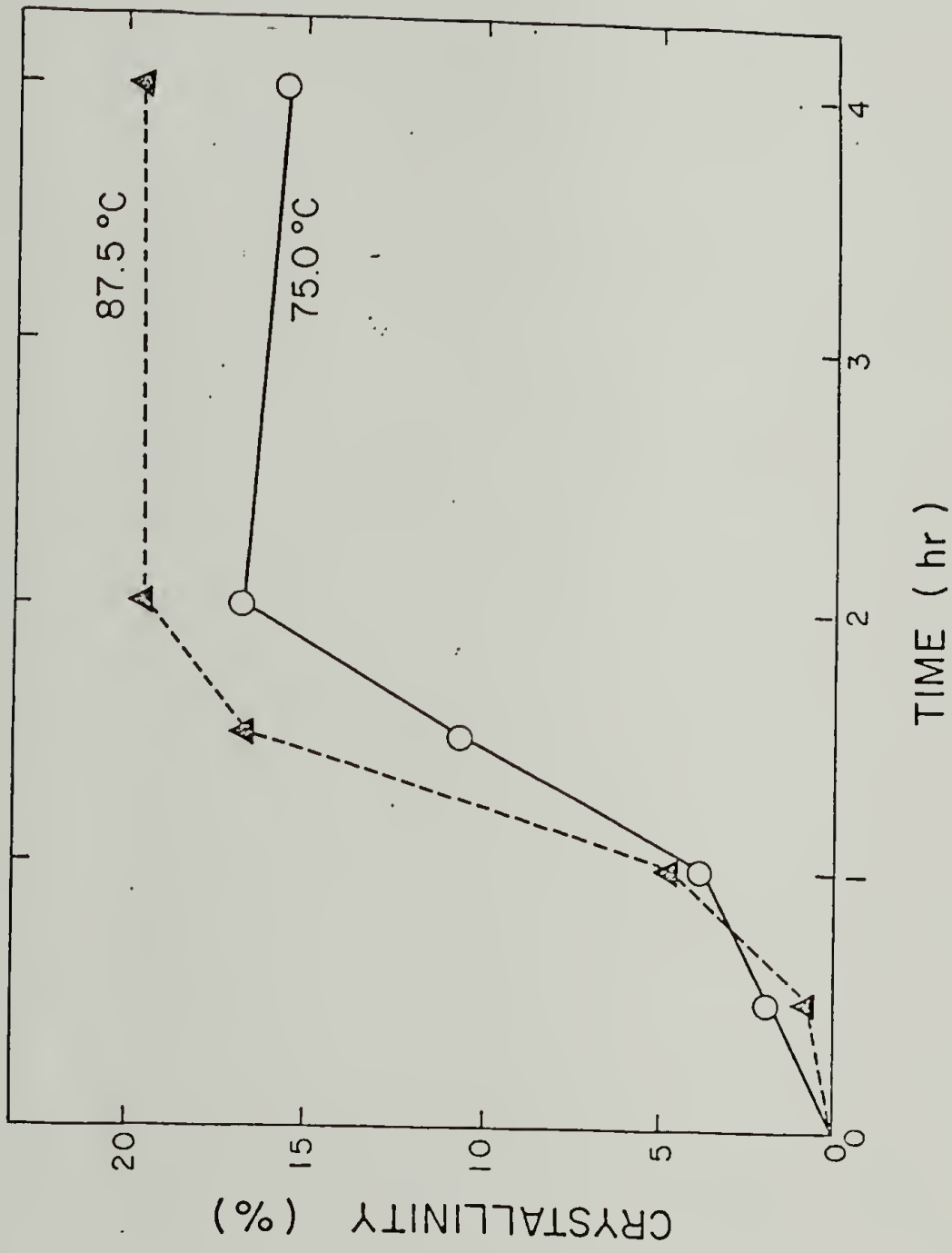


Figure 6.11

Percent crystallinity of bisphenol A polycarbonate exposed to supercritical CO₂ at 300 atm. at temperatures of 75.0 and 87.5C versus exposure time.

6.4 Predicting the T_g of Polymer-Gas Mixtures as a Function of Ambient Temperature and Pressure

6.4.1 Poly(Methyl Methacrylate)-CO₂

The determination of the binary parameters for the PMMA-CO₂ system has been described previously in Chapter 4.

The predictions of T_g as a function of CO₂ pressure using each of the three criteria are compared with data by Chiou, *et al.* [1985b], in figure (6.12). Because the T_g of CO₂ has not been reported, criteria for CO₂ (FV, S, TS) were set to zero, a reasonable approximation after noting the corresponding values for cyclohexane, which has a T_g of approx. 80K. CO₂ would be expected to have a lower T_g , if any, than cyclohexane. Again, the constant TS condition displays the most accurate prediction but that shown by the FV criterion is not far off at low pressure. As can be seen from Figure 4.14, the ΔV_m 's predicted by the MFLG model are, in general, too positive. As in the case of the PS-cyclohexane system, the binary parameters for PMMA-CO₂ were refit using a lower tolerance for the solution densities. The resulting set of parameters yields a slightly worse description of the sorption behavior (Figure 6.13), better predictions of ΔV_m (more negative) (Figure 6.14) yet a much poorer prediction of T_g versus CO₂ pressure using the constant FV criterion (Figure 6.15). This supports the contention that the FV criterion produces accurate predictions of T_g versus diluent concentration only in those systems with near-ideal ΔV_m . In addition, the predictions of the two criteria (TS and FV) differ substantially in the effect of hydrostatic pressure alone on the glass transition (see Chapter 5). The overprediction of $\partial T_g / \partial p$ by the constant FV criterion causes the T_g versus

pressure curve to level out and pass through a minimum before the constant TS-based curve.

Because both ambient pressure and temperature determine the degree of sorption of CO₂ by PMMA (and of course, the effect of pressure alone on the T_g of pure PMMA), both of these variables combine to affect the course of the T_g -P curve. Predictions of T_g versus pressure at four ambient temperatures using the constant TS condition are shown in Figure 6.16. That the curves are predicted to cross reflects the fact that the sorption isotherms are predicted to cross. A more meaningful representation of the predictions in Figure 6.17 is made by converting the data to $(T_a - T_g)$ versus pressure, where T_a is the ambient temperature. The quantity $(T_a - T_g)$ is a measure of how processable the polymer-gas mixture would be at a given T_a and pressure. As can be seen in Figure 6.17, $(T_a - T_g)$ is expected to increase rapidly up to approx. 100 bar, and at a slower rate thereafter. Values of $(T_a - T_g)$ as high as 50K could be obtained at ambient temperatures as low as 315K, over 60 degrees below the T_g of pure PMMA. In other words, a temperature of $T_g + 50$ for pure PMMA is approx 428K whereas 100 bar of CO₂ pressure drops this point by over 100K to 315K.

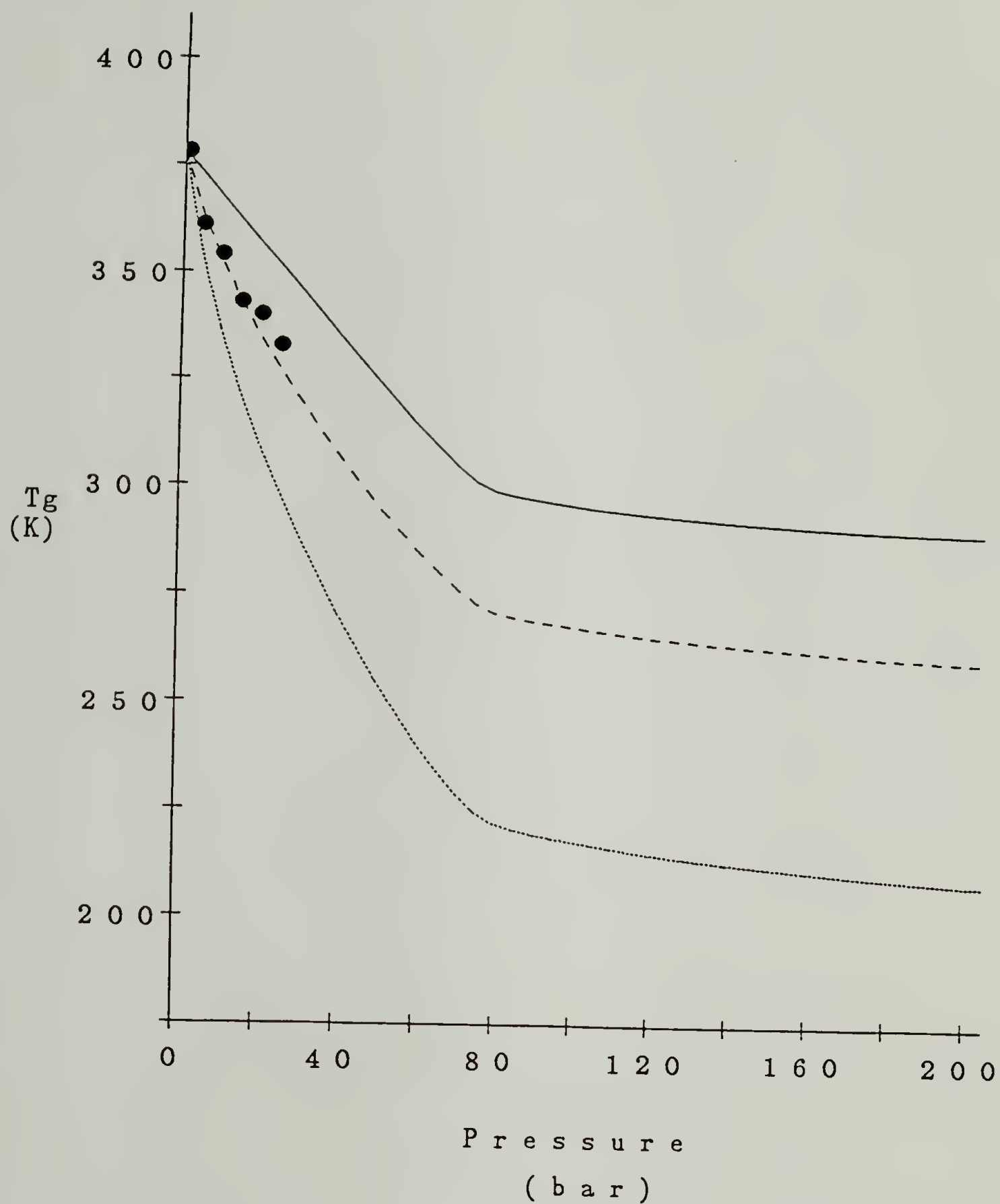


Figure 6.12

Predictions of T_g versus pressure at $T_a = 308\text{K}$ for the CO_2 -PMMA mixture using the MFLG model with the constant FV (—), S (···), and TS (- - -) conditions and data by Chiou, *et al.* [1985b] (●).

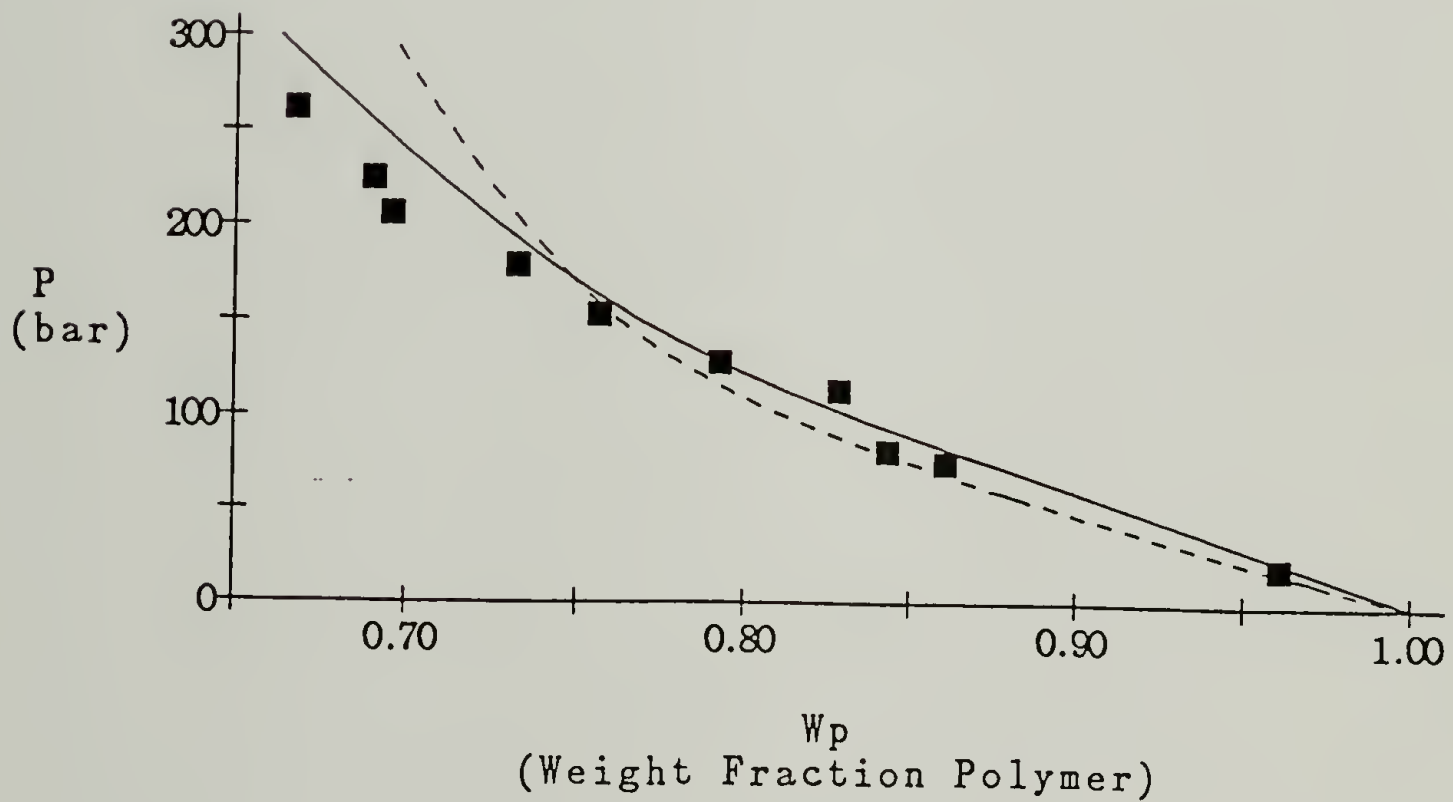
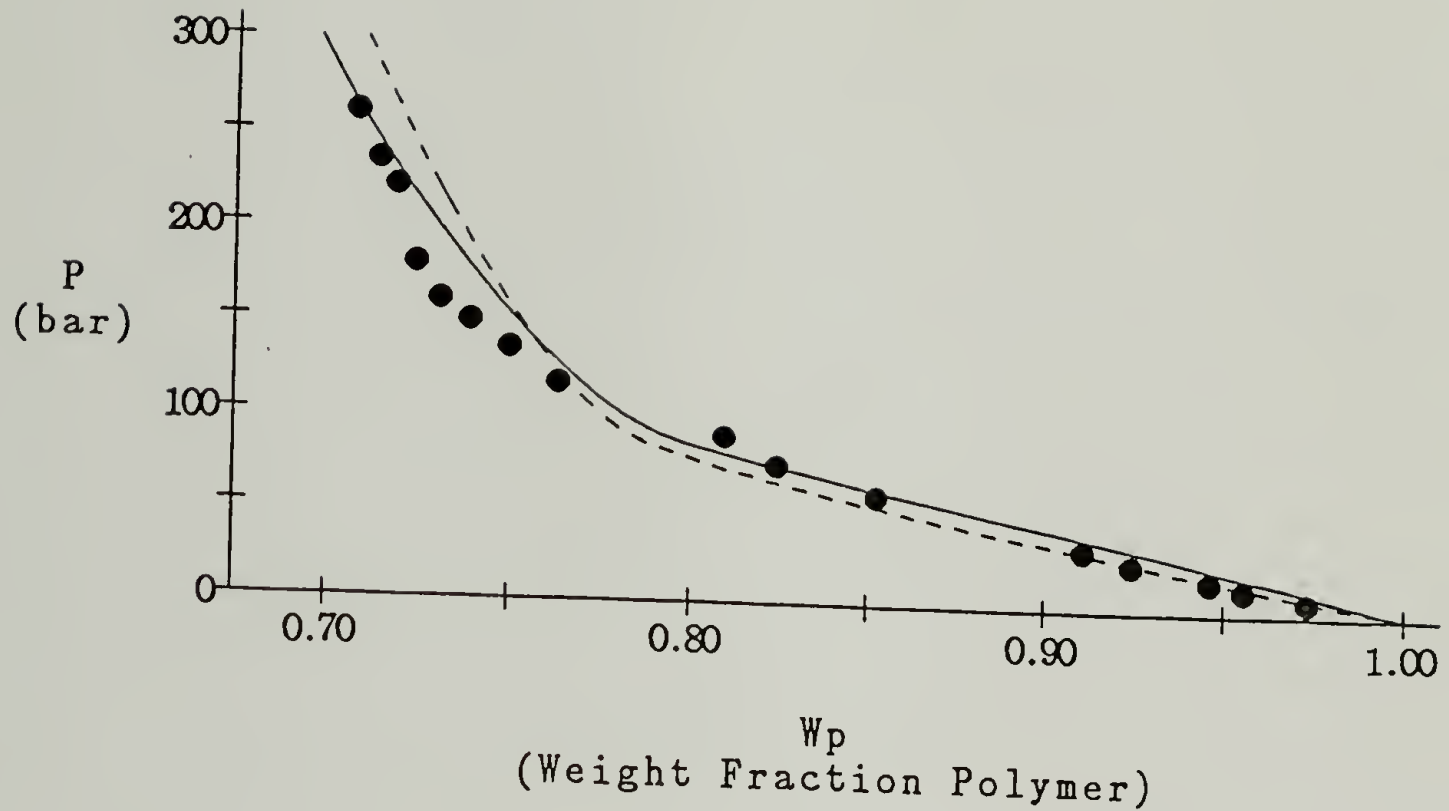


Figure 6.13

Fit of the MFLG model swelling binodal equations to sorption data by Liao and McHugh [1985] (\bullet , \blacksquare) at 315K (top graph) and 341.2K (bottom graph) using parameter set 1 (—) and parameter set 2 (- - -).

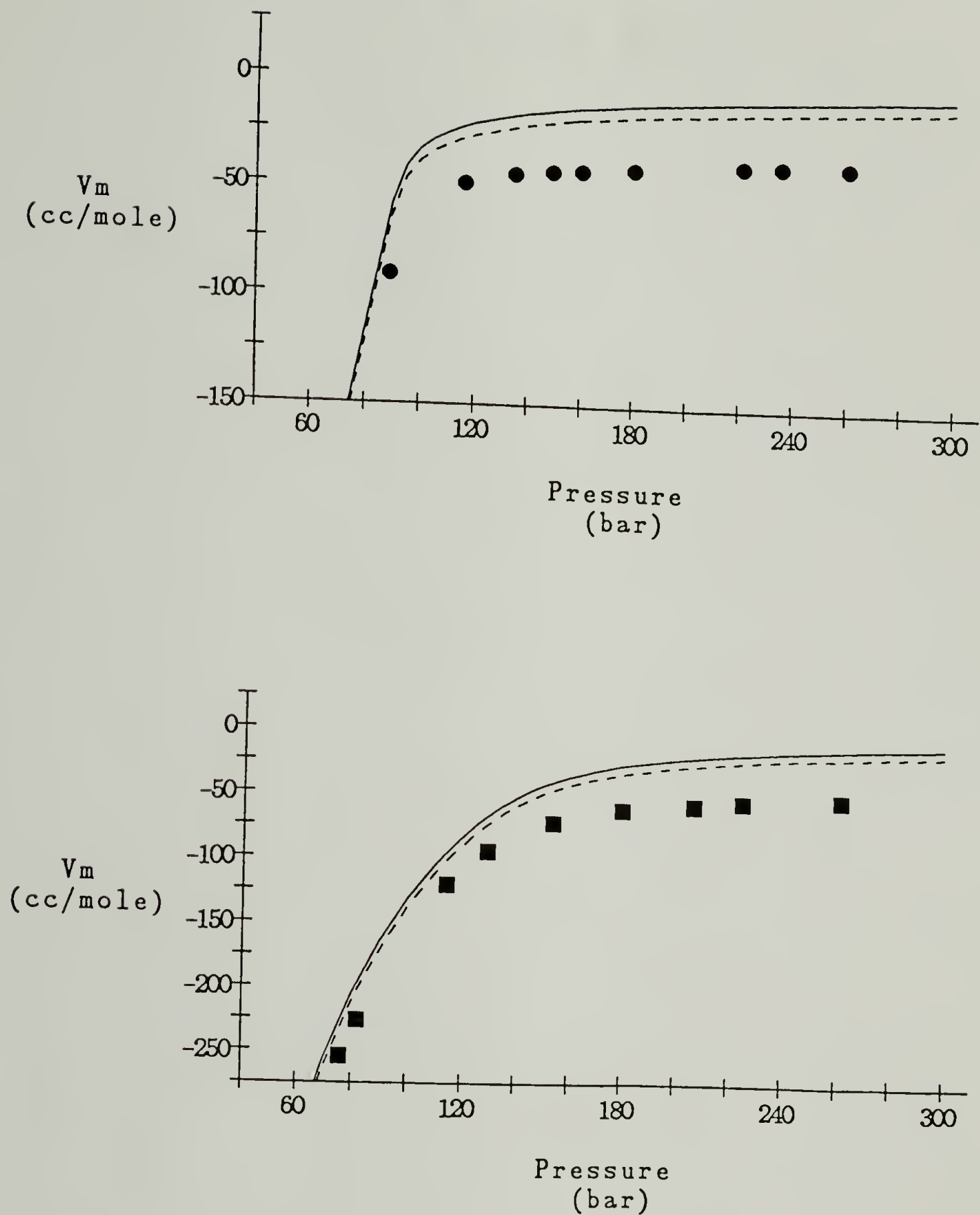


Figure 6.14

Predictions of volume change on mixing for PMMA-CO₂ mixture at 315K (top graph) and 341.2K (bottom graph) using Zero Order model and parameter set 1 [—] and parameter set 2 [- - -] and data derived from swelling measurements of Liao and McHugh [1985] [•], [■].

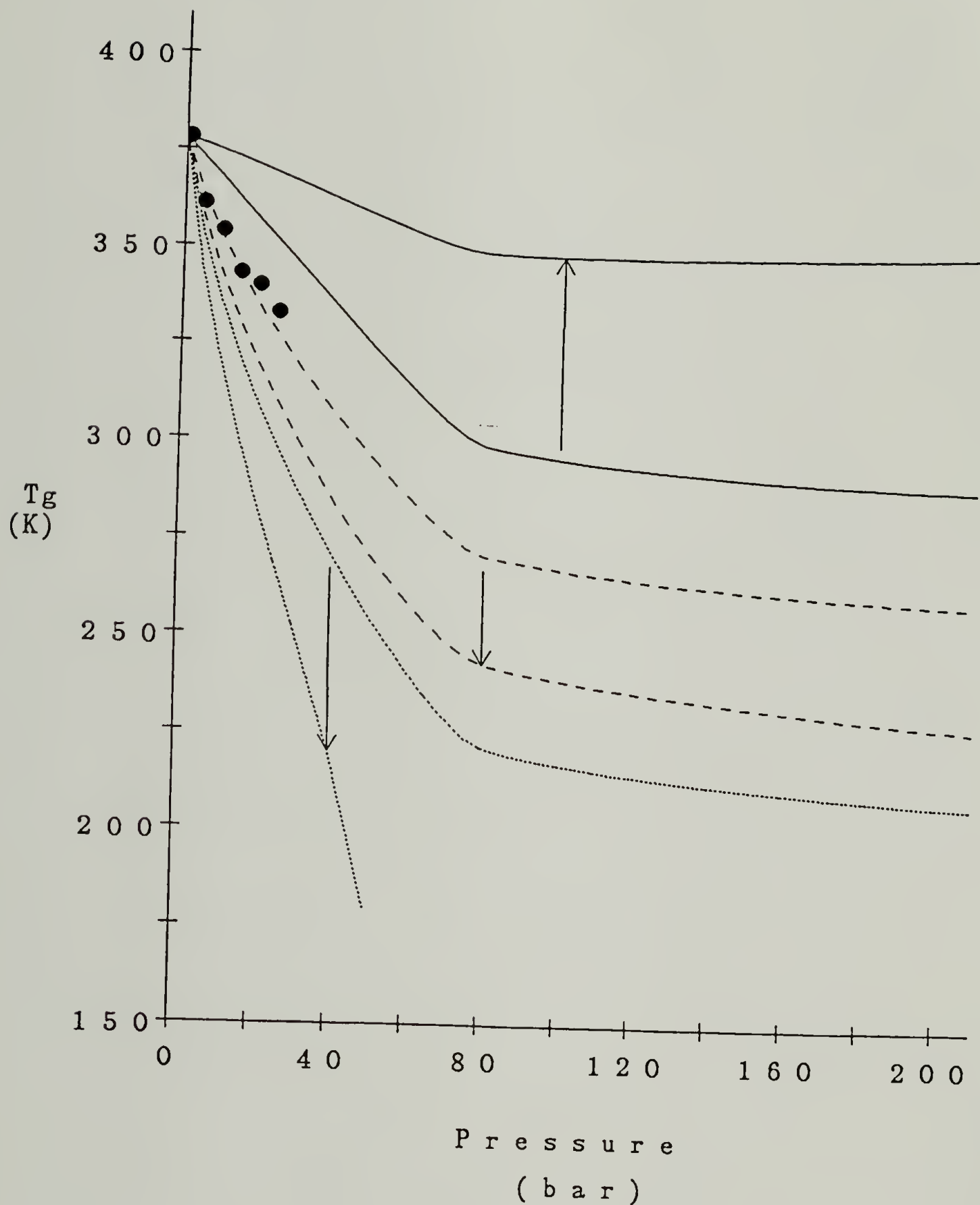


Figure 6.15

Predictions of T_g versus pressure at $T_a=308\text{K}$ for the PMMA- CO_2 mixture using the Zero Order model and the three criteria. Symbols the same as in figure (6.12). Arrows show curve shifts when binary parameters are changed from set 1 to set 2.

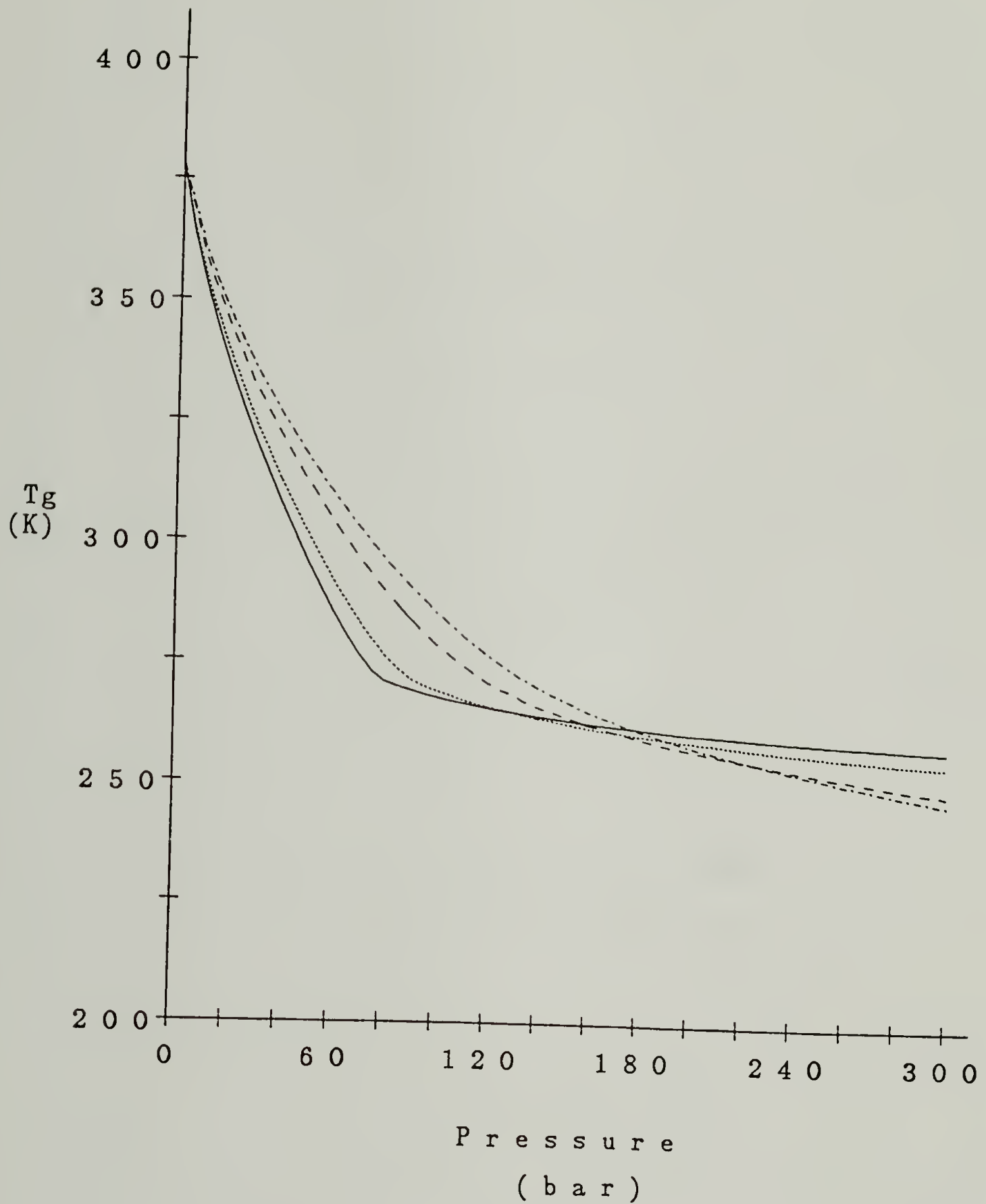


Figure 6.16

Predictions of T_g versus pressure for the CO_2 -PMMA mixture using the MFLG model and constant TS criterion at $T_a = 308\text{K}$ (—), $T_a = 315\text{K}$ (···), $T_a = 331.3\text{K}$ (- - -), and $T_a = 341.2\text{K}$ (- · - ·).

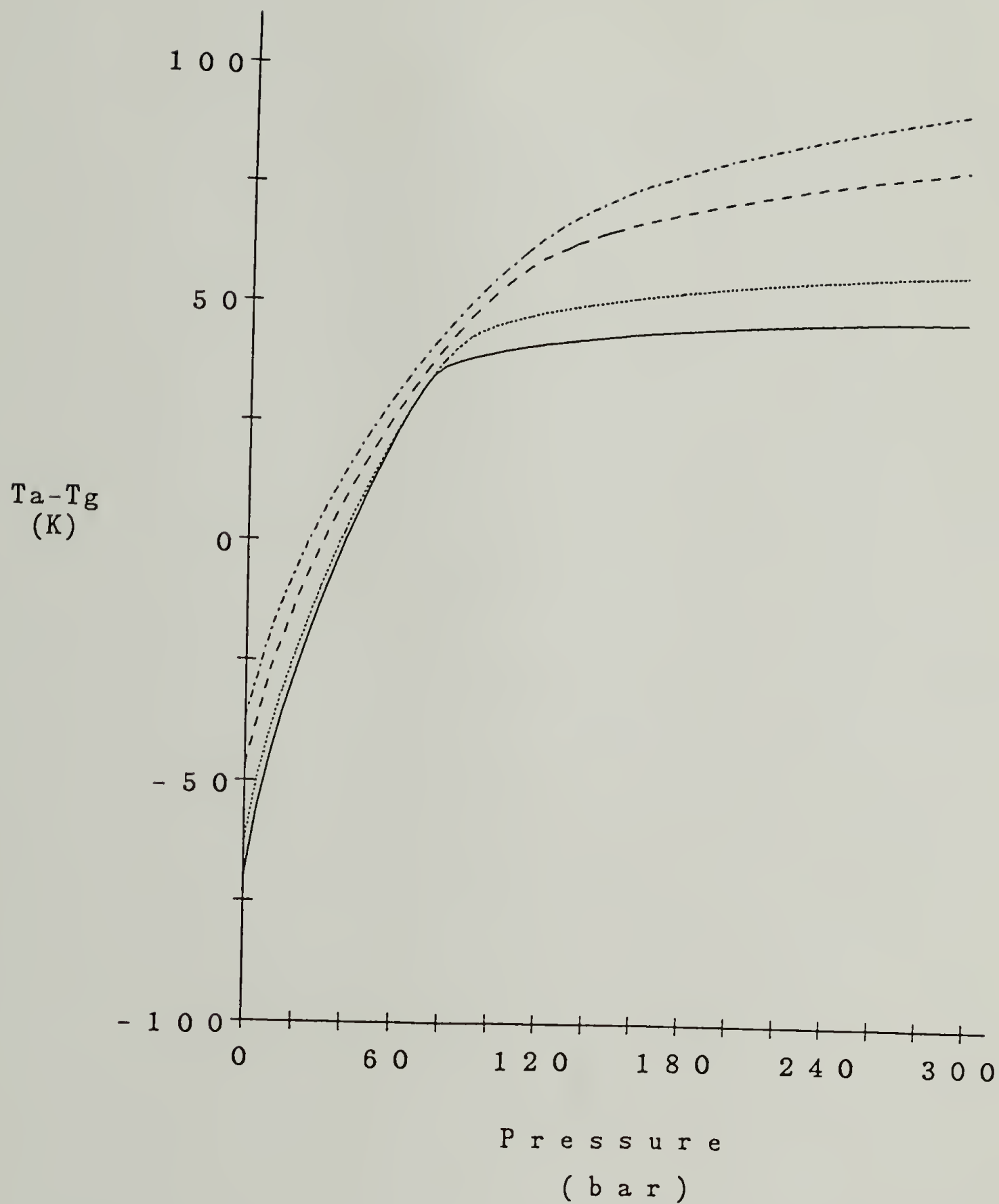


Figure 6.17

Predictions of $(T_a - T_g)$ versus pressure for the CO_2 -PMMA mixture using MFLG model and constant TS criterion at $T_a = 308\text{K}$ (—), $T_a = 315\text{K}$ (···), $T_a = 331.3\text{K}$ (- - -), and $T_a = 341.2\text{K}$ (- · · ·).

6.4.2 Polystyrene-CO₂

Although not immediately obvious, there are some fundamental differences in the behavior of T_g versus pressure in the PMMA-CO₂ and PS-CO₂ systems. Examination of the structures of the PMMA repeat unit and CO₂ would lead one to believe that CO₂ would be a relatively good solvent for PMMA. Likewise, CO₂ would be predicted to be a poorer solvent for polystyrene, which is indeed the case, as shown in Section 4.3.3. In addition, the measured value of $\partial T_g / \partial p$ ($p=0$) for PS is three times higher than that for PMMA [Olabisi and Simha, 1975; Oels, 1977]. These two characteristics should lead to a much faster development of a minimum in the T_g versus pressure curve for PS-CO₂ than for PMMA-CO₂.

The fitting of the binary parameters to the small amount of available binary data was covered in Section 4.3.3.

Predictions of T_g versus pressure using each of the three criteria are shown in Figure 6.18. As expected, the constant TS criterion provides the most accurate prediction. The FV based curve suffers from the predicted large and negative ΔV_m of the mixture, and to the over-prediction of $\partial T_g / \partial p$ for the pure polystyrene (see Chapter 5). The ambiguity in the determination of the binary parameters, resulting from the paucity of data, is also reflected by the results in Figure 6.19. The isotherms at 307K and 318K are predicted to cross, not an unlikely result, but at apparently too low a pressure, which leads to the crossing of the predicted T_g versus pressure curves whereas the data show no intersection. Despite these problems, the results for PS-CO₂ demonstrate that the constant TS criterion used with the MFLG model can provide a good first approximation of T_g versus pressure for a gas-polymer system even if very little binary data is available.

As mentioned above, the T_g of the PS-CO₂ pair should exhibit some significant differences from that of the PMMA-CO₂ mixture as pressure increases. These differences are illustrated by predictions of $(T_a - T_g)$ for PS-CO₂ at 318K and PMMA-CO₂ at 315K in Figure 6.20. The combined effects of low sorption and high $\partial T_g / \partial p$ bring $(T_a - T_g)$ barely above zero (and afterwards declining) whereas that for PMMA-CO₂ readily reaches +50 and continues to climb slowly with increasing pressure.

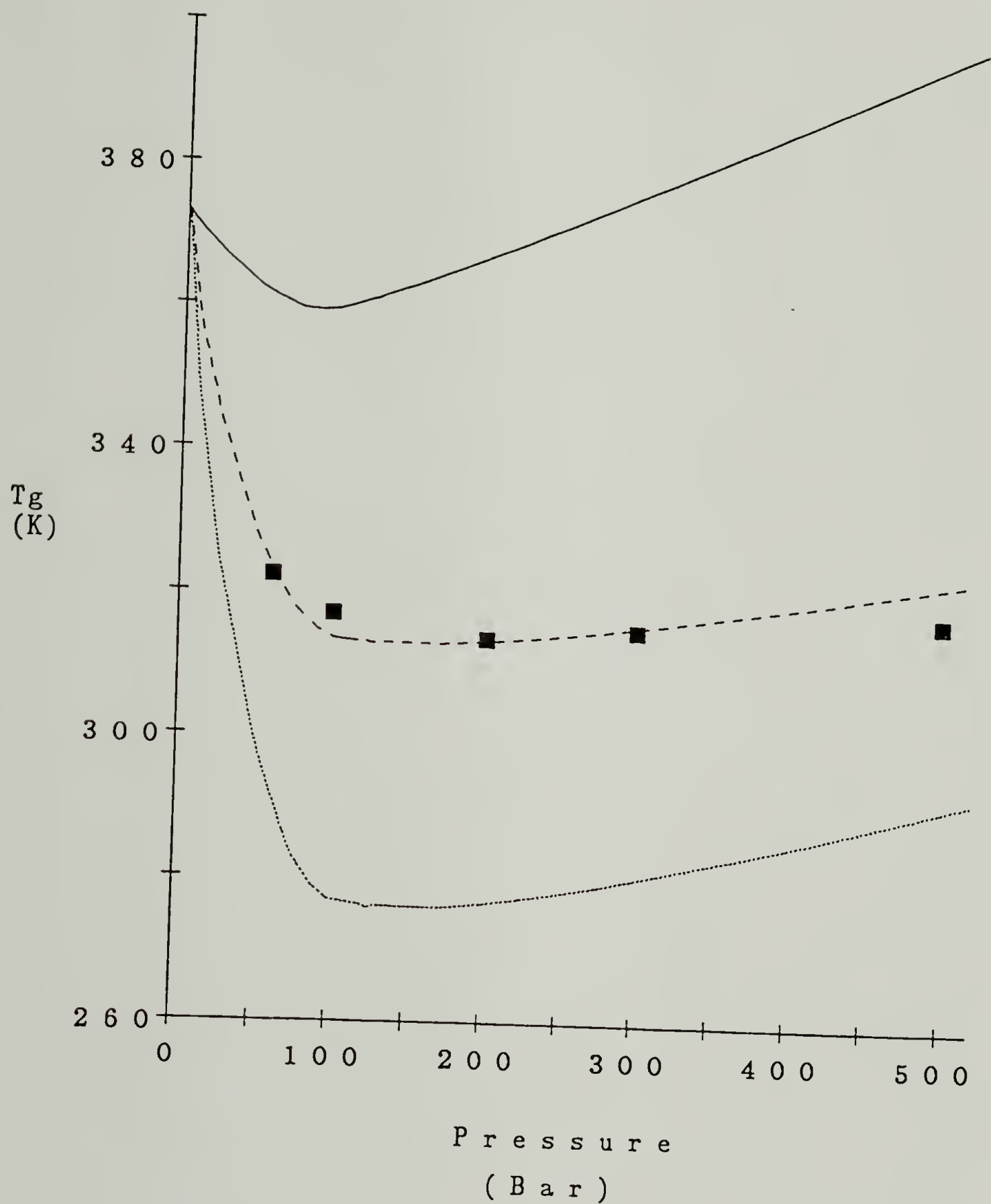


Figure 6.18

Prediction of T_g versus pressure of CO_2 -PS system using MFLG model and constant FV (—), S (···), and TS (- - -) criteria and data by Wang [1981] (•).

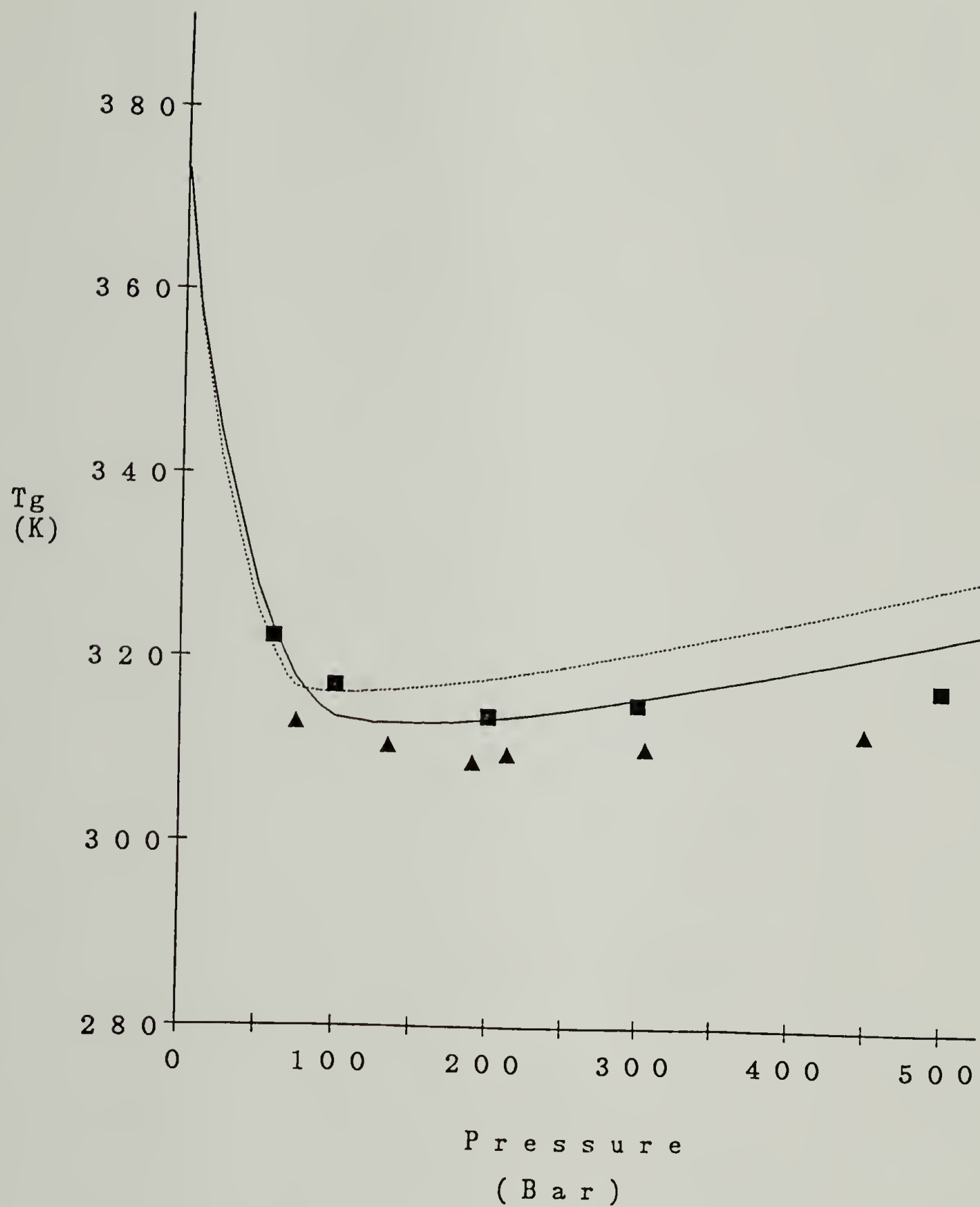


Figure 6.19

Prediction of T_g versus pressure for CO_2 -PS mixture using MFLG model and constant TS condition at $T_a = 318\text{K}$ (—) and $T_a = 307\text{K}$ (···) and data by Wang [1981] at 318K (■) and 307K (▲).

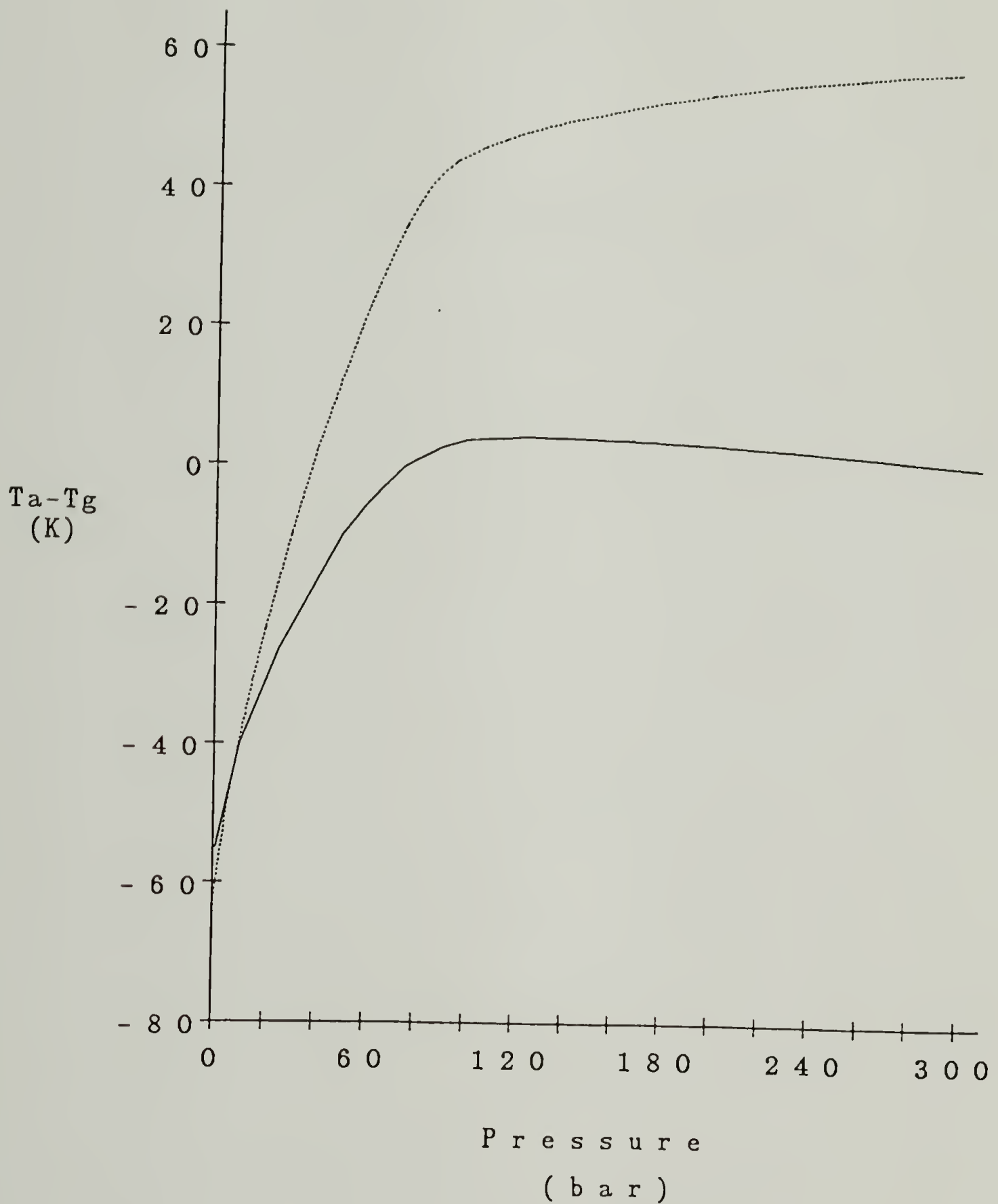


Figure 6.20

Prediction of $(T_a - T_g)$ for CO₂-PS at $T_a = 318\text{K}$ (—) and CO₂-PMMA at $T_a = 315\text{K}$ (···) using MFLG model and constant TS condition.

6.5 Summary of Chapter 6

Supercritical CO₂ readily induces crystallization in polycarbonate to an extent comparable to that achieved using acetone or other organic liquids. Carbon dioxide density, absolute pressure, and ambient temperature each influence the total crystallinity. Since the polymer degasses quickly and quantitatively at room temperature and pressure, the high T_g of the polycarbonate can be regained in the crystallized material without having to resort to vacuum treatment.

Since crystallization begins at temperatures and pressures as low as 75C and 125 atm., any attempt to extract polycarbonate with supercritical CO₂ will have to be made at temperatures between 31 and 75C, or alternatively high enough to melt any crystallites formed owing to CO₂ exposure. The latter temperature region is likely to be more promising since the lower temperature region is probably below the T_g of the polycarbonate-CO₂ mixture. Supercritical extraction of a polymer below its T_g will limit the amount of material which can be dissolved within a reasonable time [Schroeder and Van Arndt, 1976].

Use of the constant relaxation time criterion, here represented by the thermodynamic quantity TS, allows the prediction of T_g versus diluent concentration in the PS-toluene and PS-cyclohexane mixtures, and versus the combination of temperature and pressure (which determine diluent concentration) in the two gas-polymer mixtures without the need for adjustable parameters. In mixtures with near-ideal volume change on mixing, it seems likely that the TS and FV criteria would produce similar predictions of the dependence of T_g on diluent concentration. However, the effect of hydrostatic pressure alone on the T_g is

greatly overestimated by the FV criteria, which, coupled with the highly non-ideal ΔV_m of polymer-gas mixtures, disqualify the FV criterion from use in predicting the T_g of such mixtures.

The combination of the constant TS criterion and the MFLG model provide an effective means by which to predict the processability of polymers under gas pressure. A combination of a good solvent and low $\partial T_g / \partial p$ for the pure polymer can result in a high $(T_a - T_g)$ at temperatures far below the T_g of the pure polymer. Thermally unstable polymers could readily benefit from such gas plasticization during processing. Another interesting possible application concerns the reverse of the procedure described in this Chapter. Because the predicted T_g versus composition curve using the TS criteria is relatively sensitive to the values of the binary parameters, it is conceivable that T_g versus composition data, along with density versus composition, could be used to predict phase separation behavior.

CHAPTER 7

Conclusions and Proposals for Future Work

7.1 Conclusions

It has been shown that many lattice models fall into one of two broad categories, depending on whether or not the effect of segmental contact surface areas has been included. Further, those which do not employ the contact surface concept, the rigid lattice models, are specific cases of those which do, the non-rigid models. In computer modelling studies of the pVT behavior of CO₂, SO₂, CF₃H, and polystyrene, the non-rigid form of the lattice model has been demonstrated to be superior, based on the quality of the description of literature pVT data.

In the case of the non-rigid class of lattice models, it has been shown that several equations of state are specific cases of the Mean Field Lattice Gas model of Kleintjens and Koningsveld. Setting the parameter α_1 to zero yields the equation of state by Panayioutou and Vera; this requirement plus the constraint that g_{10} vanishes leads to Kanig's model. Retaining both parameters produces a superior description of the phase behavior of both the gases and polystyrene. It appears that the g_{10} parameter partially accounts for the lack of model terms which describe non-mean field density fluctuations near the critical point (in the case of the gases), and possibly makes up for neglect of a cell-like vibrational contribution to the EoS (for polystyrene). The α_1 parameter helps to fine-tune the dependence of the EoS on ϕ_0 at high densities, and as such, is possibly

required due to deviations from the simple Flory-Huggins entropy of mixing expression used to construct the MFLG model.

The fundamental nature of the heretofore MFLG empirical parameters α_1 and g_{10} was investigated via modifications to the MFLG entropy of mixing expression and subsequent computer modelling. The Flory-Huggins entropy of mixing relation was modified to attempt to account for the dependence of the total number of configurations on the distinct surface areas of the segments and holes. The resulting free energy expression, designated the First Order model, provided apparently molecular definitions for both α_1 and g_{10} and required one fewer adjustable parameter than the Zero Order model. Computer modelling of the pVT behavior of CO₂, SO₂, CF₃H, and polystyrene showed that whereas the First Order model produces a significantly better description than the case where ($\alpha_1, g_{10}=0$) or that of the general rigid lattice model, it falls short of equalling the performance of the parent model. Lacking the empirical g_{10} parameter to compensate for the segment density fluctuations in the region near T_c , the First Order model displays large errors in this regime. Consequently, in situations where critical conditions are not relevant, such as modelling of the pVT behavior of polystyrene, the First Order model performs as well as the Zero Order MFLG, despite one fewer adjustable constant.

The breakdown of the mean field approximation in the very dilute region causes significant problems if binary parameters for the MFLG models are found via use of data from this region. The use of the three binary parameters in the Zero Order model partially compensates for the dilute solution problem over small temperature ranges, but phase behavior predictions at temperatures outside the fitting range cannot be made with confidence. The MFLG models perform much better using parameters found with concentrated solution data.

While subsequent predictions of dilute phase behavior will still generally underestimate the equilibrium concentration (by overestimating the number of polymer-solvent contacts), the predicted temperature dependence and shape of the phase diagrams will be more accurate.

The prediction of phase separation behavior by the Zero Order MFLG is significantly more accurate than that of the First Order model. The two-binary-parameter description of the First Order model does not produce the proper temperature dependence of the phase diagrams, although the volume change on mixing prediction is somewhat improved. Apparently, though the First Order model properly describes the ϕ_0 dependence of the empirical parameters α_1 and g_{10} , more work needs to be done on the temperature dependence of these parameters.

The MFLG model produces an accurate description of the sorption of supercritical CO₂ by atactic PMMA in the concentration region where the mean field approximation is expected to be valid. Using the binary parameters found by fitting the appropriate model equations to the literature sorption data at temperatures between 315K and 341.2K, accurate predictions of sorption have been made at temperatures of 298.2K and 461.53K, thus demonstrating the large useful temperature range of the model. Predictions of the volume change on mixing, while displaying the proper trends versus temperature and pressure, show deviations from the data at high pressure.

In general, though correctly describing the effects of temperature, pressure, and molecular weight on dilute solution phase behavior, the model underpredicts the solubility of PMMA in CO₂. This is due both to the assumptions made during the determination of the binary parameters (that no 33,200 MW PMMA

dissolves in CO₂ up to pressures of 300 bar) and to the breakdown of the mean field approximation in very dilute polymer solutions.

The predictions in the PST-CO₂ system were made using a minimal amount of data during the fitting procedure. Despite this, the model solubility predictions qualitatively describe the dilute solution behavior, but as in the PMMA-CO₂ binary, underpredict the solubility. Not surprisingly, CO₂ is a much better solvent for PMMA than for PS.

The glass transition has been approximated as a freezing-in process involving one order parameter. Three separate parameters have been considered; free volume, entropy, and relaxation time, the latter represented by the quantity TS , as derived by Adam and Gibbs [1965]. Using the MFLG model, the $\partial T_g/\partial p$ curve has been calculated for the four amorphous polymers polystyrene, poly(methyl methacrylate), poly(vinyl acetate), and polycarbonate using each of the criteria mentioned above. Predictions of $\partial T_g/\partial p$ and $\partial \rho_g/\partial p$ employing the constant TS criterion are significantly more accurate than either the iso-entropy or iso-free volume situations for all four polymers. A modification to the MFLG model, which allows the number of segments per molecule, as well as the surface area per segment, to vary with temperature, further increases the accuracy of the predictions for three of the four polymers studied.

Supercritical CO₂ readily induces crystallization in polycarbonate to an extent comparable to that achieved using acetone or other organic liquids. Carbon dioxide density, absolute pressure, and ambient temperature each influence the total crystallinity. Since the polymer degasses quickly and quantitatively at room temperature and pressure, the high T_g of the polycarbonate can be regained in the crystallized material without having to resort to vacuum treatment. Since crystallization begins at temperatures and pressures as low as 75°C

and 125 atm., any attempt to extract polycarbonate with supercritical CO₂ will have to be made at temperatures high enough to melt any crystallites formed owing to CO₂ exposure.

Use of the constant TS criterion, allows the prediction of T_g versus diluent concentration in the PST-toluene and PST-cyclohexane mixtures, and versus the combination of temperature and pressure (which determine diluent concentration) in the two gas-polymer mixtures without the need for adjustable parameters. In mixtures with near-ideal volume change on mixing, it seems likely that the TS and FV criteria would produce similar predictions of the dependence of T_g on diluent concentration. However, the effect of hydrostatic pressure alone on the T_g is greatly overestimated by the FV criteria, which, coupled with the highly non-ideal ΔV_m of polymer-gas mixtures, disqualify the FV criterion from use in predicting the T_g of such mixtures.

Thus, the combination of the constant TS criterion and the MFLG model provide an effective means by which to predict the processability of polymers under gas pressure. A combination of a good solvent and low $\partial T_g / \partial p$ for the pure polymer can result in a high $(T_a - T_g)$ at temperatures far below the T_g of the pure polymer. Thermally unstable polymers could readily benefit from such gas plasticization during processing. Another interesting possible application concerns the reverse of this procedure. Because the predicted T_g versus composition curve using the TS criteria is sensitive to the values of the binary parameters, it is conceivable that T_g versus composition data, along with density versus composition, could be used to predict phase separation behavior.

7.2 Proposals for Future Work

7.2.1 Modelling

Whereas the MFLG model has been shown to provide a useful description of polymer-supercritical gas phase separation, as well as T_g behavior, there remains ample room for improvement. Improvements could come in three forms; addition of a dependence on segment-density fluctuations to the free energy, transformation of the model to a group-contribution format, and finally, inclusion of the concept of specific interactions. As discussed in Chapter 4, there are several possible strategies for incorporating the effect of the segment density fluctuations into the free energy. Empirical expansion of the interaction parameter [Nies, 1983], and theoretical bridging functions [Koningsveld, *et al.*, 1974; Irvine and Gordon, 1980] have proven useful in the past, yet it is the approach of Muthukumar [1986] which may hold the most promise. Muthukumar derived a temperature-dependent contribution of the effect of fluctuations on the free energy, using a field-theoretical approach, which produces extra terms which involve two new parameters. Significantly, it has been shown that the two empirical parameter (g_{i0} , α_i) approach of the MFLG model can compensate for the lack of fluctuation-dependent terms over small temperature ranges. Muthukumar's approach, which allows use of any mean field model as a starting point, could help to explain the fundamental significance of the MFLG empirical parameters and greatly extend the useful concentration range of the model.

A group contribution model, which assigns characteristic parameter values to individual chemical groups, would help to free the model from the dependence on availability of pure component data to determine material parameters. At the

same time, this transformation would eliminate one of the unrealistic attributes of the model, that a molecule such as styrene, for example, should be comprised of segments with identical shapes and sizes. Work towards this goal is proceeding at DSM in Geleen, Netherlands. If a group contribution model were to be used, it is only natural that the concept of specific interactions be introduced, since segments of one type will be attracted to segments of the same type rather than those of a different type.

7.2.2 Applications

Given the phase separation and T_g behavior of polymer-supercritical gas mixtures, several possible applications come to mind. Because the solvent can be removed very quickly, via a flash in the pressure, it is possible that supercritical gases could be used as an alternative to freeze-drying as a technique for preparing polymer blends. Besides being a fast process, the pressure flash includes a dramatic temperature quench. Thus the favorable kinetics of the process could be used to overcome thermodynamic roadblocks.

An old maxim in thermodynamics is that "like dissolves like". While overly simplistic, this simple assumption has been shown to be the case in the PMMA- CO_2 system, as well as for polyethylene, where analogies to the polymer repeat unit, such as ethane and propane, are better solvents for the polymer than the monomer, ethylene. Logically, it would seem that a good solvent for an intractable polymer such as polyacetylene would also be an analogy to the repeat unit, such as ethylene or butadiene. Such solvents could be used to plasticize the polymer or be used in an attempt to homogeneously polymerize acetylene.

As shown in Chapter 6, absorption of a supercritical gas by a polymer will lower its T_g . Thus the temperature range for processing of a polymer might be substantially broadened by using a gas as a plasticizer. Following processing, the gas could be easily removed by a pressure drop. To investigate this possible application, attempts were made to extrude mixtures of a gas and a polymer at temperatures below the T_g of the pure polymer. In each case, (PVC-CO₂, PVC-CF₃H, PET-CO₂) powdered polymer was placed in an excess of liquified gas and allowed to absorb for several hours. The tube containing the swollen polymer was then placed in liquid nitrogen in order to freeze the mixture during transfer to the extruder. The frozen mixture was placed in the barrel of the Instron rheometer and pressure applied. Unfortunately, a good seal could not be maintained around the plunger and the gas would escape very quickly after the experiment was started. Modification of the Instron barrel assembly will be necessary to properly evaluate the use of supercritical gases as plasticizers.

Recently it has been shown that very large single crystals of quartz can be grown from a supercritical water solution. It might be possible to accomplish the same result for polyethylene or poly(vinylidene fluoride) using the appropriate gas [Masse, 1987]. In addition, a supercritical gas could be used as a readily removable continuous phase in an emulsion polymerization. Finally, even the observation that generally only oligomers will dissolve in a supercritical gas may have some value. If functional oligomers were to be crosslinked while in solution with a gas, the resulting phase separation could create a foam with interesting properties.

APPENDIX A

Thermodynamic Relations for Pure Components Derived
from the First Order MFLG Free Energy ExpressionChemical Potential and Equation of State:

$$\frac{\mu_0}{RT} = \frac{-pv_0}{RT} = \ln \phi_0 + \phi_1 \left(1 - \frac{1}{m_1}\right) + \phi_1^2 \Gamma A + \phi_0 \phi_1^2 (\Gamma' A + \Gamma A') \quad (A-1)$$

$$\frac{\mu_1}{m_1 RT} = \frac{1}{m_1} \ln \phi_1 - \phi_0 \left(1 - \frac{1}{m_1}\right) + \phi_0^2 \Gamma A + \phi_0^2 \phi_1 (\Gamma' A + \Gamma A') \quad (A-2)$$

where:

$$\Gamma = \frac{(1 - \gamma_1)}{Q}$$

$$\Gamma' = -\frac{(1 - \gamma_1)Q'}{Q^2}$$

$$A = z_{00} \ln \left(\frac{Q^2}{z}\right)$$

$$A' = 2z_{00} \left(\frac{Q'}{Q}\right)$$

$$Q = (1 - \gamma_1 \phi_1)$$

$$Q' = \gamma_1 \phi_1 \text{ for } \mu_0; = -\gamma_1 \phi_0 \text{ for } \mu_1$$

Spinodal:

$$0 = \frac{1}{\phi_0} + \frac{1}{m_1 \phi_1} - 2\Gamma A + 2(\phi_0 - \phi_1)(\Gamma' A + \Gamma A') + \phi_0 \phi_1 (\Gamma'' A + 2\Gamma' A' + \Gamma A'') \quad (A-3)$$

where the symbols are the same as for equations (A-1) and (A-2) but with $Q' = -\gamma_1$ and:

$$\Gamma'' = \frac{2(1 - \gamma_1)(Q')^2}{Q^3}$$

$$A'' = -2z_{00} \left(\frac{Q'}{Q} \right)^2$$

Critical Point:

$$\begin{aligned} 0 = & \frac{1}{\phi_0^2} - \frac{1}{m_1 \phi_1^2} - 6(\Gamma' A + \Gamma A') \\ & + 3(\phi_0 - \phi_1)(\Gamma'' A + 2\Gamma' A + \Gamma A') \\ & + \phi_0 \phi_1 (\Gamma''' A + 3\Gamma'' A' + 3\Gamma' A'' + \Gamma A''') \end{aligned} \quad (A - 4)$$

where the symbols are the same as for the spinodal and, in addition:

$$\Gamma''' = -\frac{6(1 - \gamma_1)(Q')^3}{Q^4}$$

$$A''' = 4z_{00} \left(\frac{Q'}{Q} \right)^3$$

APPENDIX B

Equations Derived from First Order MFLG Model
Free Energy Expression and Defining Relations from
Table 4.1

Chemical Potential:

$$\begin{aligned} \frac{\mu_i}{m_i RT} = & \frac{1}{m_i} \ln \phi_i + \sum_{\substack{j=0 \\ j \neq i}}^2 \phi_j \left(\frac{1}{m_i} - \frac{1}{m_j} \right) \\ & + \sum_{k=1,2,m} (A_k (\Gamma_k + \Gamma'_k) + \Gamma_k A'_k) \end{aligned} \quad (B-1)$$

where:

$$i = 0, 1, 2$$

$$m_0 = 1$$

Other terms in equation (B-1) are defined in Table B.1.

Equation of State:

$$\frac{-pv_0}{RT} = \frac{\mu_0}{RT} \quad (\text{from equation B-1}) \quad (B-2)$$

Swelling Binodal:

$$\begin{aligned} \frac{\mu_0}{RT} \quad (\text{from equation B-1}) = & \ln \phi_0 + \phi_1 \left(1 - \frac{1}{m_1} \right) \\ & + A_1 \Gamma_1^0 + \Gamma_1 A_1^0 \end{aligned} \quad (B-3)$$

$$\begin{aligned} \frac{\mu_1}{RT} \quad (\text{from equation B-1}) = & \frac{1}{m_1} \ln \phi_1 + \phi_0 \left(\frac{1}{m_1} - 1 \right) \\ & + A_1 \Gamma_1^1 + \Gamma_1 A_1^1 \end{aligned} \quad (B-4)$$

where:

$$A_1 = z_{00} \ln Q^2 / z_1 + \beta_1$$

$$\Gamma_1 = \phi_0 \phi_1 (1 - \gamma_1) / Q$$

$$\Gamma_1^0 = \frac{(1 - \gamma_1) \phi_1^2}{Q} - \frac{\phi_0 \phi_1 (1 - \gamma_1) Q_1^0}{Q^2}$$

$$\Gamma_1^1 = \frac{(1 - \gamma_1) \phi_0^2}{Q} - \frac{\phi_0 \phi_1 (1 - \gamma_1) Q_1^1}{Q^2}$$

and:

$$Q = 1 - \gamma_1 \phi_1$$

$$Q_1^0 = \gamma_1 \phi_1$$

$$Q_1^1 = -\gamma_1 \phi_0$$

$$A_1^0 = 2z_{00} Q_1^0 / Q$$

$$A_1^1 = 2z_{00} Q_1^1 / Q$$

$$\phi_1 = m_1 v_0 \rho_{gas} / M_1$$

$$\phi_0 = 1 - \phi_1$$

Spinodal:

$$\Delta A_{11} \Delta A_{22} - \Delta A_{12} \Delta A_{21} = 0 \quad (B - 5)$$

where:

$$\Delta A_{ij} = \frac{\partial^2 \Delta A}{\partial \phi_i \partial \phi_j}$$

therefore:

$$\Delta A_{11} = \frac{1}{\phi_0} + \frac{1}{\phi_1 m_1} + \sum_{i=1,2,m} (\Gamma_i^{11} A_i + 2\Gamma_i^1 A_i^1 + \Gamma_i A_i^{11}) \quad (B - 6)$$

$$\Delta A_{12} = \frac{1}{\phi_0} + \sum_{i=1,2,m} (\Gamma_i^{12} A_i + \Gamma_i^1 A_i^2 + \Gamma_i^2 A_i^1 + \Gamma_i A_i^{12}) \quad (B - 7)$$

$$\Delta A_{21} = \Delta A_{12} \quad (B-8)$$

$$\Delta A_{22} = \frac{1}{\phi_0} + \frac{1}{\phi_2 m_2} + \sum_{i=1,2,m} (\Gamma_i^{22} A_i + 2\Gamma_i^2 A_i^2 + \Gamma_i A_i^{22}) \quad (B-9)$$

where:

$$\Gamma_1 = \frac{\phi_0 \phi_1 (1 - \gamma_1)}{Q}$$

$$\Gamma_1^1 = (1 - \gamma_1) \left(\frac{\phi_0 - \phi_1}{Q} - \frac{\phi_0 \phi_1 Q'}{Q^2} \right)$$

$$\Gamma_1^{11} = (1 - \gamma_1) \left(-\frac{2}{Q} - \frac{2(\phi_0 - \phi_1)Q'}{Q^2} + \frac{2\phi_0 \phi_1 (Q')^2}{Q^3} \right)$$

$$\Gamma_1^{12} = (1 - \gamma_1) \left(-\frac{1}{Q} - \frac{(\phi_0 - \phi_1)Q''}{Q^2} + \frac{2\phi_0 \phi_1 Q' Q''}{Q^3} \right)$$

$$\Gamma_1^2 = (1 - \gamma_1) \left(-\frac{\phi_1}{Q} - \frac{\phi_0 \phi_1 Q''}{Q^2} \right)$$

$$\Gamma_1^{22} = (1 - \gamma_1) \frac{2\phi_1 Q''}{Q^2} \left(1 + \frac{\phi_0 Q''}{Q} \right)$$

$$\Gamma_2 = \frac{\phi_0 \phi_2 (1 - \gamma_2)}{Q}$$

$$\Gamma_2^1 = (1 - \gamma_2) \left(-\frac{1}{Q} - \frac{\phi_0 \phi_2 Q'}{Q^2} \right)$$

$$\Gamma_2^{11} = (1 - \gamma_2) \frac{2\phi_2 Q'}{Q^2} \left(1 + \frac{\phi_0 Q'}{Q} \right)$$

$$\Gamma_2^{12} = (1 - \gamma_2) \left(-\frac{1}{Q} + \frac{\phi_2 Q''}{Q^2} - \frac{(\phi_0 - \phi_1)Q'}{Q^2} + \frac{2\phi_0 \phi_2 Q' Q''}{Q^3} \right)$$

$$\Gamma_2^2 = (1 - \gamma_2) \left(\frac{\phi_0 - \phi_1}{Q} - \frac{\phi_0 \phi_2 Q''}{Q^2} \right)$$

$$\Gamma_2^{22} = (1 - \gamma_2) \left(-\frac{2}{Q} - \frac{2(\phi_0 - \phi_2)Q''}{Q^2} + \frac{2\phi_0 \phi_2 (Q'')^2}{Q^3} \right)$$

$$\Gamma_m = \frac{\phi_1 \phi_2 (1 - \gamma_1)(1 - \gamma_2)}{Q}$$

$$\Gamma_m^1 = (1 - \gamma_1)(1 - \gamma_2) \left(\frac{\phi_2}{Q} - \frac{\phi_1 \phi_2 Q'}{Q^2} \right)$$

$$\Gamma_m^{11} = (1 - \gamma_1)(1 - \gamma_2) \frac{2\phi_2 Q'}{Q^2} \left(\frac{\phi_1 Q'}{Q} - 1 \right)$$

$$\Gamma_m^{12} = (1 - \gamma_1)(1 - \gamma_2) \left(\frac{1}{Q} - \frac{\phi_2 Q'' + \phi_1 Q'}{Q^2} + \frac{2\phi_1 \phi_2 Q' Q''}{Q^3} \right)$$

$$\Gamma_m^2 = (1 - \gamma_1)(1 - \gamma_2) \left(\frac{\phi_1}{Q} - \frac{\phi_1 \phi_2 Q''}{Q^2} \right)$$

$$\Gamma_m^{22} = (1 - \gamma_1)(1 - \gamma_2) \frac{2\phi_1 Q''}{Q^2} \left(\frac{\phi_2 Q''}{Q} - 1 \right)$$

and:

$$A_i = z_{00} \ln Q^2 / z_i + \beta_i \quad A_i^1 = 2z_{00} \frac{Q'}{Q}$$

$$A_i^{11} = -2z_{00} \left(\frac{Q'}{Q} \right)^2 \quad A_i^{12} = -2z_{00} \left(\frac{Q' Q''}{Q^2} \right)$$

$$A_i^2 = 2z_{00} \frac{Q''}{Q} \quad A_i^{22} = -2z_{00} \left(\frac{Q''}{Q} \right)^2$$

$$Q = 1 - \gamma_1 \phi_1 - \gamma_2 \phi_2 \quad Q' = -\gamma_1 \quad Q'' = -\gamma_2$$

Critical Point:

$$J_1 \Delta A_{22} - J_2 \Delta A_{21} = 0 \quad (B - 9)$$

and:

$$\begin{aligned} J_1 &= \Delta A_{111} \Delta A_{22} + \Delta A_{11} \Delta A_{221} - (\Delta A_{12} \Delta A_{211} + \Delta A_{21} \Delta A_{121}) \\ &= \Delta A_{111} \Delta A_{22} + \Delta A_{11} \Delta A_{221} - 2\Delta A_{12} \Delta A_{121} \end{aligned} \quad (B - 10)$$

$$\begin{aligned}
J_2 &= \Delta A_{112} \Delta A_{22} + \Delta A_{11} \Delta A_{222} - (\Delta A_{12} \Delta A_{212} + \Delta A_{21} \Delta A_{122}) \\
&= \Delta A_{121} \Delta A_{22} + \Delta A_{11} \Delta A_{222} - 2\Delta A_{12} \Delta A_{122}
\end{aligned} \tag{B-11}$$

where:

$$\Delta A_{ijk} = \frac{\partial^3 \Delta A}{\partial \phi_i \partial \phi_j \partial \phi_k}$$

therefore:

$$\begin{aligned}
\Delta A_{111} &= \frac{1}{\phi_0^2} + \frac{1}{m_1 \phi_1^2} \\
&\quad + \sum_{i=1,2,m} (\Gamma_i^{111} A_i + 3\Gamma_i^{11} A_i^1 + 3\Gamma_i^1 A_i^{11} + \Gamma_i A_i^{111})
\end{aligned} \tag{B-12}$$

$$\begin{aligned}
\Delta A_{222} &= \frac{1}{\phi_0^2} + \frac{1}{m_1 \phi_2^2} \\
&\quad + \sum_{i=1,2,m} (\Gamma_i^{222} A_i + 3\Gamma_i^{22} A_i^2 + 3\Gamma_i^2 A_i^{22} + \Gamma_i A_i^{222})
\end{aligned} \tag{B-13}$$

$$\begin{aligned}
\Delta A_{121} &= \frac{1}{\phi_0^2} + \sum_{i=1,2,m} (\Gamma_i^{121} A_i + 2\Gamma_i^{12} A_i^1 + 2\Gamma_i^1 A_i^{12} + \Gamma_i^{11} A_i^2) \\
&\quad + \sum_{i=1,2,m} (\Gamma_i^2 A_i^{11} + \Gamma_i A_i^{121})
\end{aligned} \tag{B-14}$$

$$\begin{aligned}
\Delta A_{221} &= \frac{1}{\phi_0^2} + \sum_{i=1,2,m} (\Gamma_i^{221} A_i + 2\Gamma_i^{12} A_i^2 + 2\Gamma_i^2 A_i^{12} + \Gamma_i^{22} A_i^1) \\
&\quad + \sum_{i=1,2,m} (\Gamma_i^1 A_i^{22} + \Gamma_i A_i^{221})
\end{aligned} \tag{B-15}$$

where:

$$\Gamma_1^{222} = -(1 - \gamma_1) \left\{ \frac{\phi_1(Q'')^2}{Q^3} \left(1 + \frac{\phi_0 Q''}{Q} \right) \right\}$$

$$\Gamma_1^{221} = (1 - \gamma_1) \left\{ \frac{-2\phi_1(Q'')^2}{Q^3} \left(1 + \frac{\phi_0 Q'}{Q} \right) + \frac{2Q''}{Q^2} \left(1 + \frac{\phi_0 Q''}{Q} \right) \left(1 - \frac{2\phi_1 Q'}{Q} \right) \right\}$$

$$\Gamma_1^{121} = (1 - \gamma_1) \left\{ \frac{2Q'}{Q^2} + \frac{2Q''}{Q^2} + \frac{4(\phi_0 - \phi_1)Q'Q''}{Q^3} - \frac{2\phi_1(Q')^2}{Q^3} \right\}$$

$$- (1 - \gamma_1) \left\{ \frac{6\phi_0\phi_1(Q')^2 Q''}{Q^4} \right\}$$

$$\Gamma_1^{111} = 6(1 - \gamma_1) \left\{ \frac{Q'}{Q^2} + \frac{(\phi_0 - \phi_1)(Q')^2}{Q^3} - \frac{\phi_0\phi_1(Q')^3}{Q^4} \right\}$$

$$\Gamma_2^{222} = 6(1 - \gamma_2) \left\{ \frac{Q''}{Q^2} + \frac{(\phi_0 - \phi_2)(Q'')^2}{Q^3} - \frac{\phi_0\phi_2(Q'')^3}{Q^4} \right\}$$

$$\Gamma_2^{221} = (1 - \gamma_2) \left\{ \frac{2Q'}{Q^2} + \frac{2Q''}{Q^2} + \frac{4(\phi_0 - \phi_2)Q'Q''}{Q^3} - \frac{2\phi_2(Q'')^2}{Q^3} \left(1 + \frac{3\phi_0 Q'}{Q} \right) \right\}$$

$$\Gamma_2^{121} = (1 - \gamma_2) \left\{ \frac{2Q'}{Q^2} - \frac{2\phi_2 Q'Q''}{Q^3} + \frac{2(\phi_0 - \phi_2)(Q')^2}{Q^3} \right\}$$

$$- (1 - \gamma_2) \left\{ \frac{2\phi_2 Q'Q''}{Q^3} \left(1 + \frac{3\phi_0 Q'}{Q} \right) \right\}$$

$$\Gamma_2^{111} = (1 - \gamma_2) \left\{ \frac{-6\phi_2(Q')^2}{Q^3} \left(1 + \frac{\phi_0 Q'}{Q} \right) \right\}$$

$$\Gamma_m^{222} = (1 - \gamma_1)(1 - \gamma_2) \left\{ \frac{6\phi_1(Q'')^2}{Q^3} \left(1 - \frac{\phi_2 Q''}{Q} \right) \right\}$$

$$\Gamma_m^{221} = (1 - \gamma_1)(1 - \gamma_2) \left\{ \frac{-2\phi_1\phi_2(Q'')^2 Q'}{Q^4} + \frac{2Q''}{Q^2} \left(\frac{\phi_2 Q''}{Q} - 1 \right) \left(1 - \frac{2\phi_1 Q'}{Q} \right) \right\}$$

$$\Gamma_m^{121} = (1 - \gamma_1)(1 - \gamma_2) \left\{ \frac{-2Q'}{Q^2} + \frac{2\phi_2 Q' Q''}{Q^3} + \frac{2\phi_1 (Q')^2}{Q^3} \right\}$$

$$+ (1 - \gamma_1)(1 - \gamma_2) \left\{ \frac{2\phi_2 Q' Q''}{Q^3} \left(1 - \frac{3\phi_1 Q'}{Q} \right) \right\}$$

$$\Gamma_m^{111} = (1 - \gamma_1)(1 - \gamma_2) \left\{ \frac{6\phi_2 (Q')^2}{Q^3} \left(1 - \frac{\phi_1 Q'}{Q} \right) \right\}$$

and:

$$A_i^{222} = 4z_{00} \left(\frac{Q''}{Q} \right)^3$$

$$A_i^{221} = 4z_{00} \frac{(Q'')^2 Q'}{Q^3}$$

$$A_i^{121} = 4z_{00} \frac{(Q')^2 Q''}{Q^3}$$

$$A_i^{111} = 4z_{00} \left(\frac{Q'}{Q} \right)^3$$

Second order derivatives are defined in the previous section concerning the spinodal.

Table B.1

Terms for Equation B-1

Term	$i = 0$	$i = 1$	$i = 2$
$\Gamma_1 + \Gamma'_1$	$\frac{(1-\gamma_1)\phi_1(\phi_1+\phi_2)}{Q} - \Gamma_{u1}$	$\frac{(1-\gamma_1)\phi_0(\phi_0+\phi_2)}{Q} - \Gamma_{u1}$	$\frac{-(1-\gamma_1)\phi_0\phi_1}{Q} - \Gamma_{u1}$
$\Gamma_2 + \Gamma'_2$	$\frac{(1-\gamma_2)\phi_2(\phi_1+\phi_2)}{Q} - \Gamma_{u2}$	$\frac{-(1-\gamma_2)\phi_0\phi_2}{Q} - \Gamma_{u2}$	$\frac{(1-\gamma_2)\phi_0(\phi_0+\phi_1)}{Q} - \Gamma_{u2}$
$\Gamma_m + \Gamma'_m$	$\frac{-(1-\gamma_1)(1-\gamma_2)\phi_1\phi_2}{Q} - \Gamma_{um}$	$\frac{(1-\gamma_1)(1-\gamma_2)\phi_2(\phi_0+\phi_2)}{Q} - \Gamma_{um}$	$\frac{(1-\gamma_1)(1-\gamma_2)\phi_1(\phi_0+\phi_1)}{Q} - \Gamma_{um}$
Γ_{u1}	$\frac{\phi_0\phi_1(1-\gamma_1)Q'}{Q}$	same as for $i = 0$	same as for $i = 0$
Γ_{u2}	$\frac{\phi_0\phi_2(1-\gamma_2)Q'}{Q}$	same as for $i = 0$	same as for $i = 0$
Γ_{um}	$\frac{\phi_1\phi_2(1-\gamma_1)(1-\gamma_2)Q'}{Q}$	same as for $i = 0$	same as for $i = 0$
Q	$1 - \gamma_1\phi_1 - \gamma_2\phi_2$	same as for $i = 0$	same as for $i = 0$
Q'	$\gamma_1\phi_1 + \gamma_2\phi_2$	$\gamma_2\phi_2 - \gamma_1(\phi_0 + \phi_2)$	$\gamma_1\phi_1 - \gamma_2(\phi_0 + \phi_1)$

Note also:

$$A_i = z_{00} \ln Q' / z_i + \beta_i$$

$$A'_i = 2z_{00} Q' / Q$$

APPENDIX C

Derivation of the Volume Change on Mixing
from the Degree of SwellingDefinition of Terms: V_i = initial volume, cc V_f = final volume, cc V_{fm} = final volume, cc/mole g_p = mass of polymer g_{CO_2} = mass of CO_2 absorbed M_i = molecular weights ρ_i = densities w_p = weight fraction polymer S = fractional volume changeDerivation of V_{fm}

$$V_f = V_i(1 + S) \quad (C - 1)$$

$$V_i = g_p / \rho_p \quad (C - 2)$$

$$\text{combine (C-1) and (C-2)} \quad V_f = \left(\frac{1 + S}{\rho_p} \right) g_p \quad (C - 3)$$

$$N_t = \frac{g_p}{M_p} + \frac{g_{CO_2}}{M_{CO_2}} \quad (\text{total moles}) \quad (C - 4)$$

$$g_{CO_2} = g_p \left(\frac{1 - w_p}{w_p} \right) \quad (C - 5)$$

Combine C-3, C-4, and C-5:

$$V_{fm} = \left(\frac{1+S}{\rho_p} \right) \left(\frac{1}{\frac{1}{M_p} + \left(\frac{1-w_p}{w_p} \right) \frac{1}{M_{CO_2}}} \right) \quad (C-6)$$

Derivation of Ideal Solution Volume

$$\begin{aligned} x_1 V_1 &= \left(\frac{\frac{g_{CO_2}}{M_{CO_2}}}{\frac{g_{CO_2}}{M_{CO_2}} + \frac{g_p}{M_p}} \right) \frac{M_{CO_2}}{\rho_{CO_2}} \\ &= \frac{1}{\rho_{CO_2}} \left(\frac{\frac{1-w_p}{w_p}}{\frac{1}{M_p} + \left(\frac{1-w_p}{w_p} \right) \frac{1}{M_{CO_2}}} \right) \end{aligned} \quad (C-7)$$

$$\begin{aligned} x_2 V_2 &= \left(\frac{\frac{g_p}{M_p}}{\frac{g_p}{M_p} + \frac{g_{CO_2}}{M_{CO_2}}} \right) \frac{M_p}{\rho_p} \\ &= \frac{1}{\rho_p} \left(\frac{1}{\frac{1}{M_p} + \left(\frac{1-w_p}{w_p} \right) \frac{1}{M_{CO_2}}} \right) \end{aligned} \quad (C-8)$$

Volume Change on Mixing

$$\begin{aligned} \Delta V_m &= V_{fm} - x_1 V_1 - x_2 V_2 \\ &= \frac{\frac{S}{\rho_p} + \left(\frac{1-w_p}{w_p} \right) \frac{1}{\rho_{CO_2}}}{\frac{1}{M_p} + \left(\frac{1-w_p}{w_p} \right) \frac{1}{M_{CO_2}}} \end{aligned} \quad (C-9)$$

which is the same as equation (4-15).

BIBLIOGRAPHY

- Adachi, K., Fujihara, F., and Ishida, Y., "Diluent Effects on Molecular Motions and the Glass Transition in Polymers. I. Polystyrene-Toluene", *J. Polym. Sci.-Polym. Phys. Ed.* (1975), 13, 2155-2171
- Adam, G., and Gibbs, J.H., "On the Temperature Dependence of Cooperative Relaxation Properties in Glass-Forming Liquids", *J. Chem. Phys.* (1965), 43, 139-146
- Albihn, P., Hedman, K., Kubat, J., "Solubility of Polystyrene in Liquid Sulfur Dioxide", *J. Appl. Poly. Sci.* (1979), 23, 2829-2836
- Albihn, P., and Kubat, J., "Phase Equilibria in the Two-Phase System Polystyrene-Liquid Sulfur Dioxide", *Br. Poly. J.* (1981), 13, 137-141
- Angell, C.A., Sare, J.M., Sare, E.J., "Glass Transition Temperatures for Simple Molecular Liquids and their Binary Solutions", *J. Phys. Chem.* (1978), 82, 2622-2629
- Arai, Y., and Saito, S., "Application of the Hole Theory to Study the P-V-T-x Relations of the CO₂-CH₄ and CO₂-N₂ Systems", *J. Chem. Eng. Jap.* (1972), 5, 107-111
- Beckman, E.J., Porter, R.S., and Koningsveld, R., "Mean Field Lattice Equations of State. II. The Role of the Segmental Surface Area in the Unification of Recent Lattice Models" *J. Phys. Chem.*, (1987) in press
- Berens, A.R., personal communication, (1987)
- Bondi, A., *Physical Properties of Molecular Crystals, Liquids, and Glasses*, Wiley, New York (1968)
- Bonner, D.C., "Solubility of Supercritical Gases in Polymers - A Review", *Polym. Eng. Sci.* (1977), 17, 65-72
- Bowman, L.M., "Dense Gas Chromatographic Studies", PhD Thesis, University of Utah, (1976)
- Carpenter, M.R., Davies, D.B., Matheson, A.J., "Measurement of the Glass Transition Temperature of Simple Liquids", *J. Chem. Phys.* (1967), 46, 2451-2454

- Chiou, J.S., Barlow, J.W., and Paul, D.R., "Polymer Crystallization Induced by Sorption of CO₂ Gas", *J. Appl. Polym. Sci.* (1985), 30, 3911-3924
- Chiou, J.S., Barlow, J.W., and Paul, D.R., "Plasticization of Glassy Polymers by Carbon Dioxide", *J. Appl. Polym. Sci.* (1985), 30, 2633-42
- Chow, T.S., "Molecular Interpretation of the Glass Transition Temperature of Polymer-Diluent Systems", *Macromolecules* (1980), 13, 362-364
- Claudy, P., Letoffe, J.M., Camberlain, Y., and Pascault, J.P., "Glass Transition of Polystyrene versus Molecular Weight", *Polym. Bull. (Ber.)* (1983), 9, 208-215
- des Cloizeaux, J., "The Lagrangian Theory of Polymer Solutions at Intermediate Concentrations", *J. Phys. (Paris)* (1975), 36, 281-291
- Costas, M., Epstein, H.I., Sanctuary, B.C., Richon, D., and Renon, H., "Equilibrium Theory of r-Mer Fluids", *J. Phys. Chem.* (1981), 85, 1264-1266
- Couchman, P.R., "Glass Transition Temperatures of Compatible Polymer Mixtures", *Phys. Lett.* (1979), 70A, 155-157
- Cowie, J.M.G., "Some General Features of T_g-M Relations for Oligomers and Amorphous Polymers", *Eur. Polym. J.* (1975), 11, 297-300
- Derham, K.W., Goldsbrough, J., and Gordon, M., "Pulse-Induced Critical Scattering (PICS) from Polymer Solutions", *Pure Appl. Chem.* (1974), 38, 97-116
- DiBenedetto, A.T., "Prediction of the Glass Transition Temperature of Polymers: A Model Based on the Principle of Corresponding States", *J. Polym. Sci. -Part B: Polym. Phys.* (1987), 25, 1949-1969
- DiMarzio, E.A., and Gibbs, J.H., "Chain Stiffness and the Lattice Theory of Polymer Phases", *J. Chem. Phys.* (1958), 28 807-813
- DiMarzio, E.A., Gibbs, J.H., Fleming, P.D., and Sanchez, I.C., "Effects of Pressure on the Equilibrium Properties of Glass-Forming Polymers", *Macromolecules* (1976), 9, 763-771

- Durrill, P.L., and Griskey, R.G., "Diffusion and Solution of Gases in Thermally Softened or Molten Polymers: Part I. Development of Technique and Determination of Data", *AIChE J.* (1966), 12, 1147-1151
- Edwards, S.F., "The Theory of Polymer Solutions at Intermediate Concentration", *Proc. Phys. Soc., London* (1966), 88, 265-280
- Ehrlich, P., "Phase Equilibria of Polymer-Solvent Systems at High Pressures Near Their Critical Loci: Polyethylene-Ethylene", *J. Polym. Sci.* (1965) A3, 131-136
- Fisher, M.E., "Renormalization of Critical Exponents by Hidden Variables", *Phys. Rev.* (1968), 176, 257-271
- Flory, P.J., *Principles of Polymer Chemistry*, Cornell Univ. Press, Ithaca, N.Y. (1953)
- Flory, P.J., Orwoll, R.A. and Vrij, A., "Statistical Thermodynamics of Chain Molecule Liquids. I. An Equation of State for Normal Paraffin Hydrocarbons", *J. Am. Chem. Soc.* (1964), 86, 3507-3514
- Flory, P.J., "Thermodynamics of Polymer Solutions", *Disc. Faraday Soc.* (1970), 49, 7-27
- Fox, T.G., "Influence of Diluent and of Copolymer Composition on the Glass Temperature of a Polymer System", *Bull. Am. Phys. Soc.* (1956), 1, 123
- Frenkel, J., *Kinetic Theory of Liquids*, Oxford University Press, London (1946); Dover reprint, New York (1955)
- Gee, G., "The Thermodynamic Analysis of the Effect of Pressure on the Glass Temperature of Polystyrene", *Polymer* (1966), 7, 177-191
- Gehrig, M., and Lentz, H., "p, V, T, Properties for Benzene in the Range 5 to 300 MPa and 323 to 683K", *J. Chem. Therm.* (1977), 9, 445-450
- Gibbs, J.H., and DiMarzio, E.A., "Nature of the Glass Transition and the Glassy State", *J. Chem. Phys.* (1958), 28, 373-383
- Gibbs, J.W., "On the Equilibrium of Heterogeneous Substances", *Trans. Conn. Acad. Arts. Sci.* (1874-78), 3, 108-248, 343-520

- Gordon, J.M., Rouse, G.B., Gibbs, J.H., and Risen, W.M., "The Composition Dependence of Glass Transition Properties", *J. Chem Phys.* (1977), 66, 4971-4976
- Gordon, M., and Taylor, J.S., "Ideal Copolymers and the Second Order Transitions of Synthetic Rubbers. I. Non-crystalline Copolymers", *J. Appl. Chem.* (1952), 2, 493-500
- Griskey, R.G., "Understanding and Predicting the Diffusion and Solution of Gases in Molten and Thermally Softened Polymers", *Soc. Plast. Eng.*, 34th ANTEC Proc., (1976), 75-78
- Guggenheim, E.A. *Mixtures*, Clarendon Press, Oxford (1952)
- Hales, J.L., and Townsend, R., "Liquid Densities from 293 to 490K of Nine Aromatic Hydrocarbons", *J. Chem. Therm.* (1972), 4, 763-772
- Hillegers, L.T., "The Estimation of Parameters in Functional Relationship Models", PhD Thesis, (1986), University of Eindhoven (Netherlands)
- Hou, Y.C., and Martin, J.J., "Physical and Thermodynamic Properties of Trifluoromethane", *AIChE J.* (1959), 5, 125-129
- Huggins, M.L., "The Thermodynamic Properties of Liquids, Including Solutions. I. Internal Energies in Monatomic Liquids and Their Mixtures", *J. Phys. Chem.* (1970), 74, 371-378
- Ichihara, S., Komatsu, A., Tsujita, Y., Nose, T., and Hata, T., "Thermodynamic Studies on the Glass Transition and the Glassy State of Polymers. I. Pressure Dependence of the Glass Transition Temperature and Its Relation to Other Thermodynamic Properties of Polystyrene", *Polym. J.* (1971), 2, 530-534
- Irvine, P., and Gordon, M., "Graph-Like State of Matter. 14. Thermodynamics of Semi-Dilute Polymer Solutions", *Macromolecules* (1980), 13, 761-772
- Jasovsky, G.A., and Gottesman, M., "Decaffeinated Roasted Coffee Blend", U.S. Patent No. 4,255,461, assigned to General Foods Corp., March 10, 1981
- Jenkel, E., and Heusch, R., "Die Erniedrigung der Entfriertemperatur Organischer Glaser durch Losungsmittel", *Kolloid Z. & Z. fur Polym.* (1953), 130, 89-105

- Kambour, R.P., Karasz, F.E., and Daane, J.H., "Kinetic and Equilibrium Phenomena in the System: Acetone Vapor and Polycarbonate Film", *J. Polym. Sci. A-2* (1966), 4, 327-347
- Kang, T.L., Hirth, L.J., Kobe, K.A., McKetta, J.J., "Pressure-Volume-Temperature Properties of Sulfur Dioxide", *J. Chem. Eng. Data* (1961), 6, 220-226
- Kanig, G., "Zur Theorie der Glastemperatur von Polymerhomologen, Copolymeren, und Weichgemachten Polymeren", *Kolloid Z. Z. Polym.* (1963), 190, 1-16
- Kehiaian, H.V., Grolier, J-P.E., and Benson, G.C., "Thermodynamics of Organic Mixtures. A Generalized Quasi-Chemical Theory in Terms of Group Surface Interactions", *J. Chim. Phys.* (1978), 75, 1031-1048
- Kehiaian, H.V., Grolier, J-P.E., Kechavarz, M.R., and Benson, G.C., "Thermodynamic Properties of Binary Mixtures Containing Ketones: VII. Analysis of the Properties of 2-Propanone + n-Alkane Mixtures in Terms of a Quasi-Chemical Group Contribution Model", *Fluid Phase Equil.* (1981), 5, 159-189
- Kelley, F.N., and Bueche, J., "Viscosity and Glass Temperature Relations for Polymer-Diluent Systems", *J. Polym. Sci.* (1961), 50, 549-556
- Kerns, W.J., Anthony, R.G., and Eubank, P.T., "Volumetric Properties of Cyclohexane Vapor", *AIChE Symp. Ser.* (1974), 70, 14-21
- Kilian, H.G., "Thermodynamik der Gleichgewichtsschmelze von Polymer-Homologen bei der Quasi-statischen Glastemperatur" *Kolloid Z. Z. Polym.* (1974), 252, 353-357
- Kilpatrick, P.K., and Chang, S.H., "Saturated Phase Equilibria and Parameter Estimation of Pure Fluids with Two Lattice-Gas Models", *Fluid Phase Equil.* (1986), 30, 49-56
- King, M.B., Kassim, K., and Bott, T.R., "Mass Transfer into Near-Critical Extractants", *Fluid Phase Equil.* (1983), 10, 249-260
- Kleintjens, L.A., "Effects of Chain Branching and Pressure on Thermodynamic Properties on Polymer Solutions", PhD Thesis, University of Essex (U.K.), (1979)

- Kleintjens, L.A., and Koningsveld, R., "Liquid-Liquid Phase Separation in Multicomponent Polymer Systems XIX. Mean Field Lattice Gas Treatment of the System n-Alkane/Linear Polyethylene", *Colloid Polym. Sci.* (1980), 258, 711-718
- Kleintjens, L.A. and Koningsveld, R., "Mean-Field Lattice-Gas Description of the System CO₂/H₂O" *Sep. Sci. Tech.* (1982), 17, 215-233
- Koningsveld, R., and Staverman, A.J., "Liquid-Liquid Phase Separation in Multicomponent Polymer Solutions IV. Coexistence Curves", *Kolloid Z. Z. Polym.* (1967), 218, 114-124
- Koningsveld, R., "Partial Miscibility of Multicomponent Polymer Solutions", *Adv. Coll. Inter. Sci.* (1968), 2, 151-215
- Koningsveld, R., Stockmayer, W.H., Kennedy, J.W., and Kleintjens, L.A., "Liquid-Liquid Phase Separation in Multicomponent Polymer Systems XI. Dilute and Concentrated Polymer Solutions in Equilibrium", *Macromolecules* (1974), 7, 73-79
- Kudchadker, A.P., Alani, G.H., and Zwolinski, B.J., "The Critical Constants of Organic Substances", *Chem. Revs.* (1968), 68, 659-735
- Kumar, S.T., Suter, U.W., and Reid, R.C., "Fractionation of Polymers with Supercritical Fluids", *Fluid Phase Equil.* (1986), 29, 373-382
- Kumar, S.K., Suter, U.W., Reid, R.C., "A Statistical-Mechanics Based Lattice Model Equation of State", *J. Chem. Phys.* (1987), in press
- Kurnik, R.T., Holla, S.J., and Reid, R.C., "Solubility of Solids in Supercritical Carbon Dioxide and Ethylene", *J. Chem. Eng. Data* (1981), 26, 47-51
- Lacombe, R.H., and Callahan, J.J., "A Theory of Glass-Forming Liquids" *Ann. N.Y. Acad. Sci.* (1981), 371, 316-317
- Lee, Y., and Porter, R.S., "Double Melting Behavior of Poly(ether ether ketone)", *Macromolecules* (1987), 20, 1336-1341
- Lemstra, P.J., Kooistra, T., and Challa, G., "Melting Behavior of Isotactic Polystyrene", *J. Polym. Sci., A-2* (1972), 10, 823-833

- Liau, I.S., and McHugh, M.A., "High Pressure Solid Polymer-Supercritical Fluid Phase Behavior", in *Supercritical Fluid Technology*, J.M.L. Penninger, M. Radosz, M.A. McHugh, and V.J. Krukoni, eds., Elsevier, Amsterdam, (1985), 415-434
- Luft, G., and Lindner, A., "Zum Einfluss des Polymermolekulargewichts auf das Phasenverhalten von Gas-Polymer-Systemen unter Hochdruck", *Angew. Makro. Chem.* (1976), 56, 99-114
- Lipatov, Y.S., "The Iso-Free Volume State and Glass Transitions in Amorphous Polymers", *Adv. Polym. Sci.* (1978), 26, 63-104
- Liu, D.D., and Prausnitz, J.M., "Calculation of Phase Equilibria for Mixtures of Ethylene and Low-Density Polyethylene at High Pressures", *IEC Proc. Des. Dev.* (1980), 19, 205-211
- de Loos, T.W., Poot, W., and Diepen, G.A.M., "Fluid Phase Equilibria in the System Polyethylene + Ethylene. 1. Systems of Linear Polyethylene + Ethylene at High Pressure", *Macromolecules* (1983), 16, 111-117
- de Loos, Th. W., Poot, W., and Lichtenthaler, R.N., "Fluid Phase Behavior in Binary Ethylene + n-Alkane Systems", *Ber. Bunsen. Phys. Chem.* (1984), 88, 855-859
- Lundberg, J.L., Mooney, E.J., and Rogers, C.E., "Diffusion and Solubility of Methane in Polyisobutylene", *J. Polym. Sci. Part A-2* (1969), 7, 947-962
- Maloney, D.P. and Prausnitz, J.M., "Solubility of Ethylene in Liquid, Low Density Polyethylene at Industrial Separation Pressures" *IEC Proc. Des. Dev.* (1976), 15, 216-220
- Masa, Z., Biro, J., and Pouchly, J., "On the Structure and Properties of Vinyl Polymers and Their Models. XV. Glass Transition Temperatures in the System Polystyrene-Diluent", *Coll. Czech. Chem. Commun.* (1973), 38, 201-207
- Masse, M., personal communication, (1987)
- McHugh, M.A., and Krukoni, V.J., *Supercritical Fluid Extraction: Principles and Practice*, Butterworths, Boston (1986)

- McKinney, J.E., Goldstein, M., J. Res. Nat. Bur. Stand., "PVT Relationships for Liquid and Glassy Poly(vinyl acetate)", (1974), 78A, 331-353
- McMaster, L.P., "Aspects of Polymer-Polymer Thermodynamics", *Macromolecules* (1973), 6, 760-773
- Mercier, J.P., Groeninckx, G., Lesne, M., "Some Aspects of Vapor-Induced Crystallization of Polycarbonate of Bisphenol A", *J. Polym. Sci. Polym. Symp.* (1967), 16, 2059-2067
- Mercier, J.P., and Legras, R., "Correlation Between the Enthalpy of Fusion and the Specific Volume of Crystallized Polycarbonate of Bisphenol A", *J. Polym. Sci. Polym. Lett. Ed.* (1970), 8, 645-650
- Mermin, N.D., "Lattice Gas with Short-Range Pair Interactions and a Singular Coexistence Curve Diameter", *Phys. Rev. Lett.* (1971), 26, 957-959
- Michels, A., and Michels, C., "Isotherms of CO₂ Between 0 and 150 and Pressures from 16 to 250 Atm. (Amagat Densities 18-206)", *Proc. Roy. Soc. (London) A* (1936), 153, 201-214
- Michels A., Michels, C., and Wouters, H., "Isotherms of CO₂ Between 70 and 3000 Atmospheres (Amagat Densities Between 200 and 600)", *Proc. Roy. Soc. (London) A* (1936), 153, 214-224
- Miller, A.A., "Kinetic Interpretation of the Glass Transition: Glass Temperatures of n-Alkane Liquids and Polyethylene", *J. Polym. Sci. A2*, (1967), 6, 249-257
- Miller, A.A., "Polymer Melt Viscosity and the Glass Transition: An Evaluation of the Adam-Gibbs and the Free Volume Models", *J. Chem. Phys.* (1968), 49, 1393-1397
- Miller, A.A., "Isomobility States in Polymer Liquids", *Macromolecules* (1978), 11, 134-137
- Miller, A.A., "A Molecular Interpretation of the Vogel Equation for Polymer Liquid Mobility", *Macromolecules* (1978), 11, 859-862
- Modell, M., and Reid, R.C., *Thermodynamics and its Applications*, Prentice Hall, Englewood Cliffs, N.J. (1971) Chapter 7

- Morel, G., and Paul, D.R., "CO₂ Sorption and Transport in Miscible Poly(phenylene oxide)/Polystyrene Blends", *J. Membr. Sci.* (1982), 10, 273-282
- Muthukumar, M., "Thermodynamics of Polymer Solutions", *J. Chem. Phys.* (1986), 85, 4722-4728
- Nanda, V.S., Simha, R. and Somcynsky, T., "Principle of Corresponding States and Equation of State of Polymer Liquids and Glasses", *J. Polym. Sci.: Part C* (1966), 12, 277-295
- Naoki, M., Owada, A., "Factors Determining Glass Transition Temperature and Relaxation Time of Poly(vinyl chloride)", *Polymer* (1984), 25, 75-83
- Nies, E., Kleintjens, L.A., Koningsveld, R., Simha, R. and Jain, R.K., "On Hole Theories for Liquids and Compressed Gases: Ethylene", *Fluid Phase Equil.* (1983), 12, 11-27
- Nies, E., Koningsveld, R., and Kleintjens, L.A., "On Polymer Solution Thermodynamics", *Prog. Coll. Polym. Sci.* (1985), 71, 1-13
- Nitsche, J.M., Teletzke, G.F., Scriven, L.E., and Davis, H.T., "Phase and Tension Behavior of Water, Carbon Dioxide, and Decane: Comparison of a Lattice-Gas Model and the Peng-Robinson Equation", *Fluid Phase Equil.* (1983), 14, 203-208
- Nitsche, J.M., Teletzke, G.F., Scriven, L.E., and Davis, H.T. "Phase Behavior of Binary Mixtures of Water, Carbon Dioxide and Decane Predicted with a Lattice-Gas Model", *Fluid Phase Equil.* (1984), 17, 243-264
- Nose, T., "A Hole Theory of Polymer Liquids and Glasses: Glass Transition and the Glassy State", *Polym. J.* (1971), 2, 427-456
- Oels, H-J., "Pressure-Volume-Temperature Measurements on Atactic Polystyrene", PhD Thesis, (1977), University of Clausthal (Fed. Rep. Germany)
- Oels, H-J., and Rehage, G., "Pressure-Volume-Temperature Measurements on Atactic Polystyrene. A Thermodynamic View", *Macromolecules* (1977), 10, 1036-1043

- Okada, M., Nose, T., "Quasi-Chemical Treatment of the Hole Theory for r-Mers. I. Pure Liquids", *Polym. J.* (1981), 13, 399-406
- Olabisi, O., and Simha, R., "Pressure-Volume-Temperature Studies of Amorphous and Crystallizable Polymers. I. Experimental", *Macromolecules* (1975), 8, 206-210
- Panayioutou C., and Vera, J.H., "Statistical Thermodynamics of r-Mer Fluids and Their Mixtures", *Polym. J.* (1982), 14, 681-694
- Panayioutou, C. and Vera, J.H., "An Improved Lattice-Fluid Equation of State for Pure Component Polymeric Fluids", *Polym. Eng. Sci.* (1982), 22, 345-348
- Patterson, D., "Role of Free Volume Changes in Polymer Solution Thermodynamics", *J. Polym. Sci.: Part C* (1968), 16, 3379-3389
- Patterson, D., "Role of Free Volume in Polymer Solution Thermodynamics", *Pure Appl. Chem.* (1972), 31, 133-149
- Paulaitis, M.E., Krukonis, V.J., Kurnik, R.T., and Reid, R.C., "Supercritical Fluid Extraction", *Rev. Chem. Eng.* (1983), 1, 179-250
- Peng, D., and Robinson, D.B., "A New Two-Constant Equation of State", *IEC Fund.* (1976), 15, 59-64
- Perry, R.H., and Chilton, C.H., eds., *Chemical Engineering Handbook, Fifth Edition*, McGraw-Hill, New York (1973)
- Prigogine, I., *The Molecular Theory of Solutions*, Interscience Publishers, New York, N.Y., (1957)
- Quach, A., and Simha, R., "Pressure-Volume-Temperature Properties and Transitions of Amorphous Polymers; Polystyrene and Poly(orthomethylstyrene)", *J. Appl. Phys.* (1971), 42, 4592-4606
- Randall, L.G. "The Present Status of Dense Gas Extraction and Dense Gas Chromatography: Impetus for DGC/MS Development", *Sep. Sci. Tech.* (1982), 17, 1-117
- Ratzsch, M., Findeisen, R., and Sernow, V.S., "Untersuchungen zum Phasenverhalten von Monomer-Polymer Systemen unter Hohen Druck", *Z. Phys. Chem. (Leipzig)* (1980), 261, 995-1000

- Reid, R.C., "Retrospective Comments on Physical Property Correlations", *Fluid Phase Equil.* (1983), 13, 1-14
- Reynolds, W.C., *Thermodynamic Properties in SI*, Department of Mechanical Engineering, Stanford University, Stanford, CA (1979)
- Saeki, S., Kuwahara, N., Konno, S, and Kaneko, M., "Upper and Lower Critical Solution Temperatures in Polystyrene Solutions", *Macromolecules* (1973), 6, 246-250
- Sanchez, I.C., and Lacombe, R.H., "An Elementary Molecular Theory of Classical Fluids. Pure Fluids", *J. Phys. Chem.* (1976), 80, 2352-2362
- Sanchez, I.C., and Lacombe, R.H., "An Elementary Equation of State for Polymer Liquids", *J. Polym. Sci. - Polym. Lett. Ed.* (1977), 15, 71-75
- Sanchez, I.C., and Lohse, D.J., "Cell Model Theory of Polymer Solutions", *Macromolecules* (1981), 14, 131-137
- Sand, M.L., "Method for Impregnating a Thermoplastic Polymer", U.S. Patent No. 4,598,006 assigned to Hercules Corp., July 1, 1986
- Sanditov, D., and Bartenev, G., "Application of Free Volume Theory to Vitreous Melts and Glasses", *Physik. Chim. Stek.* (1975), 1, 414-420
- Sayegh, S.G., and Vera, J.H., "Lattice-Model Expressions for the Combinatorial Entropy of Liquid Mixtures: A Critical Discussion", *Chem. Eng. J.* (1980), 19, 1-10
- Schneider, G.M., "Physiochemical Aspects of Fluid Extraction", *Fluid Phase Equil.* (1983), 10, 141-157
- Scholte, Th. G., "Determination of Thermodynamic Parameters of Polymer-Solvent Systems from Sedimentation-Diffusion Equilibrium in the Ultracentrifuge", *J. Polym. Sci.-Polym. Phys. Ed.* (1970), 8, 841-868
- Schottky, W., Ulich, H., and Wagner, C., *Thermodynamik*, Springer, Berlin (1929)
- Schouten, J.A., Ten Seldam, C.A., Trappeniers, N.J., "The Two-Component Lattice-Gas Model", *Physica* (1974), 73, 556-572

- Schroeder, E., Arndt, K-F., "Loslichkeit von Makromolekullen in Komprimierten Gases. II. Experimentelle Ergebnisse uber das Druckverhalten von Polyvinylchlorid, Polymethylmethacrylat und Polystyrol in Fluidem CO₂", *Faserforsch. Textiltech.* (1976), 27, 141-146
- Sefcik, M.D., "Dilation and Plasticization of Polystyrene by Carbon Dioxide", *J. Polym. Sci.-Polym. Phys. Ed.* (1986), 24, 957-971
- Simha, R., and Somcynsky, T., "On the Statistical Thermodynamics of Spherical and Chain Molecule Fluids", *Macromolecules* (1969), 2, 342-350
- Smirnova, N.A., and Victorov, A.I., "Thermodynamic Properties of Pure Fluids and Solutions from the Hole Group Contribution Model", *Fluid Phase Equil.* (1987), 34, 235-263
- Smith, J.M., and Van Ness, H.C., *Introduction to Chemical Engineering Thermodynamics, Third Edition*, McGraw-Hill, N.Y. (1975)
- Soave, G., "Equilibrium Constants from a Modified Redlich-Kwong Equation of State", *Chem. Eng. Sci.* (1972), 27, 1197-1203
- Solc, K., "Cloud-Point Curves of Polymer Solutions", *Macromolecules* (1970), 3, 665-673
- Spahl, R., and Luft, G., "Entmischungsverhalten von Ethylene und niedermolekularem Polyethylene", *Ber. Bunsenges. Phys. Chem.* (1981), 85, 379-384
- Staverman, A.J., "The Cohesive Energy of Liquid Mixtures I.", *Rec. Trav. Chim. Pays-Bas* (1937), 56, 885-890
- Staverman, A.J., "The Entropy of High Polymer Solutions", *Rec. Trav. Chim. Pays-Bas* (1950), 69, 163-174
- Stevens, J.R., Coakley, R.W., Chau, K.W., Hunt, J.L., "The Pressure Variation of the Glass Transition in Atactic Polystyrene", *J. Chem. Phys.* (1986), 84, 1006-1014
- Sweet, G.E., and Bell, J.P., "Multiple Endotherm Melting Behavior in Relation to Polymer Morphology", *J. Polym. Sci., A-2* (1972), 10, 1273-1283

- Swelheim, T., de Swaan Arons, J., and Diepen, G.A.M., "Fluid Phase Equilibrium in the System Polyethylene-Ethylene", *Rec. Trav. Chim. Pays-Bas* (1965), 84, 261-266
- Timmermans, J., *Physico-Chemical Constants of Pure Organic Compounds*, Vol. II, Elsevier (1965)
- Todoki, M., and Kawaguchi, T., "Origin of Double-Melting Peaks in Drawn Nylon 6 Yarns", *J. Polym. Sci. Polym. Phys. Ed.* (1977), 15, 1067-1076
- Trappeniers, N.J., Schouten, J.A., Ten Seldam, C.A., "Gas-Gas Equilibrium and the Two-Component Lattice-Gas Model", *Chem. Phys. Lett.* (1970), 5, 541-545
- Turnbull, D., "Under What Conditions Can a Glass be Formed?", *Contemp. Phys.* (1969), 10, 473-488
- Ueberreiter K., and Kanig, G., "Self Plasticization of Polymers", *J. Colloid Sci.* (1952), 7, 569-583
- Ueberreiter, K., and Otto-Laupenmuhlen, E., "Spezifische Warme, Spezifisches Volumen, Temperatur- and Warmeleitfahigkeit von Hochpolymeren", *Z. Naturforsch* (1953), 8a, 664-673
- Vargaftik, N.B., *Handbook of Physical Properties of Liquids and Gases*, Second Edition, Hemisphere Publ. Corp., N.Y. (1975)
- Walsh, D.J., and Dee, G.T., "Calculations of the Phase Diagrams of Polyethylene Dissolved in Supercritical Solvents", *Polymer*, in press
- Wang, W-C.V., "Environmental Effects of High Pressure Carbon Dioxide Gas on Polystyrene", PhD Thesis, Cornell University (1981)
- Wang, W-C.V., Kramer, E.J., and Sachse, W.H., "Effects of High-Pressure CO₂ on the Glass Transition Temperature and Mechanical Properties of Polystyrene", *J. Polym. Sci.- Polym. Phys. Ed.* (1982), 20, 1371-1384
- Warfield, R.W., Hartmann, B., "Pressure Dependence of Transitions", *Polymer* (1982), 23, 1835-1837

- Washburn, E.W., editor, *International Critical Tables of Numerical Data, Physics, Chemistry and Technology*, McGraw-Hill (1928)
- Wood, L.A., "Glass Transition Temperature of Copolymers", *J. Polym. Sci.* (1958), 28, 319-330
- Young, S., "Vapor Pressures and Saturated Densities of Thirty Pure Compounds", *Proc. Roy. Soc. Dublin* (1910), 12, 374-425
- Zeman, L., Biroš, J., Delmas, G. and Patterson, D., "Pressure Effects in Polymer Solution Phase Equilibria I. The Lower Critical Solution Temperature of Polyisobutylene and Polydimethylsiloxane in Lower Alkanes", *J. Phys. Chem.* (1972), 76, 1206-1213
- Zeman, L. and Patterson, D., "Pressure Effects in Polymer Solution Phase Equilibria. II. Systems Showing Upper and Lower Critical Solution Temperatures", *J. Phys. Chem.* (1972), 76, 1214-1219
- Zoller, P., Bolli, P., Hersche, E., and Foppe, U., "Das p-v-T Diagramm von Polystyrol", *Kunststoffe* (1976), 66, 363-366
- Zoller, P., "A Study of the Pressure-Volume-Temperature Relationships of Four Related Amorphous Polymers: Polycarbonate, Polyarylate, Phenoxy, and Polysulfone", *J. Polym. Sci.- Polym. Phys. Ed* (1982), 20, 1453-1464

